

**RATE EFFECTS OF RAPID LOADING
IN CLAY SOILS**

by

JUAN BALDERAS MECA

A thesis submitted to
The University of Sheffield
for the degree of
Doctor of Philosophy

Department of Civil and Structural Engineering
University of Sheffield
March 2004

ABSTRACT

RATE EFFECTS OF RAPID LOADING IN CLAY SOILS

The study of the relationship between the shear strength of the clay and the rate at which it is loaded is relevant to the application of a new rapid load pile testing technique called Statnamic. There are problems associated with interpreting the test results in clay soils due to the non linear variation in shear resistance with rate of shearing.

An investigation has been conducted for two clay soils which were used in an associated research project. These were a reconstituted kaolin clay (KSS) used for model pile tests and undisturbed glacial clay taken from a full scale prototype pile testing site near Grimsby. Monotonic and multistage strain controlled triaxial tests were carried out on both clays using a, pneumatic computer, controlled rapid load triaxial system at rates from 0.001 mm/s to 200 mm/s. The shear strength increased and the excess pore pressure decreased as the rate of shearing increased. A power law was proposed relating dynamic and static shear strength. The damping coefficients and hence the rate effects, defined as a function of strain, were similar for both clays

Based on the triaxial test results and a back analysis of Statnamic and “static” constant rate of penetration data from the associated model and full scale pile tests in both clays, a non-linear model has been proposed relating the static resistance of a pile to the measured Statnamic load taking into account the rate effects and the inertia of the pile. The non-linear model was used to develop a new multistage interpretation method for the analysis of Statnamic tests in clays.

To my family,
My parents María and José Antonio,
my sister M^a José
and Piluca.

ACKNOWLEDGEMENTS

The work presented in this thesis was carried out at the Department of Civil and Structural Engineering at the University of Sheffield and was funded by TNO Building and Construction in the Netherlands, Berminghammer Foundation Equipment and Colegio de Ingenieros de Caminos, Canales y Puertos (Spain), using a computer controlled pneumatic testing system donated by ELE International Ltd. I wish to offer my thanks for this support.

I would like to express my deepest gratitude to Dr Adrian F.L. Hyde, my supervisor, for all his generous support, advice, comprehension and help. Thanks are also due to Professor Antonio Gens at UPC, Barcelona, Spain, who always made time to discuss and comment on my work, acting as a co-supervisor during my visits to Barcelona.

I would like to thank Mike Brown, who provided all the Statnamic data and helped me during these years. I would like also to thank Dr. Toru Higuchi who helped me enormously with his technical advice. Thanks to Paul Osborne and Mark Foster for their help in the laboratory. A special mention to all my colleges in the Geotechnics Engineering Group, thanks to those who left before I did because they showed to me that there was an end and to those who will leave later because they reminded to me the hope that we all had at the beginning and that helped to renew mine everyday.

Special thanks to my friends, Sean, Nadeen, Jackie, Sam, Diego, Miguel, Jens, Maurizio, Linda, Jim, Erika, Toru, Atchan, Note, Vassilis, Emma, Klaus, Shasa, Sakthi and Paco. They made it worthy.

Especial agradecimiento para mis padres y mi hermana por creer en mi y apoyarme continuamente. Gracias a mis padres por todo lo que han hecho por mí. Finalmente gracias a Piluca por su amor, su infinita paciencia y su ayuda para hacer un sueño realidad.

TABLE OF CONTENTS

	<u>Page No.</u>
TITLE PAGE	i
ABSTRACT	ii
ACKNOWLEDGEMENTS	iii
TABLE OF CONTENTS	v
NOTATIONS	ix
CHAPTER ONE: INTRODUCTION	1
CHAPTER TWO: LITERATURE REVIEW	
2.1 Introduction.....	3
2.2 Statnamic testing.....	4
2.3 The unloading point method (UPM).....	6
2.4 Evaluation of the UPM.....	10
2.5 Rate effects in clay soils.....	12
2.5.1 Triaxial investigation.....	14
2.5.2 Ring shear tests.....	21
2.5.3 Other laboratory and field testing rate investigation.....	23
2.6 Analysis of the axial response of piles incorporating rate effects.....	26
2.7 Concluding remarks.....	29
CHAPTER THREE: TESTING PROGRAMME	
3.1 Introduction.....	39
3.2 Test Series.....	40
3.3 Preliminary tests. Soils classification and consolidation.....	40
3.4 Consolidated undrained triaxial tests.....	40
3.5 Triaxial permeability tests.....	40

3.6	Monotonic rapid loading triaxial tests.....	41
3.6.1	Reconstituted clay (KSS).....	41
3.6.2	Undisturbed clay (Grimsby).....	42
3.7	Multistage rapid loading triaxial tests.....	42
3.7.1	Reconstituted clay (KSS).....	43
3.7.2	Undisturbed Clay (Grimsby).....	44

CHAPTER FOUR: TESTING EQUIPMENT

4.1	Introduction.....	54
4.2	One-Dimensional Consolidation.....	55
4.3	Pneumatic Computer Controlled Rapid Loading Triaxial System.....	55
4.3.1	The Triaxial Cell.....	56
4.3.2	Pressure Reservoir.....	56
4.3.3	Cell Pressure System.....	56
4.3.4	Back Pressure System and Volume Change Apparatus.....	57
4.3.5	Pore Pressure Transducer.....	57
4.3.6	Immersible Load Cell.....	58
4.3.7	Deformation Transducer.....	58
4.3.8	Top Platen Loading Cap and Connecting Device.....	58
4.3.9	Control and Data Acquisition System (CDAS).....	59
4.3.10	Loading Frame.....	59
4.3.11	Electro-Pneumatic Cyclic Loading system.....	59
4.4	The Conventional Triaxial System.....	60
4.4.1	The Triaxial Cell.....	61
4.4.2	Microprocessor Controlled Hydraulic Actuators (GDS Controller)....	61
4.4.3	Back Pressure Supply and Volume Change Apparatus.....	61
4.4.4	Differential pressure transducer.....	62
4.4.5	Cell Pressure System.....	62
4.4.6	Pore Pressure Transducer.....	63
4.4.7	Immersible Load Cell.....	63
4.4.8	Deformation Transducer.....	63
4.4.9	Top Platen Loading Cap and Connecting Device.....	64
4.4.10	Data Monitoring Equipment.....	64
4.4.11	Strain Controlled Loading Frame.....	64

CHAPTER FIVE: EXPERIMENTAL PROCEDURE

5.1 Introduction.....	71
5.2 Soil Classification.....	71
5.3 Sample Preparation.....	71
5.3.1 One-Dimensional Pre-Consolidation.....	72
5.3.2 Sampling the Calibration Chamber beds.....	73
5.3.3 Boreholes on site.....	73
5.4 Setting up the Sample in Triaxial Cell.....	74
5.4.1 Pneumatic Computer Controlled Rapid Loading Triaxial System.....	74
5.4.2 The Conventional Triaxial System.....	76
5.5 Testing Procedures.....	76
5.5.1 Preliminary tests.....	77
5.5.2 Consolidated Undrained Triaxial Tests.....	78
5.5.3 Permeability Tests.....	79

CHAPTER SIX: THE MATERIALS

6.1 Introduction.....	85
6.2 The Materials.....	85
6.2.1 Soil Description and Classification.....	87
6.3 Consolidation.....	88
6.4 Monotonic Compression.....	90
6.4.1 Stress-Strain Behaviour.....	90
6.4.2 Stress Paths and Critical State Line.....	91
6.5 Permeability.....	93

CHAPTER SEVEN: RAPID LOADING TESTS

7.1 Introduction.....	108
7.2 Reconstituted clay (KSS)	108
7.2.1 Monotonic rapid loading triaxial tests (OCR1).....	108
7.2.2 Monotonic rapid loading triaxial tests (OCR4).....	112
7.2.3 Multistage rapid loading triaxial test. Static rate 0.001 mm/s (OCR1)..	113
7.2.4 Multistage rapid loading triaxial test. Static rate 0.01 mm/s (OCR1)....	117
7.2.5 Multistage rapid loading triaxial test. Static rate 0.01 mm/s (OCR4)....	120
7.2.6 Multistage rapid loading triaxial test. Static rate 0.01 mm/s (OCR8)...	120
7.3 Undisturbed clay (Grimsby).....	122

7.3.1 Multistage tests.....	122
7.3.2 Monotonic rapid loading triaxial tests.....	124
7.4 Application of multistage tests to determine critical state parameters.....	125

CHAPTER EIGHT: APPLICATION OF RATE EFFECTS TO THE ANALYSIS OF STATNAMIC TESTS

8.1 Introduction.....	202
8.2 A non-linear Statnamic analysis method.....	203
8.3 The class A prediction.....	204
8.3.1 Prediction method.....	205
8.3.2 Pile type and installation.....	205
8.3.3 Pile testing.....	206
8.3.4 Prediction results.....	207
8.3.5 Discussion of the class A prediction.....	207
8.4 Improvements to the non-linear Statnamic method.....	208
8.4.1 Triaxial damping coefficients.....	210
8.4.2 Variable non-linear model parameters. Bilinear α_{STN} model.....	211
8.4.3 Multistage Bilinear α_{STN} model.....	213

CHAPTER NINE: CONCLUSIONS

9.1 Introduction.....	228
9.2 Rapid loading tests.....	228
9.3 Application of rate effects to the analysis of Statnamic test results... ..	229
9.4 Application of multistage tests to determine critical state parameters	231
9.5 Recommendations for further Work.....	234

REFERENCES.....	233
------------------------	------------

APPENDIX

NOTATIONS

A	Activity
A_c	Cross sectional area of the sample
A_s	Static state
A_d	Dynamic state
B	Skempton's pore pressure parameter
C_L	Slope of deviator stress strain-rate lines and a function of ε
C_S	Smith's viscous damping constant
C_{sw}	Strain wave velocity
C_{UPM}	UPM method damping coefficient
C_u	Undrained shear strength
D_w	Wave length
F_{stn}	Statnamic force
F_a	Inertia force
F_v	Damping force
F_u	Equivalent static soil resistance
f_d	Dynamic loading function
f_s	Static yield function
G_s	Specific gravity
H	Differential pressure head
J	Smith's viscous damping constant for soil
J_{GC}	Gibson and Coyle's viscous damping constant for soil
J_{LP}	Litkouhi and Poskitt's point viscous damping constant for soil
J'_{LP}	Litkouhi and Poskitt's side viscous damping constant for soil
K	Plastic slider resistance
K_S	Smith's soil spring constant

k_{ah}	Adjustment parameter
k_d	Work-hardening and strain rate parameter
k_s	Work-hardening parameter
K_v	Vertical permeability
L_F	Foundation length
L_s	Sample height
M	Slope of critical state line when it is projected on to a constant volume plane (q -p' plane)
M^*	Mass of the pile
N_B	Briaud's viscous exponent
N_{GC}	Power to which velocity of sample deformation is raised in Gibson and Coyle's equation
N_{LP}	Power to which velocity of sample deformation is raised in Litkouhi and Poskitt's equation
N_p	Value of v at p' = 1kPa on the normal consolidation line
N_w	Wave Number
P_d	Dynamic strength of soil
P_s	Static strength of soil
Q	Quake
Q_{c1}, Q_{c2}	Ultimate cone resistance in time to failure t_1, t_2 .
Q_f	Flow rate
R_d	Dynamic pile resistance
$R_{dynamic}$	Smith's dynamic force resistance
$R_{Sd,e}$	Smith's resisting force under dynamic loading in the elastic zone.
R_s	Static pile resistance
R_{static}	Smith's static force resistance
R_u	Constant plastic pile resistance
T	Load duration
V	Velocity

V_{GC}	Velocity of sample deformation
V_p	Instantaneous velocity of the element of the pile.
W	Weight
X_p	Elastic deformation of the element of the pile on Smith's equation
a	Acceleration
a_1, a_2	Parameters of the equal strain contours on to the $e-p'$ plane
b_1, b_2	Parameters of the equal strain contours on to the $e-q$ plane
d	Ratio between pile head displacement and pile diameter
e	Void ratio
p'	Mean normal effective stress
q	Deviator stress
q_0	Deviator stress at static reference deformation rate, V_0
q_d	Dynamic deviator stress
q_s	Static deviator stress
u	Pore water pressure
v	Specific volume
w	Moisture content
Δu	Excess pore water pressure
ΔV	Axial rate of displacement
α, β	Triaxial damping coefficients
α_{mp}, β_{mp}	Model pile damping coefficients
α_{YJ}, β_{YJ}	Yong and Japp's parameters
α_{RD}, β_{RD}	Randolph and Deek's viscous damping parameters
$\alpha_{STN}, \beta_{STN}$	Statnamic model viscous damping parameters
ϵ	Axial strain
ϵ_0	Initial axial strain
$\epsilon_{f,YJ}$	Yong and Japp's critical axial strain
$\dot{\epsilon}$	Axial strain rate

$\dot{\epsilon}_0$	Reference axial strain rate
$\dot{\epsilon}^P$	Viscoplastic strain
ϵ_{ij}^{VP}	Viscoplastic strain tensor
ϵ_{ij}^P	Inviscid plastic strain tensor
ϵ_v	Volumetric strain
ϕ'_c	Internal friction angle for compression
κ	Slope of swelling line (negative)
λ	Slope of normal consolidation line and critical state line (negative)
Γ	Value of v at $p' = 1$ kPa on the critical state line
σ	Stress
σ_{ij}	Stress tensor
σ'_h	Horizontal effective stress
σ'_v	Vertical effective stress
σ_0	Initial stress
σ'_1	Major effective principal stress
σ'_2	Intermediate effective principal stress
σ'_3	Minor effective principal stress
θ	Temperature
τ_d	Dynamic shear resistance
τ_s	Static shear resistance
ψ	Slope of stress strain-rate lines and a function of ϵ
η	Viscous dashpot resistance
1-D	One-dimensional
CRP	Constant rate of penetration
QML	Quick maintained loading
QCL	Quick continuous loading
CSL	Critical state line
LL	Liquid limit
PI	Plasticity index

PL	Plastic limit
OCR	Over-consolidation ratio
RL	Recompression line
SL	Swelling line
UPM	Unloading point method
ln	Natural logarithm

CHAPTER ONE

INTRODUCTION

A new rapid load method of testing piles called Statnamic (Bermingham and Janes, 1989) involves the application of a short duration (about 100ms) compressive load whose reaction is given by the high acceleration of a relatively small mass. The static pile resistance is given by a process of deconvolution in which the shear strength of the soil is predicted using an assumed relationship between the measured dynamic shear resistance and the static shear resistance.

It is widely accepted that there is a relationship between the shear strength of clay and the rate at which it is loaded (Litkouhi and Poskitt, 1980). The faster the clay is sheared the greater the shear resistance of the clay. This time-dependent relationship is known as a viscous law and damping is the term used to describe the increase in strength that clay soils demonstrate under increased rates of loading.

The new method is increasingly being used as an alternative method of pile load testing. The use of a relatively straightforward analysis of the pile load/velocity relationship which takes into account pile inertia and damping effects and is known as the unloading point method (UPM) has provided a good correlation with static load test data for sandy soils (Brown, 1994). But there are problems associated with interpreting the test results in clay soils due to the non linear variation in shear resistance with rate of shearing.

The present research was focused on investigating the rate effects on clay soils.

The aims of the work were to study the relationship between dynamic shear resistance and rate of shearing in clay soils and to apply the results to refine and develop

models of soil behaviour in order to improve the current method (UPM) of analysis for Statnamic pile tests.

The objectives of the investigation were to carry out a triaxial testing programme on reconstituted clay (KSS) and undisturbed clay (Grimsby), to interpret the results in relation to current soil models, to calibrate the results against large scale model pile tests on KSS clay and in situ pile tests on Grimsby clay (Brown, 2004) and to establish models of soil behaviour taking into account rate effects for the analysis of Statnamic tests.

CHAPTER TWO

LITERATURE REVIEW

2.1 Introduction

The uncertainties associated with soil investigation and existing pile design methods that rely upon empirical correlations (Randolph, 2003), require the carrying out of in-situ load tests assessing the actual pile performance for quality control of piled foundations. Pile load tests provide a direct evaluation of the pile capacity that includes variability of ground conditions and effect of pile installation (Wood, 2003).

The Statnamic test (Bermingham & Janes, 1985) is a rapid load pile test that is increasingly being used as an alternative to both dynamic and static load tests. The existing static test methods include Maintained Load Tests (MLT) (ICE,1997), Constant Rate of Penetration Tests (CRP) (ICE, 1997) and the bottom-up Osterberg Cell (O-Cell) Test . The Statnamic test and dynamic tests have the advantage of being quicker and cheaper to carry out than the static tests although require more complex analysis and interpretation.

This literature review aims to introduce the Statnamic loading method describing the concept, the device, its advantages and disadvantages. The review will then look at the current method of analysis, its assumptions as well as their validity. The review will focus on the application of the Statnamic method in clay soil where the current method of analysis that takes into account inertia and rate effects over-predicts the static resistance. Rate effect investigations carried out by means of triaxial and other

laboratory and field testing in clay soil are examined and soil models identified. Finally current analyses of the axial response of piles incorporating rate effects are reviewed.

2.2 Statnamic testing

The Statnamic (STN) testing method was developed by Bermingham Foundation Equipment of Canada and TNO Building and Construction Research as an alternative to static (Maintained Load (ML) and Constant Rate of Penetration (CRP)) and dynamic methods. The impetus for developing the method was to find an economical solution for load testing high capacity deep foundations

“According to Fellenius (1995) the Stanamic concept was born in 1987 when he asked Patrick Bermingham to design a drop hammer for impacting a pile to perform dynamic load tests. Bermingham determined the feasibility of accelerating a mass upwards from the top of the foundation rather than dropping a mass onto the foundation and tried out several concepts of catching the reaction mass when falling back from launching.” (Middendorp, 2000)

The STN testing method has been described in detail by Berminham & Janes (1985), Hovarth (1995) and numerous others. The loading system consists of a piston with a combustion chamber placed on the pile top with a reaction mass attached to cylinder placed over the pile (Figures 2.1). A solid fuel propellant (Figure 2.2) is ignited inside the piston generating high pressure gases and accelerating the reaction mass upwards at approximately 20g producing an equal and opposite reaction which pushes the pile into the soil. The reaction weight is 20 times less than the actual maximum load. The applied force and pile top displacements are measured directly using load cell and laser beam systems (Figure 2.3). Acceleration of the top of the shaft can be measured with an accelerometer that also can serve as a backup for determining top movement . A schematic of a typical Statnamic load test setup is shown in Figure 2.4.

Bermingham and TNO realized that the long duration feature of the load allowed a fully different approach in instrumentation and analysis compared to dynamic load testing (Middendorp, 2000). Statnamic was first called inertial load testing

(Bermingham *et al*, 1989). Middendorp gave the method the present name Statnamic, realizing that the method was positioned between Static load testing and Dynamic load testing

Rapid load tests are differentiated from static and dynamic load tests by comparing the duration of the loading event with respect to the natural axial period of the foundation ($2L_F/C_{sw}$), where L_F represents the foundation length and C_{sw} represents the strain wave velocity (typical wave speeds are 5000 m/s and 4000 m/s for steel and concrete respectively). Test duration longer than $1000 L_F/C_{sw}$ are considered static loadings and those shorter than $10 L_F/C_{sw}$ are considered dynamic (Janes *et al*, 2000; Kusakabe *et al*, 2000). Tests with a duration between $10L_F/C_{sw}$ and $1000 L_F/C_{sw}$ are denoted as rapid load tests. The duration of the Statnamic test is typically 100 to 120 milliseconds, but it is dependant on the ratio of applied force to the weight of the reaction mass. Longer duration tests of up to 500 milliseconds are possible but require a larger reaction mass, (Mullin *et al*, 2002)

The advantages of the Statnamic test are that it is cheaper than a static test, quicker (several piles can be tested per day for loads up to 4MN), the load duration is of the order of 0.1 sec., exceeding that for dynamic tests and the natural period of the pile; Statnamic devices can apply load up to 30 MN; and the lateral capacity of foundations can be tested. Local available material can be used as reaction mass to reduce transport cost. A crane or crawler system is required to move the STN device over the building site. For loads up to 4MN an STN device with a hydraulic catch mechanism can be applied (Figure 2.5). For higher loads Statnamic requires a gravel catch mechanism. Testing can take between 0.5 to 2 days per pile depending on pile capacity. For hydraulic mechanisms the number of piles tested per day are in the same range as with DLT. STN can be even more efficient when the loading device and the hydraulic catch mechanism are placed on crawlers, Middendorp *et al* (2000). The direct benefit of this time efficiency is the cost savings to the client and the ability to conduct more tests within a given budget, (Mullin *et al.*, 2002).

Middendorp *et al.* (2000) compared the advantages and disadvantages of dynamic and Statnamic tests and concluded that:

1. For bored concrete piles, auger piles and caissons, the dynamic load testing method has some disadvantages and is less suitable and Statnamic load testing is the preferred method. The most important reasons for the preference of Statnamic load testing in the case of cast insitu piles are:
 - a. Accuracy of load measurements: STN is not dependent on pile material and cross section properties.
 - b. No influence of cross sectional variations: STN results are not influenced by cross sectional variations over the pile length.
 - c. No tension during compressive testing: STN's long duration loading will keep pile under compression.
 - d. Concentric loading: Easy placement of STN loading device in centre of the pile.
 - e. Pile and soil response closer to static: With STN the pile moves as a rigid body similar to static load tests. Stress wave phenomena can be neglected resulting in a simple method of analysis (Middendorp & Bielefeld, 1995).
2. For driven piles both DLT and STN methods can be applied reliably and each has its advantages and its disadvantages. A big economic advantage for DLT can be the use of the production rig for testing. A big advantage for STN is the fact that the maximum available energy can be used to mobilize capacity and that testing does not have to be stopped when tension stresses become too high like with DLT.

2.3 The unloading point method (UPM)

The most widely used procedure used to evaluate Statnamic measurements and to predict the static load versus deflection response is called the Unloading Point Method and it was outlined by Middendorp *et al.* (1992) and briefly summarised by Brown (1994) and Seidel (1996). The UPM is predicated on the assumption that the duration of the Statnamic loading pulse causes similar displacement behaviour at all

levels in the pile, the pile or shaft is assumed to behave as a rigid body subjected to time-dependent forces and accelerations. It is reasoned, therefore, that this justifies adoption of a simple model in which stress-wave phenomena do not have to be taken into account. However, it is stated that dynamic phenomena must still be taken into account.

On the basis of these assumptions, the UPM uses a rigid body model (Figure 2.6), which takes into account pile inertia and damping effects. The pile is modelled as a rigid mass M and the force in the spring represents the static soil resistance F_u , while the dashpot represents the viscous component of soil resistance and is dependent on the pile penetration velocity V such that. $F_v = C_{UPM}V$

The equation of force equilibrium is given by:

$$F_{sm} = F_u + F_v + F_a \quad \text{Equation 2.1}$$

$$F_u = F_{sm} - F_v - F_a \quad \text{Equation 2.2}$$

where,

- F_{sm} = Statnamic force
- F_a = Inertia force = $M a$
- F_v = Damping force
- F_u = Equivalent static soil resistance

The static pile resistance is derived by a process of deconvolution. A damping coefficient, C_{UPM} , is found by assuming that at the maximum displacement (point (1) in Figure 2.7) the pile velocity and hence damping is zero. i.e.

$$V_1 = 0 \quad \text{Equation 2.3}$$

$$F_{v1} = C_{UPM}V_1 = 0 \quad \text{Equation 2.4}$$

and

$$\therefore F_{u1} = F_{sm1} - F_{a1} \quad \text{Equation 2.5}$$

The soil resistance is assumed constant between the maximum load (point (2) in Figure 2.7) and the point of maximum displacement, called “Unloading Point” and assuming the coefficient to be constant the equivalent static curve can be deduced.

$$F_{u2} = F_{u1} \quad \text{Equation 2.6}$$

$$F_{u2} = F_{stn2} - C_{UPM}V_2 - F_{a2} \quad \text{Equation 2.7}$$

substituting Equations 2.7& 2.5 in Equation 2.6

$$C_{UPM} = \frac{(F_{stn2} - F_{a2}) - (F_{stn1} - F_{a1})}{V_2} \quad \text{Equation 2.8}$$

The UPM has proven to be a valuable tool in predicting damping values when the foundation acts as a rigid body. However, as the pile length increases an appreciable delay can be introduced between the movement of the pile top and the toe, hence negating the rigid body assumption. This occurrence also becomes prevalent when an end bearing condition exists; in this case the lower portion of the foundation is prevented from moving jointly with the top of the foundation (Mullins *et al.*2002).

Middendorp & Bielefeld (1995) defined a “Wave Number” (N_w) to quantify the applicability of the UPM. The wave number is calculated by dividing the wave length (D_w) by the foundation depth (L_F). D is obtained by multiplying the wave velocity C_{sw} by the load duration (T). Thus, the wave number is calculated by the following equation.

$$N_w = \frac{D_w}{L_F} = \frac{C_{sw}T}{L_F} \quad \text{Equation 2.9}$$

From empirical studies Middendorp determined that the UPM would accurately predict static capacity, from Statnamic data, if the wave number was greater than 12. Nishimura & Matsumoto (1995) established a similar threshold at a wave number of 10. Using wave speeds of 5000 m/s and 4000 m/s for steel and concrete respectively and a typical Statnamic load duration the UPM is limited to piles shorter than 50 m (steel) and 40 m (concrete). Wave number analysis can be used to determine if significant stress waves will develop in the pile. However, this does not necessarily satisfy the rigid body requirement of the UPM.

Statnamic tests cannot always have wave numbers greater than 10, and as such there have been several methods suggested to accommodate stress wave phenomena in Statnamicly tested long piles (Middendorp & Bielefeld, 1995).

Justason (1997) proposed the Modified UPM (M-UPM). The method simply involved the averaging of the top and toe velocity and acceleration for calculating the inertia and damping. The method can be applied to any length of the pile but becomes more necessary as the pile becomes longer (low N_w numbers). The standard UPM method assumes that pile top velocity and pile toe velocity are the same. The M-UPM method is particularly useful when the pile top and pile toe velocity are not in the same range (elastic pile, high toe resistance). Averaging the pile top and pile toe velocities and accelerations yields more accurate inertia and damping forces. The method yields the best results when used in conjunction with an embedded toe accelerometer.

Mullins *et al.*(2002) made an additional improvement to the M-UPM, the “Segmental Unloading Point” S-UPM. This method uses measured strain gage data to separate the pile into “segments” and perform an M-UPM on each segment. The data for each segment are added together to produce a total “derived static” load-displacement for the top of the pile. The S-UPM can be applied to any pile, so long as the pile has strain gages distributed over the pile shaft. The first application was the Taipei Financial Center in Taiwan-1999.

S-UPM extends the applicability of the M-UPM to long piles. All assumptions for the UPM remain valid. The Segmental Method assumes each segment of a pile behaves as a single degree of freedom system. The system requires embedded strain gauge data. A measure of toe displacement is desirable. All results are based on measured quantities.

SAW (Garbin, 1999) and SUPERSAW are spreadsheet-based programs that automate the application of UPM and S-UPM to Statnamic data.

Alternative procedures were proposed to evaluate Statnamic data based on automatic matching techniques (Foeken *et al.* (1998); Chin (1998); El Naggar & Baldinelli (1998)) or finite element techniques Matsumoto (1998). The results of the analysis are promising, showing good agreements with static data but interpretation suffers from complexity and highly operator dependency mainly in the determination of soil parameters for use in the analysis (Wood, 2003).

2.4 Evaluation of the UPM

The assumptions used in the UPM method and their validity are discussed by Middendorp *et al*, (1992), Brown (1994,1995), Goble *et al* (1995), Middendorp & Bielefeld (1995), Seidel (1996), and numerous others.

Brown (1994) evaluated data for eight STN load tests at six test sites and reviewed the application of the UPM. The data illustrated the good agreement of the Statnamic data with conventional static load tests for drilled shafts in sandy soil and the one test in soft clay. But the UPM tended to over predict capacity by as much as 25 or 30% in stiff overconsolidated clays. He explained these over predictions as in part due to the fact that those stiff over-consolidated clays would be expected to exhibit dilatancy during shear, and negative pore water pressure would be expected near the shaft/soil interface. This effect with the relatively plastic clays could account for more rate-dependent strength than for sandy soils with greater hydraulic conductivity. In softer clay soils, dilatancy and negative pore water pressure might not occur.

With respect to the implication that Statnamic loading may cause damage to the shaft, Brown observed no evidence of large tension stresses in any shaft tested with the Statnamic device. The load distribution along the shaft was similar for the Statnamic and static loadings in the one case study where such data were available. Finite element studies performed by Brown support the assumption that Statnamic loading should not result in significant tensile stresses in the shaft. However dynamic effects such as inertia and damping are significant with the Statnamic method and must be considered.

Brown also evaluated the effects of a surface waves propagating away from the test pile upon loading, which produces ground movement away from the test site. The relatively long wavelength (due to the long duration of the loading) and large amplitude produce a wave which can be felt a significance distance away from the test site; however, the long wavelength translates into quite low ground acceleration compared to blasting or pile driving, so that the effects on nearby structures are minimal. The most significant effect of the propagating surface wave is on the laser instrument; this instrument must be located at a sufficient distance from the test pile so that the surface wave arrival at the laser occurs after all relevant data are obtained (generally around 0.15s).

Additional analytical investigation was performed by Brown in order to examine the effect of damping factors, shaft inertia, wave propagation effects, and soil quake (displacement required to mobilize the full static resistance) on the expected response and interpretation of the response during a Statnamic type loading event. He concluded that there was a need for an improved interpretation procedure for use with the Statnamic method. The errors and over prediction of capacity noted appeared to be primarily due to the fact that the rigid body assumption in the UPM method is not appropriate for long slender shafts, especially in soils that may have high damping resistance.

The fact that the UPM has been shown to work well in some cases is likely to be due to the use of the procedure in cases where relatively short shafts have been analysed or where soil damping is relatively low (in such cases the limitations of the methods are likely to be quite small).

Goble *et al*, (1995) pointed out that the approach of considering the pile acting as a rigid body and examining the force action of the pile at the instant that motion stops (unloading point) was first suggested by Eiber (1958) for the analysis of dynamic tests. The simplest version of the methods developed was published by Goble *et al*, (1967, 1970) and later developments abandoned the rigid body assumption for a more realistic and accurate elastic model.

As has been the case regarding high-strain dynamic testing, soil damping factors are observed to vary with soil and pile types and experience is required to be able to predict a range of expected values in advance of testing (Brown,1995).

The damping coefficient, C , in the area between the points of maximum load and maximum displacement tabulated by Brown, show a surprisingly large variability (-0.4 to -5.4) for different soils. Janes(1995) presents results of Statnamic tests that show that the Statnamic damping “constant” C_{UPM} in the same area, varied on the same pile by a factor of 3 when the applied Statnamic force was doubled. The variability of the damping coefficient, C_{UPM} , along the entire pulse of a single Statnamic test was investigated and confirmed by Seidel (1996) and this extreme is also acknowledged by Mullins *et al* (2002) when they assumed the use of an average value of C_{UPM} between the points of the maximum load and displacement to apply to the UPM.

During the loading phase, the loading rate can be controlled by the amount of explosive and reaction mass. However, the unloading rate is not controlled, and large accelerations are generated, occurring near the time of load evaluation by the Statnamic equilibrium point method. Thus, the inertia term correction in the Statnamic capacity analysis can be quite sensitive to high accelerations for large shafts with a large mass; the pile mass may be further increased by some indeterminate soil mass moving with the pile. In fact the unloading phase is so short that the rigid body assumption is violated and stress waves are generated in the pile, causing large tension stresses (Goble *et al.* 1995).

To achieve soil failure, it may be necessary in some cases to load the pile substantially above the pile static capacity due to the dynamics. In normal dynamic testing, the load quickly reaches its full value; stress waves distribute the impact loading in time so that the applied force need only be similar to the pile's static capacity to achieve soil failure (Goble *et al.*, 1995). The method requires a large applied force, but the system is designed to provide a relatively large force in an efficient manner without damaging the shaft or the pile and, as with any measurement, if the load is insufficient to mobilize the full static resistance, one can only estimate the static resistance that was mobilized with that loading (Brown 1995).

Brown (1995) noted the need for improved reliability in measurements of acceleration during the Statnamic loading event. Goble *et al.*, (1995) pointed out the inconvenience of data obtained by measuring the displacement with non contact displacement measurement device that can be sensitive to vibrations from both ground and wind. He also highlighted that double differentiation to obtain acceleration magnitudes was an unreliable process, particularly when the displacement measurements are subjected to filtering in the signal conditioning and computation process, which introduces another variable.

2.5 Rate effects in clay soils.

The undrained stress-strain behaviour of clay can be significantly affected by the applied rate of loading. The change in clay soil properties with change in the loading

rate is called the strain-rate effect (Whitman,1957) or rate effect and damping is the term used in this thesis to describe the increase in strength that clay soils demonstrate under increased rates of loading , i.e. it is a viscous parameter. This phenomenon has been studied extensively since the original work of Taylor (1942) and Casagrande and Wilson (1951).

The term damping is widely used in the literature to denote either the dissipation of energy in oscillations of all types or the extent of the dissipation and decay. Damping defined as a dynamic property of a system in terms of energy dissipation can be developed by many sources the two principal ones being:

- 1) Hysteresis (or material): Damping is the result of the inelasticity in the system and represents heat and frictional losses.
- 2) Radiation (or geometric): Damping is due to the propagation of energy in the soil away from the dynamically excited system.

Viscous damping parameters used in soil models indirectly represent energy losses due to soil inertia, radiation damping, and other factors contributing to energy losses (excess pore pressure generation and dissipation, thixotropy, etc) along with viscous damping. (Paikowsky and Chernauskas, 1996).

Numerous investigations have been carried out to study the relationship between the shear strength of a clay soil and the rate at which it is loaded. There have been many attempts to define the relationship by means of empirical or constitutive equations. However there is uncertainty with regard to the fundamental mechanisms responsible for strain-rate effects.

This section reviews the work carried out by means of triaxial tests and some of the resulting soil models proposed. It also summarises the research done by means of other laboratory tests like ring shear tests, penetrometer or model pile tests and soil models suggested that could be used to predict static behaviour of the soil from rapid loading test results.

2.5.1 Triaxial investigation

Taylor (1942) investigated the strength of a clay which was remoulded at the liquid limit and then consolidated under 414 kPa. Failure was produced within the range of 4 minutes to 8 days. In these tests the strength of specimens which were failed quickly was found to be about 25 per cent greater than the strength of specimens which were failed slowly.

Casagrande & Shanon (1948), in connection with studies of the stability of slopes under the effects of bombing, investigated the rate effects using three types of apparatus developed for applying transient loads in triaxial compression and unconfined compression tests. These were pendulum apparatus, falling beam apparatus and hydraulic apparatus. The type of loading desired was a transient load in which the test specimen was subjected to a rapid loading and unloading, simulating the effect of the first stress wave created by an explosion. The value for the fastest time of loading was 1/100 second. The time for the slowest loading was determined by a desire to overlap with the fastest loading time used in static strength tests. Triaxial tests were carried out on Manchester sand, Cambridge clay, Boston clay and Stockton Clay. Casagrande and Shanon concluded that:

1. The strength of clay increases with decreasing time of loading, the transient strength for the fastest tests in this investigation being from 1.5 to 2 times the static strength. The percentage increase in strength is dependent on the static strength. Samples with a low static strength had a greater percentage increase than those with a high static strength. The increase in strength due to time of loading is independent of the method of testing.
2. The strength of sand increases only slightly with decreasing time of loading. The maximum increase for the fastest tests in this investigation was about 10%.
3. The modulus of deformation of clay for the tested transient tests in this investigation was about twice that for static. (Modulus of deformation is defined as the slope of a line drawn from the origin through the point on the stress-deformation curve corresponding to a stress of one-half the strength).

Casagrande and Willson (1951) suggested that this rate-effect upon strength might be caused by a change in the excess pore pressure generated during the shear process. Data reported by Bjerrum *et al*, (1958), Crawford (1959) and O'Neill (1962) have supported this hypothesis.

Richardson and Whitman (1963) carried out triaxial compression tests using two strain-rates at 1% strain per min and 0.002% strain per min on normally consolidated clay specimens and found that the peak shear resistance increased about 10% in passing from the slow to the fast strain-rate; at small strains, the resistance increased as much as 100%. The increase in resistance with increase in strain rate resulted: 1) at small strains, from increased strength in terms of effective stress, and 2) at large strains, from decreased excess pore pressure.

Olson and Parola (1967) performed quick triaxial compression tests on Goose Lake clay compacted at water contents ranging from 9 percent dry of optimum to 3 per cent on the wet side. The specimens were subjected to confining pressures ranging from 68.95 kPa to 689.50 kPa and were loaded to failure in times ranging from 2 ms to an hour. The average increase in compressive strength per decade reduction in time to failure, for specimens compacted at water contents near optimum, was about 2 percent for the range 100 min-10min to 18 per cent for the range 60ms-6ms. Specimens compacted at lower water contents underwent smaller strength increase in dynamic tests. The secant modulus, defined at 1 percent axial strain, increased at a rate of about 15 percent per decade reduction in time of failure.

Gibson & Coyle (1968) presented the results of a laboratory investigation of the damping properties of sands and clays. A series of dynamic (impact) and static tests were performed on a variety of sands and clays. The sands varied in grain size and grain shape, and the clays varied in plasticity and moisture content. Velocity of sample deformation, peak dynamic load, and peak static loads were measured so that damping constants for the soils could be evaluated. The objective of these tests was to determine soil damping constants by performing impact tests and to correlate these soil damping constants with common soil properties such as angle of internal shearing resistance and void ratio for granular soils and moisture content and liquidity index for clay soils.

Smith's model (Smith, 1960), which describes soil action at the point of a pile, was examined. A modification in Smith's equation (Equations 2.10 and 2.11) was made by raising velocity of deformation to an optimum power in order to obtain a J_{GC} value which was constant over the full range of loading velocities. Once an optimum power of velocity of sample deformation was obtained, an average power was determined which was convenient for all sands or clay tested. This optimum power differed for each sand and clay but all sands tested could be represented to the 0.20 power and all clay to 0.18 power without excessive error while the value of J_{GC} depends of the specific properties of each soil and could be obtained if the void ratio is known for a particular clean sand or if the moisture content is known in a particular highly plastic clay.

$$J_{GC} = \frac{\left(\frac{P_d}{P_s}\right) - 1}{V_{GC}^{N_{GC}}} \quad \text{Equation 2.10}$$

$$\left(\frac{P_d}{P_s}\right) = 1 + J_{GC} V_{GC}^{N_{GC}} \quad \text{Equation 2.11}$$

where,

P_d = Dynamic strength of soil

P_s = Static strength of soil

V_{GC} = Velocity of sample deformation

J_{GC} = Viscous damping constant for soil

N_{GC} = Power to which velocity of sample deformation is raised

The samples were tested over a range of loading velocities varying from the minimum velocity obtainable to ensure sample failure to a maximum velocity of 3.5 m/s. Pore pressures were measured in the granular materials only in "pilot" tests to observe their behaviour under dynamic loading.

Yong and Japp (1969) examined the problem of large strain performance of clays under impulsive-type loadings. The investigation was carried out in triaxial cells

on both an artificial clay and naturally occurring clay. Both soils were tested in the fully saturated state. The controlled strain-rate tester was capable of delivering uniform loading velocities of up to approximately 12.7 m/s. The tests were performed at strain rates of 30 to 2000 percent per second. Pore pressure measurements were taken at mid-height, but in view of the short times to failure involved in the compression of the soil samples, and because of the large hydraulic lag in pore pressure measurements, the results were examined in terms of total stresses. They showed from their shock loading triaxial shear tests with strain rates up to 120000%/min that the deviator stress was proportional to the logarithm of strain rate normalised with respect to a reference strain rate. If $q (= \sigma'_1 - \sigma'_3)$ for any common axial strain (ε) was plotted against $\log (\dot{\varepsilon} / \dot{\varepsilon}_0)$ where $\dot{\varepsilon}_0$ was a reference strain rate, a sensibly linear relationship was obtained (Figure 2.8). The slope of these stress strain-rate lines, $\psi(\varepsilon)$, tended to asymptotic values with increasing strains (Figure 2.9). They proposed an empirical equation expressing the constant strain rate behaviour of clays from their experiments.

$$\sigma(\varepsilon, \dot{\varepsilon}) = \sigma_0(\varepsilon, \dot{\varepsilon}_0) + \psi(\varepsilon) \log \left(\frac{\dot{\varepsilon}}{\dot{\varepsilon}_0} \right) \quad \text{Equation 2.12}$$

$$\psi(\varepsilon) = \alpha_{YJ} e^{\frac{\varepsilon_{f,YJ} - \varepsilon}{\beta_{YJ}}} \quad \text{Equation 2.13}$$

A critical strain rate was identified wherein a significant change in material response occurred. While the linear extrapolations for strength increase may be made to account for rate effects, for example for 10 percent increase in strength for every decade increase in strain rate, a critical point was reached where the simple mechanism was no longer valid. This was the critical load velocity point where material property change was great because of the mechanism in the face of the moving shock front.

The concept of a rate-dependent yield surface was recommended where a critical rate-dependent yield will exist corresponding to the critical strain-rate or critical loading velocity. The family of expanding yield surfaces is not dissimilar to those generally shown for work hardening materials.

Adachi & Okano (1974) proposed a general constitutive equation that could describe the behaviour of clays under creep, stress relaxation and constant strain rate shear processes. They extended Roscoe's critical state energy theory for clays to explain the rate sensitive properties by using Peryzyna's theory for elasto/viscoplastic continua and some empirical evidence. The equation was expressed in terms of the second order tensor field. Thus, one could apply it to three dimensional problems by means of the finite element method. They clarified that there might exist a unique stress-strain-time relation for clays by reviewing various empirical equations proposed for constant strain rate processes by Yong & Japp (1969), for stress relaxation by Murayama *et al.* (1972) and the Singh and Mitchell's equations for creep phenomena (Akai *et al.* (1972).

According to Adachi and Okano (1974), the basic concept of Peryzyna's theory of elasto/viscoplastic materials (Perzyna, 1963) is the same as a rheological model given in Figure 2.10.a. The mathematical expression for the model is given by:

$$\dot{\epsilon} = \frac{\dot{\sigma}}{E} + \frac{(\sigma - K)}{\eta} \quad \text{Equation 2.14}$$

where η is the viscous dashpot resistance. The viscoplastic deformation is governed by the excess stress $(\sigma - K)$. Generally, the slider's resistance, K , changes with the work-hardening of the material and the relation of the viscoplastic strain $\dot{\epsilon}^P$ and the excess stress $(\sigma - k)$ is non linear. Peryzyna assumed the existence of a rate sensitive loading surface, i.e. the so called "dynamic loading surface" given by $f_d(\sigma_{ij}, \theta, \epsilon_{ij}^{VP}) = k_d$ and the so called "excess stress function" F which represented the difference between the dynamic loading function and static yield function given by $f_s(\sigma_{ij}, \theta, \epsilon_{ij}^P) = k_s$. It was defined as follows:

$$F = \frac{f_d}{f_s} - 1 \quad \text{Equation 2.15}$$

where σ_{ij} is the stress tensor, θ is the temperature, ϵ_{ij}^{VP} is the viscoplastic strain tensor, ϵ_{ij}^P is the inviscid plastic strain tensor, k_d is a parameter representing both effects of work-hardening and strain rate and k_s is a work-hardening parameter.

Figure 2.10.b. shows a schematic diagram of static and dynamic loading surfaces. The difference between the stress states A_s and A_d is due to viscoplastic strain rate .

Akai *et al* (1975) conducted four types of triaxial compression tests on fully saturated normally consolidated clays under undrained conditions. Constant rate shear tests were carried out at 50, 15, 4, 1, 0.4, 0.1, 0.01 and 0.002%/min. From the experimental results they confirmed the validity of the empirical equations proposed by Yong & Japp (1969) for the behaviour under constant strain rate loading and by Murayama *et al.*(1972) for stress relaxation. The equivalency of these two was clarified and then the empirical equation for creep phenomenon by Singh and Mitchell(1968) was quantified based on those equations leading to the conclusion that a unique stress-strain –time relation existed for clay.

In order to examine the influence of strain rate on deviatoric stress and excess pore pressure, they plotted the data for deviator stress and excess pore pressure versus logarithm of strain rate using strain state as a parameter (Figure 2.11). The deviator stress increased proportional with the increase of logarithm of strain rate. The slope of the lines $\alpha(\epsilon)$ was expressed by a strain function as shown in Figure 2.12 and tended to remain constant above 1% of the vertical strain. No obvious strain rate effect on the excess pore water pressure was observed. They concluded that the pore water pressure was expressed by a function of strain. They also reported that using the experimental results of Akai *et al.* (1962) similar evidence could be recognized.

They concluded that:

1. The static stress path defined by Roscoe's original energy theory may give the equilibrium stress state in the effective stress space although within the limit of this experimental work.
2. The strain rate effect appears in stress paths evidenced by their differing from the static stress path. (Figure 2.13)
3. Equi-strain lines obtained in the effective stress space are found to be parallel to the maximum principal stress axis.

4. As consequences of 2) and 3) there exists a unique induced pore water pressure-strain relation as stated by Lo (1969) and the pore water pressure is rate insensitive.
5. Those empirical equations for behaviour of clay under various loading conditions i.e, for constant strain rate by Yong and Japp (1969), stress relaxation by Murayama *et al* (1972), and creep phenomena by Singh & Mitchell (1968), were found to be equivalent.
6. As a consequence of 5), they confirmed the existence of a unique constitutive equation for clay, which can, at least, describe those characteristics.

Adachi *and* Oka (1982) extended the Adachi *and* Okano (1974) model so that it could describe both time-dependent behaviour such as secondary compression, as well as creep and the strain rate effect. Based on the model proposed by Adachi & Oka (1982), elasto-viscoplastic constitutive models were reconstructed for overconsolidated clay by Oka (1982) and Adachi *et al* (1991).

Other triaxial rate investigations conducted on overconsolidated clay soils include the work presented by Lefebvre & LeBoeuf (1987), Sheahan *et al.* (1996) Shogaki & Shirakawa (1999) and Zhu & Yin (2000).

Lefebvre *and* LeBoeuf (1987) performed monotonic and cyclic triaxial tests on three undisturbed sensitive clays. The increase of undrained shear strength with strain rate observed in this study varied 7% to 14% per log cycle increment of strain rate, the average being 10% for destructured as well as structured clays.

Sheahan *et al.* (1996) conducted consolidated undrained triaxial compression tests on resedimented Boston blue clay. The tests were undertaken on four overconsolidation ratios (OCR= 1, 2, 4 and 8) at four axial strain rates (0.05%, 0.5%, 5% and 50%/h) .The results showed that the undrained strength (C_u) rate sensitivity (percent increase in C_u per log cycle strain rate) across the two fastest strain rates did not vary with OCR and equalled about 9%. However across the three slower rates, increase in OCR caused a consistent decrease in the rate sensitivity that reached zero at OCR=8. For high OCR clay, increases in C_u (if they occurred) were caused by lower

shear-induced pore pressures since the effective stress envelope at the peak strength did not vary with strain rate. For low OCR clay, increases in C_u were caused by both lower shear-induced pore pressures and increases in the mobilized friction angle.

Shogaki & Shirakawa (1999) presented the results of unconfined compression tests, direct shear tests and triaxial tests performed on undisturbed natural clay carried out at different rates (1%, 0.2% and 0.05%/min). The C_u values from consolidated undrained compression triaxial tests became large with increasing strain rate.

Zhu & Yin (2000) performed consolidated undrained triaxial tests on reconsolidated saturated Hong Kong marine clay in both compression and extension shear states. The specimens were prepared to four different overconsolidation ratios (OCR= 1,2,4 and 8) and sheared at three different rates (0.15%/h, 1.5%/h and 15%/h). The strain-rate dependency of undrained shear strength, pore water pressure, stress path, and secant Young's modulus were investigated. The influence of OCR was examined. Higher strain rates resulted in higher undrained shear strengths at all OCRs. Both the strain rates and the OCRs affected pore-water pressure response and effective stress paths. The strain-rate effects were more significant for extension tests than for compression tests. The higher the strain rate, the larger the secant Young's modulus. The correlation of strain-rate parameter with OCRs was not evident.

2.5.2 Ring shear tests

The existence of a significant rate effect on the residual strength of cohesive soils was first identified in the work of Lupini *et al.* (1981). Further research was carried out to investigate these rate effects (Lemos, 1986; Tika, 1989a). Tika *et al.* (1996) considered the relation between the types of displacement rate effect and the three basic shearing modes of slow residual strength (turbulent, transitional and sliding) identified by Lupini *et al.* (1981):

a) Turbulent mode (TU) occurs in soils with a high proportion of rotund particles, or possibly in soils dominated by platy particles when the coefficient of interparticle friction between these particles is high. Shearing involves rotation of the rotund particles and particle orientation has a negligible effect. The residual friction angle is high and depends primarily on the shape and packing of the rotund particles and not on

the coefficient of inter-particle friction. A shear zone, once formed, is a zone of different porosity only and it is considerably modified by subsequent stress history.

b) Sliding mode (S) occurs in soils with a high proportion of platy, low-friction particles. These particles orientate in the direction of shearing and deform predominantly by sliding on a thin polished continuous shear surface. The residual friction angle depends primarily on mineralogy, pore water chemistry and the coefficient of interparticle friction. A shear surface, once formed, is a permanent feature of the soil and is not significantly affected by subsequent stress history.

c) Transitional mode (TR) occurs in soil with no dominant particle shape. Shearing involves both turbulent and sliding behaviour in different parts of a shear zone in which orientated shear surfaces can partly be formed but are continuously disrupted by the rotund particles. In this mode the residual friction angle is sensitive to small changes in grading of the soil.

Tika *et al* (1996) presented results from a laboratory investigation into the influence of fast rate of displacement on the residual strength of soils carried out in the ring shear apparatus for a wide range of natural soils for velocities varying from 0.0145 mm/min to 6000mm/min. Tika *et al.* concluded that when shear zones are formed by slow drained shearing and then tested at alternately fast and slow rates of displacement:

1. There is a initial threshold strength in the shear zone, mobilized at a negligibly small displacement. The threshold strength increases with increasing rate of displacement and is considerably higher than the slow residual strength.
2. For soils showing a transitional or sliding shear mode, there is further increase in strength with fast displacement in the shear zone up to a maximum value, the fast peak strength. The increase in fast peak strength above the slow residual strength may be associated with volume and structure changes taking place within the shear zone during fast shearing. The fast peak strength increases with increasing rate of displacement.
3. The strength is then likely to drop with fast displacement to a minimum value, the fast residual strength. Then three types of rate effects on the residual strength are identified: positive rate effects in soil showing a fast residual strength higher

than the slow residual; a neutral rate effect in soils showing a constant fast residual strength, equal to the slow residual, irrespective of rate of displacement; and a negative rate effect in soils showing a significant drop in fast residual strength below the slow residual when sheared at rates higher than a critical value.

4. Soils with turbulent shear mode exhibit a neutral or negative rate effect. Some soils may show both types, depending on the level of normal stress. Soils with transitional shear mode exhibit a negative rate effect and soils with sliding shear mode show either a negative or positive rate effect. Degradable soils, in which platy particles may be generated by massive grain breakdown during shearing can change their type of behaviour.

The causes of the negative rate effect were investigated by Lemos (1986), Tika (1989) and Lemos (1991). According to Tika *et al.*, (1996) most of the soils exhibiting this type of behaviour were placed at low water contents, so they should have been dilatant during drained shearing and significant excess pore water pressure could not have been generated in undrained shearing. Thus the loss in strength cannot be readily attributed to the development of large excess pore pressure due to contractive behaviour of the soils.

The results from the tests presented by Tika *et al.* (1996) allow the formulation of a soil model linking the strength of a pre-existing shear zone with displacement and rate of displacement.

2.5.3 Other laboratory and field testing rate investigation

Dayal & Allen. (1975) studied the penetration rate effect on the strength of clay and sand by constant velocity cone penetration tests performed with various velocities ranging from 0.13 cm/s to 81.14 cm/s. The clay and sand targets were of various strengths and moisture contents. The construction of the penetrometer was similar to that used in static tests and in each test the cone resistance, sleeve friction and penetration velocity were recorded.

Experimental results indicated that for granular soils the effects of penetration velocity on cone and sleeve friction resistances are insignificant, whereas for cohesive soils the increase in penetration velocity causes an increase in the cone and friction resistances. It was found that for the cohesive soils the ratio of dynamic to static strength is directly proportional to the logarithm of the penetration velocity ratio. The proportionality constant of this relationship defined as soil viscosity coefficient depends on the physical properties of the soil and the soil strength and its value increases as the strength of the soil decreases and is higher for the friction sleeve than for the cone. For the tested soils various values of the soil viscosity coefficient were proposed for different penetration rates. The validity of the analytical relationship was established for penetration velocities ranging from 0.13cm/s to 550 cm/s.

Litkouhi & Poskitt (1980) investigated the form of damping which should be used in the wave equation analysis. They measured the point and side damping constants for small piles driven at constant velocity into samples of clay soil. The test procedure consisted of pushing the conical tip and the pile into the sample at 0.3mm/s in order to obtain R_s (static pile resistance). Five speeds were then selected and the conical tip and the pile were pushed in at these in order to give R_d (dynamic pile resistance). This covered the range of speeds at which piles in the field are known to move following impact from a hammer (3×10^{-4} m/s to 1.6 m/s). The tested soils were remoulded samples of London (LL=70;PL=27), Forties (LL=38;PL=20) and Magnus (LL=31;PL=17) clay. Forties clay was a normally consolidated or lightly overconsolidated silty clay and Magnus clay was a very stiff silty clay with shell fragments and scattered gravels. From published data and the results of laboratory tests on small piles they concluded that:

- a. The viscous resistance of a clay is non-linear.
- b. A J_{LP} point law of the form

$$R_d = R_s(1 + J_{LP}V^{N_{LP}}) \quad \text{Equation 2.16}$$

fits many soil types over the range of velocities encountered during most pile-driving operations. A J'_{LP} side law can be formed similarly.

- c. N_{LP} for point and side resistances lies in the region of 0.2
- d. J_{LP} (0.08-0.27) point is less than J'_{LP} (0.08-0.99) side
- e. Measurements of J_{LP} and J'_{LP} for new soil types are necessary. Correlation of field data using conventional wave equation programmes should take account of the highly non-linear viscous resistance of the soil.

Similar influence of rate on static cone resistance values was observed during CPT (Cone Penetration Test) testing on clay by Bembem & Myers (1974) for rates from 0.01 cm/s to 20 cm/s, Powell & Quaterman (1988) covering a range of penetration from 1.2 m/min to 0.01m/min and Lune *et al* (1997) for rates between 1 to 20 mm/s. Powell & Quaterman (1988) noted that it was possible to fit the rate effects curves using equations of the type

$$\frac{Q_{c1}}{Q_{c2}} = \left(\frac{t_2}{t_1} \right)^{N_B} \quad \text{Briaud } et \text{ al (1984)} \quad \text{Equation 2.17}$$

where,

Q_{c1}, Q_{c2} = ultimate cone resistance in time to failure t_1, t_2 ,

N_B = viscous exponent.

or Equation 2.15 (Litkouhi & Poskitt,1980).

Horvath (1995) carried out loading tests on a model pile embedded in clay to examine the influence of rate of loading on the capacity of the pile. The pile was loaded to failure using constant rate of penetration (CRP), quick maintained loading (QML), an quick continuous loading (QCL) methods of loading. The CRP test is a strain controlled test (2mm/min) while QML and QCL are stress controlled tests. The QCL was used to model the Statnamic loading test method and its nominal test duration was 0.1s. The QML had a total test duration ranging from 10s to 17 min. Both the QML and the QCL were significant faster than the static loading rate represented by the CRP that was used as reference. The results of the tests showed that the pile capacity (ultimate or failure load) increased with increasing loading rate. The relationship could be approximated using a straight line on a semilog plot. The rate effects were considerable in the QCL. A

30% increase in the pile capacity (ultimate or failure load) was reported in QCL tests. The results of QCL were analysed using UPM method (Section 2.3) and that improved the correlation with QML tests although still over-predicted the CRP results.

Al-Mhaidib (2001) investigated the influence of rate of loading on uplift capacity of piles in clay using a model steel pile (30 mm diameter). The experimental work consisted of uplift capacity tests carried out for rates between 0.01 mm/min to 1 mm/min and consolidated undrained triaxial tests performed under the same loading rates. Increasing the loading rate resulted in an increase of the uplift model pile capacity. Undrained shear strength of the soil increased as the loading rate increased. The relationship between loading rate, and both the undrained shear strength and the uplift capacity could be represented by a straight line on a log-log plot. Comparison of the predicted capacity based on the undrained shear strength measured in the triaxial tests at different rates with the measured capacity under the same loading rate gave a good correlation.

2.6 Analysis of the axial response of piles incorporating rate effects

The original model for analysing dynamic loading events on piles was outlined by Smith (1960). The soil is assumed to behave in an elastic-perfectly-plastic manner under static loads. The model, represented by the line segments OABC in Figure 2.14 (Gibson & Coyle, 1968) considers an initial elastic compression zone to a certain pile displacement followed by a zone of plastic deformation that takes place at a constant resistance R_u . The limit between the elastic and the plastic soil-pile behavior, denoted by Q , is defined as the soil quake. Based on this hypothesis Smith developed a numerical model to simulate the dynamic behaviour of the hammer-pile-soil system during driving. The pile is represented by a series of discrete elements, each consisting of a mass and a spring, Figure 2.15 (Turner, 1995). The soil resistance associated with each pile element is modeled by means of a spring, slider and dashpot as represented in the rheological model shown in Figure 2.16 (Gibson & Coyle, 1968). The static component of the resistance is represented by the spring in series with a frictional slider, while the dynamic component of the resistance is represented by a dashpot in parallel with the

spring/slider combination. Equation 2.17 defines resisting force under dynamic loading in the elastic zone.

$$R_{Sd,e} = K_S X_p + C_S V_p \quad \text{Equation 2.18}$$

where:

$R_{Sd,e}$ = resisting force,

K_S = soil spring constant,

C_S = a viscous damping constant,

X_p = elastic deformation

V_p = the instantaneous velocity of the element of the pile.

The frictional slider of the rheological model accounts for the constant soil resistance in the plastic zone during static loading and thus does not appear in Equation 2.17. With the purpose of including effects of pile size and shape Smith (1960) defined the viscous damping J assuming:

$$C_S = K_S X_p J \quad \text{Equation 2.19}$$

The dynamic resistancing forces (Equation 2.17) approaches a static value when the velocity approaches zero and the static force resistance can be defined as

$$R_{static} = K_S X_p \quad \text{Equation 2.20}$$

Assuming dynamic capacity of the pile element ($R_{dynamic}$) equal to resisting force ($R_{Sd,e}$) and substituting Equations 2.18 and 2.19 into Equation 2.17, the dynamic capacity is :

$$R_{dynamic} = R_{static} (1 + J V_p) \quad \text{Equation 2.21}$$

Gibson & Coyle (1968) based on applying the experimental laboratory data previously summarized in Section 5.2.1 to Smith's equation showed that Smith's J value varied with velocity of deformation for the material tested and proposed that Smith's equation could be modified (Equation 2.11) to make J_{GC} a constant for all values of load and velocity raising the velocity of deformation to the power N_{GC} , where $N_{GC} < 1$. They suggested a value for N_{GC} equal to 0.2 for clean sand and 0.18 for a highly plastic clay while the value of J_{GC} depends of the specific properties of each soil. Litkouhi & Poskitt (1980) defined the relationship between dynamic and static pile resistance on clay (Equation 2.16), both for tip and skin as per Equation 2.11 and reported that the viscous damping constant for the skin was higher than for the tip while N_{LP} lies in the region of 0.2 for both tip and skin resistance.

Randolph & Deeks (1992) proposed a similar non linear model for shaft response shown in Figure 2.17. and Equations 2.22 and 2.23. This separates the damping into viscous damping at the pile / soil interface and internal damping of the soil mass. The shaft friction under dynamic conditions is shown in the upper part of the diagram while the lower part models the non-velocity related conditions. The viscous damping of the soil along the shaft is expressed in the relationship:

$$\tau_d = \tau_s \left\{ 1 + \alpha_{RD} \left(\frac{\Delta V}{V_0} \right)^{\beta_{RD}} \right\} \quad \text{Equation 2.22}$$

$$\frac{\tau_d}{\tau_s} - 1 = \alpha_{RD} \left(\frac{\Delta V}{V_0} \right)^{\beta_{RD}} \quad \text{Equation 2.23}$$

where,

τ_d is dynamic resistance

τ_s is static resistance, defined at a low velocity of 0.01- 1 mm/s

ΔV is relative velocity between soil and pile.

V_0 is a reference velocity taken as 1 m/s

α_{RD} and β_{RD} are viscous parameters

Randolph and Deeks model should be rewritten as:

$$\tau_d = \tau_s \left\{ k_{ah} + \alpha_{RD} \left(\frac{\Delta V}{V_0} \right)^{\beta_{RD}} \right\} \quad \text{Equation 2.24}$$

where the coefficient k_{ah} should be defined so that $\tau_d = \tau_s$ under low slip velocity conditions, such that the dynamic friction ideally reverts to the static value when the slip velocity ΔV reduces to that at which τ_s was defined.

Assuming that $\tau_d = \tau_s$ when $\Delta V = 10^{-6}$ m/s

$$\text{And } k_{ah} = 1 - \alpha_{RD} (10^{-6})^{\beta_{RD}} \quad \text{Equation 2.25}$$

$$\frac{\tau_d}{\tau_s} - 1 = \alpha_{RD} \left(\frac{\Delta V}{V_0} \right)^{\beta_{RD}} - (10^{-6})^{\beta_{RD}} \quad \text{Equation 2.26}$$

Analysing data from several different researchers who carried out various types of shearing tests over a range of testing rates on different clays has shown that although the assumption for the value of $\beta_{RD} = 0.2$ in the above power law is reasonable at higher velocities, there is insufficient research data available to verify the function with any certainty over the full range of velocities from almost static upwards. In addition the magnitude of the damping constant α_{RD} is dependent on soil type, in-situ effective stress, strength and stress history; has a much wider range of values than that suggested above for sands and clays; and can change the dynamic shear resistance by an order of magnitude (Hyde *et al*, 2000).

2.7 Concluding remarks.

The Statnamic test offers the advantages of being cheaper and quicker than static tests while overcoming some of the shortcomings of dynamic testing. The longer duration of the test allows stress wave phenomena to be neglected resulting in a simpler method of analysis.

The current method of analysis of Statnamic tests (UPM), which takes into account pile inertia and damping effects, assuming a linear damping function, tends to over-predict static capacity in fine grained soils. This over-prediction amongst other things is because in reality the damping function is non-linear with respect to velocity.

It is widely accepted that there is a non-linear relationship between the shear strength of clay and the rate at which it is loaded. This time-dependent relationship is known as a viscous law and damping has been the term used to describe the increase in strength that clay soils demonstrate under increased rates of loading. There have been many attempts to define the relationship and different authors have proposed different laws and define the coefficient of damping in different ways.

There is a need for an improved interpretation procedure for use with the Statnamic test in clays. An investigation is required to examine the effect of damping, pile inertia and soil quake. Further work is required to define the behaviour of a range of clay soils with their soil properties and stress history. Using this data, models of soil behaviour could be refined to allow the better prediction of static pile behaviour from the Statnamic test.



Figure 2.1 Loading system consisted of piston with combustion chamber place on the pile top.

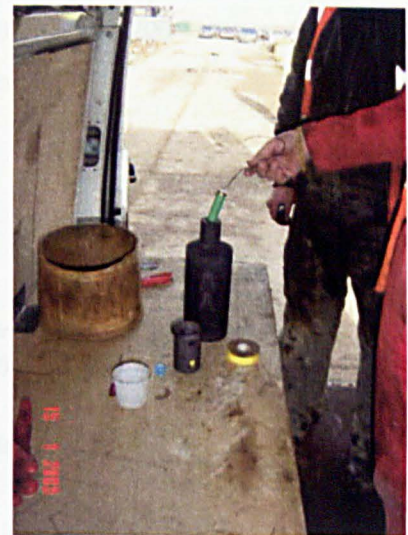


Figure 2.2 Solid fuel propellant

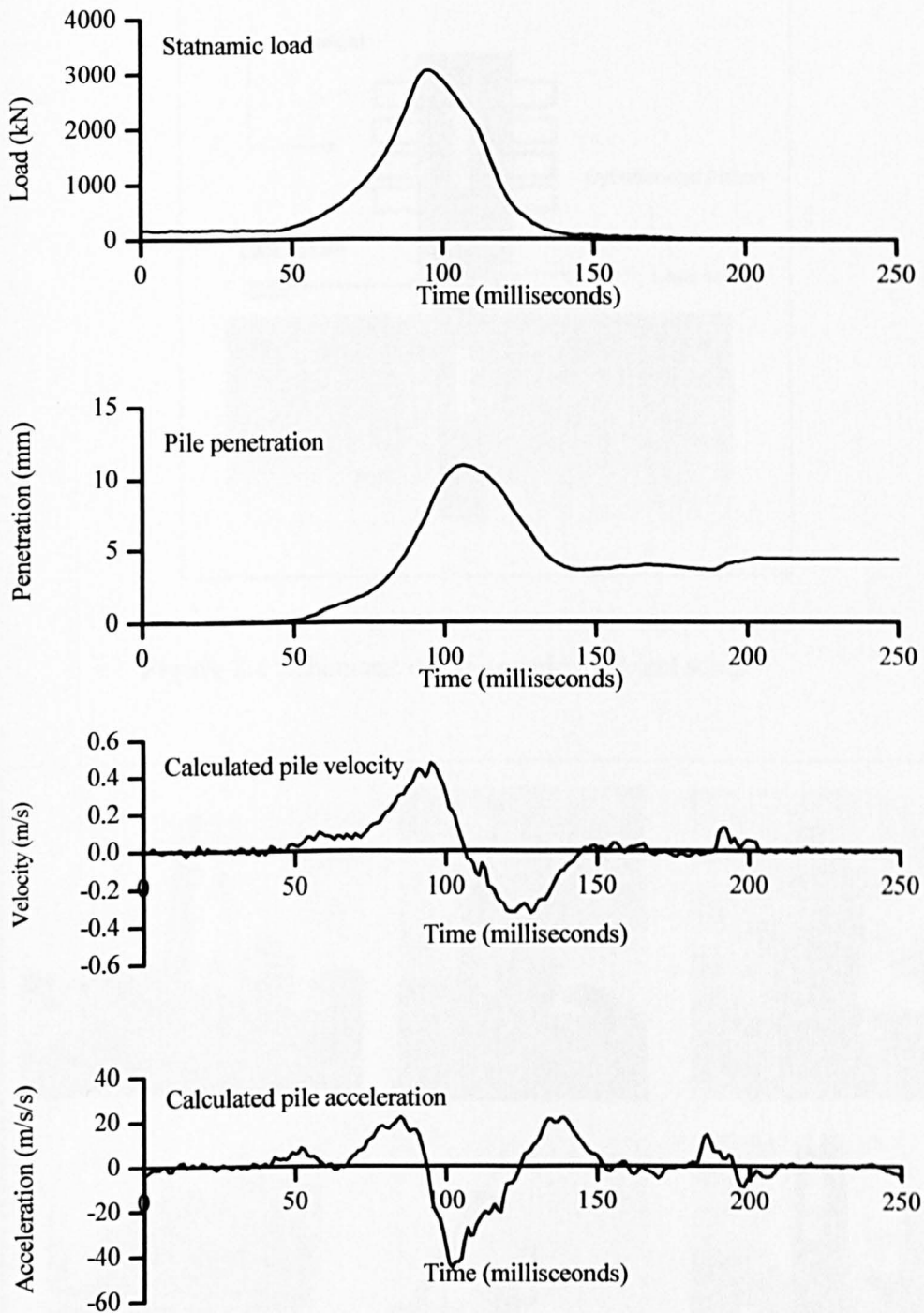


Figure 2.3 Measured and calculated results from full scale testing of an angled bored pile installed in Glacial Till (Grimsby clay) during a 30000kN Statnamic test. (After Brown, 2004)

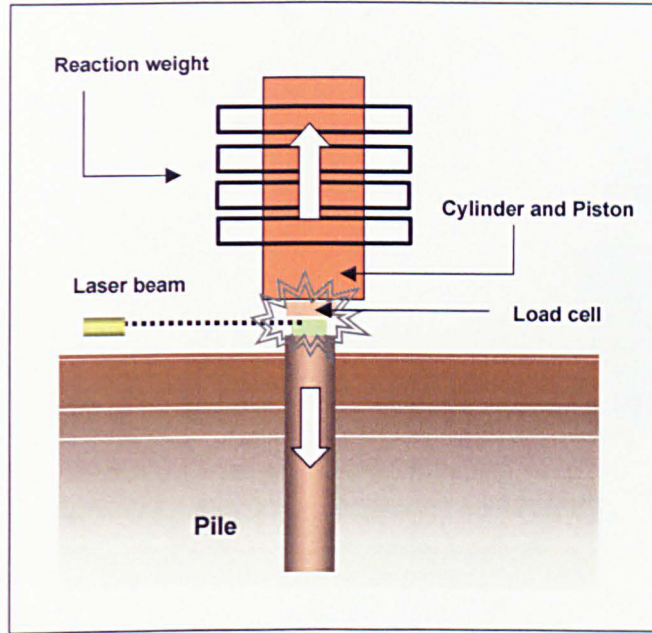


Figure 2.4 Schematic of Statnamic load test setup.



Figure 2.5 STN device with hydraulic chatch mechanism

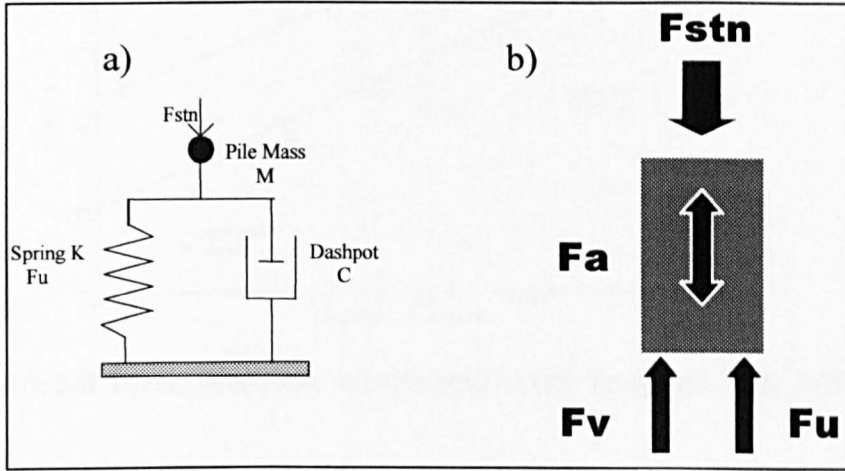


Figure 2.6 (a) UPM Rheological model, (b) UPM model of the pile as a rigid body (Middendorp, 1992)

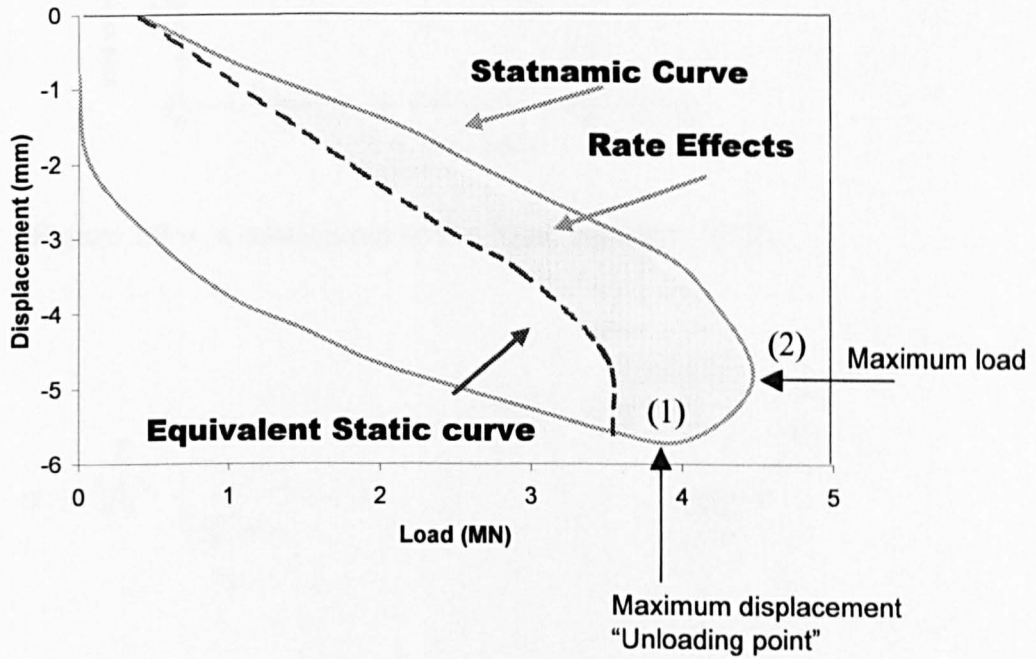


Figure 2.7 Statnamic load-displacement behaviour and equivalent static curve

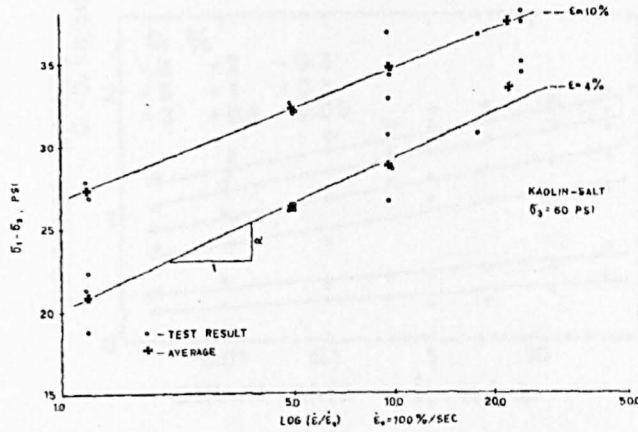


Figure 2.8 Stress, strain-rate relationship (After Yong and Japp, 1969)

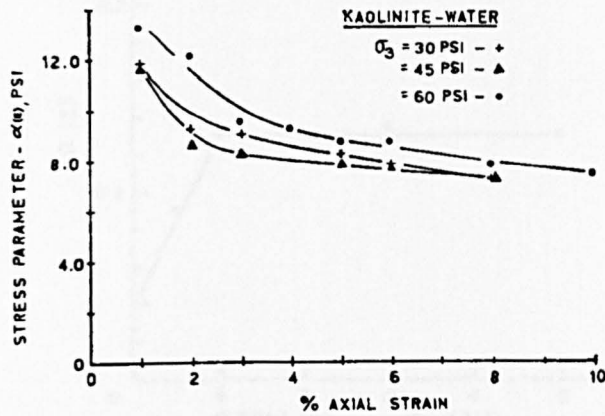


Figure 2.9 α - ϵ relationship (After Yong and Japp, 1969)

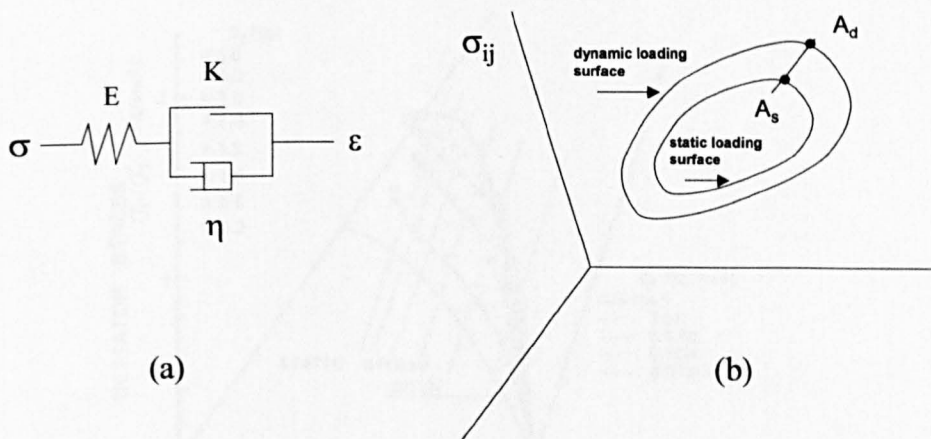


Figure 2.10 (a) Peryzna's theory rheological model. (b) Schematic diagram of static and dynamic surfaces (After Adachi and Okano, 1974)

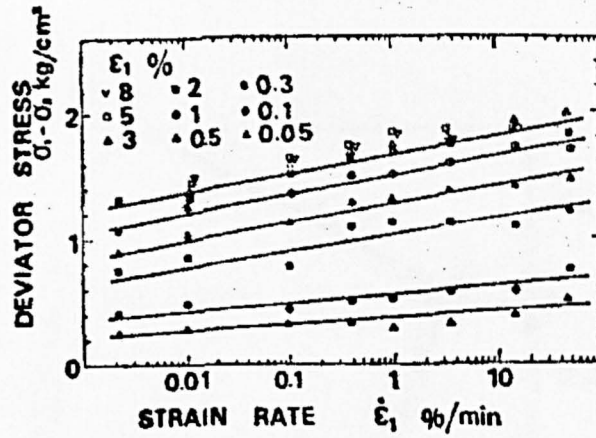


Figure 2.11 Deviator stress versus strain rate relation (After Akai *et al*, 1975)

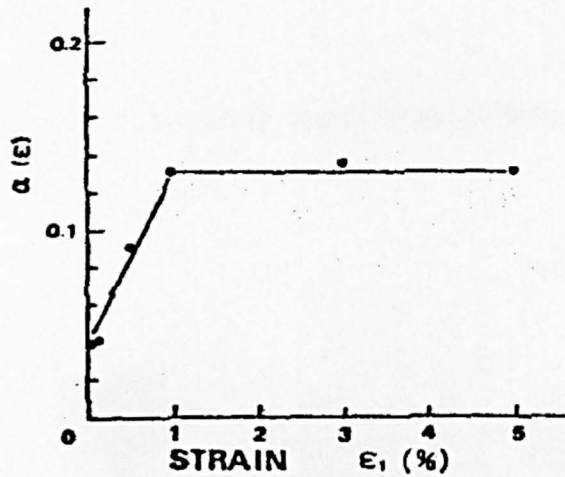


Figure 2.12 Strain dependent slope, $\alpha(\epsilon_1)$ versus strain relation (After Akai *et al*, 1975)

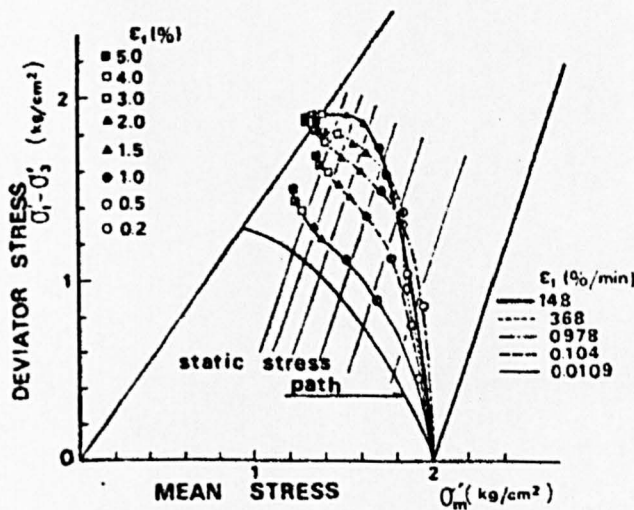


Figure 2.13 Effective stress paths and equi-strain lines for constant rate tests (After Akai *et al*, 1975)

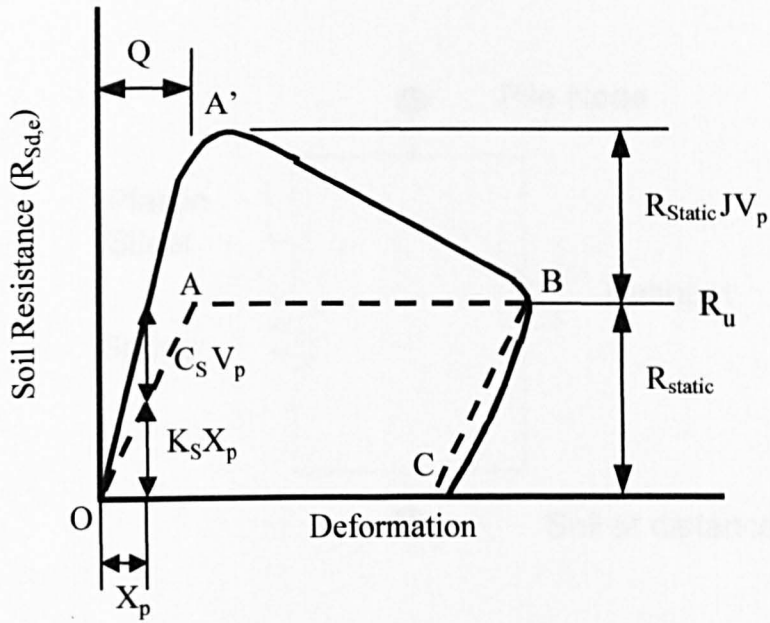


Figure 2.14 Smith's model of soil (After Gibson & Coyle, 1968)

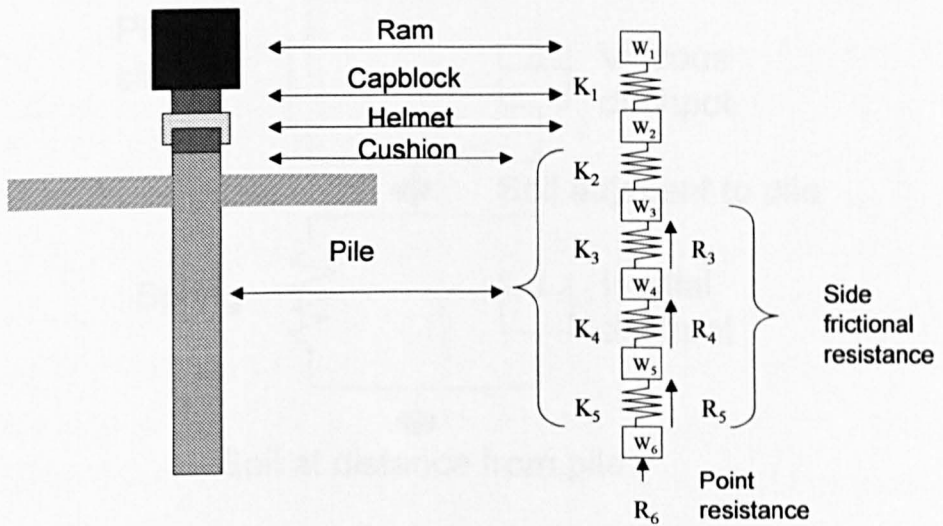


Figure 2.15 One dimensional idealisation of pile-soil interaction (After Turner, 1995)

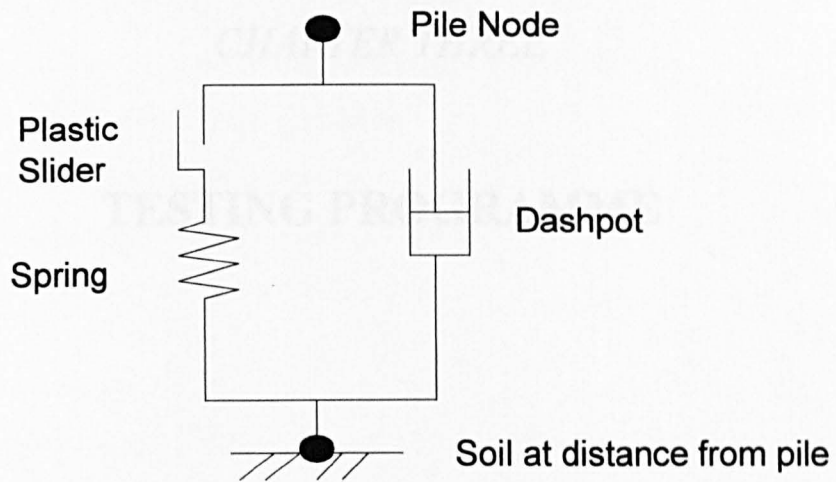


Figure 2.16 Smith's rheological model (After Gibson & Coyle, 1968)

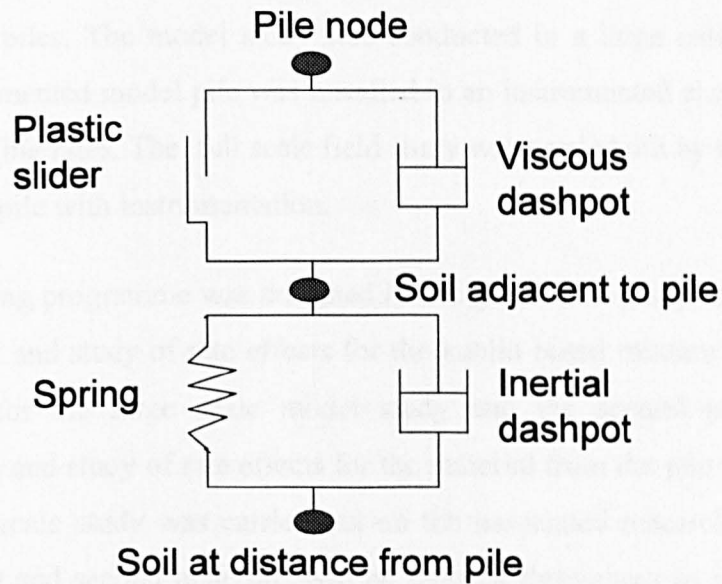


Figure 2.17 Rheological shaft model for pile driving analysis (Randolph & Deeks, 1992)

CHAPTER THREE

TESTING PROGRAMME

3.1 Introduction

The main object of the testing programme was to investigate the rate effects for two clay soils used in an associated research project (Brown, 2004) at the University of Sheffield. The associated research project consisted of a large scale model and a full scale field study aimed at getting a better understanding of soil behaviour during rapid load testing of piles. The model study was conducted in a large calibration chamber where an instrumented model pile was installed in an instrumented clay bed, and tested at different loading rates. The full scale field study was carried out by testing a 600 mm diameter bored pile with instrumentation.

The testing programme was designed in two parts. The first part consisted of the characterization and study of rate effects for the kaolin based mixture that was used in the clay bed for the large scale model study and the second part consisted of characterization and study of rate effects for the material from the pile site investigation where the full scale study was carried out on the associated research project (Brown 2004). The first and second materials will be referred throughout as reconstituted clay (KSS) and undisturbed clay (Grimsby) respectively.

For the main testing programme the KSS specimens were obtained from two different sources: 1D preconsolidated samples prepared as described in Section 5.3.1 from slurry at 80% moisture content and samples obtained by sampling the calibration chamber bed after the end of each test for different beds. The undisturbed clay samples were obtained from two boreholes at the Grimsby site.

3.2 Test Series

In the main testing programme, five test series were carried out as follows:

- (i) Preliminary tests. Soil classification and consolidation.
- (ii) Consolidated undrained triaxial tests.
- (iii) Triaxial permeability tests.
- (iv) Monotonic rapid loading triaxial tests.
- (v) Multistage rapid loading triaxial tests.

3.3 Preliminary tests. Soils classification and consolidation.

Preliminary standard tests to determine Atterberg limits, specific gravity and particle size distribution were carried out for both the reconstituted clay (KSS) and the undisturbed clay (Grimsby) to characterize the physical properties of the materials. For undisturbed clay (Grimsby) a series of three oedometer tests was performed on samples taken at different depths to determine the one dimensional consolidation and swelling lines. The results of these tests are presented in Sections 6.2 and 6.3.

3.4 Consolidated undrained triaxial tests.

Two series of consolidated undrained strain controlled triaxial tests with pore pressure measurements were conducted at 0.001mm/s on reconstituted clay (KSS) and undisturbed clay (Grimsby). The sample size was 100 mm in diameter and 200 mm in length. The tests were aimed at determining the critical state parameters for each material, and then use these parameters to establish a framework for the rate effect in the rapid loading testing programme. The test series are shown in Tables 3.1 and 3.2. The results of these tests are presented in Section 6.4.

3.5 Triaxial permeability tests.

Direct triaxial permeability tests were carried out for both reconstituted (KSS) and undisturbed clay (Grimsby). The test series are tabulated in Table 3.3 and 3.4. The

aim of the tests was to find out the vertical permeability value at the representative voids ratios for the effective consolidation stresses used on the rapid loading testing programme and check if any change in permeability gave a change in the rate effects. The results of the tests are presented in Section 6.5.

3.6 Monotonic rapid loading triaxial tests.

Consolidated undrained strain controlled triaxial tests were carried out on reconstituted clay (KSS) and undisturbed clay (Grimsby) using the pneumatic computer controlled rapid loading triaxial system, described in Section 4.3. The tests were carried out at rates from 0.001 mm/s up to 192.93 mm/s. The sample size was 100 mm in diameter and 200 mm in length and the pore water pressure was measured at mid height.

3.6.1 Reconstituted clay (KSS).

One series of seven tests was carried out to determine rate effects on reconstituted clay (KSS). The samples were prepared using the 1D pre-consolidation method, described in Section 5.3.1. They were initially one-dimensionally consolidated to an effective stress of 140 kPa, and then isotropically reconsolidated at an effective stress of 250 kPa before shearing. This was carried out in an attempt to recreate the stress conditions in the clay calibration chamber. The test series is shown in Table 3.5. The results and discussion of this series are presented on Section 7.2.1.

In order to study the influence of the stress history on the rate effects observed for normally consolidated reconstituted clay in the first series, a second series of seven tests was carried out to determine rate effects under a different stress history. The samples were obtained by sampling the clay bed in the calibration chamber. In the triaxial cell they were isotropically reconsolidated to an effective stress of 400 kPa first and then allowed to swell to an effective stress of 100 kPa before shearing. The over-consolidation ratio before test was equal to 4. The test series is tabulated in Table 3.6. The results and discussion of this series are presented on Section 7.2.2.

3.6.2 Undisturbed clay (Grimsby).

Two monotonic consolidated undrained triaxial tests were carried out at a high rate on undisturbed clay (Grimsby). The tests named GR2L and GR3L, are shown in Table 3.7. They aimed to check the validity of empirical model of soil proposed for the undisturbed clay (Grimsby) based on results from multistage tests. The results and discussion of these tests are presented in Section 7.3.2.

3.7 Multistage rapid loading triaxial tests.

The methodology used to study rate effects in series OC1 (for OCR=1) and OC4 (for OCR=4) was appropriate for reconstituted soil where an unlimited number of samples with the same controlled composition, particle soil distribution and stress conditions could be produced. However it was not suitable for the study of rate effects on undisturbed clay soil from a borehole in a site investigation where each sample might have a different composition, particle size distribution, and in situ effective stress conditions and the number of samples was limited.

To try to overcome this limitation a multistage test technique was developed to study the rate effects on a single sample. The sample in the triaxial cell was isotropically consolidated to the desired initial effective stress and then sheared at the static rate (0.001 or 0.01 mm/s) up to a certain axial strain then reconsolidated to the same initial effective stress and sheared again at higher rates to the same maximum axial strain. Four or five stages of shearing were applied to each sample starting with the static reference rate followed by the higher rates and a second static reference rate with a consolidation stage between each loading stage. Tests series are tabulated in Table 3.8 for reconstituted clay (KSS) and Table 3.9 for undisturbed clay (Grimsby). The tests were carried out using the pneumatic computer controlled rapid loading triaxial system, described in Section 4.3, on samples with 100 mm diameter and 200 mm height and pore water pressure measured at mid-height.

Using the multistage test technique it was possible to obtain rate effect parameters in a similar way as was done with the results from the calibration chamber Brown (2004), where each bed was a single sample that was tested in a multistage way. Once the model pile was installed and the soil consolidated the pile was then tested using constant rates of penetration (CRP) and Statnamic pulses, the CRP loading was undertaken at different rates from static (0.01 mm/s) up to those close to the maximum rate in a Statnamic pulse (500 mm/s) and the Statnamic loading was carried out at different stress levels, the sample being consolidated between each test allowing excess pore pressure to be dissipated.

3.7.1 Reconstituted clay (KSS).

The static rate for triaxial tests on reconstituted clay (KSS) for series OC1, OC4 and consolidated undrained triaxial was chosen as 0.001 mm/s based on the calculation made taking into account the consolidation time and calculated time of failure following the recommendations for minimum time of testing in BS1377-8:1990. The conventional static rate for testing a pile in clay is however 0.01 mm/s (BS8004:1986). It was decided to conduct a testing programme for reconstituted clay (KSS) including both rates as possible static reference rates and compare the results.

Two series of multistage tests were carried out for KSS. The test series are shown in Table 3.8. The first series with static rate equal to 0.001 mm/s consisted of a multistage test conducted at constant rate, test OC1-MR-001 (Table 3.10), and two multistage tests performed at different rates, tests OC1-M-001-1 (Table 3.11) and OC1-M-001-2 (Table 3.12). The second series with static rate equal to 0.01 mm/s consisted of two multistage tests conducted at a constant rate, tests OC1-MR-01-1 (Table 3.13) and OC1-MR-01-2 (Table 3.14), and three multistage tests performed at different rates with different initial stress conditions, tests OC1-M-01 (Table 3.15), OC4-M-01 (Table 3.16) and OC8-M-01 (Table 3.17).

In order to apply the multistage technique to study the rate effects in a single sample it was necessary to know the effects of testing in a multistage manner at a constant static reference rate to distinguish between the effects on measured deviator stress due rate of shearing and the effects on measured deviator stress due to the testing

method. The multistage tests at constant rate, both at 0.001 mm/s and 0.01 mm/s, were carried out to find out the effects of testing in a multistage manner in a single sample. Then the multistage tests at different rates were performed to study rate effects. The results and discussion of these tests are presented in Sections 7.2.3 to 7.2.6.

All the tests, apart from tests OC4-M-01 and OC8-M-01, were carried out on samples initially isotropically consolidated to an effective stress of 250 kPa, with overconsolidation ratio (OCR) equal to one and reconsolidated to the same effective stress pressure between each loading stage.

The test OC4-M-01 was conducted on a sample isotropically consolidated to an effective stress of 400 kPa and then reconsolidated to 100 kPa before shearing. The initial OCR was equal to four. During the multistage test, between each loading stage the excess pore water pressure was allowed to redistribute under undrained conditions. It was observed that after one hour the excess pore water pressure measured at mid-height of the sample disappeared and a new consolidation stage between each loading stage was unnecessary. Before test OC8-M-01 the sample was isotropically consolidated to an effective stress of 400 kPa and then reconsolidated to 50 kPa before shearing. The initial OCR was equal to eight and the sample was isotropically reconsolidated to the same initial effective stress between each loading stage. Tests OC4-M-01 and OC8-M-01 were performed to study the effect of initial stress conditions and overconsolidation ratio on the rate effects observed during a multistage rapid loading test.

3.7.2 Undisturbed Clay (Grimsby)

A series of multistage tests was carried out on undisturbed clay (Grimsby). The series is tabulated in Table 3.9. The series consisted of a multistage test at constant rate, GMR2L (Table 3.18) and three multistage rapid loading tests at different rates, GM1L (Table 3.19), GM2L (Table 3.20) and GM3L (Table 3.21). The multistage test at constant rate was undertaken to find out the effects of testing in a multistage manner on a single sample as was done for reconstituted clay (KSS). The multistage rapid loading tests at different rates were performed to study the rate effects on samples taken at different depths. The results and discussion of these tests are presented in Section 7.3.1

Test	Effective Confining Stress (kPa)	Voids ratio, e	Skempton's B	Maximum Axial Strain (%)	Sample	Triaxial System
CS-KSS-100	102	0.68	0.97	20.29	T4 2nd CC	Conventional
CS-KSS-280	281	0.65	0.99	24.33	T16 CC	
CS-KSS-375	375	0.61	0.97	11.11	T15 CC	
CS-KSS-250	247	0.650	0.99	11.33	1D Preconsolidated	Pneumatic Computer Controlled

Table 3.1. Consolidated undrained triaxial tests for reconstituted clay (KSS)

Test	Effective Confining Stress (kPa)	Voids ratio, e	Skempton's B	Maximum Axial Strain (%)	Sample	Triaxial System
CS-G1L-70	67	0.430	0.97	12.37	U3 BH2	Pneumatic Computer Controlled
CS-G1L-250	244	0.426	0.97	12.75	U5 BH2	
CS-G2L-75	76	0.463	0.96	17.10	U7 BH1	Conventional
CS-G2L-200	196	0.402	0.98	22.26	U7 BH1	
CS-G2L-300	303	0.372	0.98	24.28	U5 BH1	
CS-G3L-220	219	0.493	0.98	11.66	U12 BH2	Pneumatic Computer Controlled
CS-G3L-330	324	0.479	0.98	12.61	U13 BH2	

Table 3.2. Consolidated undrained triaxial tests for undisturbed clay (Grimsby)

Test	Consolidation	Effective Confining Stress (kPa)	OCR	Voids ratio, e
P-KSS-250	Virgin Compression	250	1	0.658
P-KSS-400		400	1	0.648
P-KSS-100	Swelling	100	4	0.662
P-KSS- 50		50	8	0.670

Table 3.3 Triaxial permeability tests for reconstituted clay (KSS)

Test	Effective Confining Stress (kPa)	Voids ratio, e
P-G-140	140	0.42
P-G-225	225	0.40

Table 3.4 Triaxial permeability tests for undisturbed clay (Grimsby)

Test	e	Skempton' B value	Rate (mm/s)	Maximum Axial strain %
OC1-1	0.65	0.99	1.00E-03	11.70
OC1-2	0.69	0.99	0.01	3.30
OC1-3	0.64	0.99	0.1	3.30
OC1-4	0.65	0.98	1.03	3.19
OC1-5	0.66	0.99	10.24	10.24
OC1-6	0.66	0.98	56.91	3.08
OC1-7	0.68	0.99	192.93	7.38

Table 3.5 Monotonic rapid loading triaxial tests for reconstituted clay (KSS).
Confining effective stress 250 kPa (OCR=1)

Test	e ₄₀₀	e ₁₀₀	Skempton' B value	Rate (mm/s)	Maximum Axial strain %
OC4-1	0.58	0.60	0.97	1.00E-03	11.71
OC4-2	0.58	0.60	0.99	0.01	10.99
OC4-3	0.58	0.60	0.98	1.01	9.92
OC4-4	0.58	0.59	0.97	8.28	8.01
OC4-5	0.58	0.59	0.99	51.76	9.56
OC4-6	0.59	0.61	0.97	157.60	6.89
OC4-7	0.55	0.58	0.99	172.35	8.17

Table 3.6 Monotonic rapid loading triaxial tests for reconstituted clay (KSS).
Confining effective stress 100 kPa (OCR=4)

Test	Effective Confining Stress	Void ratio, e	Skempton' B value	Rate (mm/s)	Maximum Axial strain (%)	Sample
GR2L	140	0.43	0.97	131.50	5.54	U6 BH1
GR3L	225	0.48	0.98	112.28	4.77	U9 BH2

Table 3.7 Monotonic rapid loading triaxial tests for undisturbed clay (Grimsby).

Test Series.	OCR	Static Reference Rate (mm/s)	Multistage loading rates	Sample Preparation
OC1-MR-001	1	0.001	Constant Rate	1D-Preconsolidation
OC1-M-001-1	1	0.001	Different Rates	1D-Preconsolidation
OC1-M-001-2	1	0.001	Different Rates	1D-Preconsolidation
OC1-MR-01-1	1	0.01	Constant Rate	1D-Preconsolidation
OC1-MR-01-2	1	0.01	Constant Rate	1D-Preconsolidation
OC1-M-01	1	0.01	Different Rates	Sampling Calibration Chamber
OC4-M-01	4	0.01	Different Rates	Sampling Calibration Chamber
OC8-M-01	8	0.01	Different Rates	Sampling Calibration Chamber

Table 3.8 Multistage rapid loading triaxial tests for reconstituted clay (KSS).

Test Series.	Static Reference Rate (mm/s)	Multistage loading rates	Sample
GMR2L	0.001	Constant Rate	U9 BH2
GM1L	0.001	Different Rates	U3 BH1
GM2L	0.001	Different Rates	U6 BH1
GM3L	0.001	Different Rates	U9 BH1

Table 3.9 Multistage rapid loading triaxial tests for undisturbed clay (Grimsby).

Test	Voids ratio, e	Consolidation time	Rate (mm/s)	Maximum Axial strain %
OC1-MR-001-A	0.684	24h 00m	0.001	2.67
OC1-MR-001-B	0.666	33h 40m	0.001	2.60
OC1-MR-001-C	0.652	12h 07m	0.001	2.85
OC1-MR-001-D	0.640	36h 42m	0.001	2.13
OC1-MR-001-E	0.633	6h 31m	0.001	2.29
OC1-MR-001-F	0.625	65h 00m	0.001	2.61

Table 3.10 Multistage triaxial test OC1-MR-001 at constant loading rate. Static reference rate 0.001 mm/s

Test	Voids ratio, e	Consolidation time	Rate (mm/s)	Maximum Axial strain %
OC1-M-001-1-A	0.657	24h 00m	0.001	3.12
OC1-M-001-1-B	0.630	24h 07m	126.50	4.64
OC1-M-001-1-C	0.613	20h 06m	116.35	4.80
OC1-M-001-1-D	0.602	21h 57m	0.001	3.14
OC1-M-001-1-E	0.592	24h 37m	59.60	3.85

Table 3.11 Multistage rapid loading triaxial test OC1-M-001-1 at different loading rates. Static reference rate 0.001 mm/s

Test	Voids ratio, e	Consolidation time	Rate (mm/s)	Maximum Axial strain %
OC1-M-001-2-A	0.651	24h 14m	0.001	3.06
OC1-M-001-2-B	0.638	5h 09m	1	3.03
OC1-M-001-2-C	0.624	16h 55m	64.62	2.73
OC1-M-001-2-D	0.615	6h 38m	80.28	3.08
OC1-M-001-2-E	0.604	17h 38m	0.001	2.73

Table 3.12 Multistage rapid loading triaxial test OC1-M-001-2 at different loading rates. Static reference rate 0.001 mm/s

Test	Voids ratio, e	Consolidation time	Rate (mm/s)	Maximum Axial strain %
OC1-MR-01-1-A	0.676	24h 31m	0.001	3.75
OC1-MR-01-1-B	0.653	22h 23m	0.001	3.60
OC1-MR-01-1-C	0.637	22h 57m	0.001	3.73
OC1-MR-01-1-D	0.622	23h 29m	0.001	3.81

Table 3.13 Multistage triaxial test OC1-MR-01-1 at constant loading rate. Static reference rate 0.01 mm/s

Test	Voids ratio, e	Consolidation time	Rate (mm/s)	Maximum Axial strain %
OC1-MR-01-2-A	0.667	23h 18m	0.001	3.21
OC1-MR-01-2-B	0.652	18h 25m	0.001	3.55
OC1-MR-01-2-C	0.636	22h 48m	0.001	3.85
OC1-MR-01-2-D	0.623	27h 34m	0.001	3.65

Table 3.14 Multistage triaxial test OC1-MR-01-2 at constant loading rate. Static reference rate 0.01 mm/s

Test	Voids ratio, e	Consolidation time	Rate (mm/s)	Maximum Axial strain %
OC1-M-01-A	0.694	24h 00m	0.01	3.32
OC1-M-01-B	0.670	24h 07m	1.02	3.14
OC1-M-01-C	0.654	20h 06m	47.62	3.65
OC1-M-01-D	0.642	21h 57m	32.53	1.79
OC1-M-01-E	0.627	24h 37m	0.01	1.31

Table 3.15 Multistage rapid loading triaxial test OC1-M-01 at different loading rates. Static reference rate 0.01 mm/s. Effective confining stress 250 kPa (OCR=1).

Test	Voids ratio, e	Consolidation time (100 kPa)	Rate (mm/s)	Maximum Axial strain (%)
OC4-M-01-A	0.599	4h 24m	0.01	3.26
OC4-M-01-B	0.599	-	10.31	3.06
OC4-M-01-C	0.599	-	54.23	2.97
OC4-M-01-D	0.599	-	154.86	4.06
OC4-M-01-E	0.596	18h 25m	0.01	4.33

Table 3.16 Multistage rapid loading triaxial test OC4-M-01 at different loading rates. Static reference rate 0.01 mm/s. Effective confining stress 100 kPa (OCR=4).

Test	Voids ratio, e	Consolidation time (50 kPa)	Rate (mm/s)	Maximum Axial strain %
OC8-M-01-A	0.625	24h 18m	0.01	3.12
OC8-M-01-B	0.622	24h 56m	1.04	3.22
OC8-M-01-C	0.62	45h 47m	55.91	2.99
OC8-M-01-D	0.619	24h 04m	171.46	6.47
OC8-M-01-E	0.618	1h 10 m	0.01	4.45

Table 3.17 Multistage rapid loading triaxial test OC8-M-01 at different loading rates. Static reference rate 0.01 mm/s. Effective confining stress 50 kPa (OCR=8).

Test	Voids ratio, e	Consolidation time	Rate (mm/s)	Maximum Axial strain (%)
GMR2L-A	0.441	73h 00m	0.001	3.00
GMR2L-B	0.434	25h 05m	0.001	3.65
GMR2L-C	0.430	24h 07m	0.001	3.19
GMR2L-D	0.427	24h 00m	0.001	2.99
GMR2L-E	0.426	24h 01m	0.001	3.01
GMR2L-F	0.424	20h 30m	0.001	4.83

Table 3.18 Multistage triaxial test GMR2L at constant loading rate. Static reference rate 0.01 mm/s. Effective confining stress 145 kPa

Test	Voids ratio, e	Consolidation time	Rate (mm/s)	Maximum Axial strain (%)
GM1L-A	0.48	48h 00m	0.001	2.54
GM1L-B	0.476	23h 32m	1.03	2.27
GM1L-C	0.475	24h 07m	54.01	2.98
GM1L-D	0.474	24h 00m	113.03	2.31
GM1L-E	0.471	25h 41m	0.001	5.23

Table 3.19 Multistage rapid loading triaxial test GM1L at different loading rates. Static reference rate 0.01 mm/s. Effective confining stress 70 kPa

Test	Voids ratio, e	Consolidation time	Rate (mm/s)	Maximum Axial strain %
GM2L-A	0.432	52h 46m	0.001	2.50
GM2L-B	0.426	24h 19m	1	2.47
GM2L-C	0.423	24h 01m	60.94	2.36
GM2L-D	0.419	23h 55m	0.001	3.30
GM2L-E	0.418	20h 51m	0.05	4.70

Table 3.20 Multistage rapid loading triaxial test GM2L at different loading rates. Static reference rate 0.01 mm/s. Effective confining stress 135 kPa

Test	Voids ratio, e	Consolidation time	Rate (mm/s)	Maximum Axial strain %
GM3L-A	0.467	73h 00m	0.001	2.57
GM3L-B	0.462	26h 46m	1.05	2.27
GM3L-C	0.458	23h 04m	49.4	1.86
GM3L-D	0.455	24h 17m	49.11	2.27
GM3L-E	0.453	20h 49m	0.001	2.97
GM3L-F	0.451	24h 00m	0.1	4.78

Table 3.21 Multistage rapid loading triaxial test GM3L at different loading rates. Static reference rate 0.01 mm/s. Effective confining stress 220 kPa

CHAPTER FOUR

TESTING EQUIPMENT

4.1 Introduction

The main object of the testing programme carried out for this research was to investigate the rate effects of rapid loading in clay soils and to apply the results to refine and develop models of soil in order to improve the current method (UPM) of analysis for Statnamic pile tests. Therefore the testing rates aimed to reflect those encountered in both “static” (Constant rate of penetration tests) and Statnamic tests.

A computer servo controlled pneumatic cyclic triaxial system and a conventional triaxial system were used to conduct rapid loading triaxial tests and complementary elemental tests respectively. Pre-consolidated reconstituted clay (KSS) samples were prepared from a slurry using a one-dimensional consolidation system.

The computer servo controlled cyclic system, with a 100 mm diameter sample cell, was used to carry out consolidated undrained triaxial tests for a full range of rates from 0.001mm/s up to 200 mm/s. This system was originally designed for cyclic triaxial tests and allowed the carrying out of monotonic tests under higher rates than in the conventional triaxial systems.

The conventional triaxial system, with a 100 mm diameter sample cell, was used to carry out isotropic consolidation, permeability and consolidated undrained triaxial tests. The consolidated undrained triaxial tests were carried out at low rate (0.001 mm/s) up to 20 % axial strain with the purpose of defining the critical state parameters of the soil.

Preliminary standard tests, such as particle size distribution analysis, specific gravity, Atterberg limit and oedometer consolidation tests were carried out using standard equipment specified in British Standard 1377 (1990).

This chapter describes the details of the equipment used for this research.

4.2 One-Dimensional Consolidation.

One-dimensionally consolidated samples for the triaxial tests were reconstituted from a homogeneous slurry at a moisture content of 80% (approximately twice the Liquid Limit), mixed in a Hobart mixer and using one-dimensional consolidation moulds (Figure 4.1). The consolidation moulds (U100 tubes 460 mm high and 105 mm internal diameter) were fitted with a porous stone and drainage line both on the top and on the base plate. Filter papers were used on the surface of the porous stones to prevent clogging of the drainage paths. A cross-section of a consolidation mould can be seen in Figure 4.2. The consolidation pressure (140 kPa) was applied by means of an actuator connected to a compressed air supply. The consolidation pressure was measured by means of a pressure transducer attached to the top drainage line. The pore pressure transducer was manufactured by Bell and Howell Limited, model type 4-366-0001-02 MO. It had a range of 0 to 700 kPa and a resolution of ± 0.5 kPa and was calibrated using a Budenberg dead weight tester oil interface. The transducer was connected to a transducer indicator manufactured by RDP Electronic Ltd, model type E307. After consolidation 100 mm diameter samples were extruded from U100 tubes.

4.3 Pneumatic Computer Controlled Rapid Loading Triaxial System

A computer controlled closed-loop cyclic triaxial system manufactured by ELE International Ltd. was used to run strain controlled undrained compression tests at different rates. The system consisted of a triaxial cell, a loading frame fitted with a double acting actuator connected to a pneumatic servo-valve and a Control and Data Acquisition System (CDAS) linked to a computer (Figures 4.3 and 4.4). The triaxial cell was equipped with a miniature pore pressure transducer, immersible load cell,

deformation transducer and two pneumatic servo-valves for control of cell and back pressure fitted with pressure transducers for each valve. The three pneumatic servo-valves had clean air pressure supplied by a steady pressure reservoir. Computer software processed the data, as well as monitoring, logging and sending control commands.

The specimen was loaded using a double acting actuator controlled by an electro-pneumatic valve and a displacement transducer mechanically coupled to the actuator piston, enabling displacement control in addition to force control. The details of this system will be described in the following sections.

4.3.1 The Triaxial Cell

A triaxial cell for 100 mm samples manufactured by Wykeham Farrance Ltd. was used and was fitted with a miniature pore pressure transducer, immersible load cell and axial deformation transducer. These transducers were connected to the CDAS for data logging.

4.3.2 Pressure Reservoir

To preserve a steady air pressure supply to the high precision servo-valves a pressure reservoir was used. This was kept at a pressure of 700 kPa. The reservoir had two water/oil traps at both inlet and outlet ports to make sure the air was clean.

4.3.3 Cell Pressure System

The system consisted of an electro-pneumatic servo valve, pressure transducer, bladder type air/water pressure interface tank and pressure gauge. The air pressure regulated by a servo valve was supplied to the air/water interface tank, which in turn pressurised the water in the tank.

The servo valve was manufactured by Festo Co. and gives a pressure output range of 0 – 1000 kPa for an input range of 0 – 10 V. The mechanism of the servo valve is described in Section 4.3.11.a. The pressure was manually regulated using the CDAS in “manual control” mode, and was controlled by software when the system was

running in “closed-loop” mode. In both control modes cell pressure was controlled via the servo valve.

A pressure transducer, manufactured by ELE International Ltd., was located next to the output port of the servo valve and had a range of 0 – 1000 kPa and a resolution of ± 0.5 kPa. It was calibrated by using a Budenberg dead weight tester with 100 kPa increments.

4.3.4 Back Pressure System and Volume Change Apparatus

The same type of system as that used for the cell pressure, was used to control and monitor back pressure. However the water outlet of the air/water interface tank was connected to a volume change measurement apparatus, and then to the cell base to apply back pressure to the sample.

The volume change measuring apparatus used was manufactured by ELE International Ltd (Figure 4.5) and had a capacity of 80 cm³ in volume and a resolution of ± 4 mm³. The apparatus consisted of a cylinder, piston fitted with a bellofram and a linear variable differential transformer (LVDT). The lower chamber of the cylinder was connected to the air/water pressure assembly while the upper chamber was attached to the cell base. The LVDT was attached to the piston and the movement of the piston was monitored to calculate the volume change in association with the area of piston.

The volume change unit was calibrated under 220 kPa back pressure to avoid errors caused by expansion of the system. For calibration, a 10ml graduated glass burette, readable to 0.02 ml, mounted in an acrylic outer tube was used. The outer acrylic tube was filled with de-aired and de-ionised water. By alternately filling and then bleeding the burette, the full range of the transducer was calibrated in about 10 ml increments (Figure 4.6). Two drainage lines were used, one was fitted on the base pedestal and another one on the top platen loading cap.

4.3.5 Pore Pressure Transducer

The pore water pressure was measured at mid-height of the specimen following Hight (1982) and Pierpoint (1996), using a Druck, type PCDR81, miniature transducer

(Figure 4.7). It had a range of 0-1000 kPa and a resolution of ± 0.5 kPa. The same type of transducer were used by Bond *et al* (1991) and Brown *et al* (2002) . They were found to respond to step load of 100kPa within 10-24 ms. It was essential that the porous element at the tip of the miniature pressure transducer was initially de-aired to ensure a suitably linear calibration. This was carried out by placing the transducer in de-aired water, under a vacuum, for several hours. The miniature pore pressure transducer was calibrated with a Budenberg air dead weight tester with air-water interface.

4.3.6 Immersible Load Cell

The axial load was monitored using an immersible load cell manufactured by Wykeham Farrance. This had a load range of ± 5 kN, with a final resolution of ± 2.5 N. The load cell was calibrated by using a Budenberg oil dead weight tester with load cell calibration frame.

4.3.7 Deformation Transducer

Vertical deformation was measured using an LVDT manufactured by ELE which had a linear range of 50 mm and an resolution of ± 0.01 mm. The body of the LVDT was clamped to the loading ram, and a post and bracket for the LVDT was clamped to the top of the triaxial cell. The measured displacement was displayed on the monitor and recorded by the software. The calibration was determined using a 0.001 mm resolution Mitutoya digital micrometer.

4.3.8 Top Platen Loading Cap and Connecting Device

The top platen loading cap and connection method was specially designed following Higuchi (2001) to minimise disturbance during sample preparation and when connecting the top cap to a threaded stub on the base of the load cell. The connection between the top cap and the screw was made using resin. The top cap had a hollow for the resin to be poured into. The resin used was mixed with hardener. The proportions of the mix was determined from a series of trials such that it hardened after 20 minutes. After testing the connection was easily broken by unscrewing and a new hollow for the next test was made by drilling out the hardened resin.

The connection between the top end of the loading piston and the bottom of the actuator rod (Figure 4.8) was redesigned in order to minimise the friction effects during loading. The new device consisted of a universal joint (Figure 4.9) attached to a tension coupling (Figure 4.10).

4.3.9 Control and Data Acquisition System (CDAS)

The Control and Data Acquisition System (CDAS) was manufactured by IPC Ltd. and provided all critical control, timing and data acquisition functions for the triaxial testing system. The CDAS was linked to a PC through a standard serial communication link. All control, communication and transducer cables terminated in connectors located on the front panel of the CDAS.

The CDAS automatically controlled the operation of the loading for each type of test. The CDAS directly controlled the actuator's servo valve to apply the requested loading rate, magnitude and waveform. It also controls the other two servo valves for cell and back pressures to adjust the air pressure to the required level for tests. While the sample was being subjected to loading forces, the CDAS captured data from the transducers and transferred these to the PC for processing for feedback, display and storage.

4.3.10 Loading Frame

The loading frame was manufactured by ELE International Ltd. and consisted of flat base plate, supported on four levelling screws, and two threaded columns supporting a crosshead beam. Loading forces were applied through a pneumatic actuator mounted in the centre of the crosshead.

4.3.11 Electro-Pneumatic Cyclic Loading system.

The electro-pneumatic cyclic loading system consisted of an electro-pneumatic servo valve and double acting actuator both linked to a PC via the CDAS. The equipment was controlled by the software provided (Universal Testing Machine).

Figure 4.11 shows a schematic diagram of the principal elements of the electro-pneumatic closed-loop system as described by Higuchi (2001). The double acting actuator was coupled to the sample via the load cell and the electro-pneumatic servo valve controlled the actuator. Transducer feedback of load and displacement was compared with a command signal including the amplitude and frequency within the CDAS. The error signal between the command signal and the feedback was amplified to drive the servo valve towards reducing the error to zero, thus closing the loop.

(a) Electro-Pneumatic Servo Valve

The electro-pneumatic servo valve was manufactured by Festo Co. and gave a pressure output range of 0 – 1000 kPa. A conditioned electric signal was continuously applied to the valve by the CDAS to drive in closed-loop mode. The controlled pressure was then applied to the actuator. The flow of air pressure was controlled by the servo valve in which a small electric current was used to open and close the control spool of the valve.

(b) Double Acting Actuator

A 100 mm diameter double acting actuator with 30 mm stroke manufactured by SMC Pneumatics Ltd. was used and was mounted in the centre of the crosshead. Both pressures for upper chamber and lower chamber of the actuator were controlled by the electro-pneumatic servo valve. Energy generated by the pressure difference was transmitted to the sample via the piston, loading rod and load cell. The actuator had a ± 25 mm LVDT, manufactured by Solartron Ltd., mechanically coupled to the actuator piston. This enabled displacement control in addition to force control.

4.4 The Conventional Triaxial System.

Isotropic consolidation, permeability and consolidated undrained triaxial tests were performed using a conventional triaxial system (Figure 4.12) with a 50 kN standard loading frame capable of strain controlled testing. Besides the loading frame it consisted of a triaxial cell, two microprocessor-controlled hydraulic actuators for back pressure, a differential pressure transducer, a cell pressure system, a pressure transducer

for pore pressure, a deformation transducer, and data monitoring equipment linked to a computer.

4.4.1 The Triaxial Cell

A triaxial cell for 100 mm samples manufactured by Wykeham Farrance Ltd. was used for sample testing fitted with a cell pressure transducer, pore water pressure transducer, immersible load cell and axial deformation transducer. These transducers were connected to an analogue/digital conditioning unit for data logging.

4.4.2 Microprocessor Controlled Hydraulic Actuators (GDS Controller)

The microprocessor controlled hydraulic actuators were manufactured by GDS Instruments Ltd. They were used for precise regulation and measurement of liquid pressure and liquid volume change. Control algorithms were built into the programmable memory to cause the controller to seek a target pressure or step to a target volume change as can be seen in Figure 4.13. The controllers were used in stand-alone mode operation for the purpose of applying cell pressure, back pressure and measuring pore pressure and volume change. These controllers have a range of 0 - 2000 kPa, an accuracy of ± 0.1 kPa and a capacity of 200 cm³ in volume.

4.4.3 Back Pressure Supply and Volume Change Apparatus

The samples were isotropically consolidated in the triaxial cell under a known cell pressure and against a 220 kPa back pressure. The back pressure was supplied by a GDS controller, and the amount of moisture entering or leaving the sample during saturation and isotropic consolidation were measured by the GDS controller.

During permeability tests the back pressure was supplied independently to the top and the base of the sample by two different GDS controllers and the difference of pore pressure between both extremes of the sample was measured by a differential pressure transducer connected to both drainage lines.

4.4.4 Differential pressure transducer

A 20kPa differential pressure transducer, manufactured by Huba Control (Model No. 692.905011041) was used to measure the applied pressure difference across the soil sample during permeability tests.

Figure 4.14 shows a schematic diagram of the arrangement used for calibrating the differential pressure transducer. The calibration was performed according to the procedure described by Srisaktihivel (2003). The differential pressure source consisted of two 10 ml graduated glass burettes, mounted in acrylic outer tubes. They were fixed to a vertical frame side by side, one above the other with a small overlap. The outer acrylic tubes were filled with deaired water and connected with plastic tubing to the air pressure supplier system. Each burette was connected with plastic tubing at the upper end to the air pressure line and at the lower end to an air-water interface tank, which was filled with deaired water. The higher burette was connected to the high pressure end of the differential pressure transducer and the other burette was connected to the low pressure end. The whole system was kept under a 220 kPa back pressure by applying this pressure to both the air-water interface tank and to the air pressure line connected to the burettes. This back pressure was applied to eliminate any effects caused by residual air bubbles and to simulate the actual testing conditions.

The differential pressure was applied to the transducer varying the water levels in the burettes individually by raising and/or lowing the air-water interface tank. The applied head difference was recorded using a vertical scale, readable to 1mm, mounted between the outer acrylic tubes of the burettes. As a result, the accuracy of the calibration was limited to 0.02kPa. The transducer was calibrated from 0 to 10 kPa.

4.4.5 Cell Pressure System

The system consisted of an air/water cylinder, air regulator and pressure gauge. The air regulator was connected to the main air supply to control the required cell pressure. The pressure range was 0 to 700 kPa. The regulated air was supplied to the top of the cylinder, which in turn pressurised the water at the bottom. The required pressure was monitored by a pressure gauge accurate to ± 0.5 kPa. The pressure gauge was calibrated by using a Budenberg dead weight tester with 100 kPa increments. The

air/water cylinder was filled with deionized water which was changed regularly. Connections for cell pressure were made using push fit connectors and 4 mm and 8 mm diameter nylon tubing.

4.4.6 Pore Pressure Transducer

The purpose of the transducer was to measure the generation and dissipation of pore pressure inside the sample. The pore pressure transducer used was a PDCR 810 manufactured by Druck Ltd. It had a range of 0 to 1000 kPa and a combined non-linearity and hysteresis of $\pm 0.1\%$. The transducer were mounted on a close-coupled transducer mounting block outside the triaxial cell and calibrated by using a Budenberg dead weight tester with an oil interface.

4.4.7 Immersible Load Cell

The axial load was monitored using an immersible precision Imperial College load cell. It has a maximum load rating of 4.5 kN and a non-linearity of $\pm 0.5\%$ of full range output. The load cell was specifically designed for the measurement of axial loads inside triaxial cells, in order to eliminate the frictional load loss incurred by external load. The load cell was calibrated by using a Budenberg oil dead weight tested with a load cell calibration frame.

4.4.8 Deformation Transducer

Vertical deformation was measured using a linear variable differential transformer (LVDT) manufactured by MPE Transducers Ltd. It had a linear range of 50 mm and linearity of $\pm 0.1\%$ of full scale output. The body of the transducer was clamped to the column of the loading frame, and the post and the bracket for the transducer was clamped to the top of the triaxial cell. The measured displacement corresponds to a shortening or lengthening of the sample. The linear calibration was derived using a 0.001 mm resolution Mitutoya digital micrometer.

4.4.9 Top Platen Loading Cap and Connecting Device

The top platen loading cap was fitted with an integral hemispherical dome and a drainage line.

4.4.10 Data Monitoring Equipment

The data monitoring equipment consisted of a computer with a data logger card and an analogue to digital (A/D) conditioning unit. In operation, the transducers were connected to an A/D conditioning unit and interfaced to the data acquisition card installed in the computer. This unit manufactured by RDP Electronics had 8 separate channels but only 4 channels were used. Each transducer was connected to one channel. The computer was installed with the MetraByte Das-8 A/D card and the Strawberry Tree "Workbench" software for readings to be taken automatically. The output data was stored to the hard disc of the computer.

4.4.11 Strain Controlled Loading Frame

The tests were performed with the triaxial cell set up in the strain controlled loading frame. The loading frame used was manufactured by Soiltech Co. and had the facility to carry out strain controlled monotonic compression tests with a speed range of 0.01 – 1.52 mm/min and a maximum load capacity of 9.8 kN.



Figure 4.1 One-dimensional consolidation system.

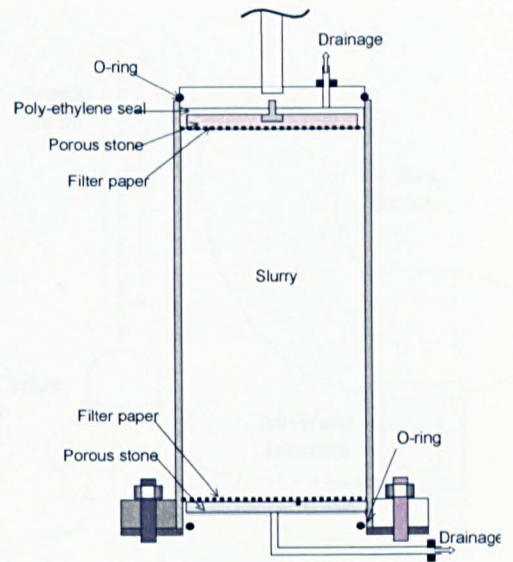


Figure 4.2 Cross-sectional area of a consolidation mould

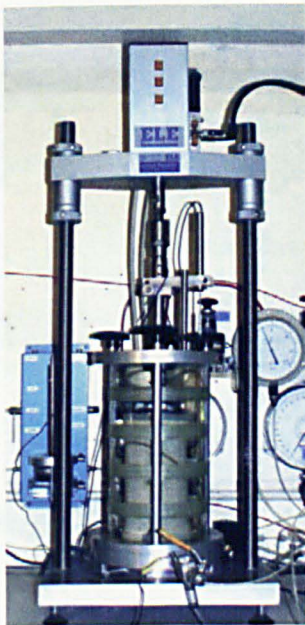


Figure 4.3 Triaxial Cell

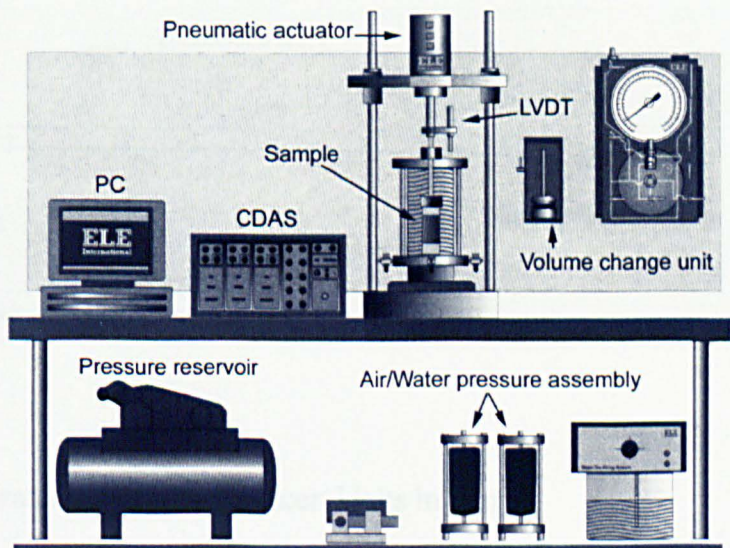


Figure 4.4 Schematic diagram of computer controlled closed-loop cyclic triaxial system. After Higuchi (2001).

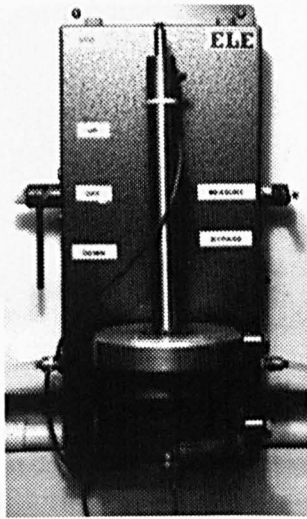


Figure 4.5 Volume change apparatus

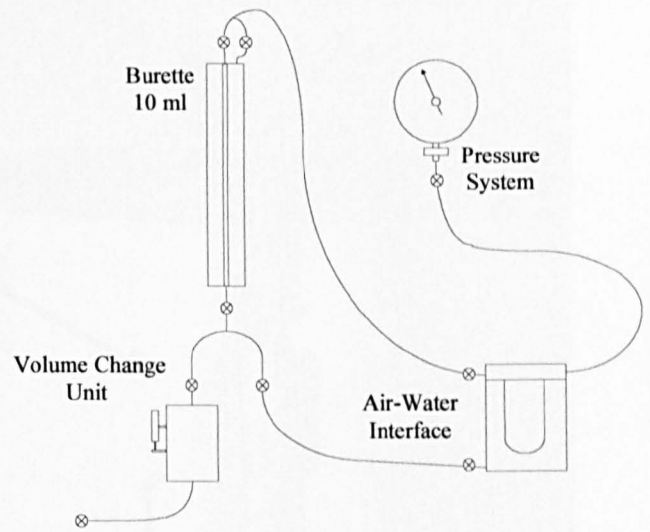


Figure 4.6 Volume change unit calibration

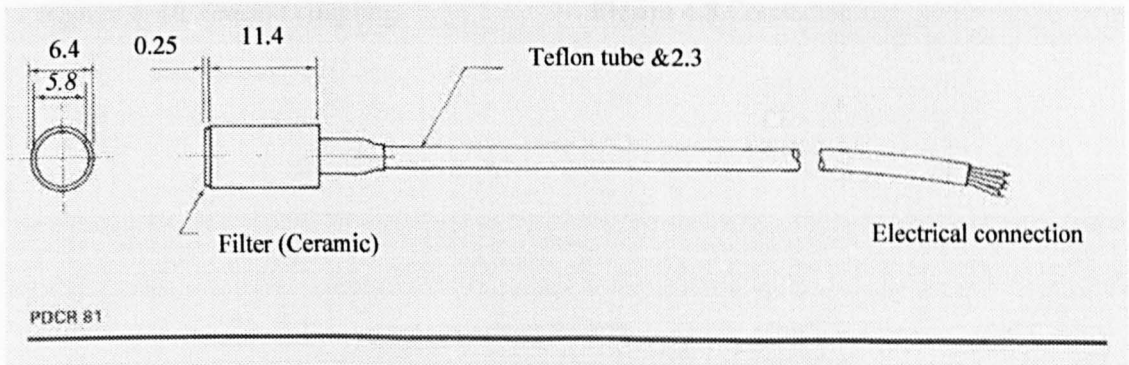


Figure 4.7 Miniature pore water pressure transducer. Units in mm



Figure 4.9. Universal joint.

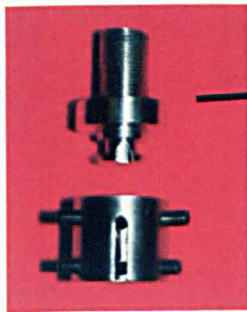


Figure 4. 10 Tension coupling.

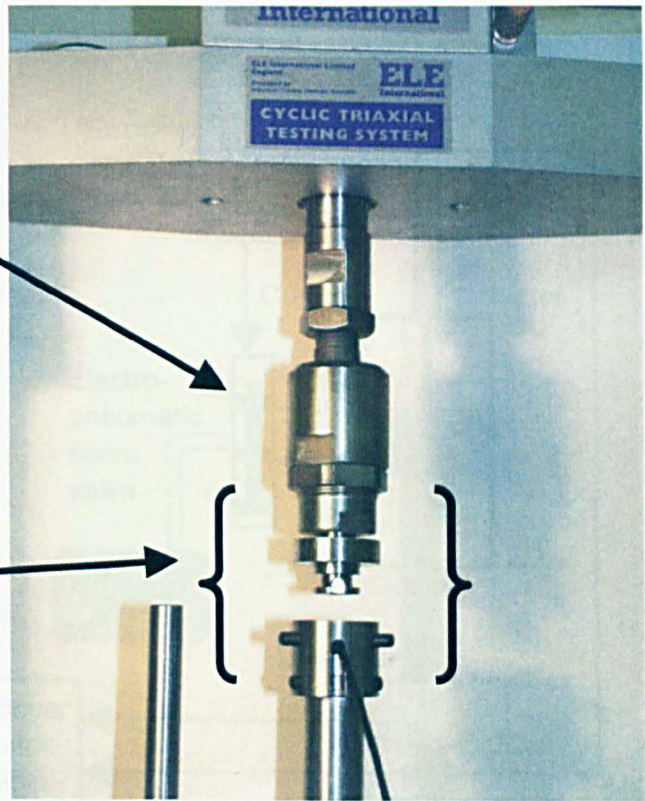


Figure 4.8.Connector

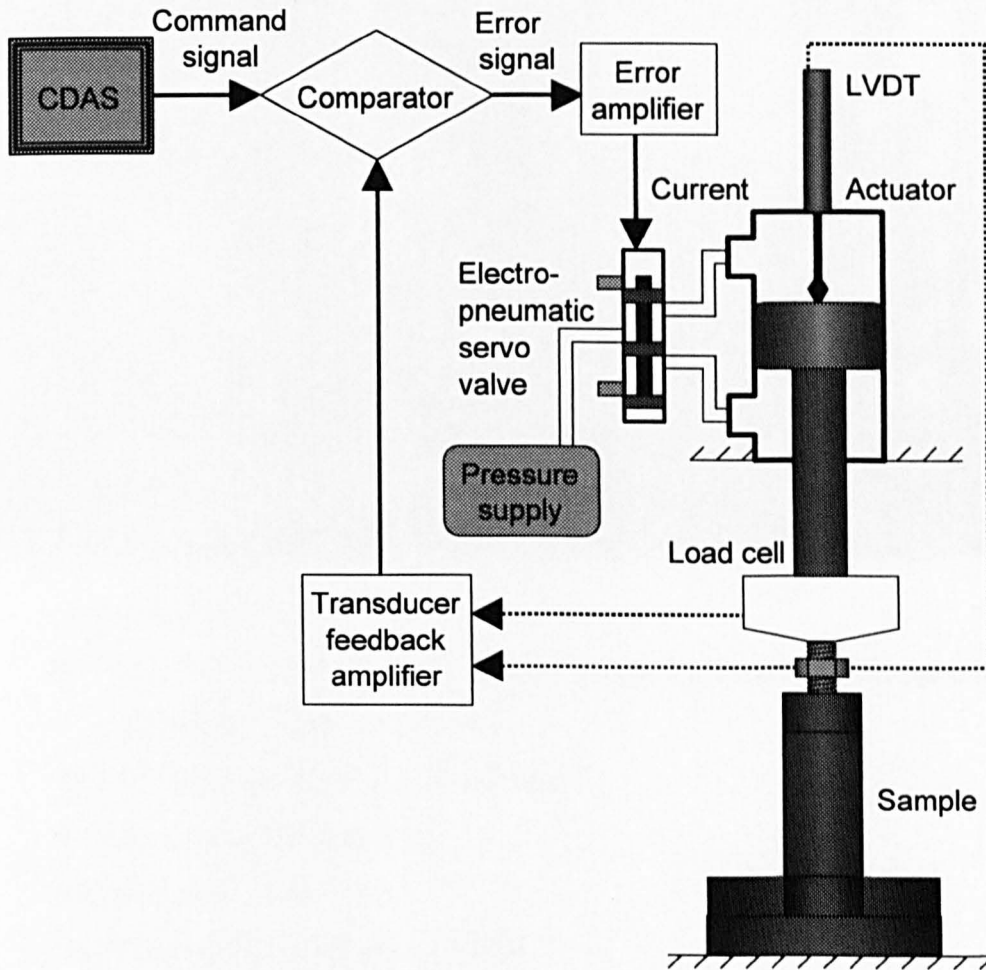
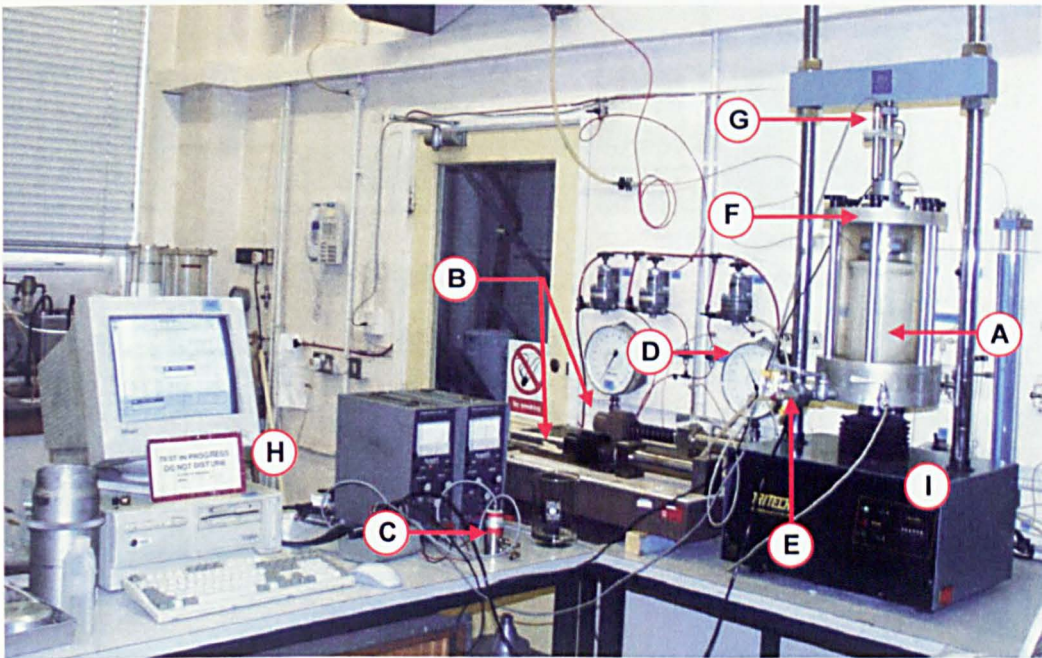


Figure 4.11 Schematic diagram of electro-pneumatic closed-loop system.
After Higuchi (2001)



- A. Triaxial Cell
- B. Back Pressure Supply and Volume Change Apparatus (GDS controller)
- C. Differential Pressure Transducer
- D. Pressure gauge (Cell pressure system)
- E. Pore Pressure Transducer
- F. Immersible Load Cell
- G. Deformation Transducer (LVDT)
- H. Data Monitoring Equipment
- I. Strain Controlled Loading Frame

Figure 4.12 Conventional triaxial system

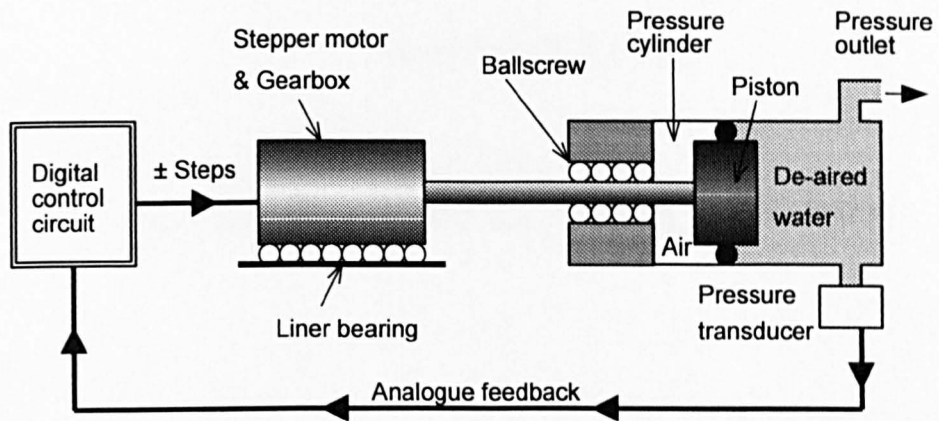


Figure 4.13 Diagram layout of GDS controller. After Higuchi (2001)

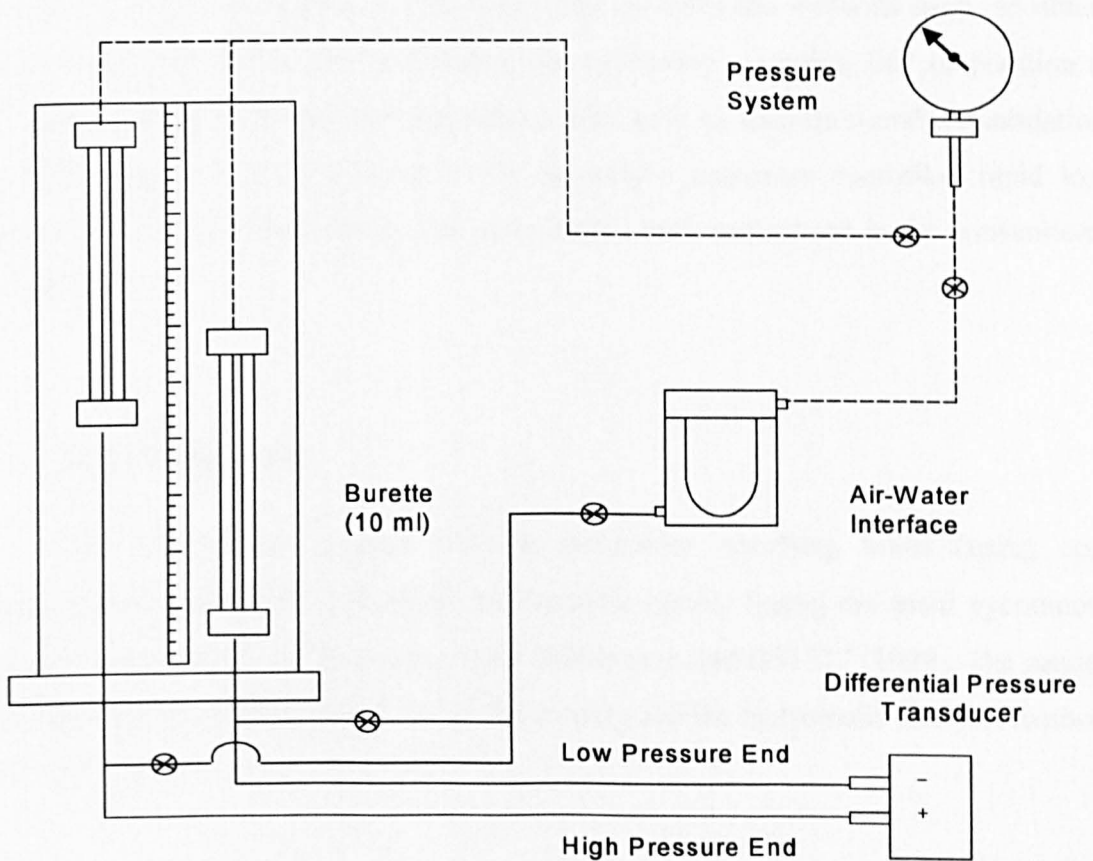


Figure 4.14 Schematic diagram of the differential pressure transducer calibration system

CHAPTER FIVE

EXPERIMENTAL PROCEDURES

5.1 Introduction

This chapter describes the details of the sample preparation, and test procedures employed during the research programme. This includes the methods used to obtain reconstituted clay (KSS) and undisturbed clay (Grimsby) samples, the preparation of the sample before each test, the preliminary tests such as saturation and consolidation, the rapid loading tests conducted in the pneumatic computer controlled rapid load triaxial system, and compression and permeability tests carried out in the conventional triaxial system.

5.2 Soil Classification

The preliminary standard tests to determine Atterberg limits (using cone penetrometer method for liquid limit) and specific gravity (using the small pycnometer method) were carried out according to the British standard BS1377 (1990). The particle size distribution was determined using the sieving and the hydrometer analysis methods (BS1377: 1990).

5.3 Sample Preparation

Three different techniques were used to prepare samples for the main testing programme. Reconstituted clay (KSS) specimens were obtained from a slurry using a

one dimensional pre-consolidation method or by sampling the clay bed in the calibration chamber. The undisturbed clay (Grimsby) specimens were obtained from boreholes undertaken on site. The procedures for each technique are described in the following sections.

5.3.1 One-Dimensional Pre-Consolidation

KSS Samples were initially consolidated in a one-dimensional consolidation mould from a slurry. Samples from the moulds were then extruded into 100 mm diameter thin-walled samplers and were stored until testing.

(a) Slurry Preparation

The kaolin based slurry was obtained by mixing 25% sand, 25% silt and 50% Speswhite kaolin previously oven dried at 105°C. Sufficient material was prepared for to fill three consolidation moulds. The powdered and air dried Speswhite kaolin, sand and silt were weighed out in batches of 6 kg, 3 kg and 3kg, respectively. This was mixed in a Hobart mixer with de-aired de-ionised water at a moisture content of 80 % (Figure 5.1). The Speswhite kaolin and the water were initially mixed for five minutes, then the silt was added and mixed for another five minutes before the sand was added and the mixing restarted. After mixing for an hour, the slurry was considered to be homogeneous and therefore ready to be poured into the consolidation moulds.

(b) One Dimensional Consolidation

The base of the consolidation moulds and the piston had porous stone discs which were initially de-aired in de-aired de-ionized water in a bell jar under a vacuum of minus 1 Atm., for 1 hour (Figure 5.2). A filter paper was cut and placed, wet, over the porous base disc to prevent clogging of the drainage paths with clay and silt particles. A 105 mm diameter steel cylinder was then screwed to the base. The drainage tube, on the bottom, was blocked by filling the base with distilled de-aired water, to a depth of about 3 mm just enough to cover the base platen and the drainage tube. Then the slurry was poured slowly into the mould using a funnel with a hose on the tip. When

the mould was full, it was vibrated lightly to allow the release of any air bubbles that might be trapped during the filling process.

A filter paper was placed over the slurry to prevent the top porous stone from clogging. The piston with the drainage assembly was gradually lowered into the mould, allowing air to escape through the drainage line until some water came out from the top drainage line, then the line was closed to allow the pore water pressure to be measured before consolidation. An actuator, connected to a compressed air supply, provided the 140 kPa consolidation pressure. This pressure was measured by means of a pressure transducer attached to the top drainage line. It was not necessary to measure the actuator ram friction, as the measured pore water pressure was equal to the consolidation pressure applied to the slurry. The top platen displacement and the discharged water were monitored. Consolidation was completed within 3 days. The sample was then extruded into three 100 mm internal diameter thin walled steel tubes. The ends were waxed and the samples stored in plastic bags in a controlled temperature room at about $20^{\circ}\text{C} \pm 2^{\circ}\text{C}$.

5.3.2 Sampling the Calibration Chamber beds

In addition to samples prepared using the one dimensional pre-consolidation method described above, following the tests in the calibration chamber (Brown 2004), KSS samples were taken from the soil bed for triaxial shear testing. The clay bed sample was carefully stripped down. The stripping down process involved the excavation of the clay bed to expose the transducers and associated wiring. The clay was sampled using U100 tubes carefully pushed into the sample for laboratory triaxial testing, and U38 tubes for additional study (Figure 5.3). Then the ends were waxed and the samples, sealed in plastic bags, were stored in a controlled temperature room ($20^{\circ}\text{C} \pm 2^{\circ}\text{C}$) prior to testing.

5.3.3 Boreholes on site

U100 samples of undisturbed clay from the full scale pile investigation site of the associated research project (Brown 2004) were taken by means of two cable percussive

boreholes (Figure 5.4) sunk close to the piles. Further details of the boreholes and ground investigation carried out are given in Section 6.2.

5.4 Setting up the Sample in Triaxial Cell

5.4.1 Pneumatic Computer Controlled Rapid Loading Triaxial System

Prior to each triaxial test, conducted on the rapid loading system, the sample was set up according to following procedure.

- (1) The triaxial cell base including the pedestal and the top cap with a drainage line was flushed with de-aired water.
- (2) The sample was extruded from the one-dimensional consolidation mould into a previously weighed split former of 100 mm internal diameter and 200 mm height. After trimming both ends, the former and the sample were weighed to get the bulk density of the sample. Soil trimmings were used to obtain a value of pre-test water content.
- (3) A porous disk of 100 mm diameter, which had been previously de-aired in a vacuum desiccator was placed over the base pedestal. A moist disk of filter paper was placed over the porous disk to prevent clogging of the drainage paths. The sample was carefully retrieved from the former and put on the porous disk. The initial height and diameter of the sample were measured three times at different sections by a vernier calliper. A moist filter paper side drain was placed around the sample and a membrane was stretched over the sample and fastened to the pedestal of the cell base by two O-rings. To remove air trapped by the latex membrane, the sample, was gently stroked in an upward direction, as suggested by Bishop and Henkel (1964). A moist filter paper and a 100 mm diameter porous stone previously de-aired and the top cap were placed over the sample. A hollowed top cap with a drainage line was put on top of the sample. Any air remaining between the cap and the sample was removed by flowing some water

through the drainage line. Then two O-rings were placed on the top cap using a split O-ring stretcher.

- (4) A miniature pore pressure transducer was installed at the periphery of the sample following the procedures described by Hight (1982) and Pierpoint (1996). Before the installation, the porous stone and the cavity between the stone and sensor were de-aired by immersing the transducer in de-aired water under vacuum overnight. For installation a hole was cut in the latex rubber membrane at its mid-height. A silicone rubber grommet was formed (Figure 5.5) The rubber grommet, inserted in the hole with its shaft protruding, housed the transducer and provided a former for extending the latex rubber membrane by painting on successive layers of prevulcanized latex as can be seen in Figure 5.6 (A, B and C). To ensure intimate contact between the sample periphery and the porous stone of the transducer, a pad of saturated clay, about 5 mm thick, was placed on the stone before installation. After pushing the transducer into its housing, and avoiding any penetration of the sample, which would increase interference effects, the assembly was sealed with two O-rings. For additional security against leakage, prevulcanized latex was painted around the installed transducer. (Figure 5.6 D). The cables from the transducer passed through the base of the testing apparatus through an O-ring seal.
- (5) Approximately 4 ml of resin mixed with hardener was poured into the hollow in the sample top cap (Figure 5.7). Then, the cell lid was fastened in place and the top end of the load cell (loading ram) was connected to the bottom of the actuator rod using a connector designed for this research (Section 4.3.8). The load cell with a threaded stub on its base was lowered into the resin-filled hollow of the sample top cap, making sure that the load cell did not register any load. The connection between the top cap and the screw was made using resin in order to minimise disturbance during sample set up and to guarantee a tight fit. The load cell was maintained in this position for 20 minutes until the resin hardened. This was done according to the method proposed by Higuchi (2001).
- (6) The water was then let into the cell from the air/water pressure assembly. An LVDT was clamped on to the loading ram so that the sample deformation could

be measured externally. The air was allowed to bleed out from the top of the cell, and when there was no more air trapped inside the cell, the screw on top of the cell was tightened.

5.4.2 The Conventional Triaxial System

(a) *Monotonic Consolidated Undrained Triaxial Tests*

Before the compression tests were carried out in the Conventional Triaxial System previously described in Section 4.4, the samples were set up following the same procedure that has been described in Section 5.3.1 with the following exceptions.

Instead of the miniature pore water pressure transducer, a base pedestal pore water pressure transducer was used (Section 4.4.6). During step (1), the base of the cell including the pedestal, the pore water pressure transducer and the top cap with a drainage line were flushed with de-aired water to guarantee the saturation of the system.

Instead of the hollowed top cap, a top loading cap, fitted with an integral hemispherical dome, was used. On step (5), the cell lid was fastened in place, the loading ram was lowered and guided onto the top cap and stopped just before loading it.

(b) *Permeability Tests*

When permeability tests were carried out in the Conventional Triaxial System, the samples were set up according to the procedure described in Section 5.3.2 apart from the following details.

The size of the sample was 100 mm diameter and 100 mm height. No side filter paper was fitted around the sample. Two latex membranes, thickness 0.32 mm, were used instead of one, they were soaked in de-aired water for at least 2 hours before use, in order to reduce absorption of water from the sample and to lower the water permeability of the membranes. The loading ram was not connected to the top cap.

5.5 Testing Procedures

Two types of triaxial testing system were used as described in Sections 4.3 and 4.4. The testing procedures for each testing system will be described in the following sections.

5.5.1 Preliminary tests

For consistency purposes, all the tests carried out in any of the systems started with saturation, followed by isotropic consolidation.

(a) Saturation

Prior to testing a saturation stage was conducted to ensure that all trapped air in the sample was dissolved by using a back pressure. The saturation was done by ramping the back pressure alternately with the cell pressure. The initial cell pressure was set at 25 kPa and ramped to 225 kPa for reconstituted clay (KSS) and 300 kPa for undisturbed clay (Grimsby). The back pressure started initially from 20 kPa and was ramped to 220 kPa for reconstituted clay (KSS) and 295 kPa for undisturbed clay (Grimsby). The increment of the pressures was set to 25 kPa for each step and the duration of ramping fixed at one hour.

The back pressures were sufficient to saturate the samples such that the pore pressure response to an undrained isotropic stress increment gave an average B value (Skempton 1954), greater than 0.98. However, any sample, which did not reach a B value of at least 0.96, were discarded.

(b) Isotropic Consolidation

In all tests, samples were initially isotropically consolidated. The back pressure was set at 220 kPa or 295 kPa as described above. Consolidation was allowed to occur by setting a cell pressure and allowing pore water to flow out of the test sample.

The cell pressure was set initially at 225 kPa, for reconstituted clay (KSS), or 300 kPa, for undisturbed clay (Grimsby), after saturation and hence the effective stress was 5 kPa. Then the effective stress was increased to the desired pressure in three steps.

After each step the sample was allowed to consolidate for half an hour but the final pressure was maintained for twenty-four hours on reconstituted clay (KSS) and seventy-two hours on undisturbed clay (Grimsby) to complete the consolidation, i.e., when there was no further measurable volume change.

In the pneumatic computer controlled rapid loading system, monitoring the exact height of the sample during saturation and consolidation was made possible because the sample was rigidly attached to the load cell before saturation.

5.5.2 Consolidated Undrained Triaxial Tests

(a) Pneumatic Computer Controlled Rapid Loading Triaxial System

The pneumatic computer controlled closed-loop cyclic triaxial system, described in Section 4.3, was used in the present research to carry out monotonic strain controlled consolidated undrained triaxial tests and multistage rapid loading tests at different rates from 0.001 mm/s up to 200 mm/s.

The apparatus was capable of applying cyclic and stress and strain-controlled monotonic loads. The software used to control the system, called UTM (Universal Testing Machine), allowed the operator to enter the initial sample dimensions, back pressure, cell pressure, isotropic consolidation conditions, load cycle frequency, load amplitude, displacement amplitude, load wave shapes, termination strain/stress level, termination cycle count, and, for safety reasons, maximum load and displacement. Test parameters and results were stored on the hard disk of the PC in a binary file. The information logged every 0.01 seconds and stored in the binary file allowed tests to be reviewed and an ASCII file to be created that provided a means of importing test results into a spreadsheet program.

The monotonic tests carried out at rates up to 0.1 mm/s were performed using the rate mode under strain-controlled conditions. The monotonic tests carried out at rates higher than 0.1 mm/s were performed using the cyclic mode. In that case the wave shape of the load was defined as a ramp function and the rate of shearing was introduced by means of the slope of the function defined as the ratio between the

maximum axial strain and time of loading. The theoretical maximum rate depended on the maximum axial strain and the minimum allowable time which it was possible to select. They were found to be 10% and 100 ms respectively giving a rate of 200 mm/s for a 200 mm height sample. However the actual performance of the equipment and hence the feasible rate depended on the stiffness of the different soils under varying stress conditions and ultimately on the capacity of the system to apply the load in the required time. The maximum feasible rates in this testing programme were 192.93 mm/s for reconstituted clay (KSS), at $OCR = 1$, isotropically consolidated to 250 kPa effective stress, and 131.50 mm/s for undisturbed clay (Grimsby), isotropically consolidated to 140 kPa effective stress.

(b) The Conventional Triaxial System

After the completion of the consolidation the loading ram was brought into contact with the ball bearing until it was just seated on the top cap. The samples were sheared under undrained monotonic test conditions up to 25% or 15% axial strain. All the tests were performed at a constant strain rate of 0.001 mm/s. The connection to the GDS controller that was used to apply back pressure was closed to prevent drainage during a test. The readings of pore water pressure, load and deformation were recorded automatically on the computer.

5.5.3 Permeability Tests

Triaxial permeability tests were carried out on the conventional triaxial apparatus using two back pressure systems, described in Section 4.4. The samples were set up, saturated and consolidated in stages. Vertical permeability measurements were performed at different void ratios after finishing each consolidation or swelling stage. At the end of each consolidation or swelling stage, a constant pressure difference was applied across the sample such that the induced flow of water was from the bottom to the top. The induced flow rate across the sample was monitored in both the inflow and the outflow pressure systems. Throughout the permeability tests, the differential pressure across the sample did not exceed 10-15% of the applied vertical effective stress as was recommended by Little *et al* (1992). A final moisture content sample was taken to permit the calculation of void ratios at various stages of the test.

Each permeability test was repeated with at least three different differential pressures. The tests were conducted until the rates of flow observed through the two pressure systems were practically equal and a steady state flow conditions could be assumed across the sample. The applied differential pressure was then plotted against the induced flow rate to establish a linear relationship passing through the origin. The gradient of the line was used for permeability calculation. (Equation 5.1)

$$K_v = \left(\frac{L_s}{A_c} \right) \left(\frac{Q_f}{H} \right) \quad \text{Equation 5.1}$$

where k_v is the vertical permeability, L_s is the sample height, A_{sp} is the cross sectional area of the sample, Q_f is the flow rate and H is the differential pressure head.

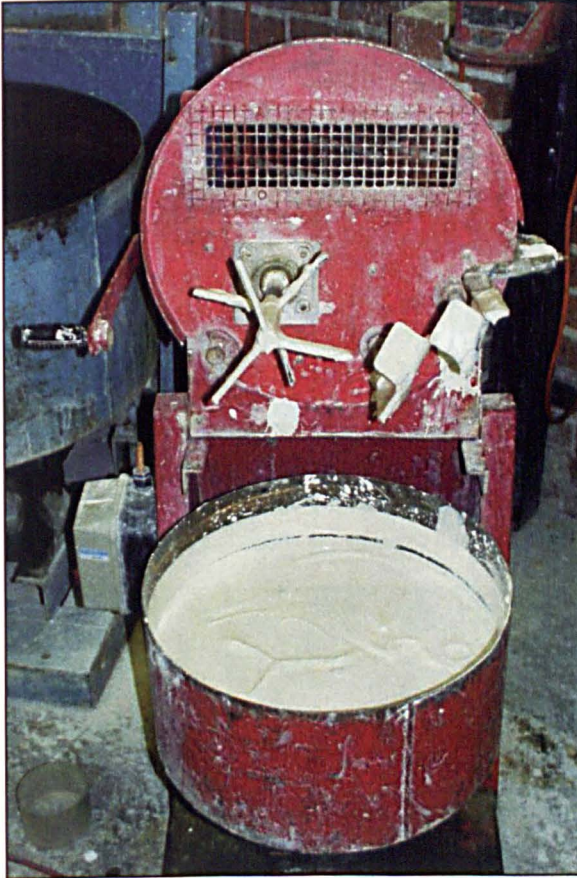


Figure 5.1 Slurry preparation.
Hobart mixer.

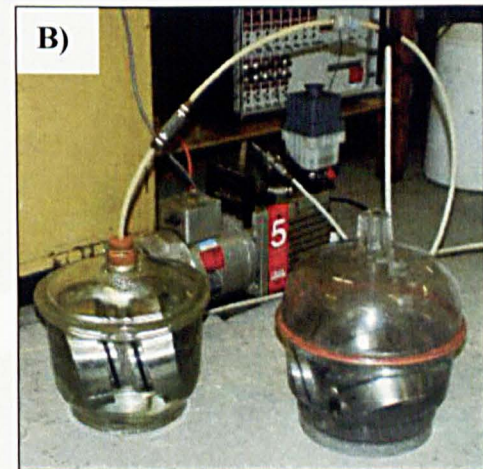


Figure 5.2 De-airing the top pistons
and bases of the consolidation moulds.

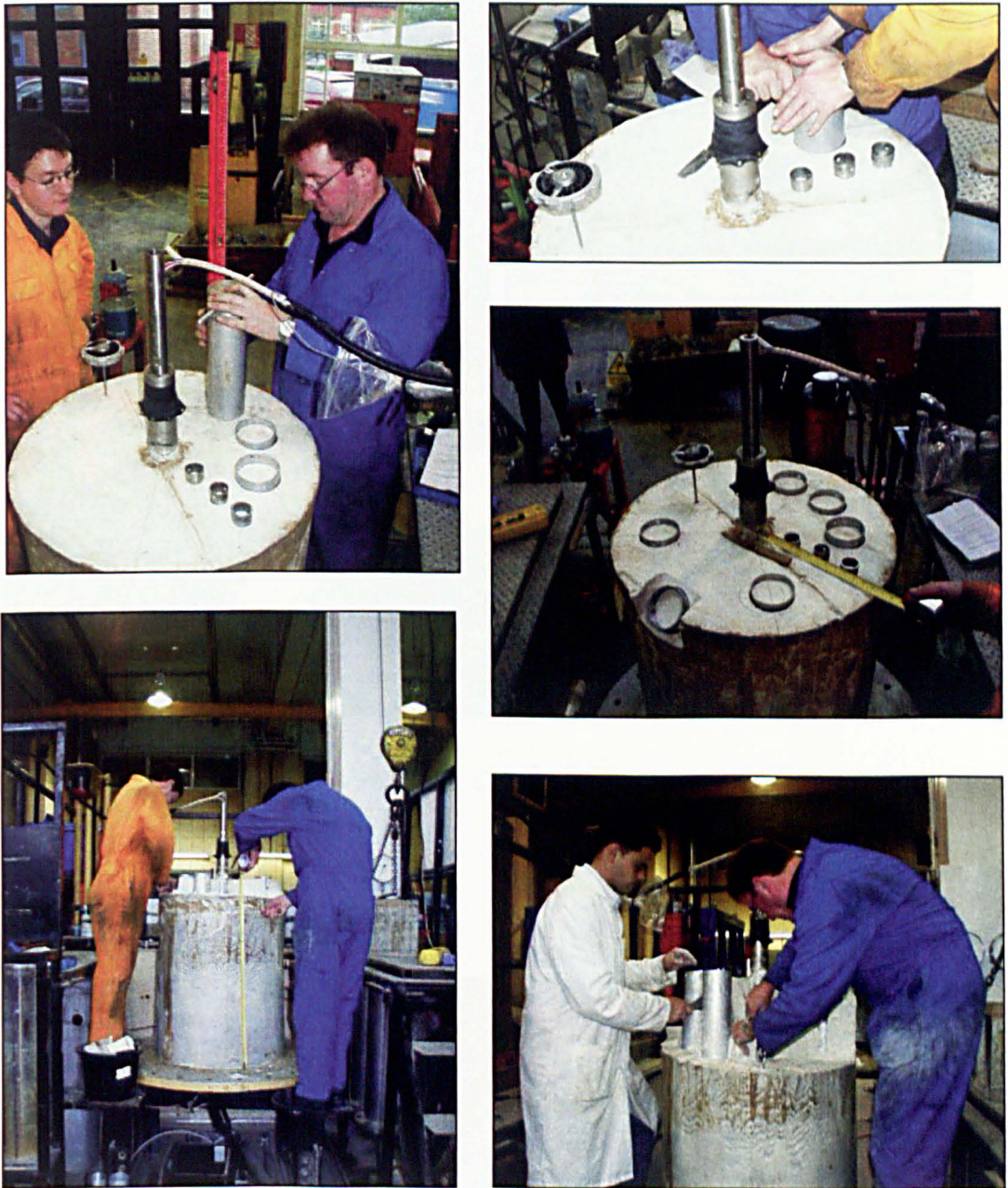


Figure 5.3 Sampling the calibration chamber bed.



Figure 5.4 Cable percussive borehole at Grimsby.

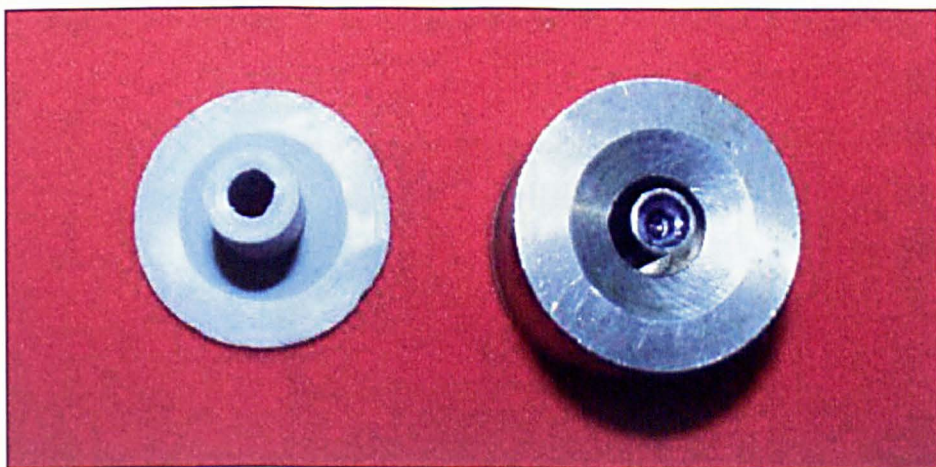


Figure 5.5 Silicone rubber grommet and the mould used to form it .

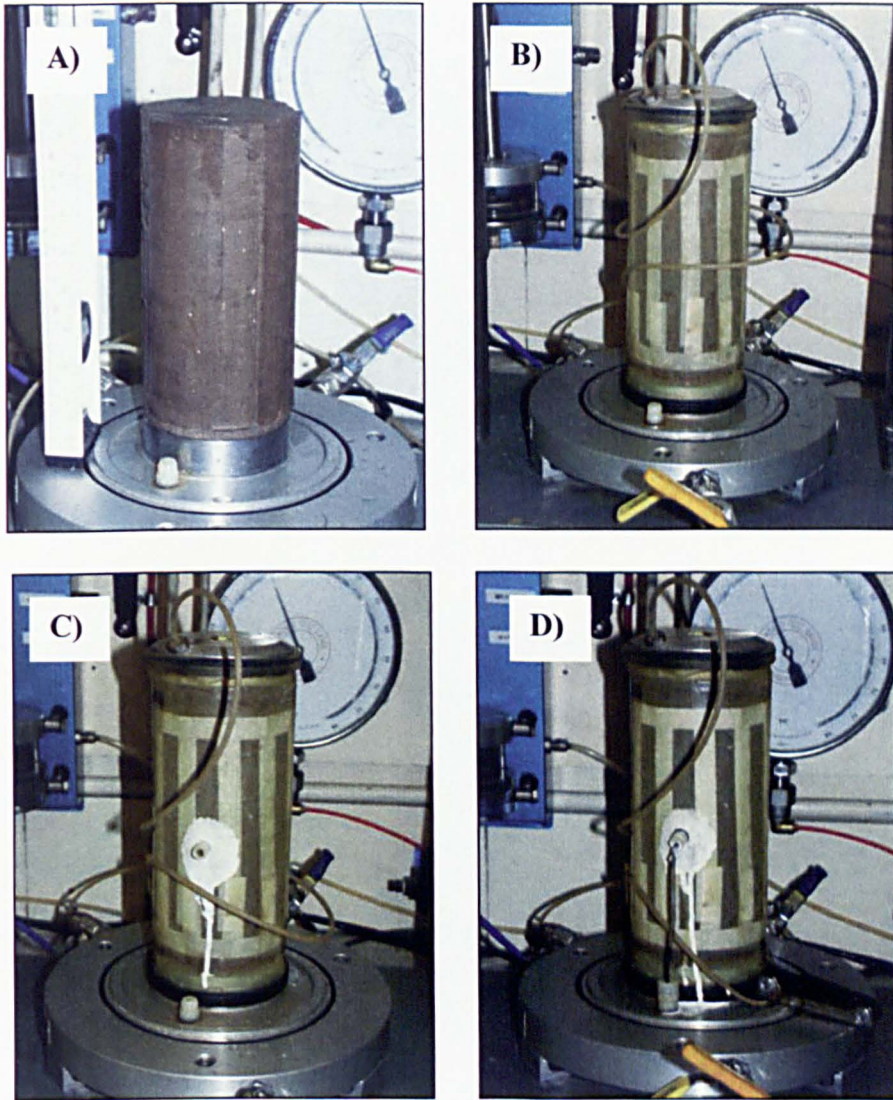


Figure 5.6 Setting up the miniature pore water pressure transducer.



Figure 5.7 Resin mixed with hardener being poured into the hollow in the sample top cap

CHAPTER SIX

THE MATERIALS

6.1 Introduction

This chapter deals with the basic characterisation of the materials used. The physical properties of the materials as well as the results from the consolidated undrained triaxial tests and the triaxial permeability tests will be presented and discussed. The object of the consolidated undrained triaxial and permeability tests was to obtain a framework for later discussion of the results of monotonic and multistage rapid loading tests.

6.2 The Materials

Two clay soils, reconstituted clay (KSS) and undisturbed Grimsby clay, were used for the research. The same materials were used in the associated project (Brown 2004) previously introduced in Section 3.1. The reconstituted clay was the same as the soil that was used for the calibration chamber and the undisturbed clay samples were obtained from the Grimsby site.

Although previous studies in the clay calibration chamber had used 100% kaolin (Anderson *et al*, 1991), it was considered to be more appropriate to use a material that would more closely resemble natural clays in terms of grading and material properties, although the bed preparation process would not recreate the soil fabric found with natural deposits (Anderson *et al*, 2003). The kaolin based mixture used for this study

and for the associated research project in the calibration chamber was similar to that proposed by Rossato *et al* (1992;1994) which consisted of a mix of kaolin, sand and silt (KSS). The mixture material consisted of 50% of Speswhite kaolin, 25% silt and 25% fine sand. The Speswhite kaolin powder, the sand and the silt were from the same batch as used by Brown (2004). A summary of the material properties as provided by the suppliers can be found in Table 6.1.

The full scale investigation site was within Expanded Piling's head office and depot (Cheapside Works), situated near to Waltham on the outskirts of Grimsby, North East Lincolnshire and 7.5 Km Southwest the coast. A plan showing the site location is shown in Figure 6.1 and an aerial photograph is shown in Figure 6.2.

Previous research projects were carried out in the past, on the same site, by Taylor (1966), James (1967) and Bell (2001). The boreholes for the previous ground investigations were located on the south side of the workshops, near the service road, within 200m of the current research site. The soil description quoted by Taylor (1966) is shown in Table 6.2. British Geological Survey records, Cheapside Farm (527930,401710), include a borehole located 100 m north of the site. It was a drinking water well where the water table and chalk bedrock were encountered at 10.67 m and 28.65 m below ground level, respectively.

The current ground investigation carried out for this project and the associated research project (Brown 2004) consisted of two cable percussive boreholes and piezocone penetration tests. The first borehole (BH1) was conducted to a depth of 20.35 m below ground level (BGL) and included alternate driven U100 samples and Standard Penetration Tests (SPT) while the second borehole (BH2) extending to a depth of 15.40 m just included driven U100 samples. The borehole logs showing the strata encountered can be seen in Fig 6.3. For BH1 and Fig 6.4 for BH2. On completion of the first borehole, a standpipe piezometer was installed with its tip at 12.9m BGL although no water seepage was noticed during the investigation. The U100 samples of undisturbed clay from the site were waxed on site and then transported to the University of Sheffield where they were stored in plastic bags in a controlled temperature room at $20^{\circ}\text{C} \pm 2^{\circ}\text{C}$ prior to testing.

A summary of the strata encountered based on the borehole logs and U100 inspection, quoted by Brown (2004), is presented in Table 6.3. and Figure 6.5 A. The information from the SPT N values with depth is shown in Figure 6.5 B

Additional investigation included three electronic piezocone CPTs (static cone penetration test) and one SCPT (seismic cone penetration test) to 20 m BGL and multistage 100 mm diameter quick undrained triaxial tests. Typical outputs from PCPT and SCPT tests can be seen in Figs.6.5 C and D, respectively. The results of the multistage triaxial testing with additional hand vane measurements taken on site and results from Taylor (1966) can be seen in Figure 6.6 A. Values of bulk density and Atterberg limits of samples at different depths are presented in Figure 6.6 B and C, respectively.

6.2.1 Soil Description and Classification

(a) Reconstituted clay (KSS)

A particle size analysis was performed on representative batch samples using the sieving and the hydrometer analysis methods (BS1377:1990). The particle size distribution curve for this material is shown in Figure 6.7, and the results of the particle size distribution test are listed as follows:

Sand -	(> 0.06 mm)	-	34 %
Silt - <i>Coarse</i>	(0.02 - 0.06 mm)	-	8 %
- <i>Medium</i>	(0.006 - 0.02 mm)	-	8 %
- <i>Fine</i>	(0.002 - 0.006 mm)	-	12 %
Clay -	(< 0.002 mm)	-	38 %

Tests for specific gravity and Atterberg limits gave the following results:

Specific gravity, G_s	-	2.64
Liquid limit, LL	-	37 %
Plastic limit, PL	-	17 %
Plasticity index, PI	-	20 %
Activity, A	-	0.53

According to the Unified Soil Classification System (BS 5930: 1981) as seen in Figure 6.8, the composite material can be classified as CI, i.e. clay of intermediate plasticity.

(b) Undisturbed Grimsby clay

A particle size analysis was performed on representative batch samples using the sieving and the hydrometer analysis methods (BS 1377:1990). The particle size distribution curve for this material is shown in Figure 6.7, and the results of the particle size distribution test are listed as follows:

Sand -	(> 0.06 mm)	-	39-44 %	($A_v = 41$ %)
Silt - <i>Coarse</i>	(0.02 - 0.06 mm)	-	8 %	($A_v = 8$ %)
- <i>Medium</i>	(0.006 - 0.02 mm)	-	11-12 %	($A_v = 11$ %)
- <i>Fine</i>	(0.002 - 0.006 mm)	-	11-13 %	($A_v = 12$ %)
Clay -	(< 0.002 mm)	-	25-29 %	($A_v = 28$ %)

Tests for specific gravity and Atterberg limits gave the following results:

Specific gravity, G_s	-	2.69
Liquid limit, LL	-	20-36 % ($A_v = 28$ %)
Plastic limit, PL	-	12-18 % ($A_v = 16$ %)
Plasticity index, PI	-	7-20 % ($A_v = 12$ %)
Activity, A	-	0.5-0.6

Results from Atterberg limits and moisture content testing versus depth can be seen in Figure 6.6 C. According to the Unified Soil Classification System (BS 5930: 1981) as seen in Figure 6.8, the composite material can be classified as CL, i.e. clay of low compressibility and high plasticity.

6.3 Consolidation

(a) KSS

Two one-dimensional oedometer consolidation tests were carried out up to 800 kPa vertical stress on reconstituted clay (KSS) samples obtained by sampling the

calibration chamber bed. The author's colleague, at Sheffield University, Srisaktihivel (2003) carried out 1-D consolidation tests for the same material (KSS) from a slurry using 254 mm diameter Rowe cells up to an effective confining pressure of 400 kPa.

The average one-dimensional normal compression and swelling lines from those tests are plotted in Figure 6.9 in $v, \ln \sigma_v'$ space (where v is the specific volume and σ_v' is the vertical effective stress). The oedometer tests results only achieved values close to the normal compression line for a stress level between 400 kPa and 800 kPa; that was due to the stress history of the samples that had been previously isotropically consolidated in the calibration chamber to 280 kPa.

During one-dimensional compression, the vertical effective stress (σ_v') is proportional to the mean effective stress (p') (Equation 6.1) and hence the slope of the one-dimensional normal compression line in $v, \ln \sigma_v'$ space should be the same as that of the isotropic compression line in $v, \ln p'$ space.

$$p' = \frac{1}{3}(\sigma_v' + 2\sigma_h') = \left(\frac{1}{3} + 2K_0\right)\sigma_v' \quad \text{Equation 6.1}$$

$$\text{where, } K_0 = \frac{\sigma_h'}{\sigma_v'} \quad \text{Equation 6.2}$$

and K_0 is constant during one-dimensional compression.

The results from the one-dimensional consolidation tests both in the oedometer cell and the Rowe cell can be used to obtain the slope of the normal consolidation line in v - $\ln \sigma_v'$ space and hence the slope, $-\lambda$, of isotropic consolidation lines in $v, \ln p'$. The gradient of this line for reconstituted clay (KSS), obtained by least squares regression, in Figure 6.9, was -0.10 .

However, the intercept of the normal compression line with the v -axis (at $\ln p' = 0$ or $p' = 1$ kPa), will be different. Therefore the results from one-dimensional consolidation could not be used to define the position of the isotropic normal consolidation line.

In one dimensional swelling, the ratio σ_h'/σ_v' is not constant, but increases as unloading continues. Hence the ratio σ_v'/p' changes during unloading, and the one-dimensional and isotropic unload/reload lines are not parallel and the results from oedometer and Rowe cells could not be used to obtain the slope of the isotropic swelling lines.

(b) Grimsby clay

Oedometer consolidation tests were carried out on three samples from BH2 at different depths. The results from these tests, plotted in $v - \ln \sigma_v'$ space, can be seen in Figure 6.10. Although the position of the line differed for different tests, the slopes lie within a range of -0.03 to -0.04.

6.4 Monotonic Compression

The summary of results for consolidated undrained triaxial compression tests on specimens isotropically consolidated to various stress histories are shown in Table 6.4 and Table 6.5 for reconstituted clay (KSS) and undisturbed Grimsby clay, respectively. The aim of the tests was to define the value of the critical state parameters for both materials, and use them to establish a framework for further discussion of the rate effect investigation in the main testing programme.

6.4.1 Stress-Strain Behaviour

(a) KSS

The stress-strain results from the strain controlled consolidated undrained triaxial tests on reconstituted clay (KSS) are presented in Figure 6.11. All the tests were carried out to at least 11% axial strain (ϵ) and the assumed critical state values are summarized in Table 6.4. For the normally consolidated specimens, the stress-strain relationships are dependent on the value of the effective consolidation pressure, p' . The specimens that were consolidated to higher values of p' and hence lower values of specific volume,

sustained higher values of q at failure, but the shape of the q - ϵ curves were similar for all the tests.

(b) Grimsby clay

The stress-strain results from the strain controlled consolidated undrained triaxial tests on undisturbed Grimsby clay are presented in Figure 6.12. The samples were isotropically consolidated to different stress histories. Initial mean effective stress values after consolidation varied between 70 kPa and 330 kPa. All the tests were carried out to at least 11% axial strain (ϵ). For tests carried out to axial strains higher than 15%, the deviator stress became approximately constant after reaching a limiting value, without reaching a peak (Figure 6.12). For tests carried out to axial strains lower than 15% the deviator stress did not reach either a peak or a limiting value. For further analysis aimed at obtaining the critical state parameters of the soil, the critical state values were assumed to be the values at maximum strains for each test as is summarized in Table 6.5.

6.4.2 Stress Paths and Critical State Line

The stress paths, in q - p' space, for the undrained triaxial tests carried out on samples isotropically consolidated to various stress histories are shown in Figure 6.13 and 6.14 for reconstituted clay (KSS) and undisturbed Grimsby clay respectively. The critical states summarized in Tables 6.4 and 6.5 define a straight line through the origin in q - p' space (Figure 6.13 and 6.14) for each material. This line is the critical state line (CSL) (The notion of a critical state line is part of the critical state theory, which was outlined in a series of papers on the yielding of soils by Roscoe *et al.*, (1958), Poorooshasb & Roscoe (1961), Roscoe & Poorooshab (1963) and Roscoe *et al.*, (1963). It has been described by Schofield & Wroth (1968) and explained by Atkinson & Bransby (1978) and Wood (1990)).

The projection of the critical state line onto the q - p' plane in Figures 6.13 and 6.14 is described by:

$$q = Mp' \qquad \text{Equation 6.3}$$

where M is its gradient. From the least squares regression analysis, M was found to be 1.05 for reconstituted clay (KSS) and 1.07 for undisturbed Grimsby clay.

The angle of the internal friction for compression, ϕ'_c , can be calculated from the Equation 6.4 (Atkinson & Bransby, 1978)

$$M = \frac{6 \sin \phi'_c}{3 - \sin \phi'_c} \quad \text{Equation 6.4}$$

Therefore,

$$\phi'_c = \sin^{-1} \left(\frac{3M}{6 + M} \right) \quad \text{Equation 6.5}$$

Hence for $M = 1.05$, $\phi'_c = 26.5^\circ$ for reconstituted clay (KSS) and for $M = 1.07$, $\phi'_c = 27^\circ$ for undisturbed Grimsby clay.

The projection of the critical state line onto the v - p' plane is curved, but if the same points are plotted with axes v - $\ln p'$, the points fall close to a straight line, and the gradient of this line is the same as the gradient of the corresponding normal compression line (Atkinson & Brandy 1978). The critical state line is described by

$$v = \Gamma - \lambda \ln p' \quad \text{Equation 6.6}$$

where Γ is defined as the value of v at $p' = 1 \text{ kPa}$ on the critical state line and $-\lambda$ is the slope of the critical state line and the normal consolidation line. Equations 6.3 and 6.6 together define the position of the critical state line in the q - p' - v space and M , Γ , and λ are soil constants.

The critical state line, for reconstituted clay (KSS), is plotted in v - p' space in Figure 6.15. The gradient of this line, obtained by regression analysis, is the same as the gradient of the one dimensional normal consolidation line discussed in Section 6.3.a and the isotropic normal consolidation line obtained from the specific volumes of samples before the tests for series CS-KSS. For the reconstituted clay (KSS), the soil constant Γ , N_p , and λ , were found to be equal to 2.19, 2.23 and 0.10 respectively.

For undisturbed Grimsby clay the data of the triaxial tests summarized in Table 6.5 are plotted in Figure 6.16, in the v - p' plane. The data was too scattered and it was not possible to define the position of either the critical state line (CSL) or the normal consolidation line (NCL) in v - p' space.

From the 1-D consolidation tests, and the consolidated undrained compression tests, the summary critical state parameters obtained for both materials is shown in Table 6.6.

6.5 Permeability

Direct triaxial vertical permeability tests were carried out in a triaxial apparatus, with two back pressure systems, for both KSS and Grimsby clay soil. A detailed description of the experimental set up and the procedure used is given in Sections 4.4 and 5.5.3 respectively.

(a) KSS

Measurements of the vertical permeability were performed on a KSS sample obtained by sampling the calibration chamber bed. After setting up the sample in the triaxial cell, on completion of saturation, the specimen was isotropically reconsolidated in two loading stages to 250 kPa and 400 kPa and two swelling stages to 100 kPa and 50 kPa. Direct vertical permeability tests were then conducted at different void ratios after finishing each consolidation or swelling stage. The aim of the test was to find out the value of the vertical permeability at representative void ratios for the effective consolidation stresses used on the main testing programme i.e 250 kPa (OCR=1), 100 kPa (OCR=4) and 50 kPa (OCR =8). A summary of the triaxial permeability tests results for reconstituted clay is shown in Table 6.7.

(b) Grimsby clay

The sample U8 from BH2 (6.50-7.20 m depth) was isotropically reconsolidated after saturation in two loading stages to 40 kPa and 225 kPa effective stress, the same consolidation effective stress that was used for tests GM2L and GM3L on the

multistage rapid load testing. After each consolidation stage a constant differential pressure head permeability test was conducted. Table 6.8 shows a summary of the results of the triaxial permeability tests conducted on undisturbed Grimsby clay.

SPESWHITE KAOLIN	
<i>Supplier</i>	Whitchem, Staffordshire
<i>Product</i>	Speswhite Powder China Clay
SAND	
<i>Supplier</i>	Hanson Aggregates
<i>Product</i>	Buckland P30 Silica Sand
<i>Location</i>	Heath & Reach, Bedfordshire
<i>Geological Type</i>	Lower Greensand of the Cretaceous Period
<i>Grain Shape</i>	Mostly sub-angular with some sub-rounded and occasional rounded
<i>Silica sand</i>	97% Minimum
SILT	
<i>Supplier</i>	Hepworth Minerals & Chemicals, Cheshire
<i>Product</i>	Oakamoor HPF4 Silica Flour
<i>Location</i>	Oakamoor, Staffordshire
<i>Geological Type</i>	Carboniferous Upper Millstone Grit
<i>Description</i>	High purity quartz sand, dry ground and classified

Table 6.1 Individual material descriptions as provided by the suppliers

Depth (m)	Soil Description
0-0.6	Topsoil
0.6-1.5/2.1	Medium stiff light brown CLAY with gravel.
1.5/2.1-10.0	Very stiff to firm dark brown gravelly CLAY, gravel medium to coarse with occasional cobbles. Thin beds of silty sand at 4.5 m.

Table 6.2 Grimsby soil description (Taylor 1966)

Depth (m)	Soil Description
0-0.3	Firm to stiff, slightly sandy, mottled orange brown CLAY with occasional black organic fragments
0.3-2.4	Firm to very stiff, slightly gravelly, light orangey brown CLAY, with occasional black organic fragments and extremely closed spaced thin lamina of silt, gravel is fine to medium, rounded to sub-rounded.
2.4-20.35	Firm to very stiff, gravelly, greyish brown to dark brown, CLAY, with occasional coarse gravel and rare cobbles, gravel is fine to medium, rounded to sub-rounded. 4.2m Firm to stiff 10.45m becoming Stiff

Table 6.3 Grimsby soil description (Brown 2004)

Test	Effective Confining Stress (kPa)	Specific Volume, $v = 1+e$	Axial Strain (%)	Mean normal effective stress, p' (kPa)	Deviator stress, q (kPa)
CS-KSS-100	102	1.68	20.29	112	112
CS-KSS-280	281	1.65	24.33	167	167
CS-KSS-375	375	1.61	11.12	209	223
CS-KSS-250	248	1.65	11.33	149	167

Table 6.4 Summary results of consolidated undrained triaxial tests for reconstituted KSS clay

Test	Effective Confining Stress (kPa)	Specific Volume, $v = 1+e$	Axial Strain (%)	Mean normal effective stress, p' (kPa)	Deviator stress, q (kPa)
CS-G1L-70	67	1.43	12.37	235	281
CS-G1L-250	244	1.43	12.75	368	399
CS-G2L-75	76	1.46	17.10	163	155
CS-G2L-200	196	1.40	22.26	219	256
CS-G2L-300	303	1.37	24.28	331	368
CS-G3L-220	219	1.49	11.66	370	390
CS-G3L-330	324	1.48	12.61	368	367

Table 6.5 Summary results of consolidated undrained triaxial tests for undisturbed Grimsby clay

Critical state parameters	Reconstituted clay	Undisturbed clay
	(KSS)	(Grimsby)
M	1.05	1.07
λ	0.10	0.03-0.04
Γ at 1 kPa	2.19	-
N_p at 1 kPa	2.23	-

Table 6.6 Critical state parameters for reconstituted KSS clay and undisturbed Grimsby clay.

Test	Consolidation	Effective Confining Stress (kPa)	OCR	Voids ratio, e	Vertical permeability, k_v (m/s)
P-KSS-250	Virgin Compression	250	1	0.658	1.03E-09
P-KSS-400		400	1	0.648	9.25E-10
P-KSS-100	Swelling	100	4	0.662	8.49E-10
P-KSS-50		50	8	0.670	1.02E-09

Table 6.7 Triaxial permeability tests on reconstituted KSS clay

Test	Effective Confining Stress (kPa)	Voids ratio, e	Vertical permeability, k_v (m/s)
P-G-140	140	0.42	4.85E-11
P-G-225	225	0.40	3.64E-11

Table 6.8 Triaxial permeability tests on undisturbed Grimsby clay

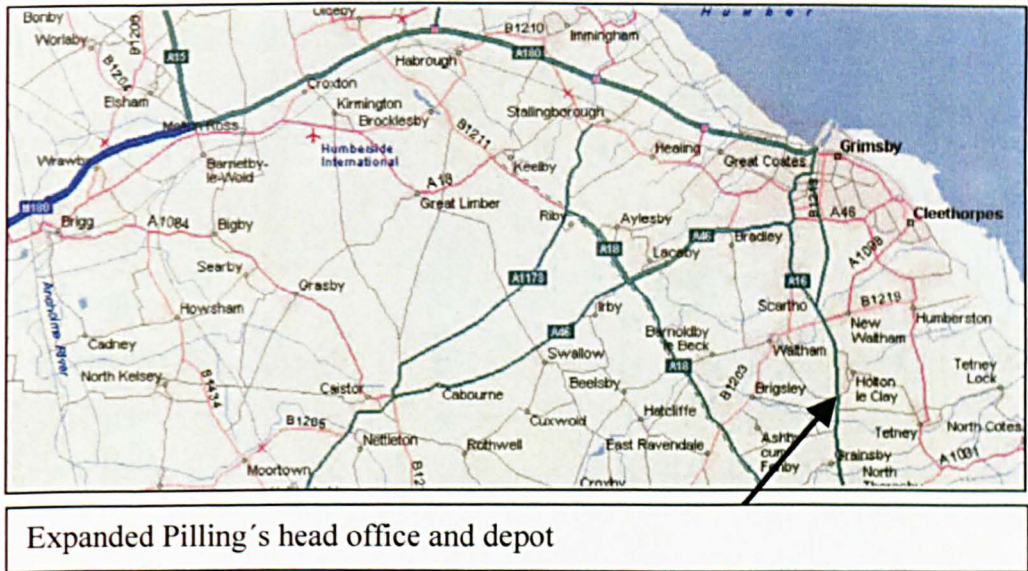


Figure 6.1 Site location plan. Expanded Piling. Cheapside Works, Grimsby. (after Bell, 2001)



Figure 6.2 Aerial photograph. Expanded Piling. Cheapside Works, Grimsby (after Bell, 2001).

Description	Depth & Thickness (m)	Depth (m)	Samples		Test	Field Records
			Type	No.		
Brown, mottled rust brown silty, slightly clay containing fragments of brick, small stones and other assorted gravel	0.30	0.20	D	1		
Made Ground		0.40	D	2		
Firm to stiff, light orange brown, mottled light grey, silty, sandy Clay containing assorted fine gravel	0.90	0.85	U	1		60 blows
Stiff, brown, mottled light grey, silty, sandy Clay containing assorted fine gravel		1.55	D	3	SPT	3,4,5,6,7,8
Stiff, dark brown, occasionally mottled light grey, silty, slightly sandy Clay containing chalk and other assorted gravel	2.00	2.00	U	2		99 blows
		2.65	D	4	SPT	2,2,3,3,5,7
Stiff, dark brown, occasionally mottled light grey, silty, slightly sandy Clay containing chalk and other assorted gravel		3.10	U	3		55 blows
		3.70	D	5	SPT	2,2,3,4,4,5
Glacial Till (Boulder Clay)		4.20	U	4		50 blows
		4.80	D	6	SPT	1,1,2,2,3,5
Firm to stiff between 5.00 m to 7.50 m		5.30	U	5		47 blows
		6.00	D	7	SPT	1,1,2,2,3,4
Firm to stiff between 5.00 m to 7.50 m		6.50	U	6		40 blows
		7.20	D	8	SPT	1,2,3,3,4,4
Firm to stiff between 5.00 m to 7.50 m		7.70	U	7		52 blows
		8.55	D	9	SPT	2,2,3,4,4,5
Firm to stiff between 5.00 m to 7.50 m		9.15	U	8		43 blows
		9.85	D	10	SPT	2,2,3,4,5,6
Firm to stiff between 5.00 m to 7.50 m		10.45	U	9		48 blows
		11.15	D	11	SPT	2,2,4,5,6,6
Firm to stiff between 5.00 m to 7.50 m		11.75	U	10		52 blows
		12.60	D	12	SPT	2,3,3,5,5,6
Firm to stiff between 5.00 m to 7.50 m		13.20	U	11		50 blows
		13.90	D	13	SPT	2,3,4,5,7,8
Firm to stiff between 5.00 m to 7.50 m		14.60	U	12		58 blows
		15.30	D	14	SPT	2,3,5,6,8,8
<u>Ground water observations</u>		15.85	U	13		55 blows
No ground water seepages were encountered within the depth penetrated		16.50	D	15	SPT	2,3,4,5,6,8
Standpipe installed in dry hole at 12.80 m b.g.l		17.05	U	14		70 blows
End of borehole	20.35	17.80	D	16	SPT	2,4,5,7,8,9
		18.45	U	15		70 blows
End of borehole	20.35	19.10	D	17	SPT	2,4,5,6,7,8
		19.75	U	16		60 blows

U = Undisturbed Sample
D = Disturbed Sample

Figure 6.3 Borehole record (T.L.P. Ground Investigations). Borehole 1 (24-05-2001)

Description	Depth & Thickness (m)	Depth (m)	Samples	
			Type	No.
Loose, assorted brick and concrete rubble in a matrix of brown silty and sandy "soil". Brown, silty, sandy clay containing fragments of coal, sandstone, brick and other assorted gravel. Made Ground	0.50			
Firm to stiff, brown, silty, slightly sandy Clay containing occasional small fragments of coal, sandstone, old red sandstone and other assorted gravel	0.90			
Glacial Till (Boulder Clay) Stiff to very stiff, brown, mottled orange brown and grey silty, slightly sandy Clay containing occasional small fragments of chalk and other assorted gravel Generally stiff, dark brown, silty, slightly sandy Clay containing occasional small fragments of chalk, coal and other assorted gravel Glacial Till (Boulder Clay)		1.05 - 1.75	U	1
		1.80 - 2.50	U	2
		2.50 - 3.20	U	3
		3.25 - 3.95	U	4
	3.90	4.05 - 4.75	U	5
		4.90 - 5.60	U	6
		5.70 - 6.40	U	7
		6.50 - 7.20	U	8
		7.25 - 7.95	U	9
		8.00 - 8.70	U	10
		8.80 - 9.50	U	11
Thin lens of wet, brown, silty Sand.	9.25			
		9.70 - 10.40	U	12
		10.60 - 11.30	U	13
		11.40 - 12.10	U	14
Ground water observations		12.25 - 12.95	U	15
Slight groundwater seepage was encountered at 9.25 m emanating from a thin lens of water bearing silty sand.		13.05 - 13.75	U	16
After 15 mins. no water had accumulated in the base of the borehole		13.85 - 14.55	U	17
On completion borehole remained dry after borehole casing was withdrawn		14.70 - 15.40	U	18
End of borehole	15.40			

U = Undisturbed sample
D = Disturbed Sample

Figure 6.4 Borehole record (T.L.P. Ground Investigations). Borehole 2 (27-03-2002)

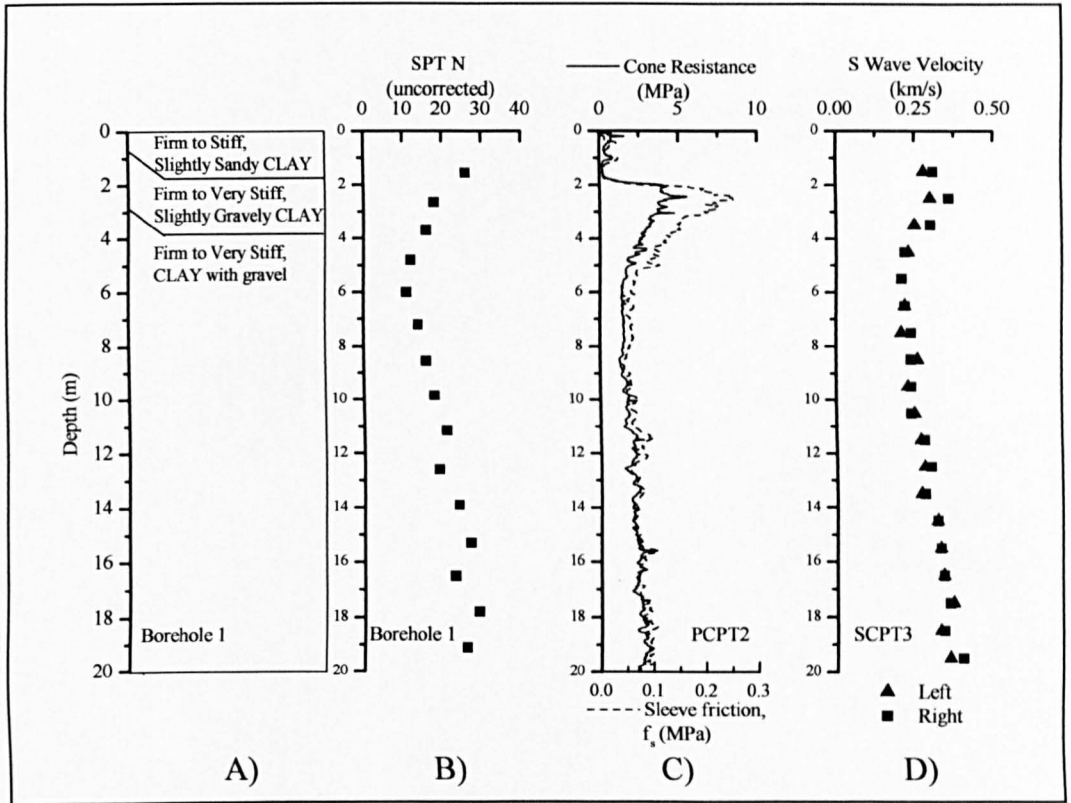


Figure 6.5 Information from SPT, CPT and SCPT at Grimsby. (after Brown 2004)

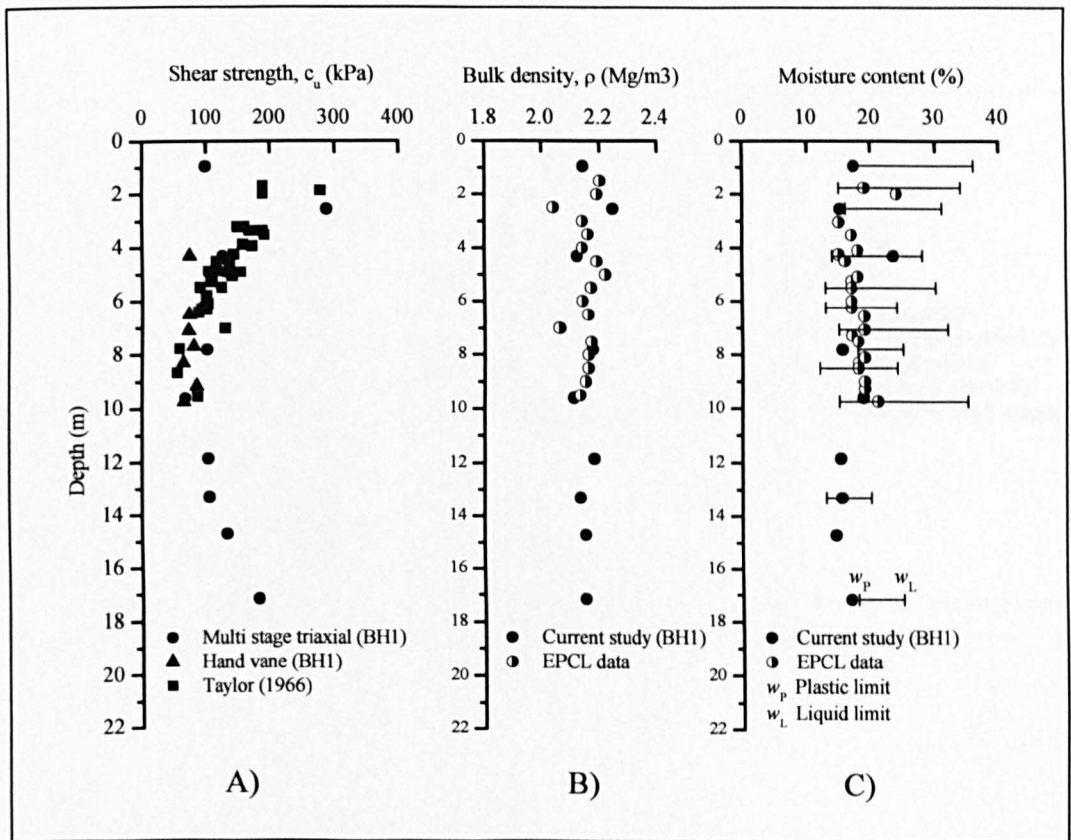


Figure 6.6 Shear strength from multistage quick undrained triaxial tests, bulk density and Atterberg limits of undisturbed Grimsby clay. (after Brown, 2004)

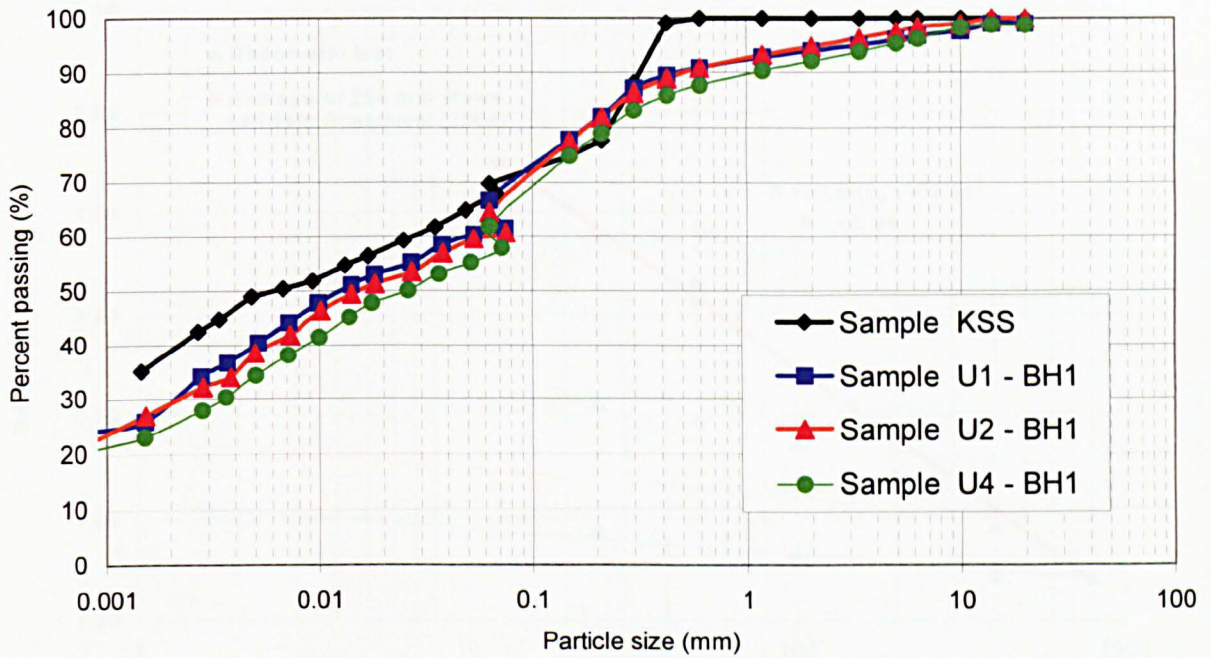


Figure 6.7 Particle size distributions of the reconstituted clay (KSS) and the undisturbed Grimsby clay

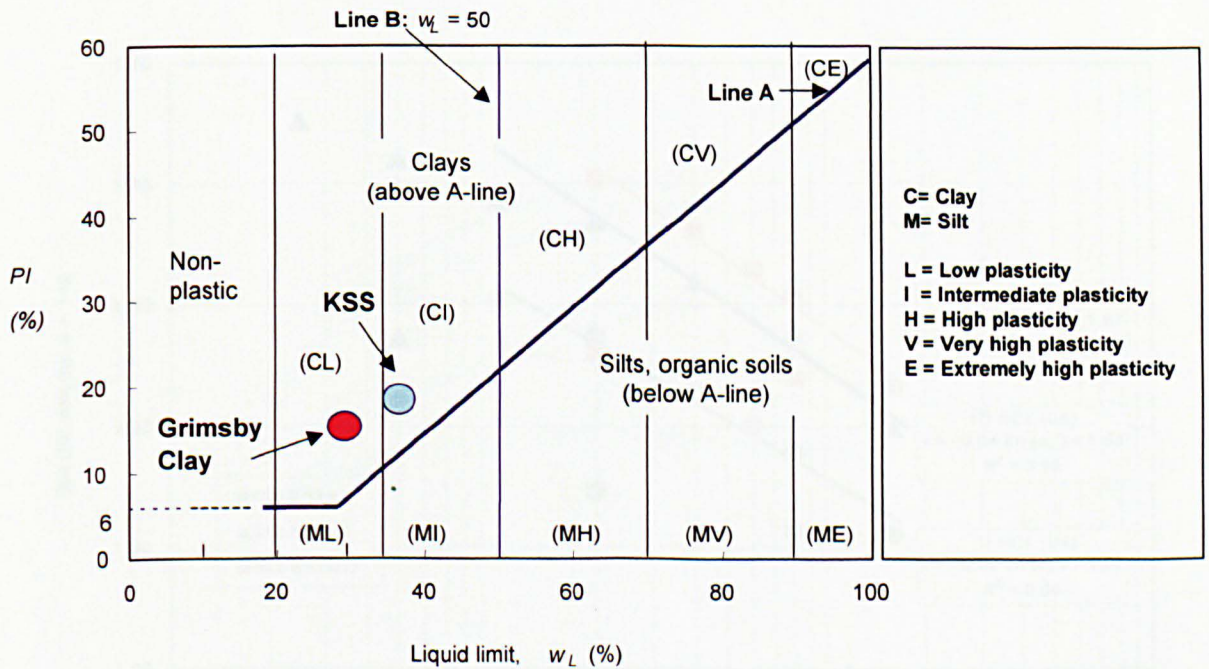


Figure 6.8 Classification of KSS and Grimsby Clay (modified from BS 5930:1981)

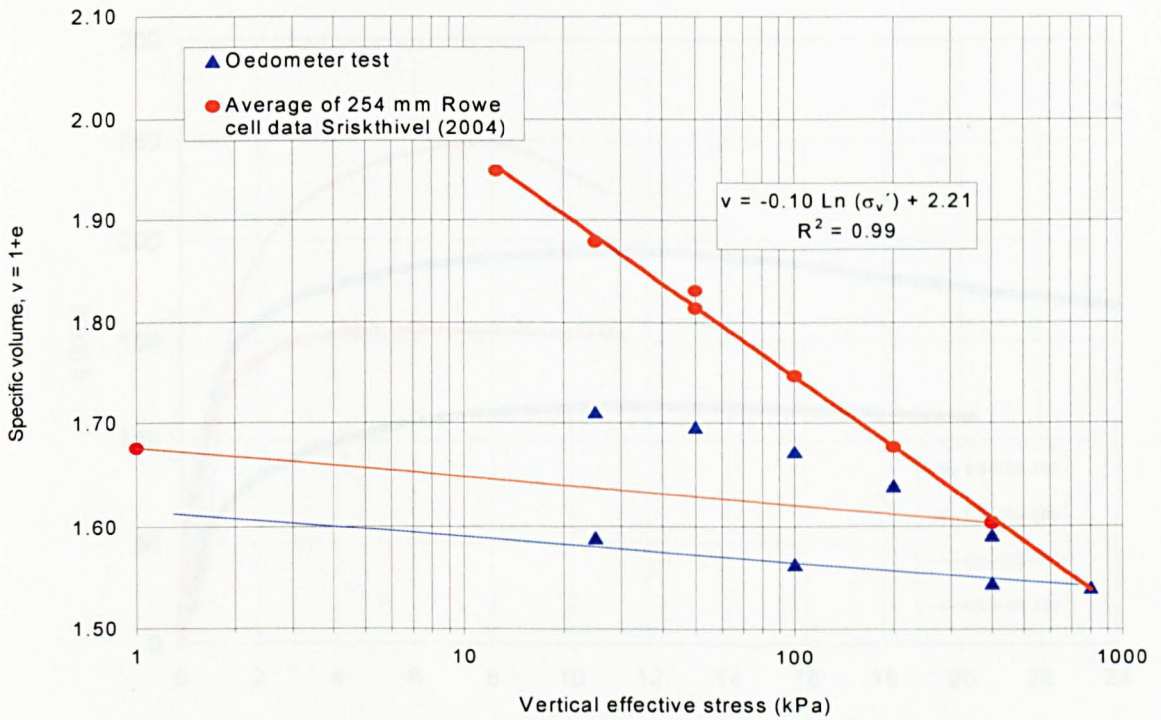


Figure 6.9 Specific volume versus vertical effective stress from 1D consolidation oedometer test and 254mm Rowe cell. Reconstituted KSS clay

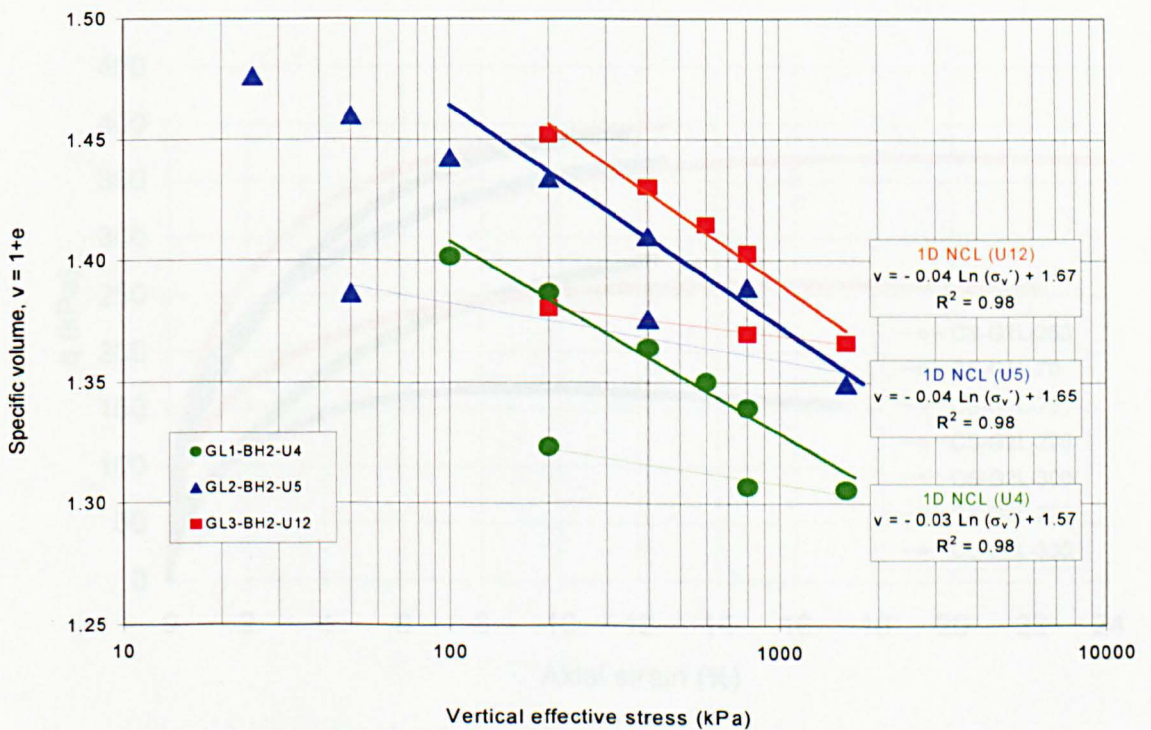


Figure 6.10 Specific volume versus vertical effective stress from 1-D consolidation oedometer tests for undisturbed Grimsby clay

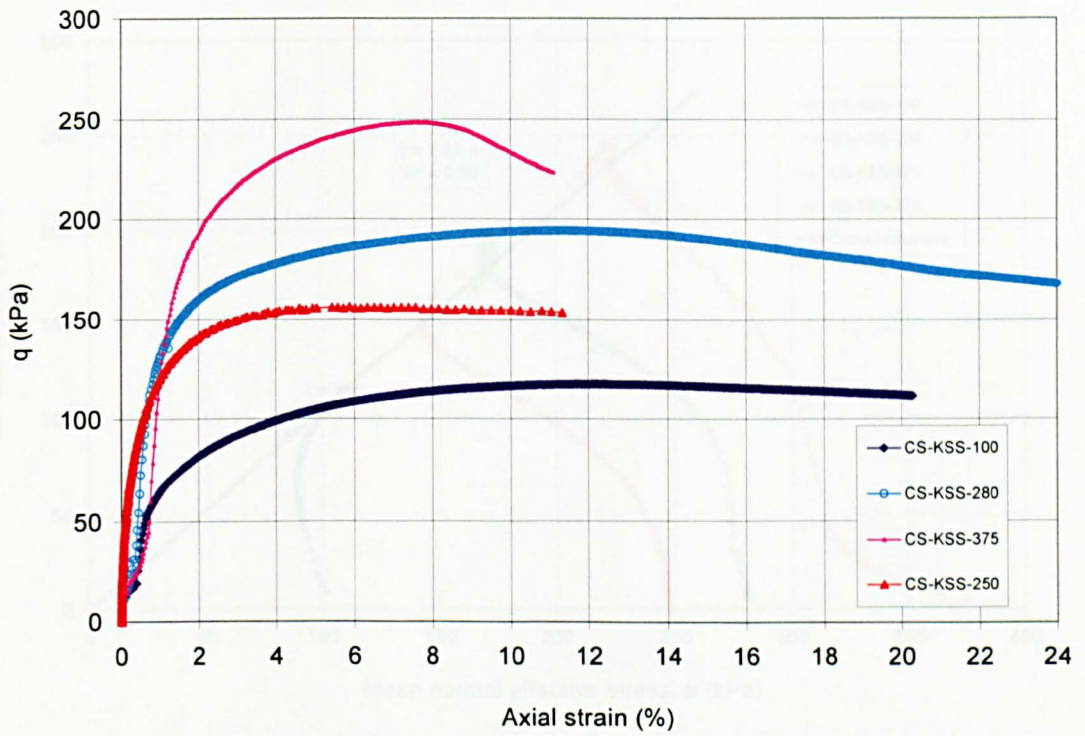


Figure 6.11 Deviator stress versus axial strain. Tests series CS-KSS. Reconstituted KSS clay

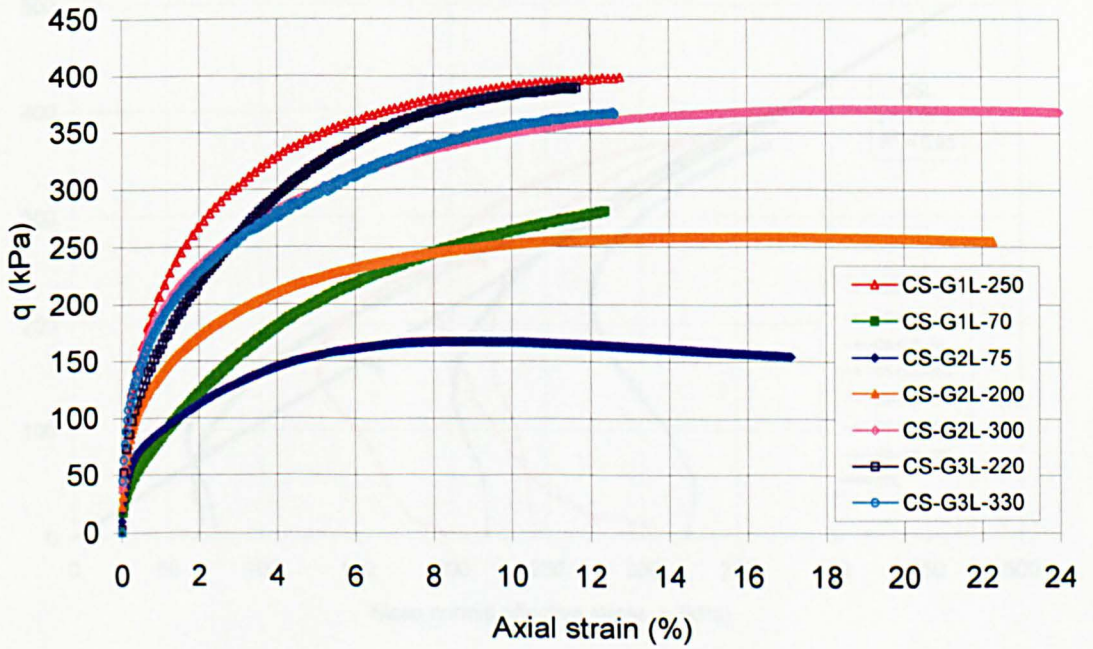


Figure 6.12 Deviator stress versus axial strain. Tests series CS-G. Undisturbed Grimsby clay

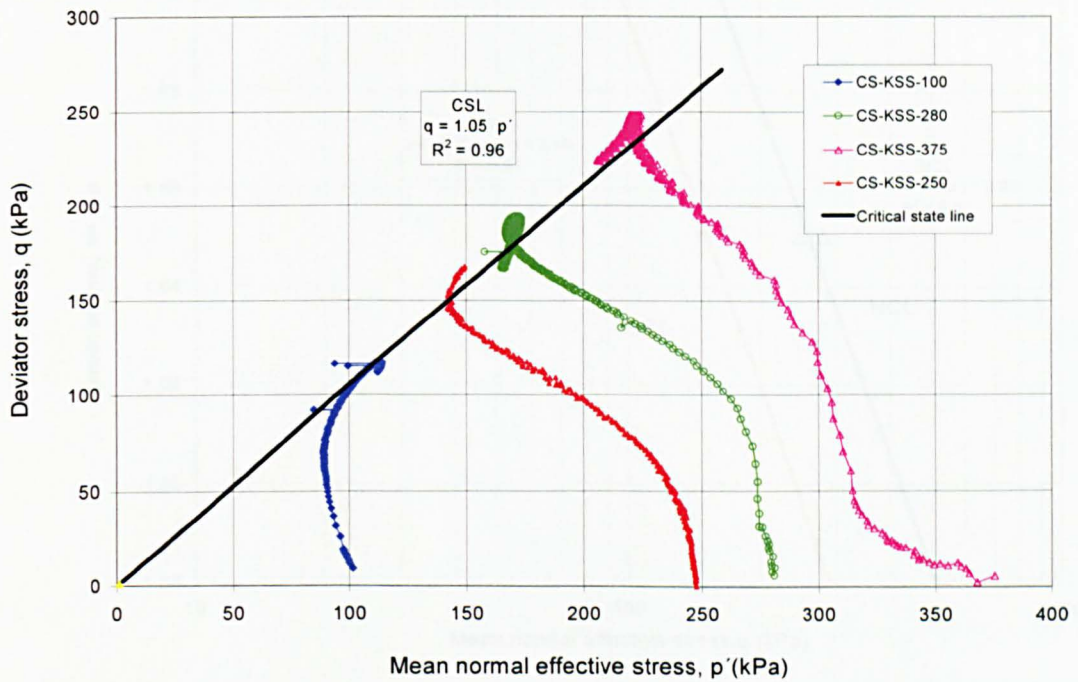


Figure 6.13 Stress paths and critical state line for tests series CS-KSS. Reconstituted KSS clay

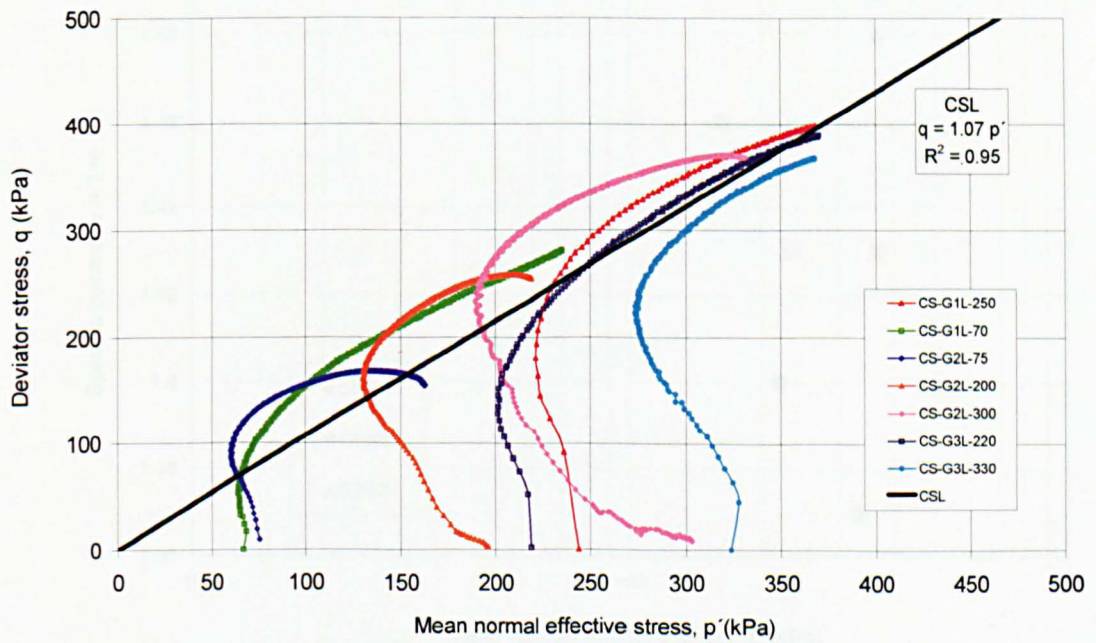


Figure 6.14 Stress paths and critical state line for tests series CS-G. Undisturbed Grimsby clay

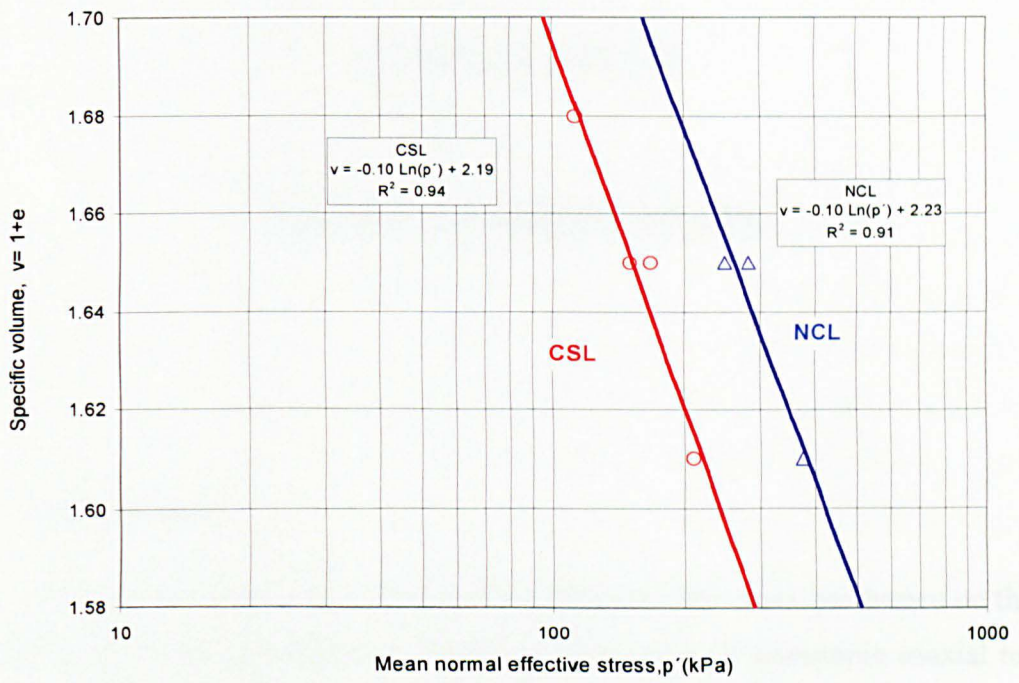


Figure 6.15 Specific volume versus mean normal effective stress from consolidated undrained triaxial tests for reconstituted KSS clay

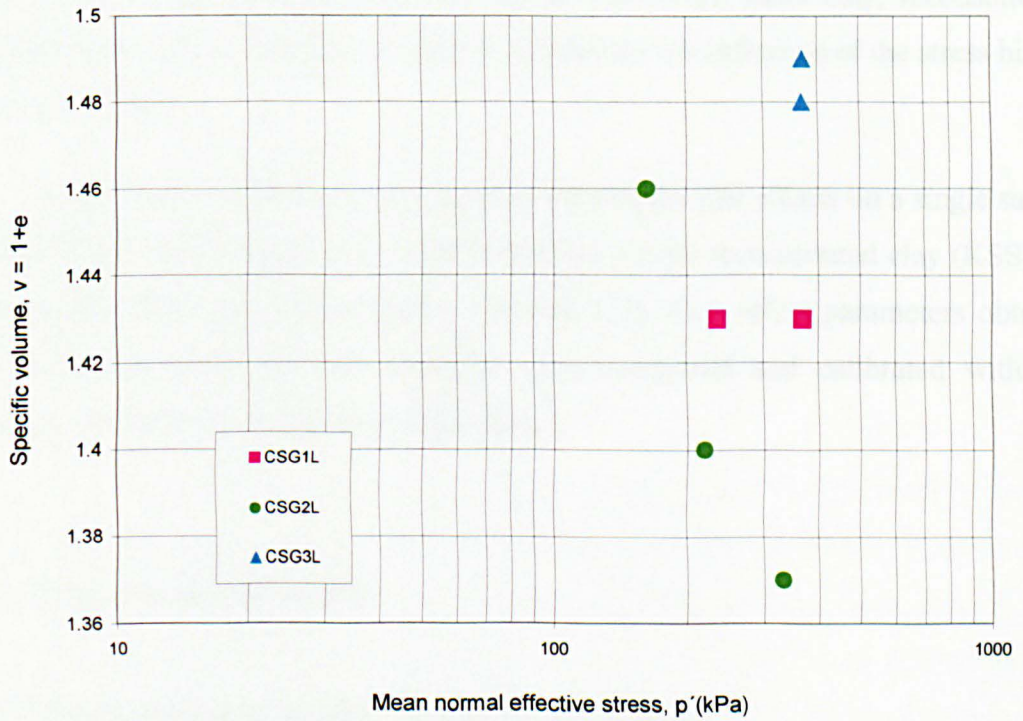


Figure 6.16 Specific volume versus mean normal effective stress from consolidated undrained triaxial tests for undisturbed Grimsby clay

CHAPTER SEVEN

RAPID LOADING TESTS

7.1 Introduction

Consolidated undrained triaxial tests at different rates were performed on the two clay soils previously introduced in Chapter 6. One series of monotonic triaxial tests at seven different rates from 0.001 mm/s up to 200 mm/s was undertaken on the reconstituted clay (KSS) normally consolidated to the same effective stress as that applied in an associated research project in the calibration chamber (Brown, 2004). A similar series of triaxial tests was also carried out on the same clay, reconsolidated under different stress conditions in order to investigate the influence of the stress history on the rate effects.

A multistage method was developed to investigate rate effects on a single sample and multistage rapid loading tests were carried out on the reconstituted clay (KSS) and on the undisturbed clay from Grimsby (Section 6.2). Rate effect parameters obtained from multistage tests for both materials were compared and calibrated with rate parameters obtained from the monotonic tests.

7.2 Reconstituted clay (KSS)

7.2.1 Monotonic rapid loading triaxial tests (OCR=1)

A series of seven tests was carried out to determine rate effects on shear strength of reconstituted clay. The samples were prepared as described in Chapter 5. They were

initially one-dimensionally consolidated to an effective stress of 140 kPa, and then isotropically reconsolidated at an effective stress of 250 kPa before shearing. This was carried out in an attempt to recreate the stress conditions in the clay calibration chamber (Brown, 2004).

Consolidated undrained strain controlled triaxial tests, called OC1-1 to OC1-7, were carried out at 0.001, 0.01, 0.1, 1.03, 10.24, 56.91 and 192.93 mm/s. The sample size was 100 mm in diameter and 200 mm in length and the pore water pressure was measured at mid height. The results of the triaxial shear tests are shown in Figures 7.1 to 7.3. Figure 7.1 shows the deviator stress versus axial strain curves. The deviator stress and hence the shear strength increases as the rate of shearing increases. Figure 7.2 presents the excess pore pressure versus axial strain. The excess pore pressure decreases as the rate of shearing increases. That agrees with the pore pressure response on rapid loading reported by Casagrande & Willson (1951) and Richardson & Whitman (1963) and disagrees with the findings of Adachi & Okano (1974) and Akai *et al.*, (1975) who reported no obvious rate effect on the excess pore pressure and concluded that the excess pore water pressure depends on strain but not strain rate.

During the rapid loading tests for rates higher than 10 mm/s the cell pressure increased due to the rapid change in volume caused by the ram as it penetrated the cell. The pore pressure measured was thus the sum of the excess pore pressure caused during shearing plus an excess pore pressure equal to the increase in cell pressure since the samples were fully saturated before shearing. In order to investigate the rate effects in pore pressure, the excess pore pressure values were corrected for this increase in cell pressure and are plotted in Figure 7.2. A complete description of this phenomenon and the corrections carried out are presented in Appendix 1.

The seven effective stress paths corresponding to the seven different constant strain rates are plotted in Figure 7.3. The strain rate effect caused the dynamic stress path to move away from the static stress path as a consequence of reduced excess pore pressure and hence increase in mean effective stress. Adachi & Okano (1974) reported the same experimental evidence in undrained shear tests at different strain rates presented by Akai *et al.*, (1962), Richardson & Whitman (1963) and Akai *et al.*, (1973), and suggested the existence of dynamic loading surfaces, in the q - p' - v space, that due to

strain rate effects are outside the static state boundary surface given by Roscoe's original critical state energy theory (Roscoe *et al.*, 1958). Yong & Japp (1969) proposed a similar concept of a rate-dependent yield surface, which expands with increasing rates of shearing up to a critical strain rate.

The void ratio, rate of vertical displacement, deviator stress (q) and ratio between dynamic and static deviator stresses (q_d/q_s) at different levels of strain are summarized in Table 7.1. In order to examine the influence of deformation rate on shear strength the data are plotted on deviator stress versus logarithm of normalized axial rate ($\Delta V/V_0$) for different axial strains in Figure 7.4. The rate effects have been evaluated at equal strain states. The increase in deviator stress at each strain state is proportional to the logarithm of normalized deformation rate and hence an empirical model (Equation 7.1) can be used to fit the experimental data,

$$q(\varepsilon, V) = q_0(\varepsilon, V_0) + C_L(\varepsilon) \log\left(\frac{\Delta V}{V_0}\right)$$

Equation 7.1

where $q(\varepsilon, V)$ is dynamic deviator stress, ε is the axial strain, ΔV is the deformation rate (mm/s), V_0 is a static reference deformation rate (0.001 mm/s), $q_0(\varepsilon, v_0)$ is deviator stress at V_0 and $C_L(\varepsilon)$ (with units of stress) is the strain dependent absolute value of the slope of the straight lines obtained when the results of the triaxial tests are plotted in terms of deviator stress versus logarithm of the normalized vertical displacement rate ($\Delta V/V_0$). Figure 7.5 shows the values of $C_L(\varepsilon)$ for the best fit of Equation 7.1 to data from the series of monotonic rapid loading tests on KSS clay at OCR1.

The model proposed (Equation 7.1), is similar to those proposed by Yong & Japp (1969) (Equation 2.11) with data from shock loading triaxial shear tests with strain rates up to 120,000 %/min and Akai *et al.* (1975) for triaxial tests at different constant rates from 0.002 %/min to 50 %/min. The results for $C_L(\varepsilon)$ (Figure 7.5) agree with those reported by Yong & Japp (1969) and Akai *et al.* (1975). The stress parameter $\psi(\varepsilon)$ (Equation 2.11) (with unit of stress), equivalent to $C_L(\varepsilon)$ (Equation 7.1), decreases with strain from a maximum value at small strain (2%) and then tends to asymptotic values

with increasing strains for the tests reported by Yong & Japp (1969) Figure 2.9. For the tests reported by Akai et al (1975) the values increase linearly from zero to an asymptotic value at about 1% strain (Figure 2.12). The results in Figure 7.5 combine both models showing values of $C_L(\varepsilon)$ increasing from zero to a maximum at axial strain lower than 1% and then decreasing from this point to an asymptotic value with increasing strains.

Figures 7.6a, 7.6b, 7.6c and 7.6d show the same data plotted as a deviator stress ratio versus normalised axial displacement rate for different axial strains. Graphs A-1 to M-1 show the results at axial strains from 0.05% to 7% with a best fit to a power law of the form given in Equation 7.2

$$\frac{q_d}{q_s} = 1 + \alpha \left(\frac{\Delta V}{V_0} \right)^\beta - \alpha \left(\frac{0.001}{V_0} \right)^\beta \quad \text{Equation 7.2}$$

where α and β are damping coefficients, as defined by Gibson & Coyle (1968) and Randolph & Deeks (1992), ΔV is axial rate of displacement in mm/s that is normalised by $V_0 = 1000$ mm/s, q_d is the dynamic deviator stress and q_s is the deviator stress at the static reference rate of 0.001 mm/s. The graphs A-2 to M-2 show the same results fitted with the same power law but this time with β fixed equal to 0.20.

The power law in Equation 7.2 is the same non-linear model as that proposed by Gibson & Coyle (1968), Randolph & Deeks (1992) and Hyde et al (2000) and by fixing β equal to 0.20 it is possible to get an expression similar to the laws proposed by Heerema (1979) and Litkouhi & Poskitt (1980) for calculation of pile carrying capacity and driveability using dynamic formulae. They published findings indicating that for end bearing in clays and sands and for skin friction in clays, damping is dependent on the fifth root of velocity (Equation 2.15).

The analysis of the graphs A-1 to M-1 in Figures 7.6a to 7.6c shows that both coefficients, α and β vary with axial strain but by fixing the value of β equal to 0.20 it is possible to define α as function of axial strain as is shown in Figure 7.7 where α remains approximately constant for axial strains of more than 1%. And hence a new expression can be proposed where α is strain dependent (Equation 7.3).

$$\frac{q_d}{q_s} = 1 + \alpha(\varepsilon) \left(\frac{\Delta V}{V_0} \right)^{0.20} - \alpha(\varepsilon) \left(\frac{0.001}{V_0} \right)^{0.20} \quad \text{Equation 7.3}$$

7.2.2 Monotonic rapid loading triaxial tests (OCR=4)

A second series of seven tests was carried out to investigate the influence of the stress history on rate effects. Consolidated undrained strain controlled triaxial tests were carried out at 0.001, 0.01, 1.01, 8.29, 51.76, 157.60 and 172.35 mm/s. The over-consolidation ratio before testing was equal to 4. The results of the triaxial shear tests, called OC4-1 to OC4-7, are shown in Figures 7.8, 7.9 and 7.10. Figure 7.8 shows the deviator stress versus axial strain curves. Figure 7.9 presents the excess pore pressure versus axial strain. The same correction for pore pressure and cell pressure was applied as in the OCR 1 series and was done according with the procedure summarized in Appendix 1. The seven effective stress paths corresponding to the seven different constant strain rates are plotted in Figure 7.10.

The measured deviator stress increased while in the most cases the excess pore pressure decreased when the rate of shearing increased and the rate effects were manifested by the stress paths varying from static stress path as was observed for the OCR1 series. The results from tests OC4-3 and OC4-4 in Figure 7.9 and Figure 7.10 seem to contradict the model but this could be due to the need for pore pressure and cell pressure corrections that were incorrectly assumed negligible for rates lower than 10 mm/s according to the calibration procedure summarized in Appendix 1.

The void ratio, rate of vertical displacement, measured deviator stress (q) and ratio of dynamic to static deviator stresses (q_d/q_s) at different strain states are summarized in Table 7.2. . The rate effects are evaluated at equal strain states as was done before for OCR1 plotting the data as deviator stress versus logarithm of normalized axial rate (V/V_0) for different axial strains in Figure 7.11 and Equation 7.1 is used to fit the experimental data. The deviator stress increase is proportional to the logarithm of the normalized axial rate at all levels of strain as was observed for OCR1. Figure 7.12 shows the values of $C_L(\varepsilon)$ for the best fit of Equation 7.1 to data from series at OCR4.

The same data are also plotted on the ratio of dynamic deviator stress to static deviator stress versus normalised axial displacement rate for different axial strains. The power law in Equation 7.2 is used to fit the results shown in Figures 7.13a, 7.13b, and 7.13c. The graphs A-1 to M-1 show the results at axial strains from 0.05% to 7%, with best fit values of damping coefficients α and β . The graphs A-2 to M-2 in Figures 7.13a, 7.13b and 7.13c show the results fitted with the same power law but with β fixed equal to 0.20.

The analysis of the graphs A-1 to M-1 in Figures 7.13a to 7.13c shows that both coefficients, α and β vary with axial strain. Fixing the value of β equal to 0.20 it is possible to define α as a function of axial strain as is shown in Figure 7.14 where the data are plotted together with data for the OCR1 and OCR4 series. Although the shape of the function $\alpha(\epsilon)$ is similar for both series, the values are higher for OCR1 than for OCR4. The same observation is valid for $C_L(\epsilon)$ in Equation 7.4 (Figure 7.15).

7.2.3 Multistage rapid loading triaxial test. Static rate 0.001 mm/s (OCR=1)

The methodology used for series OC1 and OC4 was appropriate for working with reconstituted soil where a large number of samples could be produced under the same controlled conditions. However it was not suitable to apply the same methodology to study rate effects on undisturbed clay soil from a site investigation borehole where each sample and in situ effective stress conditions varied and the number of samples was limited. Therefore a multistage test technique was developed to study the rate effects on a single sample. A sample was isotropically consolidated in the triaxial cell to the desired initial effective stress and then sheared at 0.001 mm/s up to a 3% axial strain then reconsolidated to the same initial effective stress and sheared again at higher rates up to 3% axial strain. Four or five stages of shearing, with consolidation between each stage, were applied to each sample starting with the static reference rate followed by the higher rates and then a second static reference rate.

Using the multistage test technique it was possible to get rate effect parameters in a similar way as was done with the calibration chamber tests, Brown (2004), where each bed was tested in a multistage way. Once the model pile was installed and the soil

consolidated the pile was then tested under constant rate of penetration (CRP) and Statnamic conditions. The CRP tests were carried out at different rates from static (0.01 mm/s) up to those close to the maximum rate in a Statnamic pulse (500 mm/s) and the Statnamic tests were carried out at different stress levels with the sample being consolidated between each test allowing the excess pore pressure to be dissipated .

(a) Multistage tests at constant rate (0.001 mm/s)

To apply the multistage technique to study the rate effects in single sample it was necessary to know the effects of testing in a multistage manner at a constant static reference rate to distinguish between the effects on measured deviator stress due rate of shearing and the effects on measured deviator stress due to the testing method.

One sample, OC1-MR-001, was prepared in the same way as for series OC1, and was tested using the multistage technique with a constant rate. The sample was initially one-dimensionally consolidated to an effective stress of 140 kPa and then isotropically reconsolidated at an effective stress of 250 kPa before shearing . By testing the sample in a multistage manner with different stages of loading, all at the rate of 0.001 mm/s, it was found that the deviator stress increased at each stage as shown in Figure 7.16. The increase in shear strength was due to the decrease in specific volume during reconsolidation at the initial effective stress before each new loading stage (Figure 7.17) along with fabric changes during loading stages. The void ratio, deviator stress (q) and mean effective stress (p') at different levels of strain are summarized in Table 7.3 for all the stages. In Figure 7.18 the stress paths of the six consecutive tests are plotted, the shape of the curves clearly indicates that the soil became more over-consolidated at each stage. The equal strain contours, as defined by Worth & Loudon (1967), plotted in Figure 7.19 show a linear relationship between the mean effective stress (p') and the deviator stress (q) for all the strains. The value of the slope changes and tends to the critical state value M as the axial strain increases. When the same strain contours are plotted in terms of mean effective stress (p') versus void ratio (e) in Figure 7.20 the strain contour data can be fitted to an expression of the type:

$$e = a_1 \ln p' + a_2 \quad \text{Equation 7.4}$$

where a_1 tends to λ and a_2 tends to $(\Gamma+1)$ as the axial strain increases. M , λ and Γ being the critical state values (Roscoe *et al*, 1958)(Atkinson & Bransby ,1978) as reported in Chapter 6 (Table 6.6). Values of a_1 and a_2 for different strain contours are presented in Table 7.4.

The strain contours can also be plotted in terms of deviator stress (q) versus void ratio (e) using an expression of the type:

$$e = b_1 \ln q + b_2 \quad \text{Equation 7.5}$$

to fit the data as show in Figure 7.21. Values of b_1 and b_2 for different strain contours are presented in Table 7.4.

(b) Multistage tests at different rates

Two samples, prepared as described in Chapter 5, were tested in a multistage manner at different rates to study the rate effects on reconstituted clay. The samples were initially one-dimensionally consolidated to an effective stress of 140 kPa and then isotropically reconstituted at an effective stress of 250 kPa before shearing. The stress conditions were the same as in series OC1 and in test OC1-MR-001. The tests were named OC1-M-001-1 and OC1-M-001-2 .

During the first multistage test, named OC1-M-001-1, the sample was sheared at five strain-controlled loading stages at 0.001, 126.50, 116.35, 0.001 and 59.60 mm/s with a consolidation stage at 250 kPa effective stress between each loading stage. During the second multistage test, named OC1-M-001-2, the sample was sheared at five strain-controlled loading stages at 0.001, 1, 64.62, 80.28 and 0.001 mm/s with a consolidation stage at 250 kPa effective stress between each loading stage.

The results of the triaxial tests at different rates are plotted in terms of deviator stress versus axial strain in Figure 7.22 for OC1-M-001-1 and in Figure 7.23 for OC1-M-001-2. By increasing the rate of shearing the strength increased but there was also an increase in strength when the void ratio decreased during consecutive consolidation stages as was reported before for the multistage test at constant rate OC1-MR-001. The strength for each test depends not only on the rate of shearing but also on the fabric

changes and void ratio of the sample at each test as was observed first in test OC1-MR-001. In order to investigate the rate effects, the measured deviator stress had to be normalized. By testing the sample at 0.001 mm/s a second time at a different void ratio it was possible, in the same way as was done before for OC1-MR-001, to define equal strain contour lines for a rate of 0.001 mm/s in terms of deviator stress versus void ratio as shown in Figure 7.24 for OC1-M-001-1 and Figure 7.25 for OC1-M-001-2 .

The equal strain contour lines represent the deviator stress expected if the tests were performed at 0.001 mm/s for all the loading stages and could be used to predict the static deviator stress at each stage. The value of the void ratio before shearing is known for all the tests and the static deviator stress can be deduced from the equations of the the equal strain contour lines as shown in Figure 7.24 for OC1-M-001-1 and Figure 7.25 for OC1-M-001-2 .

For each loading stage at rates higher than 0.001 mm/s there was a measured deviator stress from now on called the dynamic deviator stress q_d and a deduced deviator stress for 0.001 mm/s that lies on the equal strain contour line which is from now on called the static deviator stress q_s , as shown in Figure 7.24 for OC1-M-001-1 and Figure 7.25 for OC1-M-001-2 . Void ratio, vertical rate of displacement, measured deviator stress, static deviator stress and ratio between dynamic and static deviator stress are summarized on Table 7.5 for OC1-M-001-1 and Table 7.6 for OC1-M-001-2.

The results are plotted as dynamic to static deviator stress ratio versus axial displacement rate for various axial strains. The same power law (Equation 7.2) as was used for series OC1 and OC4 has been fitted to the data in Figure 7.26 for OC1-M-001-1 , in Figure 7.27 for OC1-M-001-2.and for both tests together in Figure 7.28.

The analysis of the graphs A to H in Figures 7.26, 7.27 and 7.28 shows that assuming $\beta = 0.20$ is possible to define α as function of axial strain as is shown in Figure 7.29 for each test separately and in Figure 7.30 for the data of both tests together, where α remains approximately constant above an axial strain of 1%.

The validity of applying the non linear model (Equation 7.2) to the experimental data from multistage rapid loading tests was assumed based on the analysis of

experimental data from monotonic rapid loading series (Sections 7.2.1 and 7.2.2) and evidence reported by researchers such as Gibson & Coyle (1968) or Randolph & Deeks (1992). The α values obtained from single stage tests on reconstituted clay (KSS) (Figure 7.7) were however lower than those obtained from corresponding multistage tests (Figure 7.30). The limited amount of data obtained from a multistage test, usually consisting of a set of data from a maximum of four to five different rates, constituted the main shortcoming of the method since the non linear model (Equation 7.2) had to be fitted to a small number of data points. The α values obtained fitting the non linear model to experimental data had an associated standard error (Figures 7.6, 7.26, 7.27 and 7.27) that should be considered when damping parameters from different tests or different soils are compared. The average standard errors of α for series OC1, tests OC1-M-001-1, OC1-M-001-2, and OC1-M-001-1&2 considered together were respectively ± 0.05 , 0.09, 0.16, and 0.10.

Based on the results plotted in Figure 7.29 the author considered the multistage tests on reconstituted clay (KSS) to be repeatable, considering $\alpha \pm$ standard error for each test. When the multistage method is used to investigate rate effects it is also recommended that more than one multistage test be carried out in order to obtain a bigger set of data and hence a better fit to determine rate effects parameters in Equation 7.2 as was done for reconstituted clay (KSS) (Figures 7.28 and 7.30).

7.2.4 Multistage rapid loading triaxial test. Static rate 0.01 mm/s (initial OCR=1)

The static rate for triaxial tests on reconstituted clay for series OC1, OC4 and tests OC1-MR-001, OC1-M-001-1 and OC1-M-001-2 was 0.001 mm/s based on a calculation taking into account consolidation time and calculated time to failure following the recommendations for minimum rate of testing in BS 1377-8:1990. The conventional static rate for constant rate of penetration (CRP) pile testing is however 0.01 mm/s (ICE, 1997). It was decided therefore to carry out a multistage testing programme with 0.01 mm/s as a static reference rate and compare the results with the results from tests with 0.001 mm/s as static rate.

(a) Multistage tests at constant rate (0.01 mm/s)

Two samples of reconstituted clay were tested in a multistage manner at a constant rate. Both samples were prepared as described in Chapter 5. The stress conditions were the same as in tests OC1-MR-001 and OC1-M-001-1 and OC1-M-001-2. The tests were named OC1-MR-01-1 and OC1-MR-01-2.

The aims of these tests was to define equal strain contour lines at 0.01 mm/s as was done for OC1-MR-001 at 0.001 mm/s and check the repeatability of the multistage testing method for a constant rate.

During the multistage test OC1-MR-01-1, the sample was sheared at four strain controlled loading stages at 0.01mm/s with a consolidation stage at 250 kPa effective stress between each loading stage. The tests were undertaken up to a maximum axial strain of 3%. During the multistage test OC1-MR-01-2, the sample was sheared at five strain controlled loading stages at 0.01 mm/s with a consolidation stage at 250 kPa effective stress between each loading stage. The tests were undertaken up to a maximum axial strain of 3%.

The results of the tests are plotted in Figure 7.31 for OC1-MR-01-1 and Figure 7.32 for OC1-MR-01-2 in terms of deviator stress versus axial strain. In both tests the shear strength increased at each stage as was observed before in OC1-MR-001 and as in that case the stress paths plotted in Figure 7.33 for OC1-MR-01-1 and Figure 7.34 for OC1-MR-01-2 show that the samples became more over-consolidated after each new loading and reconsolidation stage. The equal-strain contours in Figure 7.35 for OC1-MR-01-1 and Figure 7.36 for OC1-MR-01-2 again show a linear relationship between the mean effective stress (p') and the deviator stress (q) for all the strains. The void ratio, deviator stress (q) and mean effective stress (p') at different strain states are summarized in Table 7.7 for OC1-MR-01-1 and Table 7.8 for OC1-MR-01-2.

Equation 7.4 and Equation 7.5 used before for OC1-MR-001 were also fitted to data from multistage tests where the static reference rate was 0.01 mm/s as shown in Figures 7.37 , 7.38, 7.39 and 7.40. Values of a_1 , a_2 , b_1 and b_2 for different strain contours are presented in Table 7.9 for OC1-MR-01-1 and Table 7.10 for OC1-MR-01-2 .

These results confirm the validity of the concept of equal strain contour lines, as defined in Section 7.2.3.a, for multistage tests carried out at 0.01 mm/s and provide evidence of good repeatability of the results obtained for multistage tests at constant loading rate.

(b) Multistage tests at different rates

A further sample of reconstituted clay was tested in a multistage manner at different rates. The stress conditions were the same as in previous tests for OCR 1.

During the multistage test, OC1-M-01, the sample was sheared at five strain-controlled loading stages at 0.01, 1.02, 47.62, 32.53 and 0.01 mm/s with a consolidation stage at 250 kPa effective stress between each loading stage.

The results of the triaxial tests at different rates are plotted in terms of axial strain versus deviator stress in Figure 7.41. There was an increase in the measured deviator stress due to the increase in the rate of shearing, the fabric changes during loading each loading stage and the reduction of void ratio during consecutive consolidation stages. With the data from the loading stages carried out at 0.01 mm/s, it was possible to define the equal strain contour lines for the rate of 0.01 mm/s in the same way as was done before for OC1-M-001-1 and OC1-M-001-2 in terms of deviator stress versus void ratio as shown in Figure 7.42, where the equal strain contour lines represent the static deviator stress (q_s) at 0.01 mm/s expected at each stage and the measured deviator stress for rates higher than 0.01 mm/s represent the dynamic deviator stress (q_d). Void ratio, vertical rate of displacement, measured deviator stress, static deviator stress and ratio between dynamic and static deviator stress are summarized in Table 7.11. The ratio of dynamic to static deviator stress versus rate of shearing are plotted on Figure 7.43 a and Figure 7.43 b. The power law (Equation 7.2), used for series OC1 and OC4 and tests OC1-M-001-1 and OC1-M-001-2, was also used here to fit the data. Graphs A-1 to F-1 show the results at different axial strains from 0.1% up to 2% with variable α and β . The graphs A-2 to F-2 show the results fitted to the same power law but with β fixed equal to 0.20.

7.2.5 Multistage rapid loading triaxial test. Static rate 0.01 mm/s (initial OCR=4)

One sample of reconstituted clay was tested in a multistage manner at different rates as in Section 7.2.4b but at OCR = 4, not 1. The sample, prepared as described in Chapter 5, was initially one-dimensionally consolidated to an effective stress of 140 kPa, then isotropically reconsolidated at an effective stress of 400 kPa and allowed to swell to 100 kPa before shearing. The initial OCR was 4.

During the multistage test, OC4-M-01, the sample was sheared at five strain-controlled loading rates of 0.01, 10.31, 54.23, 154.86 and 0.01 mm/s. Between each loading stage the excess pore water pressure was allowed to redistribute under undrained conditions. It was observed that after one hour the measured excess pore water pressure at mid-height disappeared and a new consolidation stage between each loading stage was unnecessary. The results of the triaxial tests at different rates are plotted in terms of axial strain versus deviator stress in Figure 7.44. In this case there was no volume change between loading stages as shown in Figure 7.45, the void ratio stayed constant and the increase in measured deviator stress can be assumed to be due to rate effects. The measured deviator stress for the first loading stage carried out at 0.01 mm/s represents the static deviator stress (q_s) at 0.01 mm/s expected for all the loading stages and the measured deviator stress for rates higher than 0.01 mm/s represents the dynamic deviator stress (q_d). Void ratio, vertical rate of displacement, measured deviator stress, static deviator stress and the ratio between dynamic and static deviator stress are summarized in Table 7.12. The ratio of dynamic to static deviator stress versus rate of shearing are plotted on Figure 7.46 a and Figure 7.46 b. The power law (Equation 7.2), used before for series OC1 and OC4 and multistage tests at OCR 1, was used to fit the data. Graphs A-1 to H-1 show the best fit results at different axial strains from 0.1% up to 3% where α and β were allowed to vary. Graphs A-2 to H-2 show the results fitted with the same power law but with β fixed at 0.20.

7.2.6 Multistage rapid loading triaxial test. Static rate 0.01 mm/s (initial OCR=8)

One sample of reconstituted clay was tested in a multistage manner at different rates as in Section 7.2.4b and 7.2.5 but at OCR = 8, not 1 or 4. The sample, prepared as described in Chapter 5, was initially one-dimensionally consolidated to an effective

stress of 140 kPa, then isotropically reconsolidated at an effective stress of 400 kPa and allowed to swell to 50 kPa before shearing. The initial OCR was equal to 8.

During the multistage test, OC8-M-01, the sample was sheared at five strain-controlled loading rates of 0.01, 1.04, 55.91, 171.46 and 0.01 mm/s with consolidation at 50 kPa effective stress between each loading stage.

The results of the triaxial tests at different rates are plotted in terms of axial strain versus deviator stress in Figure 7.47. There was an increase in the measured deviator stress due to the increase in the rate of shearing, the fabric changes during each loading stage and the reduction of void ratio during consecutive consolidation stages. With the data from the loading stages carried out at 0.01 mm/s, it was possible to define the equal strain contour lines for the rate of 0.01 mm/s in the same way as was done before for OC1-M-01-1 in terms of deviator stress versus void ratio as shown in Figure 7.48, where the equal strain contour lines represent the static deviator stress (q_s) at 0.01 mm/s expected at each stage and the measured deviator stress for rates higher than 0.01 mm/s represent the dynamic deviator stress (q_d). Void ratio, vertical rate of displacement, measured deviator stress, static deviator stress and ratio of dynamic to static deviator stress are summarized in Table 7.13. The ratio of dynamic to static deviator stress versus rate of shearing are plotted on Figure 7.49 a and Figure 7.49 b. The power law (Equation 7.2) used before for series OC1 and OC4 and multistage tests at OCR 1 and 4, was used to fit the data. Graphs A-1 to H-1 show the results at different axial strains from 0.1% up to 3% with variable α and β . The graphs A-2 to H-2 show the best fit with the same power law but with β fixed at 0.20.

Figure 7.50 shows that, considering $\beta = 0.20$, similar α values were obtained for multistage tests carried out on samples initially consolidated to OCR1, 4 and 8. The correlation of the damping parameter α with OCRs was not evident. For OCR1, the values of α obtained for multistage rapid loading tests with static reference rate equal to 0.001 mm/s (Figure 7.30) are similar to those obtained with static reference rate equal to 0.01 mm/s (Figure 7.50), therefore the author felt justified in assuming there was a negligible influence on the determination of rate effect parameters using multistage rapid loading tests from selecting static rates based either on recommendations for minimum rate of testing in BS 1377- 8:1990 (0.001 mm/s) or based on the definition of

conventional static rate for constant rate of penetration (CRP) pile testing (0.01 mm/s) (ICE, 1997).

7.3 Undisturbed clay (Grimsby)

7.3.1 Multistage tests

(a) Multistage test at constant rate (0.001 mm/s)

One multistage triaxial test at a constant rate was carried out on undisturbed clay. The sample U-9 BH1 (10.45 m depth), was taken from Bore Hole 1 at the Grimsby site (Section 6.2). Before testing the sample was saturated and isotropically reconsolidated to the in situ overburden effective pressure (145 kPa).

The aim of this test was to define equal strain contour lines at 0.001 mm/s on undisturbed clay (Grimsby) as was done for OC1-MR-001 for reconstituted clay.

During the multistage test, GMR2L, the sample was sheared at six strain controlled loading stages at 0.001mm/s with a consolidation stage at 145 kPa effective stress between each loading stage.

The results of the test are plotted in Figure 7.51 in terms of deviator stress versus axial strain. The measured deviator stress increased at each stage as was observed before in OC1-MR-001 for reconstituted clay and as in that case the stress paths plotted in Figure 7.52 show that the sample became more over-consolidated after each new loading and reconsolidation stage. The equal-strain contours in Figure 7.53 show a linear relationship between the mean effective stress (p') and the deviator stress (q) for all the strains, as was observed for OC1-MR-001, although this relationship is clearer for strains greater than 1.5% when the value of the slope tends to the critical state value M . Void ratio, deviator stress (q) and mean effective stress (p') at different strain states are summarized in Table 7.14.

Equations 7.5 and 7.6 used before for OC1-MR-001 were also fitted to data from multistage tests at a constant rate on undisturbed clay in GMR2L as shown in

Figures 7.54 and 7.55 respectively. Values of a_1 , a_2 , b_1 and b_2 for different strain contours are presented in Table 7.15 .

The results of this test corroborate the existence of equal strain contour lines for undisturbed clay (Grimsby) and justify their use in multistage rapid loading tests to determine the corresponding static deviator stress (at 0.001 mm/s) for each loading stage. It was found as was observed before for reconstituted clay (KSS) that as the strain increases the slope of the equal strain contour lines in the q - p' space tended to M , and the parameter a_1 in Equation 7.5 that fits the equal strain contour lines in the e - p' space tended to λ , M and λ being the critical state parameters for undisturbed clay (Grimsby) (Table 6.6).

(b) Multistage tests at different rates

Three samples of undisturbed clay were tested in a multistage manner at different rates. The aim of the tests, called GM1L, GM2L and GM3L, was to investigate the rate effects on undisturbed clay (Grimsby) on samples obtained at different depths at Grimsby site (Section 6.2). The samples were isotropically reconsolidated to the in situ effective overburden pressure.

During the first multistage test, GM1L, the sample was sheared at five strain-controlled loading stages at 0.001, 1.03, 54.01, 113.03 and 0.001 mm/s with a consolidation stage at 70 kPa effective stress between each loading stage. During the second multistage test, GM2L, the sample was sheared at five strain-controlled loading rates of 0.001, 1, 60.94, 0.001 and 0.05 mm/s with a consolidation stage at an effective stress of 135kPa between each loading stage. During the third multistage test, GM3L, the sample was sheared at five strain-controlled loading stages at 0.001, 1, 49.40, 49.11, 0.001 and 0.1 mm/s with a consolidation stage at 220 kPa effective stress between each loading stage.

The results of the triaxial tests at different rates are plotted in terms of axial strain versus deviator stress in Figure 7.55 for GM1L, Figure 7.56 for GM2L, and Figure 7.57 for GM3L. There was an increase in shear strength due to the increase in the rate of shearing, the fabric changes during each loading stage and the reduction of void ratio during consecutive consolidation stages. With the data from the loading

stages carried out at 0.001 mm/s, it was possible to define the equal strain contour lines for the rate of 0.001 mm/s in the same way as was done for multistage tests on reconstituted clay (KSS).

The results are plotted in terms of deviator stress versus void ratio in Figure 7.59 for GM1L, Figure 7.60 for GM2L and Figure 7.61 for GM3L, where the equal strain contour lines represent the static deviator stress (q_s) at 0.001 mm/s expected at each stage and the measured deviator stress represents the dynamic deviator stress (q_d) for rates higher than 0.001 mm/s. Void ratio, rate of vertical displacement, measured deviator stress, static deviator stress and ratio between dynamic and static deviator stress are summarized in Table 7.16 for GM1L, Table 7.17 for GM2L and Table 7.18 for GM3L. The ratios of dynamic to static deviator stress versus rate of shearing are plotted on Figure 7.62 a and Figure 7.62 b for GM1L, Figure 7.63 a and Figure 7.63 b for GM2L, Figure 7.64 a and Figure 7.64 b for GM3L and Figure 7.65 a and 7.65 b for all the data together. The power law, used before for reconstituted clay (Equation 7.2), was used to fit the data. Graphs A-1 to G-1 show the results at different axial strains from 0.1% up to 2.5% where α and β were allowed to vary. The graphs A-2 to G-2 show the results fitted with the same power law but with β fixed at 0.20.

Figure 7.66 shows that, assuming $\beta = 0.20$, similar α values were obtained for tests carried out on undisturbed clay (Grimsby) samples taken at different depths. It was reasonable therefore to consider all the data from the three tests together to define a unified rate effect soil model for the clay at the site in Grimsby. The model is shown in Figure 7.67, where α varies with strain and tends to 0.90 for strains higher than 0.5%.

7.3.2 Monotonic rapid loading triaxial tests

In order to check the validity of the empirical models proposed in 7.3.1 based on Equation 7.2 with values of α and β at different depths from multistage tests GM1L, GM2L and GM3L, two monotonic consolidated undrained triaxial tests were carried out at a high rate. The tests were named GR2L, and GR3L.

The undisturbed sample U-6 BH1 from bore hole 1 at Grimsby site (Section 6.2) was used for test GR2L. The sample was saturated and isotropically reconsolidated to

the same initial stress conditions applied for the multistage tests GM2L and then sheared at 131.50 mm/s. The result of this test together with the first loading stage for GM2L at 0.001 mm/s (renamed as GS2L) are plotted in Figure 7.68 in terms of axial strain versus deviator stress. The values of the deviator stress at different axial strains on GS2L were used as static deviator stress (q_s) at 0.001 mm/s and the measured deviator stress on GR2L was used as the dynamic deviator stress (q_d) at 131.50 mm/s in the power law in Equation 7.2 with β equal to 0.20. Hence the values of α were deduced for different strains and compared with the values obtained for GM1L, GM2L and GM3L (Figures 7.70 and 7.71).

The undisturbed sample U-9 BH2 from bore hole 2 at the Grimsby site (Section 6.2) was used for test GR3L. The sample was saturated and reconsolidated to the same initial stress conditions applied for the multistage tests GM3L and then sheared at 112.28 mm/s. The result of this test together with the first loading stage for GM3L at 0.001 mm/s (renamed as GS3L) are plotted in Figure 7.69 in terms of axial strain versus deviator stress. The values of the deviator stress at different axial strains on GS3L were used as static deviator stress (q_s) at 0.001 mm/s and the values of the measured deviator stress on GR2L were used as the dynamic deviator stress (q_d) at 131.50 mm/s in the power law in Equation 7.2 with β equal to 0.20. Hence values of α were deduced for different strains and compare with the values obtained for GM1L, GM2L and GM3L (Figure 7.70 and 7.71).

Figure 7.71 shows a good agreement between α values obtained from single stage tests (GS2L versus GR2L and GS3L versus GR3L) and those corresponding to multistage tests (GM1L, GM2L and GM3L) that validated the use of multistage rapid loading tests to obtain reliable damping coefficient parameters (α and β) in Equation 7.2 for undisturbed clay (Grimsby).

7.4 Application of multistage tests to determine critical state parameters

The results from multistage triaxial tests at constant rate (0.001 mm/s) carried out on KSS and Grimsby clay reported in Section 7.2.3.a and Section 7.3.1.a show that the slope of the equal strain contour lines defined in the q - p' space (Figures 7.19 and

7.53) and the parameters a_1 and a_2 (Tables 7.4 and 7.15) in Equation 7.5 that fit the same equal strain contours lines in the $e-p'$ space (Figures 7.20 and 7.54) might be used to determine the critical state parameters, M , λ and Γ (Roscoe *et al*, 1958)(Atkinson & Bransby, 1978) (Table 6.6), since the slope of the equal strain contour lines in $q-p'$ tends to M and a_1 and a_2 tend to λ and $(\Gamma+1)$ respectively.

The results from multistage tests at constant rate (0.01 mm/s) on reconstituted clay (KSS) reported in Section 7.2.4 (Figures 7.35 and 7.36 and Tables 7.9 and 7.10) confirm the repeatability of the method although the slope of the equal strain contour lines in the $q-p'$ space, the parameter a_1 and a_2 and hence the corresponding deduced M , λ and Γ values slightly differ from those obtained from multistage test at 0.001 mm/s and single stage consolidated undrained triaxial tests carried out at 0.001 mm/s (Section 6.4) almost certainly due to the different testing rate.

The multistage test at constant rate as defined in Sections 7.2.3.a and 7.3.1a. represents a method of obtaining a good approximation of the critical state parameters, M , λ and Γ by testing on a single sample instead of carrying out a series of monotonic consolidated undrained (or drained) triaxial tests and isotropic consolidation tests that require the use of a set of similar samples not always available. The application of such a technique could be appropriate for site investigation boreholes where samples and in situ effective stress conditions may vary and the number of samples are limited. The results of tests carried out on reconstituted KSS clay and undisturbed Grimsby clay are encouraging but further research is required to check the validity of the method on different soils and at stress conditions.

Test		OC1-1	OC1-2	OC1-3	OC1-4	OC1-5	OC1-6	OC1-7
e		0.65	0.69	0.64	0.65	0.66	0.66	0.68
Rate (mm/s)		1.00E-03	0.01	0.1	1.03	10.24	56.91	192.93
$\varepsilon = 0.05\%$	q (kPa)	62	64	77	77	103	93	105
	qd/qs	1.00	1.03	1.24	1.24	1.66	1.50	1.69
$\varepsilon = 0.1\%$	q (kPa)	74	89	92	107	148	121	127
	qd/qs	1.00	1.20	1.24	1.45	2.00	1.64	1.72
$\varepsilon = 0.3\%$	q (kPa)	97	111	119	131	148	159	167
	qd/qs	1.00	1.14	1.23	1.35	1.53	1.64	1.72
$\varepsilon = 0.5\%$	q (kPa)	109	121	128	138	154	165	182
	qd/qs	1.00	1.11	1.17	1.27	1.41	1.51	1.67
$\varepsilon = 1.0\%$	q (kPa)	123	134	133	150	163	168	189
	qd/qs	1.00	1.09	1.08	1.22	1.33	1.37	1.54
$\varepsilon = 1.5\%$	q (kPa)	130	140	138	157	167	168	190
	qd/qs	1.00	1.08	1.06	1.21	1.28	1.29	1.46
$\varepsilon = 2.0\%$	q (kPa)	134	143	146	163	171	178	195
	qd/qs	1.00	1.07	1.09	1.22	1.28	1.33	1.46
$\varepsilon = 2.5\%$	q (kPa)	141	148	153	166	176	178	196
	qd/qs	1.00	1.05	1.09	1.18	1.25	1.26	1.39
$\varepsilon = 3.0\%$	q (kPa)	145	150	169	170	180	182	198
	qd/qs	1.00	1.03	1.17	1.17	1.24	1.26	1.37
$\varepsilon = 4.0\%$	q (kPa)	150	--	--	--	185	--	206
	qd/qs	1.00	--	--	--	1.23	--	1.37
$\varepsilon = 5.0\%$	q (kPa)	152	--	--	--	190	--	210
	qd/qs	1.00	--	--	--	1.25	--	1.38
$\varepsilon = 6.0\%$	q (kPa)	157	--	--	--	194	--	213
	qd/qs	1.00	--	--	--	1.24	--	1.36
$\varepsilon = 7.0\%$	q (kPa)	163	--	--	--	198	--	216
	qd/qs	1.00	--	--	--	1.21	--	1.33

Table 7.1 Result of monotonic rapid loading tests on KSS (OCR=1).

Test		OC4-1	OC4-2	OC4-3	OC4-4	OC4-5	OC4-6	OC4-7
e_{400}		0.58	0.58	0.58	0.58	0.58	0.59	0.55
e_{100}		0.60	0.60	0.60	0.59	0.59	0.61	0.58
Rate (mm/s)		1.00E-03	0.01	1.01	8.28	51.76	157.60	172.35
$\varepsilon = 0.1\%$	q (kPa)	55	55	74	--	88	90	86
	qd/qs	1.00	1.00	1.35	--	1.60	1.64	1.56
$\varepsilon = 0.3\%$	q (kPa)	71	78	91	--	--	119	115
	qd/qs	1.00	1.10	1.28	--	--	1.68	1.62
$\varepsilon = 0.5\%$	q (kPa)	81	89	103	108	115	135	130
	qd/qs	1.00	1.10	1.27	1.33	1.42	1.67	1.60
$\varepsilon = 1.0\%$	q (kPa)	109	109	120	124	124	150	134
	qd/qs	1.00	1.00	1.10	1.14	1.14	1.38	1.23
$\varepsilon = 1.5\%$	q (kPa)	120	122	132	138	132	167	155
	qd/qs	1.00	1.02	1.10	1.15	1.10	1.39	1.29
$\varepsilon = 2.0\%$	q (kPa)	134	132	142	148	143	177	163
	qd/qs	1.00	0.99	1.06	1.10	1.07	1.32	1.22
$\varepsilon = 2.5\%$	q (kPa)	141	140	149	157	149	184	172
	qd/qs	1.00	0.99	1.06	1.11	1.06	1.30	1.22
$\varepsilon = 3.0\%$	q (kPa)	146	147	155	164	157	190	177
	qd/qs	1.00	1.01	1.06	1.12	1.08	1.30	1.21
$\varepsilon = 4.0\%$	q (kPa)	158	158	168	175	169	204	191
	qd/qs	1.00	1.00	1.06	1.11	1.07	1.29	1.21
$\varepsilon = 5.0\%$	q (kPa)	167	166	178	184	180	213	201
	qd/qs	1.00	0.99	1.07	1.10	1.08	1.28	1.20
$\varepsilon = 6.0\%$	q (kPa)	173	172	187	193	191	220	209
	qd/qs	1.00	0.99	1.08	1.12	1.10	1.27	1.21
$\varepsilon = 7.0\%$	q (kPa)	179	177	195	199	198	--	217
	qd/qs	1.00	0.99	1.09	1.11	1.11	--	1.21

Table 7.2 Results of monotonic rapid loading tests on KSS (OCR=4)

Test		OC1-MR-001-A	OC1-MR-001-B	OC1-MR-001-C	OC1-MR-001-D	OC1-MR-001-E	OC1-MR-001-F
e		0.684	0.666	0.652	0.64	0.633	0.625
$\varepsilon = 0.5\%$	q (kPa)	98	138	167	174	186	201
	p' (kPa)	198	211	225	229	238	243
$\varepsilon = 1.0\%$	q (kPa)	113	159	194	216	234	253
	p' (kPa)	173	195	217	232	246	259
$\varepsilon = 1.5\%$	q (kPa)	121	166	203	230	248	270
	p' (kPa)	158	186	213	231	247	265
$\varepsilon = 2.0\%$	q (kPa)	126	170	207	235	254	275
	p' (kPa)	149	179	209	231	248	268
$\varepsilon = 2.5\%$	q (kPa)	130	173	209	--	--	278
	p' (kPa)	143	176	206	--	--	270

Table 7.3 Results of multistage test at constant rate (0.001 mm/s) on KSS.

Axial strain		$\varepsilon = 0.5\%$	$\varepsilon = 1.0\%$	$\varepsilon = 1.5\%$	$\varepsilon = 2.0\%$	$\varepsilon = 2.5\%$
p'-e	a ₁	-0.283	-0.146	-0.115	-0.101	-0.101
	a ₂	2.182	1.438	1.266	1.190	1.188
	R ²	0.99	0.99	0.99	0.99	0.99
q-e	b ₁	-0.082	-0.073	-0.074	-0.076	-0.077
	b ₂	1.062	1.033	1.041	1.052	1.061
	R ²	0.95	0.98	0.99	0.99	0.99

Table 7.4 Parameters a₁, a₂, b₁, b₂ for equal strain contours on multistage test OC1-MR-001

Test		OC1-M-001-1-A	OC1-M-001-1-B	OC1-M-001-1-C	OC1-M-001-1-D	OC1-M-001-1-E
e		0.657	0.63	0.613	0.602	0.592
Rate (mm/s)		1.00E-03	126.5	116.35	1.00E-03	59.6
$\varepsilon = 0.1\%$	q_d (kPa)	64	134	135	72	144
	q_s (kPa)	64	68	71	72	74
	q_d/q_s	1.00	1.97	1.90	1.00	1.95
$\varepsilon = 0.2\%$	q_d (kPa)	78	175	185	102	169
	q_s (kPa)	78	89	97	102	107
	q_d/q_s	1.00	1.97	1.91	1.00	1.58
$\varepsilon = 0.5\%$	q_d (kPa)	102	227	226	149	215
	q_s (kPa)	102	123	138	149	160
	q_d/q_s	1.00	1.85	1.64	1.00	1.34
$\varepsilon = 1.0\%$	q_d (kPa)	120	260	262	191	277
	q_s (kPa)	120	148	171	188	205
	q_d/q_s	1.00	1.76	1.53	1.02	1.35
$\varepsilon = 1.5\%$	q_d (kPa)	128	270	294	216	310
	q_s (kPa)	127	163	191	212	233
	q_d/q_s	1.01	1.66	1.54	1.02	1.33
$\varepsilon = 2.0\%$	q_d (kPa)	135	276	310	231	329
	q_s (kPa)	132	172	202	225	248
	q_d/q_s	1.02	1.60	1.53	1.03	1.33
$\varepsilon = 2.5\%$	q_d (kPa)	139	278	317	237	338
	q_s (kPa)	132	172	202	225	248
	q_d/q_s	1.05	1.62	1.57	1.05	1.36
$\varepsilon = 3.0\%$	q_d (kPa)	142	279	323	241	343
	q_s (kPa)	146	189	223	248	274
	q_d/q_s	0.97	1.48	1.45	0.97	1.25

Table 7.5 Results of multistage rapid loading test OC1-M-001-1 on KSS.

Test		OC1-M-001-2-A	OC1-M-001-2-B	OC1-M-001-2-C	OC1-M-001-2-D	OC1-M-001-2-E
e		0.651	0.638	0.624	0.615	0.604
Rate (mm/s)		1.00E-03	1	64.62	80.28	1.00E-03
$\varepsilon = 0.1\%$	q_d (kPa)	61	120	150	150	80
	q_s (kPa)	60	65	70	74	79
	q_d/q_s	1.02	1.85	2.14	2.03	1.01
$\varepsilon = 0.2\%$	q_d (kPa)	73	150	185	185	116
	q_s (kPa)	72	82	94	102	114
	q_d/q_s	1.01	1.83	1.97	1.81	1.02
$\varepsilon = 0.5\%$	q_d (kPa)	97	191	241	242	167
	q_s (kPa)	98	114	134	148	168
	q_d/q_s	0.99	1.68	1.80	1.64	0.99
$\varepsilon = 1.0\%$	q_d (kPa)	120	217	287	305	215
	q_s (kPa)	129	152	181	203	233
	q_d/q_s	0.93	1.43	1.59	1.50	0.92
$\varepsilon = 1.5\%$	q_d (kPa)	132	225	305	333	241
	q_s (kPa)	129	152	182	204	235
	q_d/q_s	1.02	1.48	1.68	1.63	1.03
$\varepsilon = 2.0\%$	q_d (kPa)	140	230	316	351	255
	q_s (kPa)	147	173	207	232	268
	q_d/q_s	0.95	1.33	1.53	1.51	0.95
$\varepsilon = 2.5\%$	q_d (kPa)	146	232	320	360	268
	q_s (kPa)	143	168	201	225	259
	q_d/q_s	1.02	1.38	1.59	1.60	1.03
$\varepsilon = 3.0\%$	q_d (kPa)	151	235	332	365	271
	q_s (kPa)	147	172	205	230	264
	q_d/q_s	1.03	1.37	1.62	1.59	1.03

Table 7.6 Results of multistage rapid loading test OC1-M-001-2 on KSS.

Test		OC1-MR-01-1-A	OC1-MR-01-1-B	OC1-MR-01-1-C	OC1-MR-01-1-D
e		0.676	0.653	0.637	0.622
$\varepsilon = 0.5\%$	q (kPa)	110	168	198	204
	p' (kPa)	194	221	237	242
$\varepsilon = 1.0\%$	q (kPa)	125	189	229	250
	p' (kPa)	171	212	241	258
$\varepsilon = 1.5\%$	q (kPa)	130	197	240	270
	p' (kPa)	158	208	241	263
$\varepsilon = 2.0\%$	q (kPa)	137	201	245	278
	p' (kPa)	152	204	240	267
$\varepsilon = 2.5\%$	q (kPa)	140	203	248	282
	p' (kPa)	148	200	239	269
$\varepsilon = 3.0\%$	q (kPa)	142	205	249	285
	p' (kPa)	145	199	239	271
$\varepsilon = 3.5\%$	q (kPa)	145	206	249	286
	p' (kPa)	144	197	238	272

Table 7.7 Results of multistage test at constant rate (0.01 mm/s) OC1-MR-01-1

Test		OC1-MR-01-2-A	OC1-MR-01-2-B	OC1-MR-01-2-C	OC1-MR-01-2-D
e		0.667	0.652	0.636	0.623
$\varepsilon = 0.5\%$	q (kPa)	111	161	185	192
	p' (kPa)	196	215	227	234
$\varepsilon = 1.0\%$	q (kPa)	124	181	219	238
	p' (kPa)	171	206	231	248
$\varepsilon = 1.5\%$	q (kPa)	132	189	231	258
	p' (kPa)	137	201	232	256
$\varepsilon = 2.0\%$	q (kPa)	135	192	235	266
	p' (kPa)	150	196	231	260
$\varepsilon = 2.5\%$	q (kPa)	140	194	238	269
	p' (kPa)	146	193	231	261
$\varepsilon = 3.0\%$	q (kPa)	142	196	239	270
	p' (kPa)	143	191	229	262
$\varepsilon = 3.5\%$	q (kPa)	--	197	240	272
	p' (kPa)	--	189	228	262

Table 7.8 Results of multistage test at constant rate (0.01 mm/s) OC1-MR-01-2

Axial strain		$\varepsilon = 0.5\%$	$\varepsilon = 1.0\%$	$\varepsilon = 1.5\%$	$\varepsilon = 2.0\%$	$\varepsilon = 2.5\%$	$\varepsilon = 3.0\%$	$\varepsilon = 3.5\%$
p'-e	a ₁	-0.252	-0.139	-0.11	-0.099	-0.095	-0.085	-0.083
	a ₂	2.01	1.396	1.235	1.177	1.151	1.101	1.09
	R ²	0.95	0.97	0.98	0.98	0.98	0.99	0.99
q-e	b ₁	-0.088	-0.082	-0.078	-0.08	-0.081	-0.076	-0.078
	b ₂	1.094	1.074	1.058	1.073	1.081	1.056	1.068
	R ²	0.87	0.94	0.96	0.97	0.97	0.98	0.99

Table 7.9 Parameters a₁, a₂, b₁, b₂ for equal strain contours on multistage test OC1-MR-01-1

Axial strain		$\varepsilon = 0.5\%$	$\varepsilon = 1.0\%$	$\varepsilon = 1.5\%$	$\varepsilon = 2.0\%$	$\varepsilon = 2.5\%$	$\varepsilon = 3.0\%$	$\varepsilon = 3.5\%$
p'-e	a ₁	-0.295	-0.156	-0.087	-0.08	-0.075	-0.072	-0.088
	a ₂	2.228	1.263	0.999	1.069	1.044	1.026	1.112
	R ²	0.94	0.97	0.92	0.97	0.98	0.98	0.99
q-e	b ₁	-0.071	-0.064	-0.063	-0.064	-0.066	-0.067	-0.089
	b ₂	1.005	0.977	0.977	0.981	0.994	1.000	1.125
	R ²	0.87	0.93	0.95	0.96	0.97	0.97	0.99

Table 7.10 Parameters a₁, a₂, b₁, b₂ for equal strain contours on multistage test OC1-MR-01-2

Test		OC1-M-01-A	OC1-M-01-B	OC1-M-01-C	OC1-M-01-D	OC1-M-01-E
e		0.694	0.67	0.654	0.642	0.627
Rate (mm/s)		0.01	1.02	47.62	32.53	0.01
$\varepsilon = 0.1\%$	q_d (kPa)	85	117	141	146	124
	q_s (kPa)	85	97	107	114	125
	q_d/q_s	1.00	1.21	1.32	1.28	0.99
$\varepsilon = 0.2\%$	q_d (kPa)	99	149	188	175	150
	q_s (kPa)	99	115	127	137	150
	q_d/q_s	1.00	1.30	1.48	1.28	1.00
$\varepsilon = 0.5\%$	q_d (kPa)	115	188	231	222	196
	q_s (kPa)	115	140	158	174	196
	q_d/q_s	1.00	1.34	1.46	1.28	1.00
$\varepsilon = 1.0\%$	q_d (kPa)	128	209	275	273	238
	q_s (kPa)	127	159	185	206	237
	q_d/q_s	1.01	1.31	1.49	1.33	1.00
$\varepsilon = 1.5\%$	q_d (kPa)	133	217	289		257
	q_s (kPa)	134	169	197		257
	q_d/q_s	0.99	1.28	1.47		1.00
$\varepsilon = 2.0\%$	q_d (kPa)	137	221	302		265
	q_s (kPa)	137	174	203		265
	q_d/q_s	1.00	1.27	1.49		1.00
$\varepsilon = 2.5\%$	q_d (kPa)	141	221			268
	q_s (kPa)	141	178			269
	q_d/q_s	1.00	1.24			1.00

Table 7.11 Results of multistage rapid loading test OC1-M-01. (OCR=1)

Test		OC4-M-01-A	OC4-M-01-B	OC4-M-01-C	OC4-M-01-D	OC4-M-01-E
e		0.599	0.599	0.599	0.599	0.596
Rate (mm/s)		0.01	10.31	54.23	154.86	0.01
$\varepsilon = 0.1\%$	q_d (kPa)	52	75	20	71	46
	q_s (kPa)	52	52	52	52	46
	q_d/q_s	1.00	1.44	0.38	1.37	1.00
$\varepsilon = 0.2\%$	q_d (kPa)	63	100	25	89	54
	q_s (kPa)	63	63	63	63	54
	q_d/q_s	1.00	1.59	0.40	1.41	1.00
$\varepsilon = 0.5\%$	q_d (kPa)	83	125	117	120	73
	q_s (kPa)	84	84	84	84	74
	q_d/q_s	0.99	1.49	1.39	1.43	0.99
$\varepsilon = 1.0\%$	q_d (kPa)	102	158	155	148	99
	q_s (kPa)	102	102	102	102	99
	q_d/q_s	1.00	1.55	1.52	1.45	1.00
$\varepsilon = 1.5\%$	q_d (kPa)	113	171	181	182	122
	q_s (kPa)	113	113	113	113	122
	q_d/q_s	1.00	1.51	1.60	1.61	1.00
$\varepsilon = 2.0\%$	q_d (kPa)	122	179	193	203	141
	q_s (kPa)	123	123	123	123	141
	q_d/q_s	0.99	1.46	1.57	1.65	1.00
$\varepsilon = 2.5\%$	q_d (kPa)	130	185	200	211	153
	q_s (kPa)	130	130	130	130	153
	q_d/q_s	1.00	1.42	1.54	1.62	1.00
$\varepsilon = 3.0\%$	q_d (kPa)	137	191	214	216	161
	q_s (kPa)	138	138	138	138	162
	q_d/q_s	0.99	1.38	1.55	1.57	0.99

Table 7.12 Results of multistage rapid loading test OC4-M-01. (OCR=4)

Test		OC8-M-01-A	OC8-M-01-B	OC8-M-01-C	OC8-M-01-D	OC8-M-01-E
e		0.625	0.622	0.62	0.619	0.618
Rate (mm/s)		0.01	1.04	55.91	171.46	0.01
$\varepsilon = 0.1\%$	q_d (kPa)	37	45	58	60	32
	q_s (kPa)	37	35	33	32	32
	q_d/q_s	1.00	1.29	1.76	1.88	1.00
$\varepsilon = 0.2\%$	q_d (kPa)	44	60	64	81	42
	q_s (kPa)	44	43	42	42	42
	q_d/q_s	1.00	1.40	1.52	1.93	1.00
$\varepsilon = 0.5\%$	q_d (kPa)	61	83	103	105	61
	q_s (kPa)	61	61	61	61	61
	q_d/q_s	1.00	1.36	1.69	1.72	1.00
$\varepsilon = 1.0\%$	q_d (kPa)	79	111	123	127	87
	q_s (kPa)	79	82	85	86	87
	q_d/q_s	1.00	1.35	1.45	1.48	1.00
$\varepsilon = 1.5\%$	q_d (kPa)	92	124	142	141	102
	q_s (kPa)	92	96	99	101	102
	q_d/q_s	1.00	1.29	1.43	1.40	1.00
$\varepsilon = 2.0\%$	q_d (kPa)	102	132	153	159	111
	q_s (kPa)	102	106	109	110	111
	q_d/q_s	1.00	1.25	1.40	1.45	1.00
$\varepsilon = 2.5\%$	q_d (kPa)	110	138	162	170	117
	q_s (kPa)	109	112	114	115	116
	q_d/q_s	1.01	1.23	1.42	1.48	1.01
$\varepsilon = 3.0\%$	q_d (kPa)	117	144	167	174	121
	q_s (kPa)	117	118	120	120	121
	q_d/q_s	1.00	1.22	1.39	1.45	1.00

Table 7.13 Results of multistage rapid loading test OC8-M-01. (OCR=8)

Test		GMR2L-A	GMR2L-B	GMR2L-C	GMR2L-D	GMR2L-E	GMR2L-F
e		0.441	0.434	0.43	0.427	0.426	0.424
$\varepsilon = 0.25\%$	q (kPa)	90	105	105	105	105	106
	p' (kPa)	152	158	158	159	160	161
$\varepsilon = 0.5\%$	q (kPa)	117	146	148	149	149	149
	p' (kPa)	149	165	168	170	172	175
$\varepsilon = 1.0\%$	q (kPa)	152	210	219	227	226	221
	p' (kPa)	151	188	197	205	207	209
$\varepsilon = 1.5\%$	q (kPa)	175	241	270	283	290	290
	p' (kPa)	156	201	224	237	243	249
$\varepsilon = 2.0\%$	q (kPa)	194	257	293	310	319	323
	p' (kPa)	162	208	238	256	265	273
$\varepsilon = 2.5\%$	q (kPa)	208	266	303	323	331	335
	p' (kPa)	168	216	248	268	278	287
$\varepsilon = 3.0\%$	q (kPa)	–	197	240	272		
	p' (kPa)	–	189	228	262		

Table 7.14 Results of multistage test at constant rate (0.001 mm/s) GMR2L

Axial strain		$\varepsilon = 0.25\%$	$\varepsilon = 0.5\%$	$\varepsilon = 1.0\%$	$\varepsilon = 1.5\%$	$\varepsilon = 2.0\%$	$\varepsilon = 2.5\%$	$\varepsilon = 3.0\%$
p'-e	a ₁	-0.285	-0.068	-0.049	-0.035	-0.032	-0.031	-0.031
	a ₂	1.872	0.977	0.691	0.619	0.602	0.6	0.601
	R ²	0.93	0.95	0.93	0.98	0.99	0.99	0.99
q-e	b ₁	-0.085	-0.057	-0.037	-0.031	-0.032	-0.034	-0.038
	b ₂	0.826	0.713	0.625	0.602	0.608	0.622	0.637
	R ²	0.75	0.76	0.81	0.94	0.97	0.98	0.98

Table 7.15 Parameters a₁, a₂, b₁, b₂ for equal strain contours on multistage test GMR2L

Test		GM1L-A	GM1L-B	GM1L-C	GM1L-D	GM1L-E
e		0.48	0.476	0.475	0.474	0.471
Rate (mm/s)		1.00E-03	1.03	54.01	113.03	1.00E-03
$\varepsilon = 0.1\%$	q_d (kPa)	30	45	59	77	36
	q_s (kPa)	30	32	33	34	36
	q_d/q_s	1.00	1.41	1.79	2.28	1.00
$\varepsilon = 0.2\%$	q_d (kPa)	41	63	87	92	56
	q_s (kPa)	41	47	49	50	56
	q_d/q_s	1.00	1.34	1.78	1.84	1.00
$\varepsilon = 0.5\%$	q_d (kPa)	59	94	114	112	87
	q_s (kPa)	59	70	73	76	87
	q_d/q_s	1.00	1.34	1.56	1.47	1.00
$\varepsilon = 1.0\%$	q_d (kPa)	78	131	156	152	129
	q_s (kPa)	77	97	103	109	129
	q_d/q_s	1.01	1.35	1.51	1.39	1.00
$\varepsilon = 1.5\%$	q_d (kPa)	86	149	188	196	157
	q_s (kPa)	86	112	119	127	155
	q_d/q_s	1.00	1.33	1.58	1.54	1.01
$\varepsilon = 2.0\%$	q_d (kPa)	97	160	204	237	184
	q_s (kPa)	97	130	139	149	185
	q_d/q_s	1.00	1.23	1.47	1.59	0.99
$\varepsilon = 2.5\%$	q_d (kPa)	105	170	221	261	190
	q_s (kPa)	106	138	147	157	192
	q_d/q_s	0.99	1.23	1.50	1.66	0.99

Table 7.16 Results of multistage rapid loading test GM1L

Test		GM2L-A	GM2L-B	GM2L-C	GM2L-D	GM2L-E
e		0.432	0.426	0.423	0.419	0.418
Rate (mm/s)		1.00E-03	1	60.94	1.00E-03	0.05
$\varepsilon = 0.1\%$	q_d (kPa)	49	72	84	60	68
	q_s (kPa)	49	54	56	60	61
	q_d/q_s	1.00	1.33	1.50	1.00	1.11
$\varepsilon = 0.2\%$	q_d (kPa)	62	101	117	74	88
	q_s (kPa)	62	67	70	74	75
	q_d/q_s	1.00	1.51	1.67	1.00	1.17
$\varepsilon = 0.5\%$	q_d (kPa)	85	143	167	115	129
	q_s (kPa)	85	97	104	114	117
	q_d/q_s	1.00	1.47	1.61	1.01	1.10
$\varepsilon = 1.0\%$	q_d (kPa)	108	194	237	168	194
	q_s (kPa)	108	132	146	168	173
	q_d/q_s	1.00	1.47	1.62	1.00	1.12
$\varepsilon = 1.5\%$	q_d (kPa)	125	216	281	213	252
	q_s (kPa)	125	160	181	214	223
	q_d/q_s	1.00	1.35	1.55	1.00	1.13
$\varepsilon = 2.0\%$	q_d (kPa)	138	231	309	243	286
	q_s (kPa)	138	180	204	243	254
	q_d/q_s	1.00	1.28	1.51	1.00	1.13
$\varepsilon = 2.5\%$	q_d (kPa)	149	248	332	258	301
	q_s (kPa)	149	192	218	259	270
	q_d/q_s	1.00	1.29	1.52	1.00	1.11

Table 7.17 Results of multistage rapid loading test GM2L

Test		GM3L-A	GM3L-B	GM3L-C	GM3L-D	GM3L-E	GM3L-F
e		0.467	0.462	0.458	0.455	0.453	0.451
Rate (mm/s)		0.001	1.05	49.40	49.11	0.001	0.10
$\varepsilon = 0.1\%$	q_d (kPa)	69	99	113	101	75	89
	q_s (kPa)	69	71	73	74	75	76
	q_d/q_s	1.00	1.39	1.55	1.36	1.00	1.17
$\varepsilon = 0.2\%$	q_d (kPa)	83	130	146	141	98	118
	q_s (kPa)	83	88	92	95	97	100
	q_d/q_s	1.00	1.48	1.59	1.48	1.01	1.18
$\varepsilon = 0.5\%$	q_d (kPa)	116	185	218	201	152	170
	q_s (kPa)	116	128	138	146	152	158
	q_d/q_s	1.00	1.45	1.58	1.38	1.00	1.08
$\varepsilon = 1.0\%$	q_d (kPa)	144	247	296	280	214	244
	q_s (kPa)	144	166	186	203	215	228
	q_d/q_s	1.00	1.49	1.59	1.38	1.00	1.07
$\varepsilon = 1.5\%$	q_d (kPa)	164	277	358	354	267	311
	q_s (kPa)	164	196	225	250	268	287
	q_d/q_s	1.00	1.41	1.59	1.42	1.00	1.08
$\varepsilon = 2.0\%$	q_d (kPa)	182	296		403	308	360
	q_s (kPa)	183	220		287	309	333
	q_d/q_s	0.99	1.35		1.40	1.00	1.08
$\varepsilon = 2.5\%$	q_d (kPa)	193			438	331	384
	q_s (kPa)	193			306	331	357
	q_d/q_s	1.00			1.43	1.00	1.08

Table 7.18 Results of multistage rapid loading test GM3L

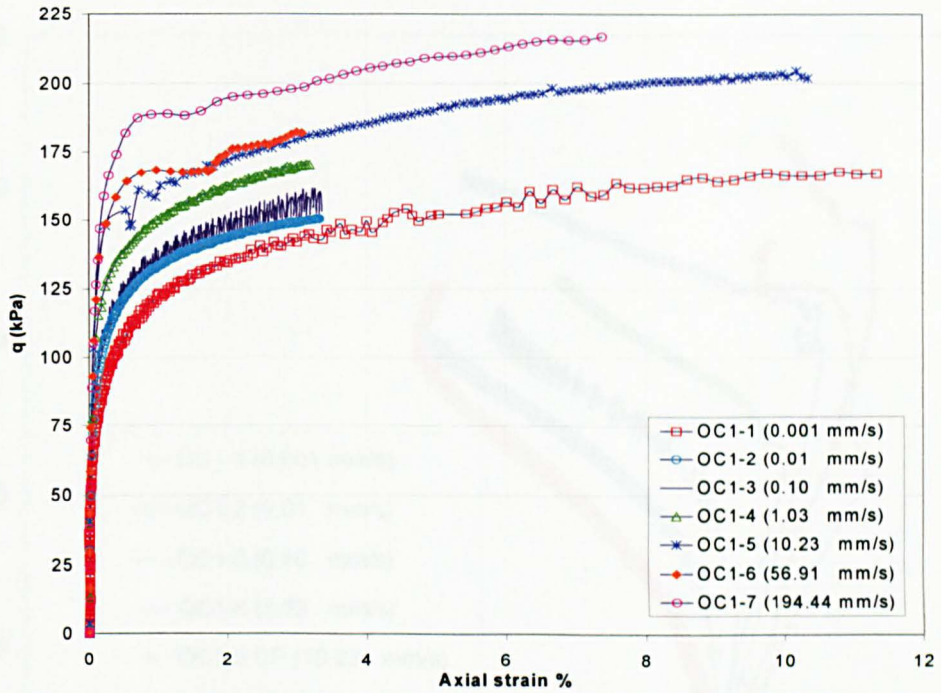


Figure 7.1 Deviator stress versus axial strain curves for monotonic consolidated undrained triaxial tests at different rates. (OCR=1)

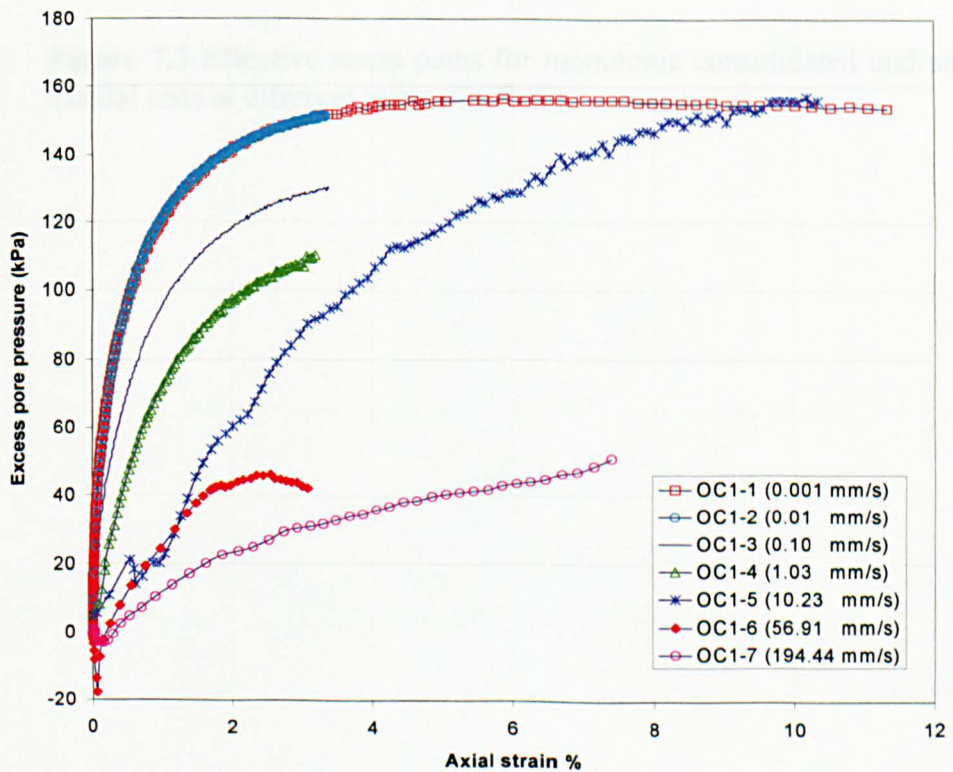


Figure 7.2 Excess pore pressure versus axial strain for monotonic consolidated undrained triaxial tests at different rates. (OCR=1)

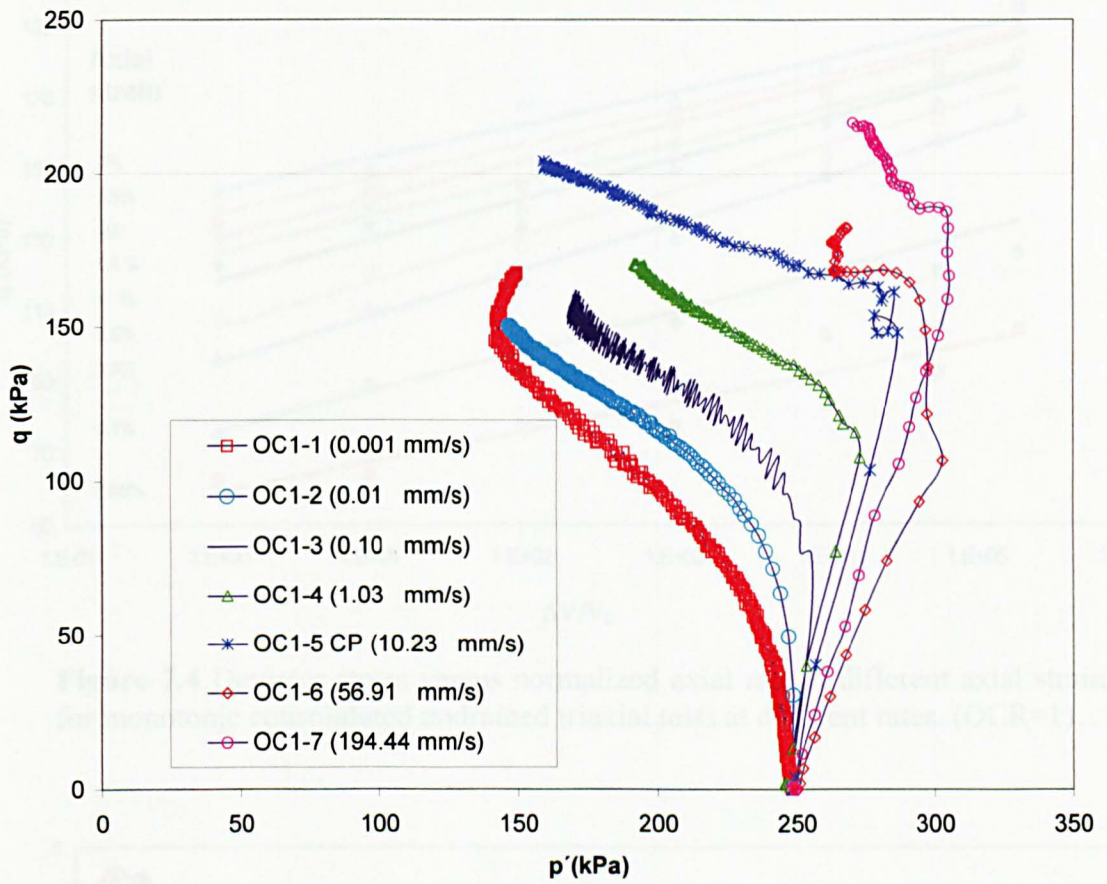


Figure 7.3 Effective stress paths for monotonic consolidated undrained triaxial tests at different rates. (OCR=1).

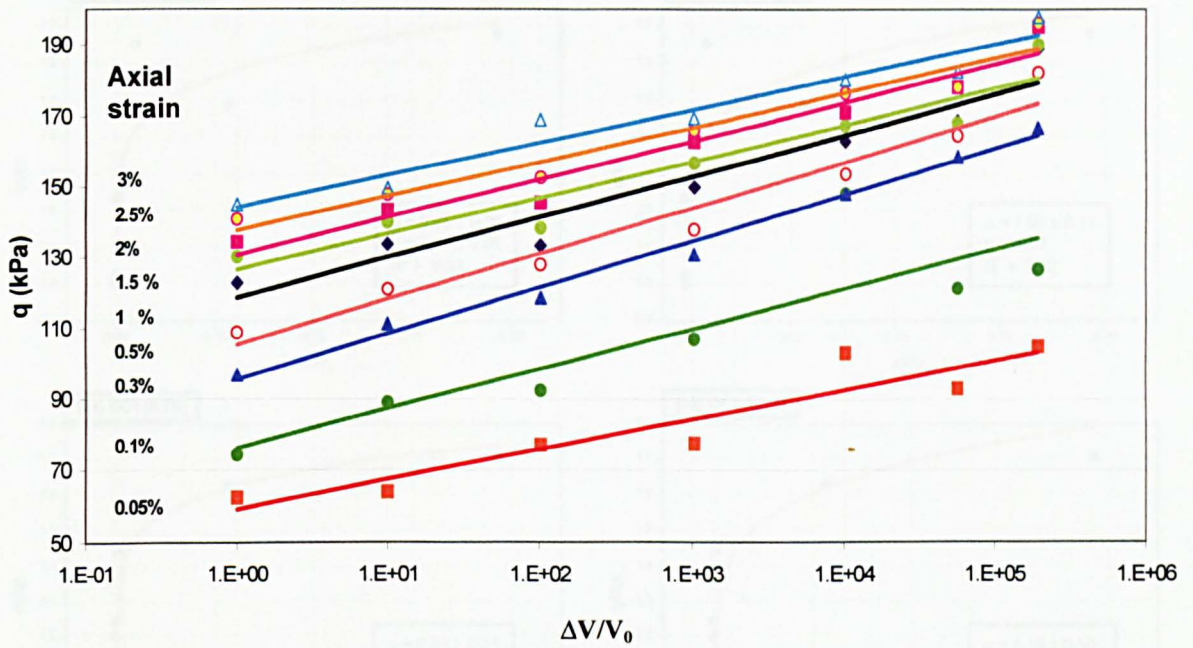


Figure 7.4 Deviator stress versus normalized axial rate at different axial strains for monotonic consolidated undrained triaxial tests at different rates. (OCR=1).

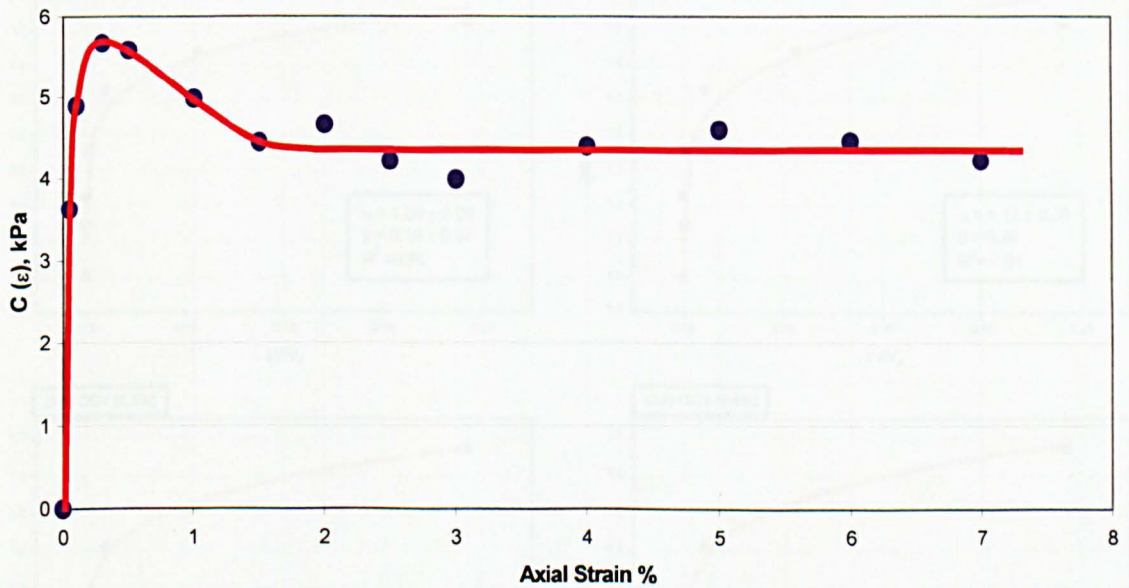


Figure 7.5 Coefficient C versus axial strain for monotonic consolidated undrained triaxial tests at different rates. (OCR=1).

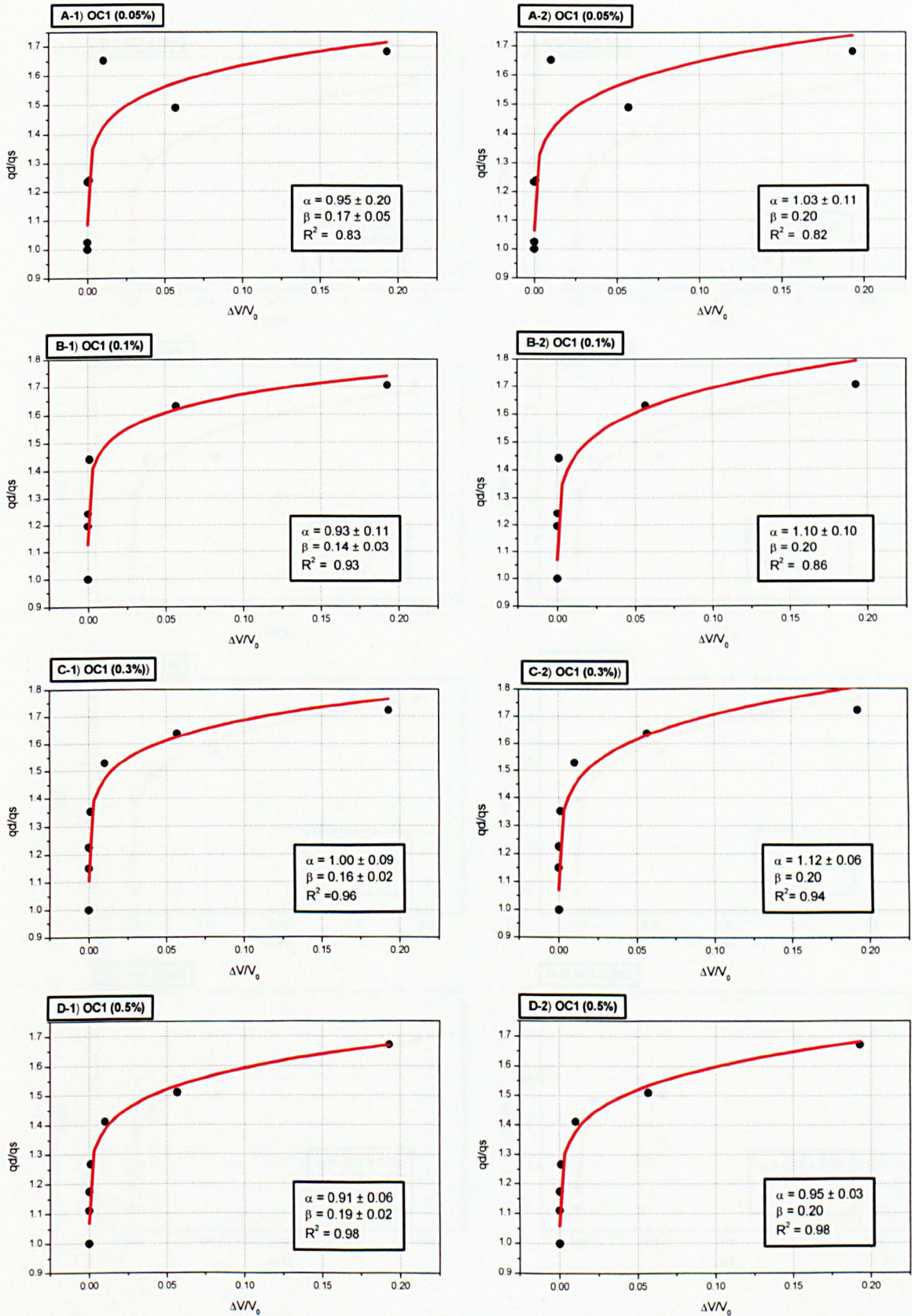


Figure 7.6 a Deviator stress versus normalized axial displacement rate ($\Delta V/V_0$) for monotonic consolidated undrained triaxial tests at different rates. (OCR = 1)

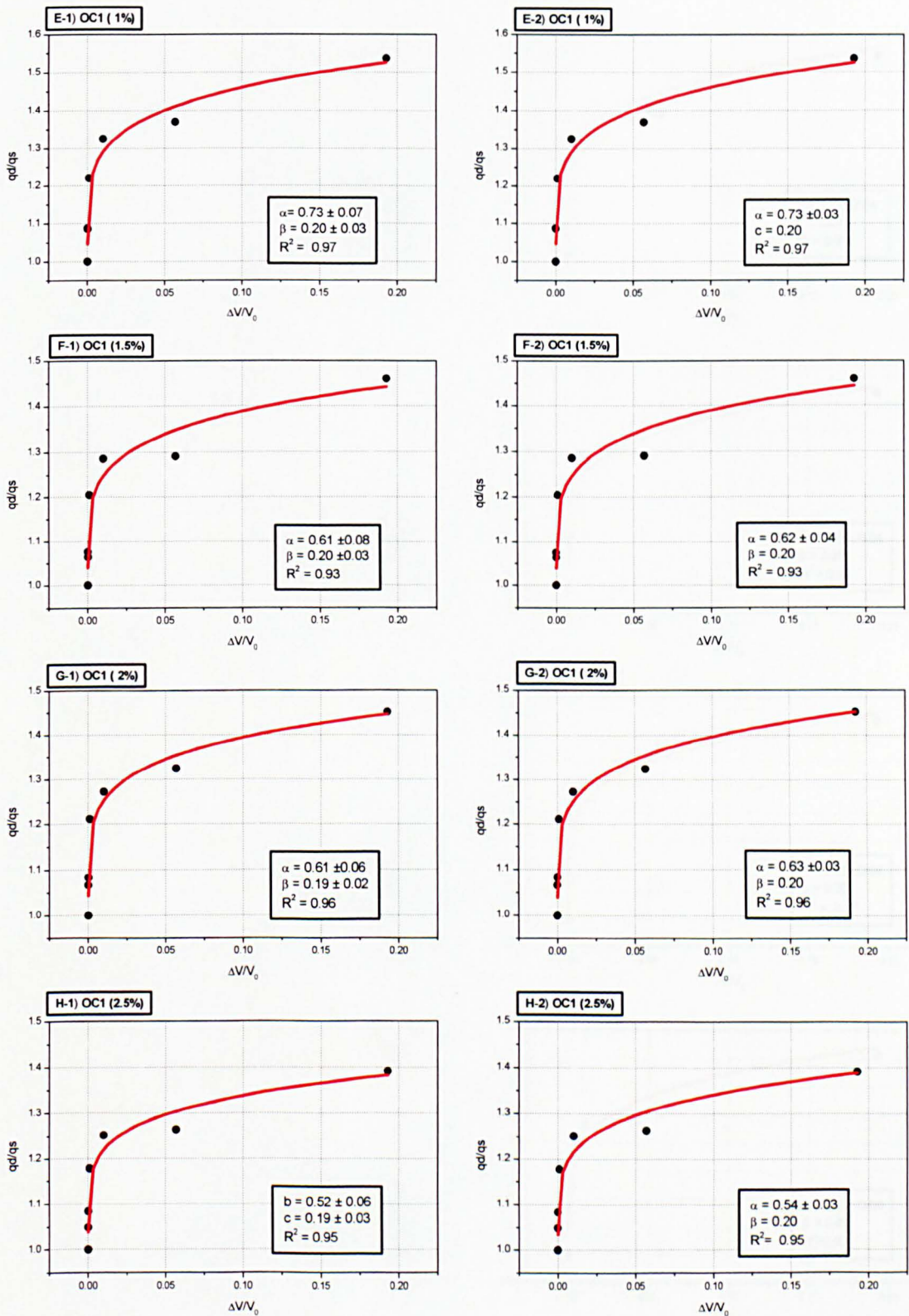


Figure 7.6 b Deviator stress versus normalized axial displacement rate ($\Delta V/V_0$) for monotonic consolidated undrained triaxial tests at different rates. (OCR = 1)

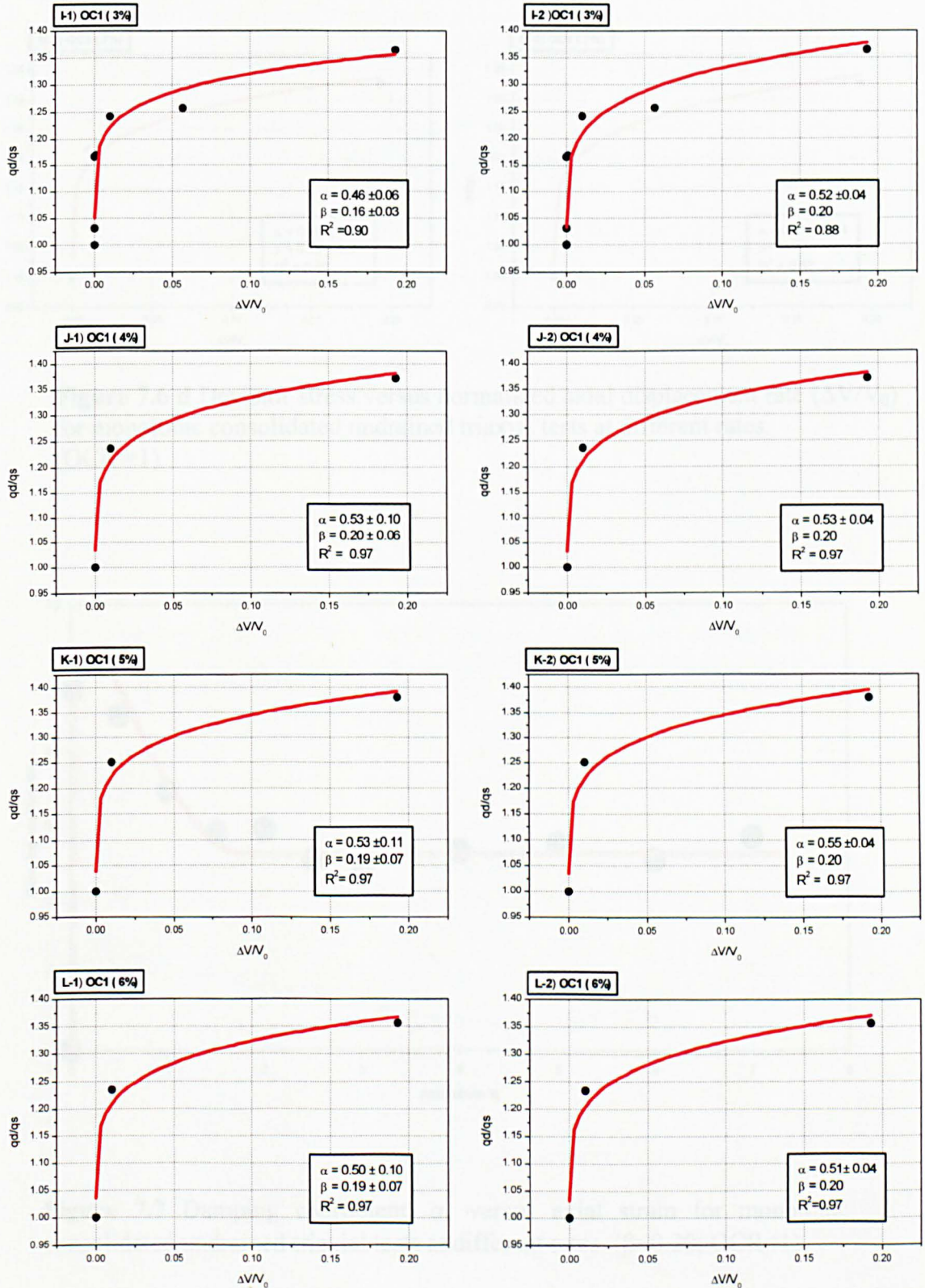


Figure 7.6 c Deviator stress versus normalized axial displacement rate ($\Delta V/V_0$) for monotonic consolidated undrained triaxial tests at different rates. (OCR = 1)

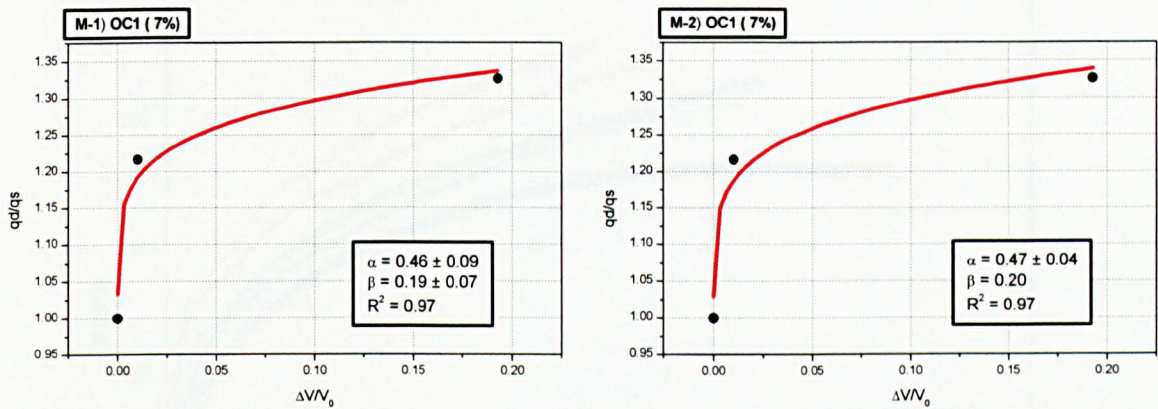


Figure 7.6 d Deviator stress versus normalized axial displacement rate ($\Delta V/V_0$) for monotonic consolidated undrained triaxial tests at different rates. (OCR = 1)

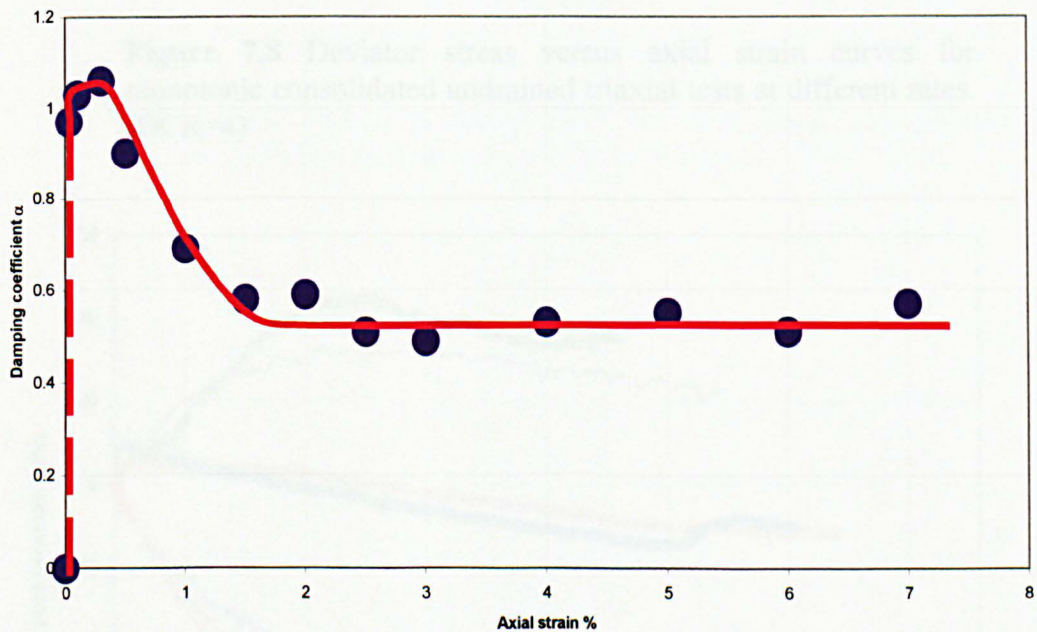


Figure 7.7 Damping coefficient, α , versus axial strain for monotonic consolidated undrained triaxial tests at different rates. ($\beta=0.20$; OCR=1)

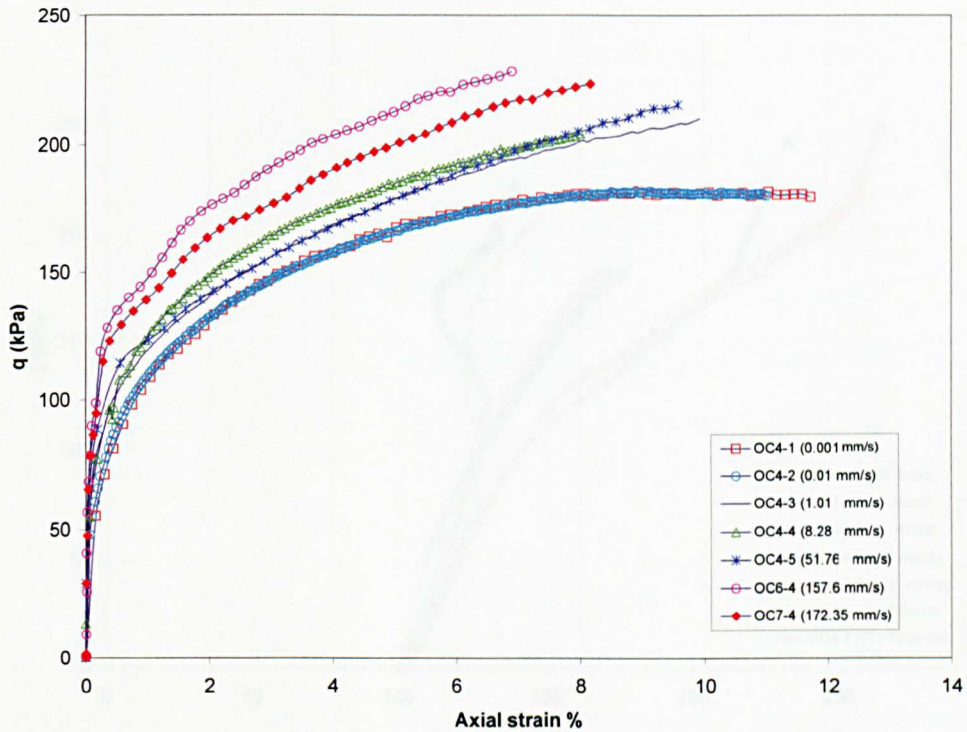


Figure 7.8 Deviator stress versus axial strain curves for monotonic consolidated undrained triaxial tests at different rates. (OCR=4)

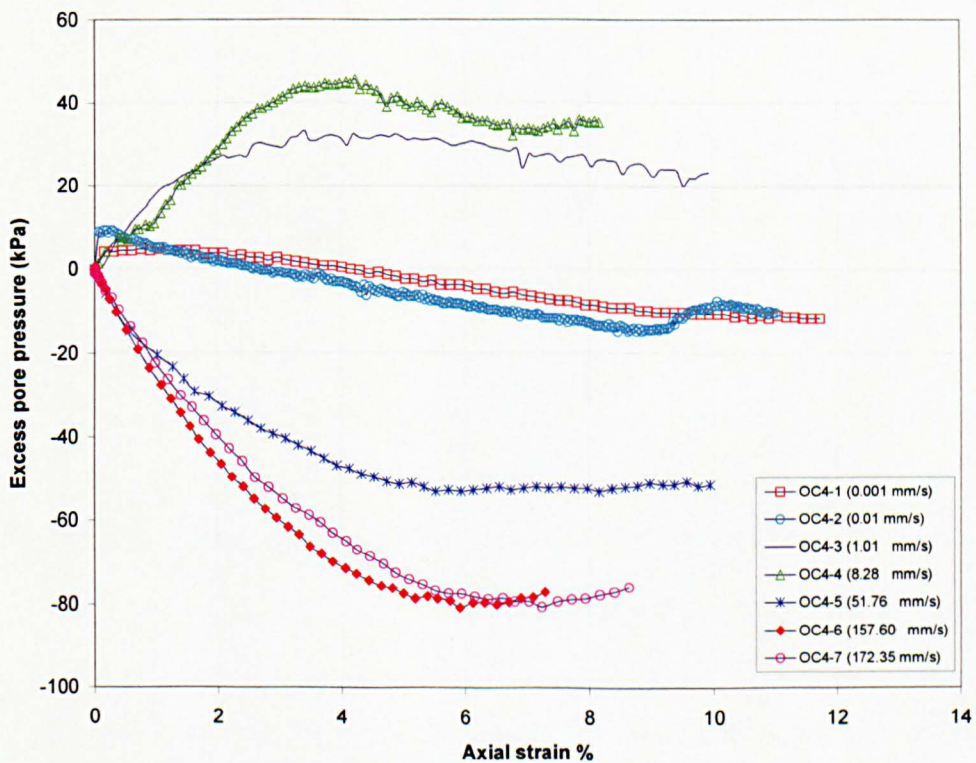


Figure 7.9 Excess pore pressure versus axial strain for monotonic consolidated undrained triaxial tests at different rates. (OCR=4)

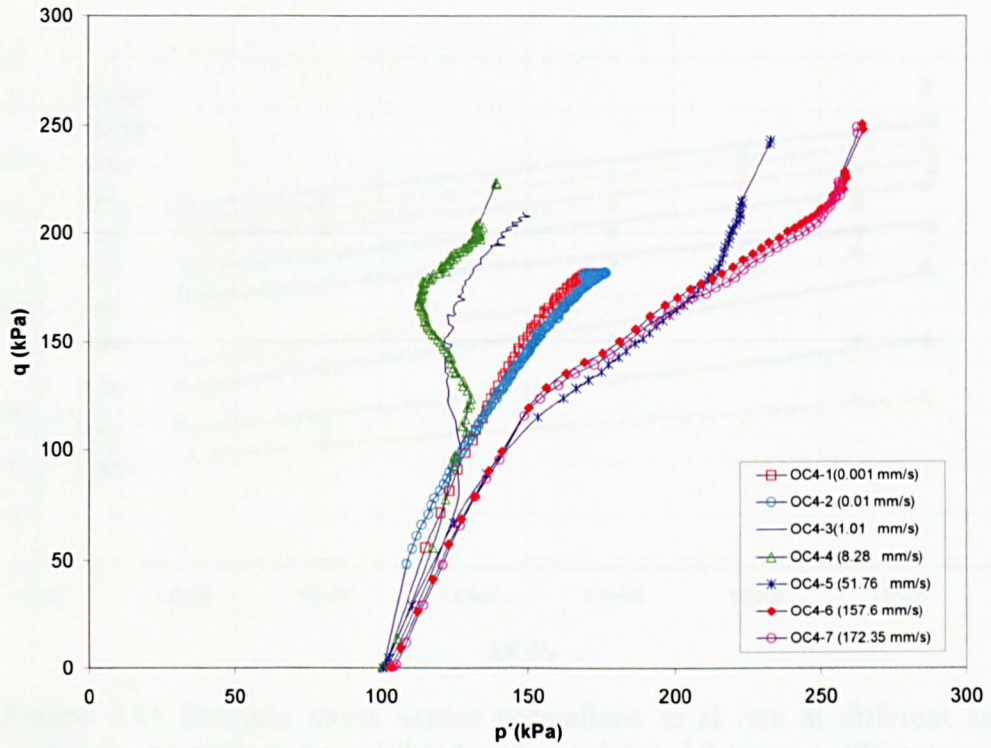


Figure 7.10 Effective stress paths for monotonic consolidated undrained triaxial tests at different rates. (OCR=4).

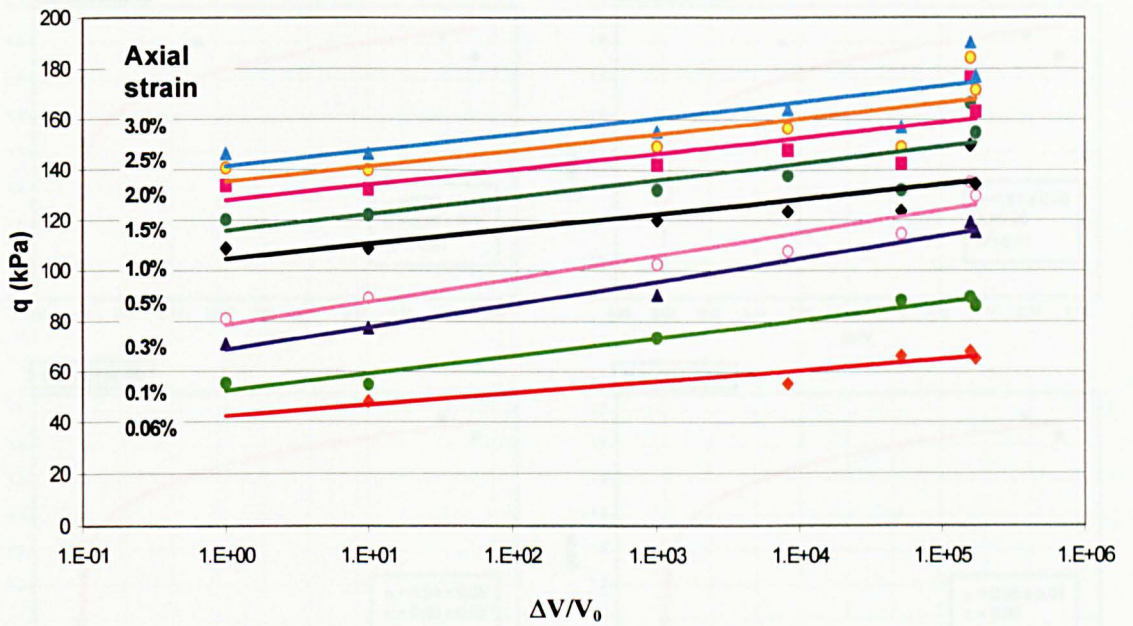


Figure 7.11 Deviator stress versus normalized axial rate at different axial strains for monotonic consolidated undrained triaxial tests at different rates. (OCR=4).

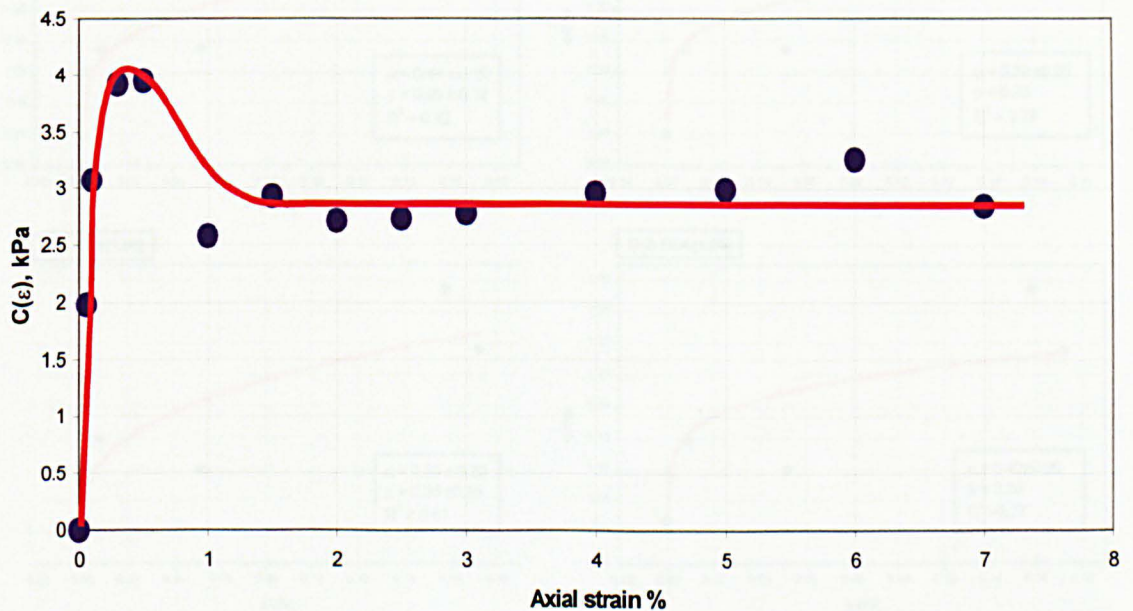


Figure 7.12 Coefficient C versus axial strain for monotonic consolidated undrained triaxial tests at different rates. (OCR=4).

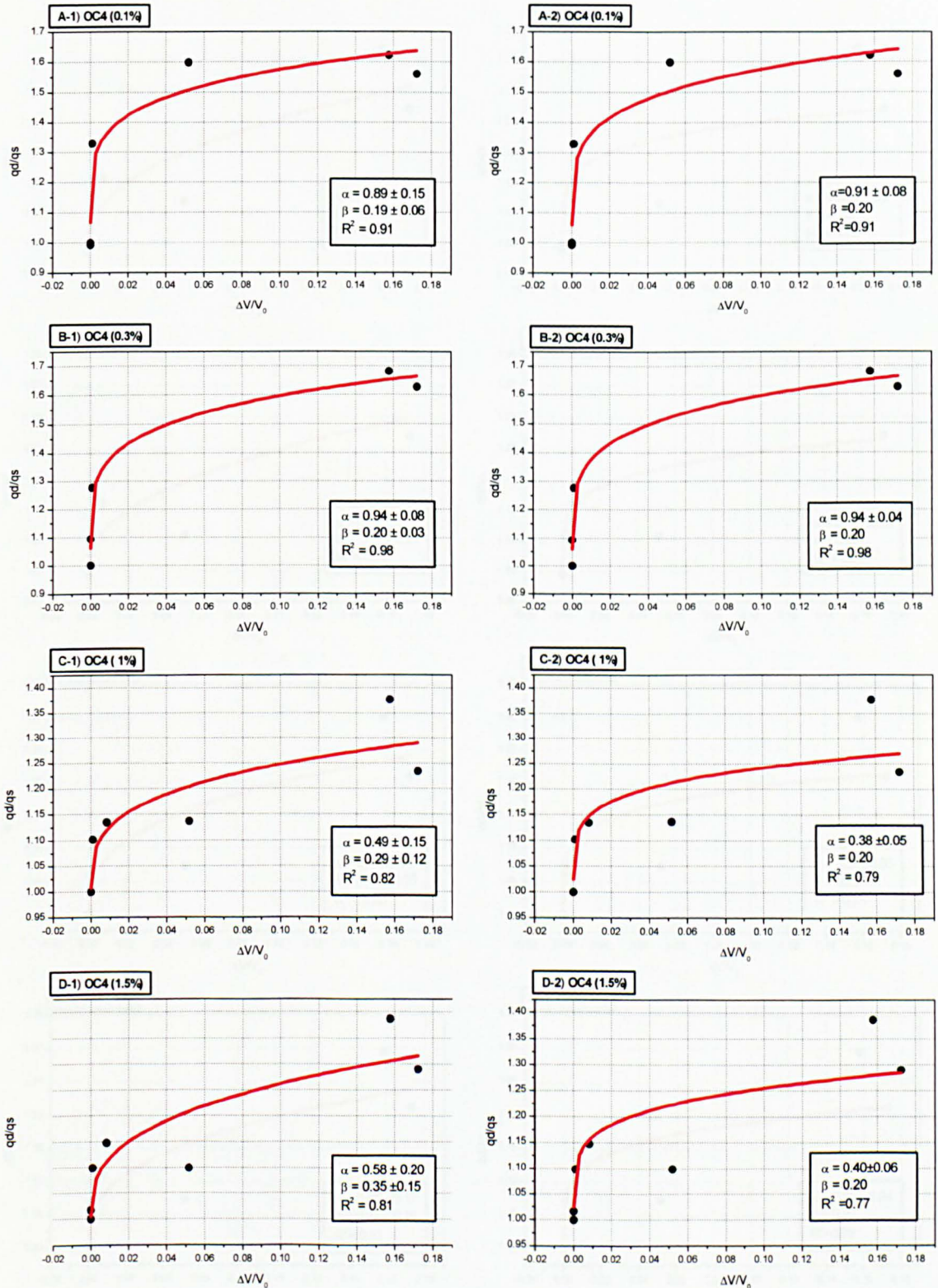


Figure 7.13 a Deviator stress versus normalized axial displacement rate ($\Delta V/V_0$) for monotonic consolidated undrained triaxial tests at different rates. (OCR = 4)

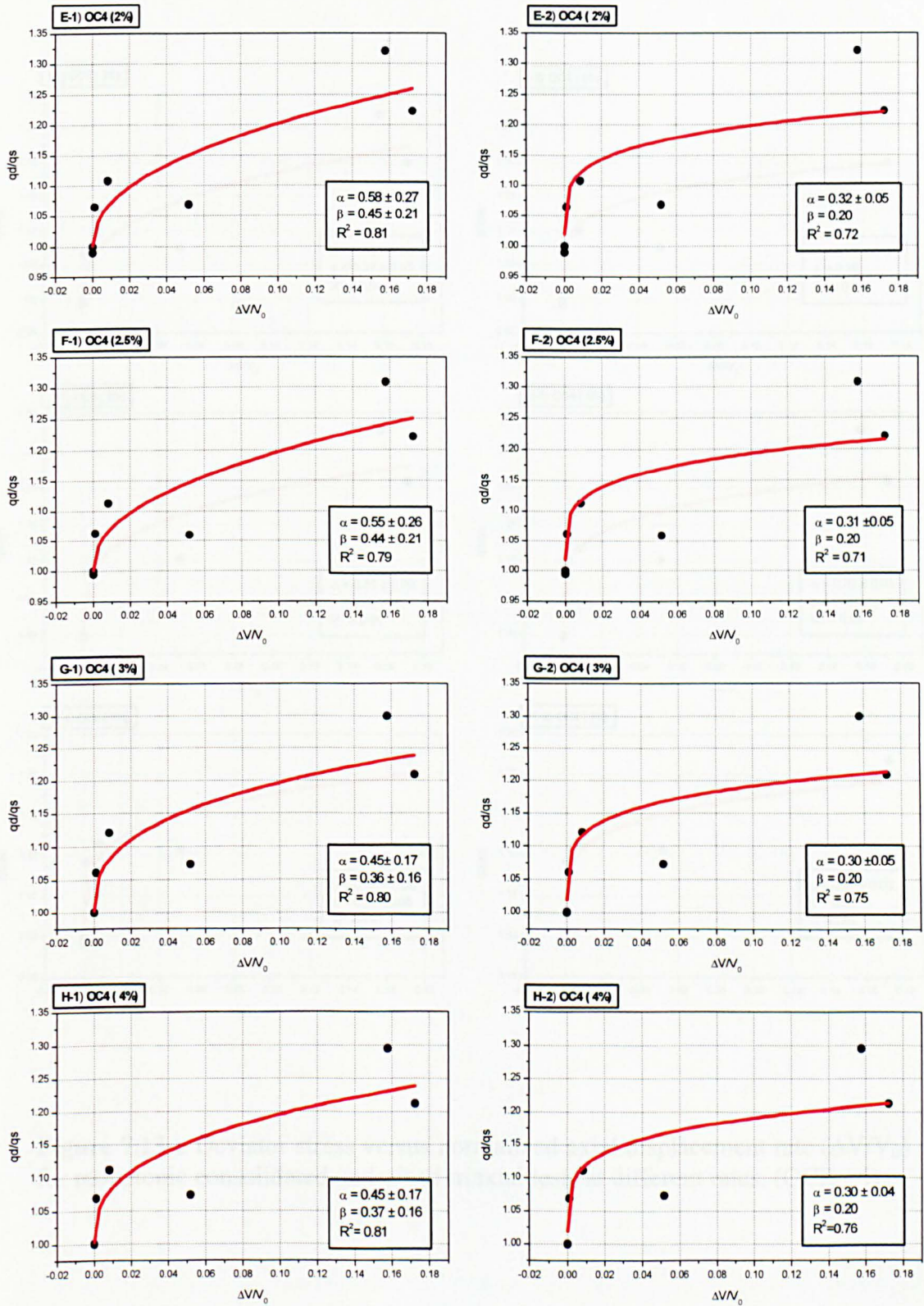


Figure 7.13 b Deviator stress versus normalized axial displacement rate ($\Delta V/V_0$) for monotonic consolidated undrained triaxial tests at different rates. (OCR = 4)

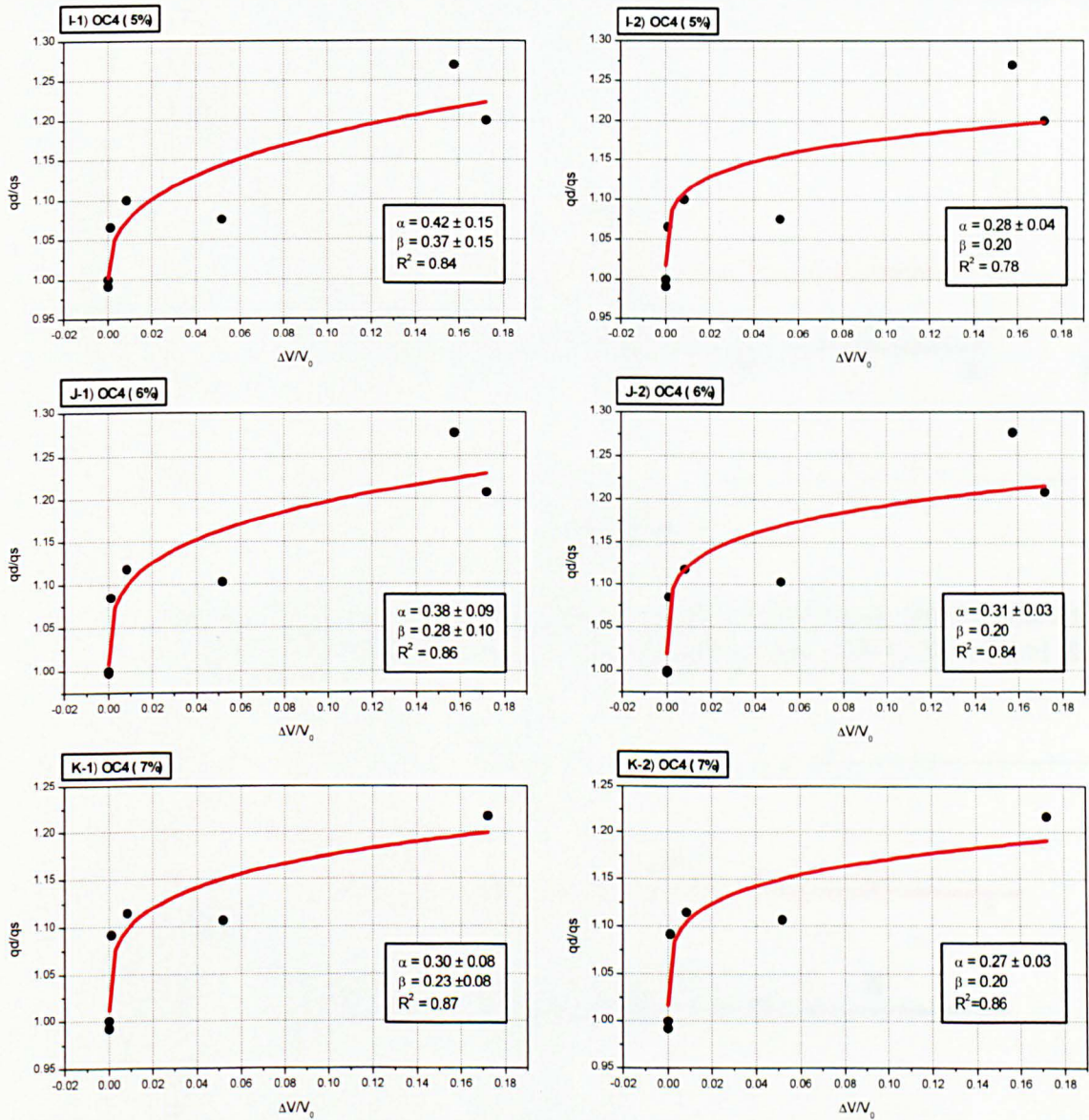


Figure 7.13 c Deviator stress versus normalized axial displacement rate ($\Delta V/V_0$) for monotonic consolidated undrained triaxial tests at different rates. (OCR = 4)

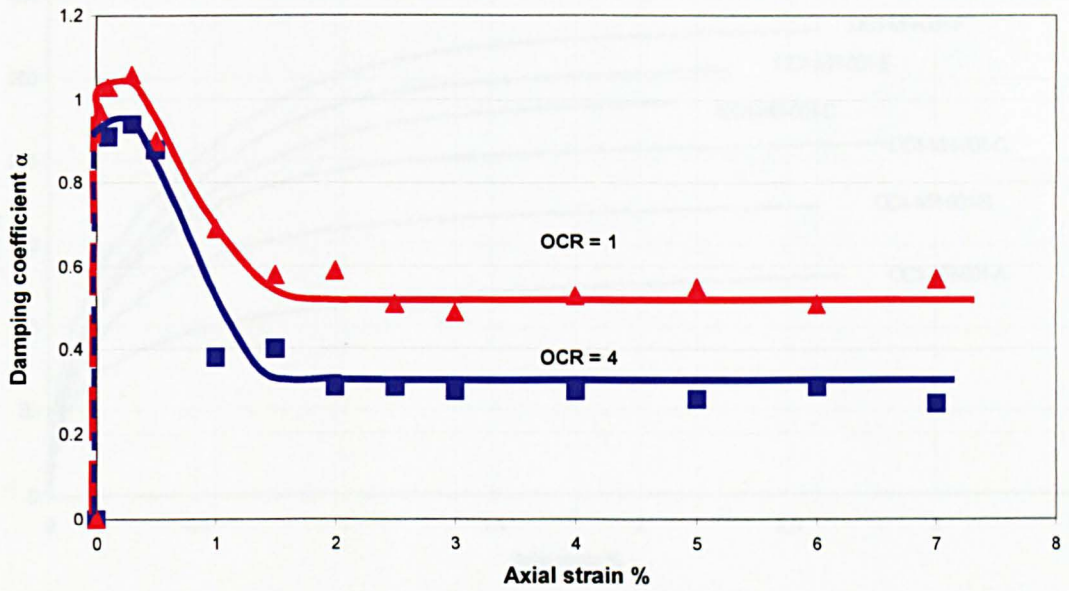


Figure 7.14 Damping coefficient, α , versus axial strain for monotonic consolidated undrained triaxial tests at different rates. ($\beta=0.20$; OCR=1 & OCR = 4)

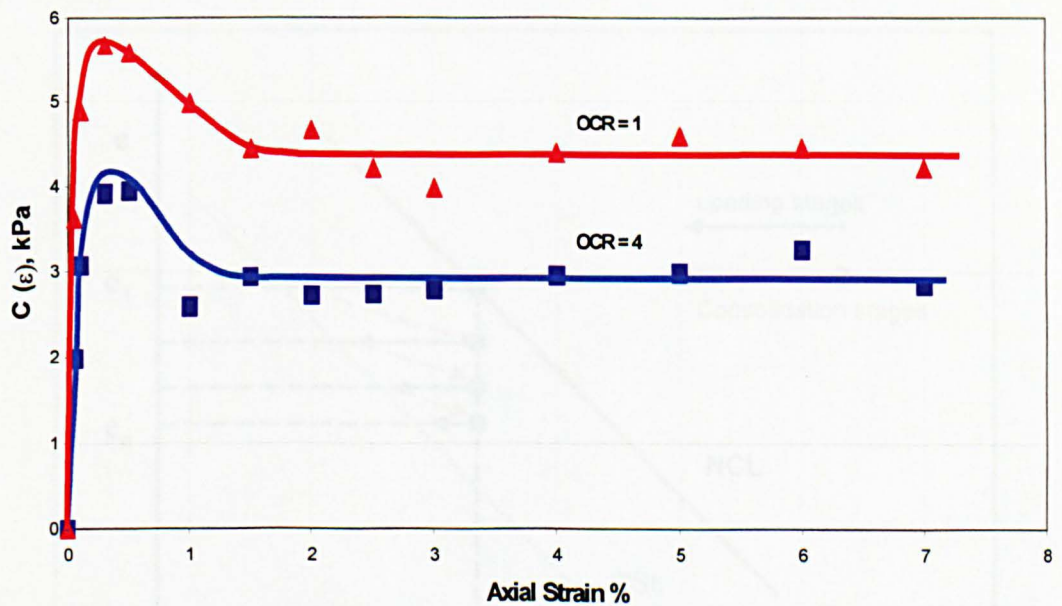


Figure 7.15 Coefficient, C, versus axial strain for monotonic consolidated undrained triaxial tests at different rates. (OCR=1 & OCR =4).

Figure 7.17 Schematic stress path diagram during multiple test.

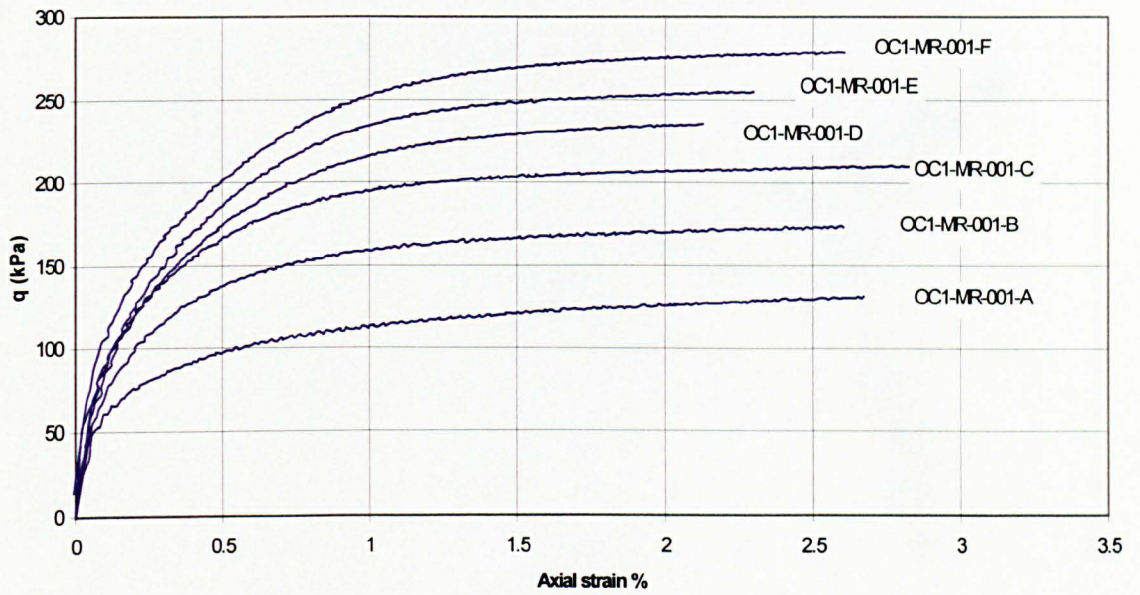


Figure 7.16 Deviator stress versus axial strain for multistage test OC1-MR-001 at constant rate (0.001 mm/s).

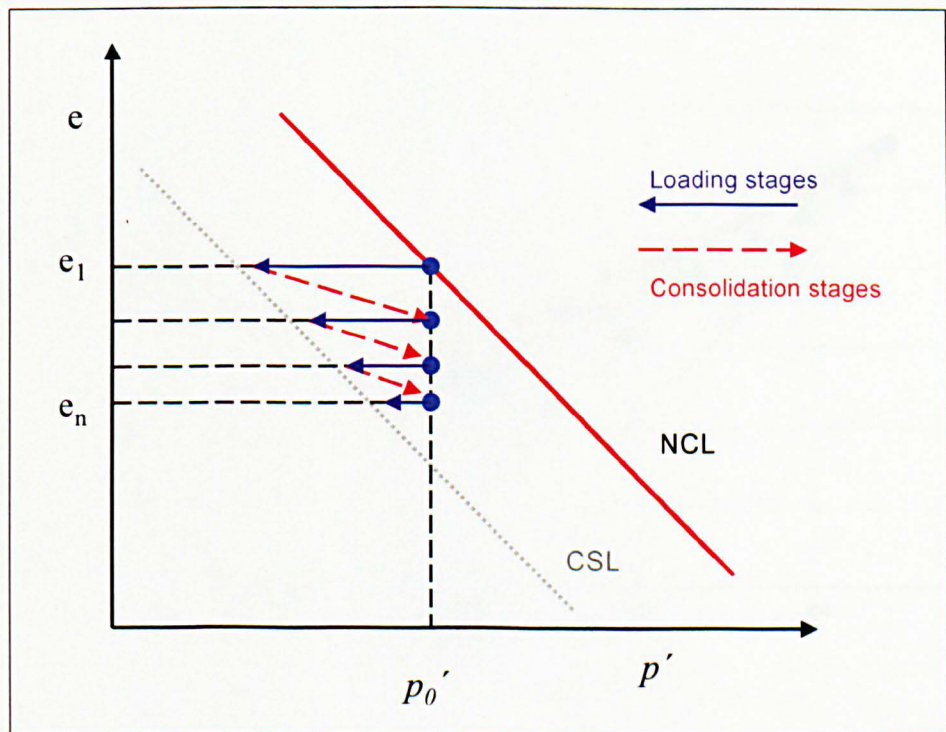


Figure 7.17 Schematic stress path diagram during multistage test.

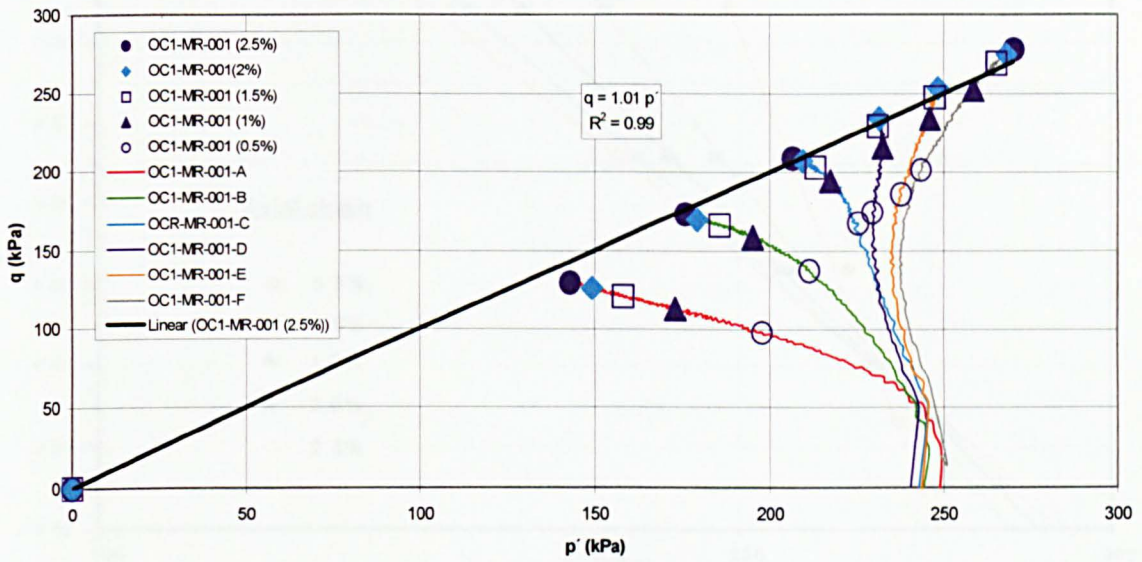


Figure 7.18 Effective stress paths for multistage test OC1-MR-001 at constant rate (0.001 mm/s).

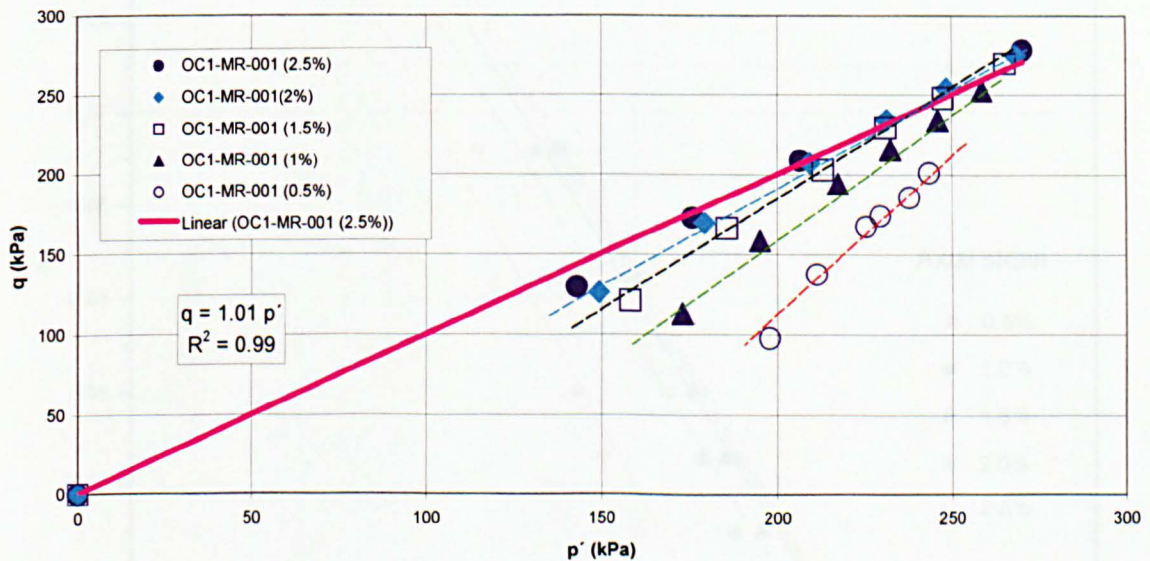


Figure 7.19 Equal strain contours for multistage test OC1-MR-001 at constant rate (0.001 mm/s). Deviator stress versus mean effective stress.

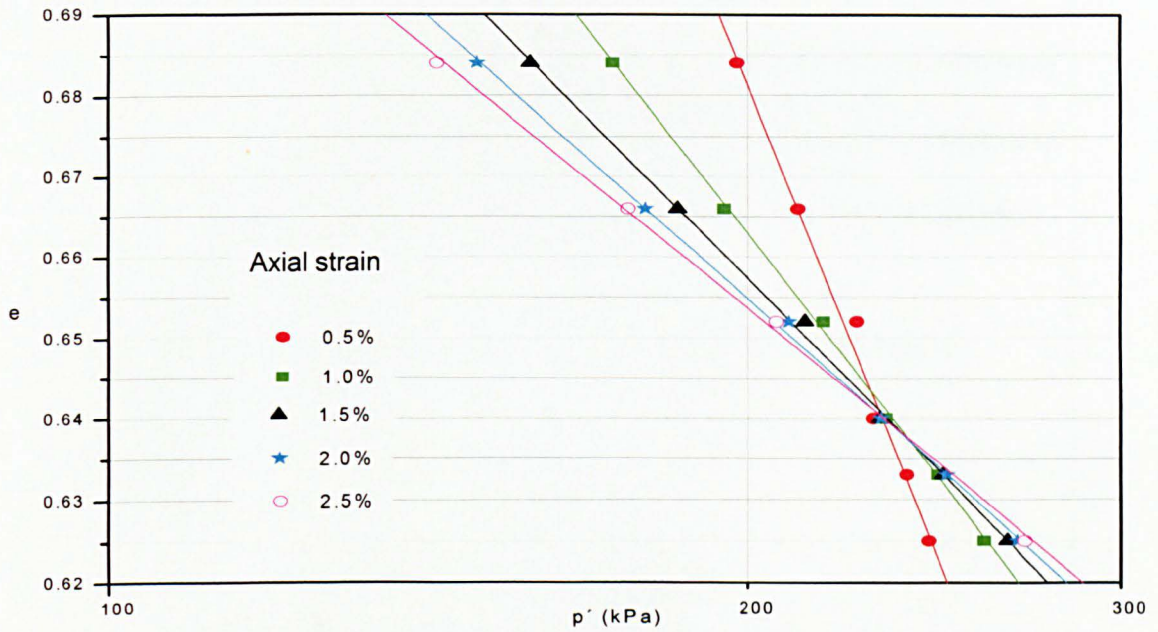


Figure 7.20 Equal strain contours for multistage test OC1-MR-001 at constant rate (0.001 mm/s). Voids ratio versus mean effective stress.

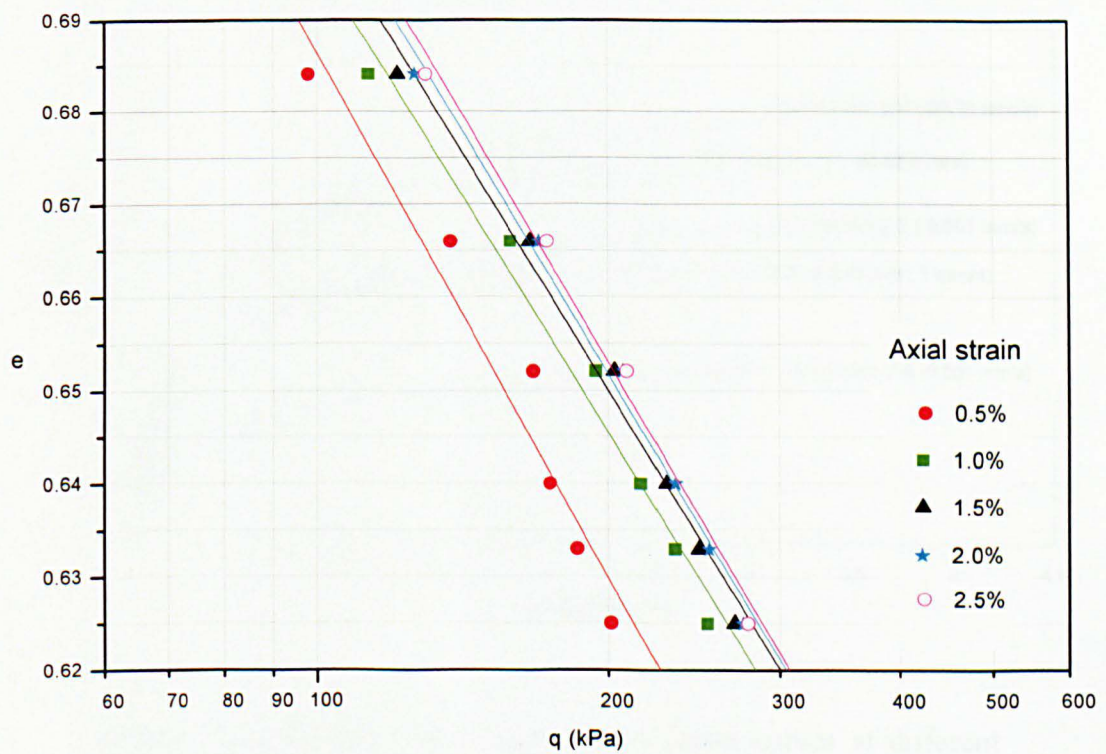


Figure 7.21 Equal strain contours for multistage test OC1-MR-001 at constant rate (0.001 mm/s). Voids ratio versus deviator stress.

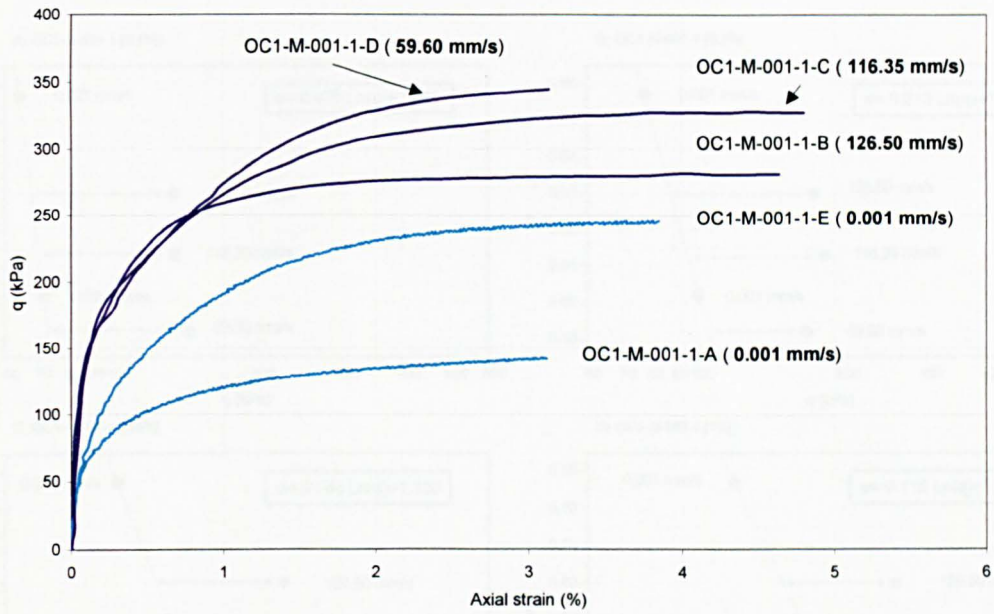


Figure 7.22 Deviator stress versus axial strain curves at different rates for multistage test OC1-M-001-1.

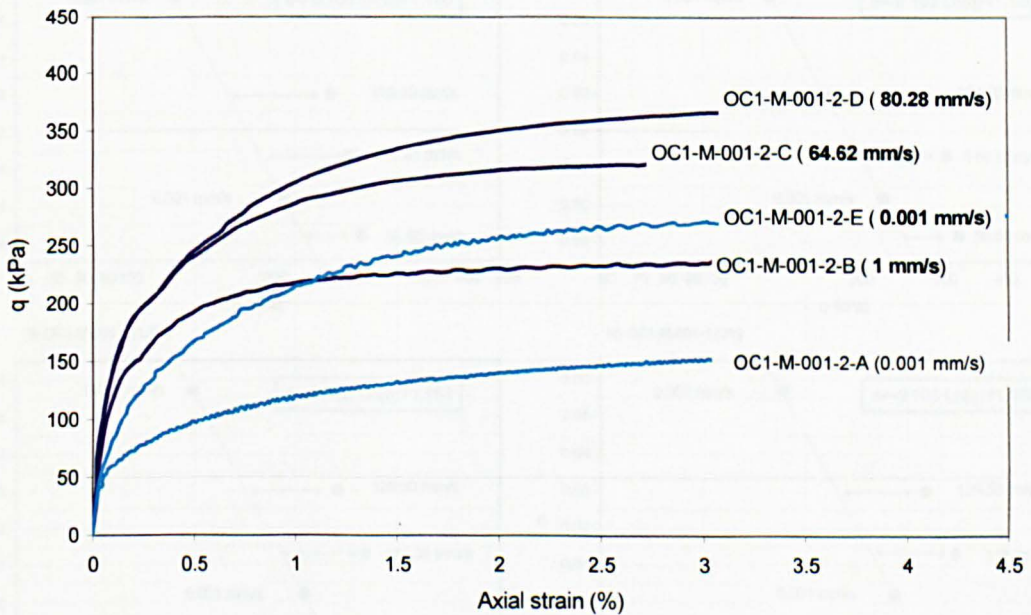


Figure 7.23 Deviator stress versus axial strain curves at different rates for multistage test OC1-M-001-2.

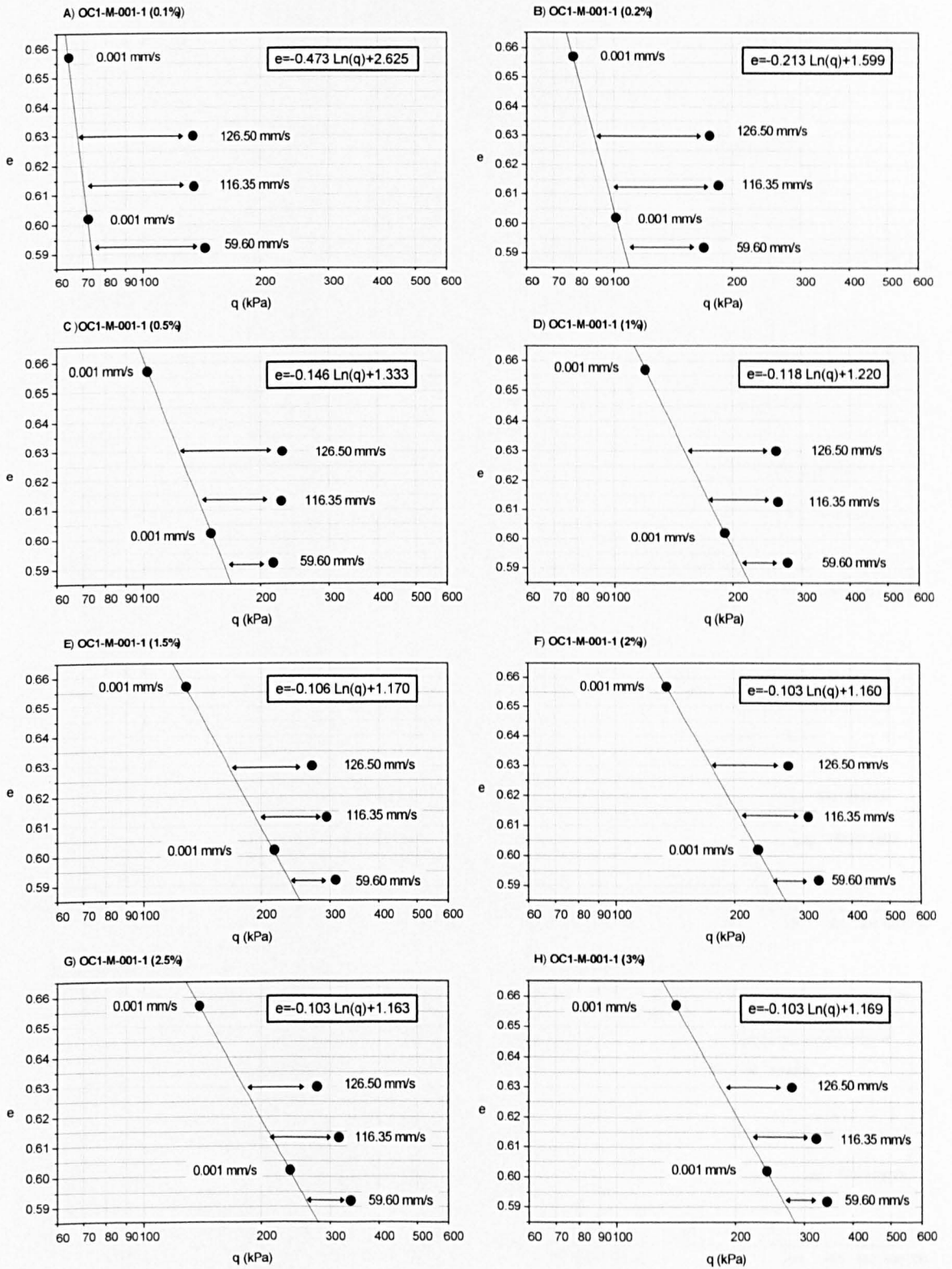


Figure 7.24 Deduced equal strain contours at 0.001 mm/s for multistage test OC1-M-001-1. Voids ratio versus deviator stress.

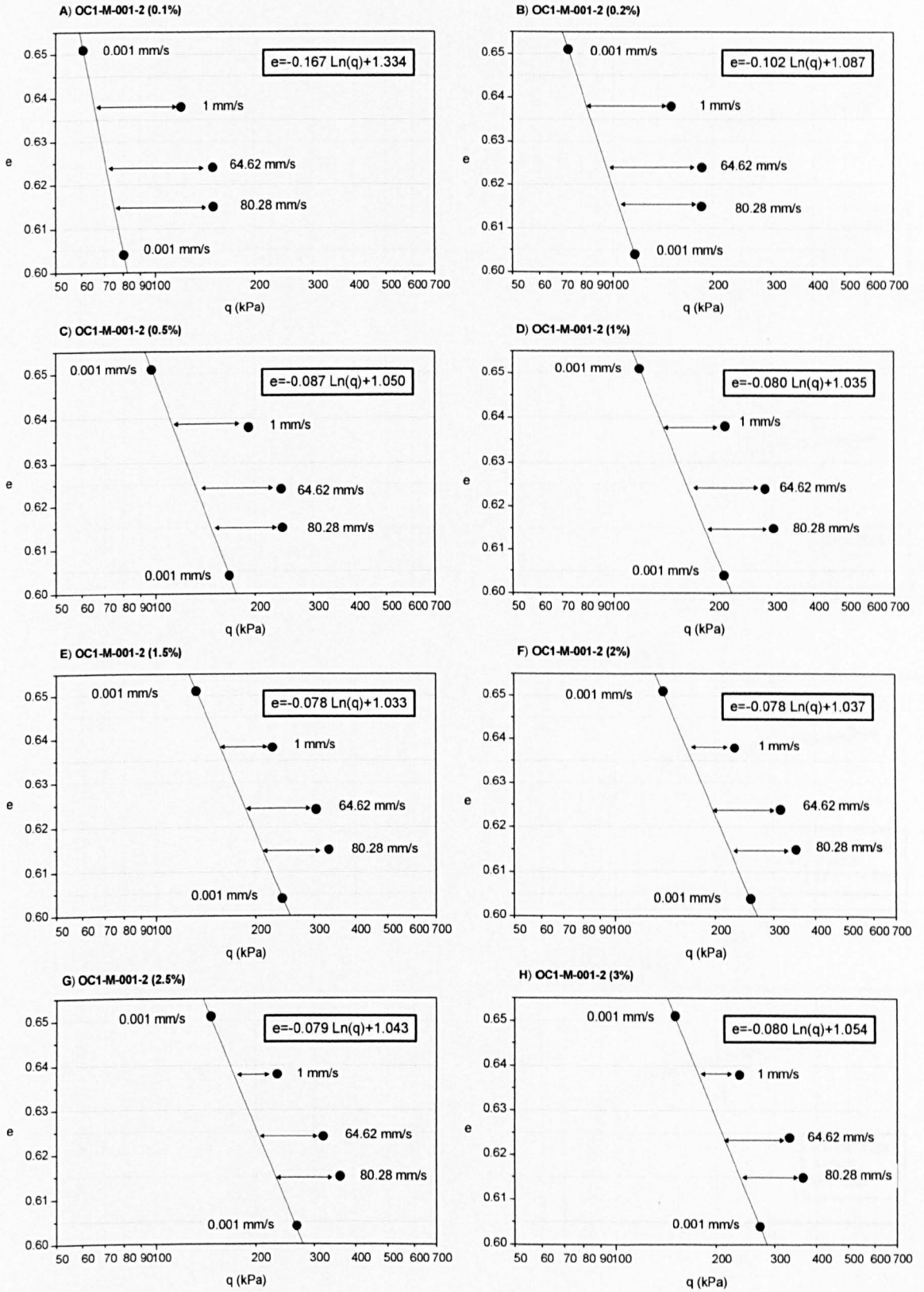


Figure 7.25 Deduced equal strain contours at 0.001 mm/s for multistage test OC1-M-001-2. Voids ratio versus deviator stress.

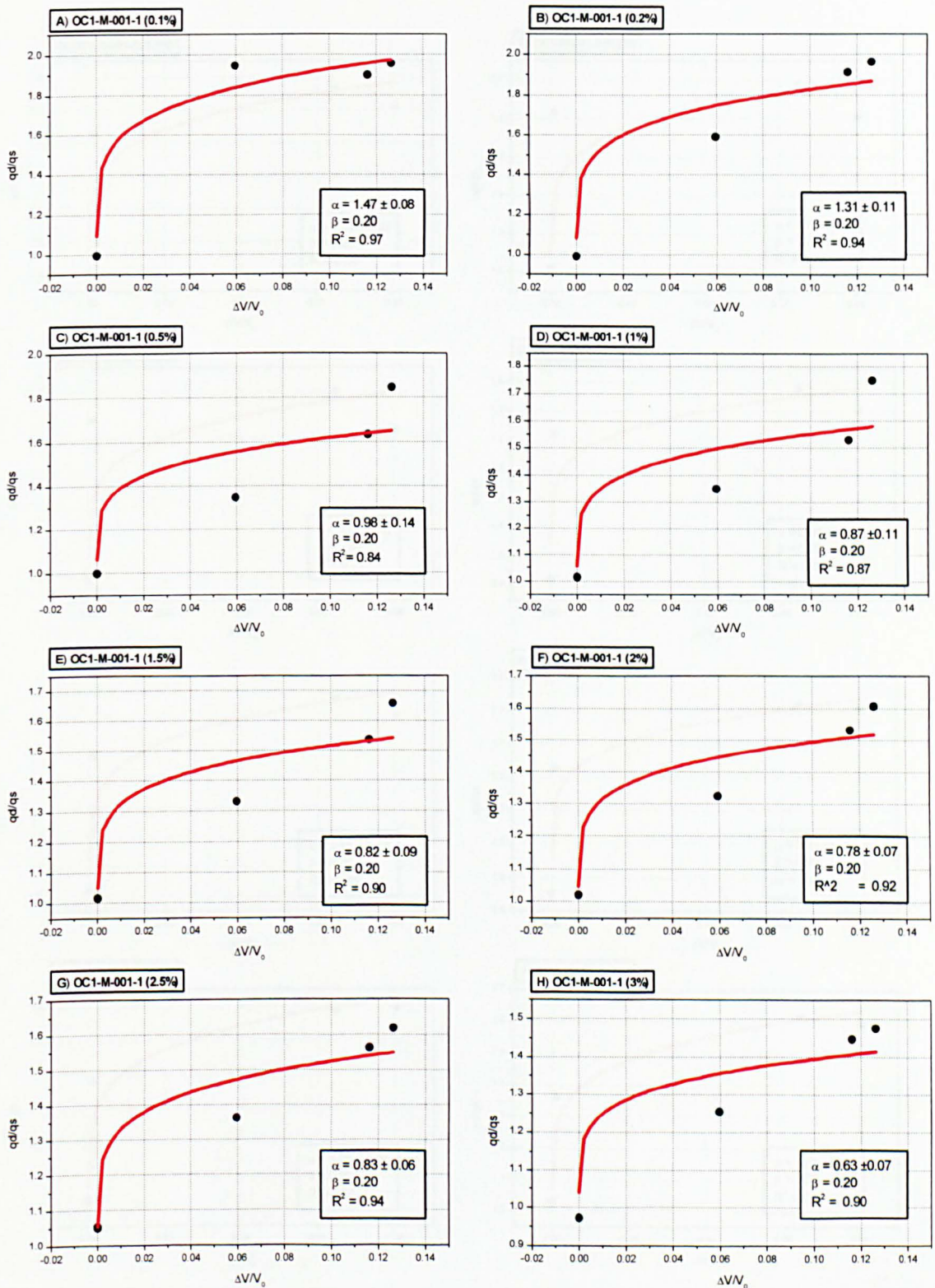


Figure 7.26 Deviator stress versus normalized axial displacement rate ($\Delta V/V_0$) at different strain states for multistage test at different rates, OC1-M-001-1.

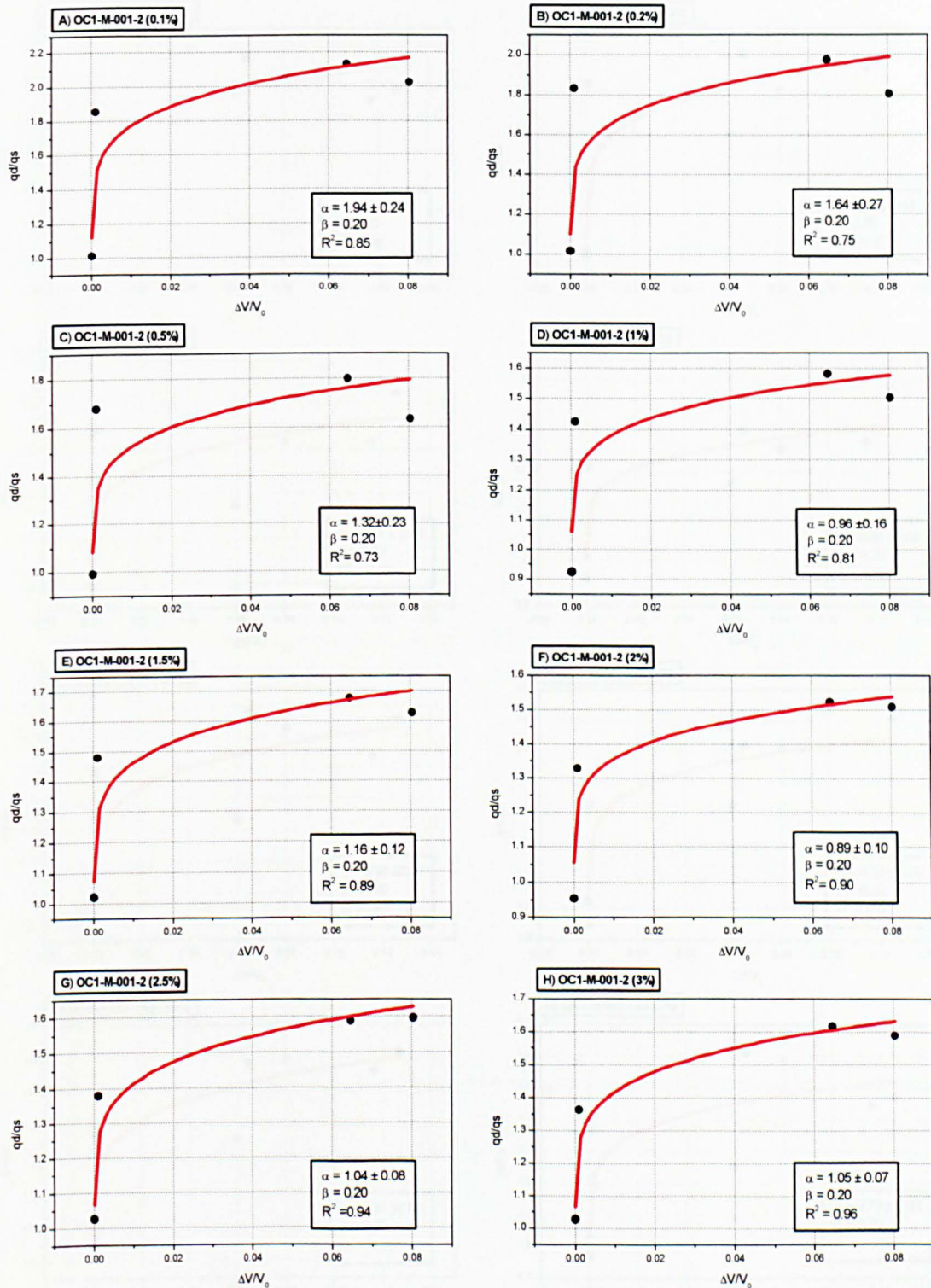


Figure 7.27 Deviator stress versus normalized axial displacement rate ($\Delta V/V_0$) at different strain states for multistage test at different rates, OC1-M-001-2.

Figure 7.28 Deviator stress versus normalized axial displacement rate ($\Delta V/V_0$) at different strain states for multistage test at different rates, OC1-M-001-2.

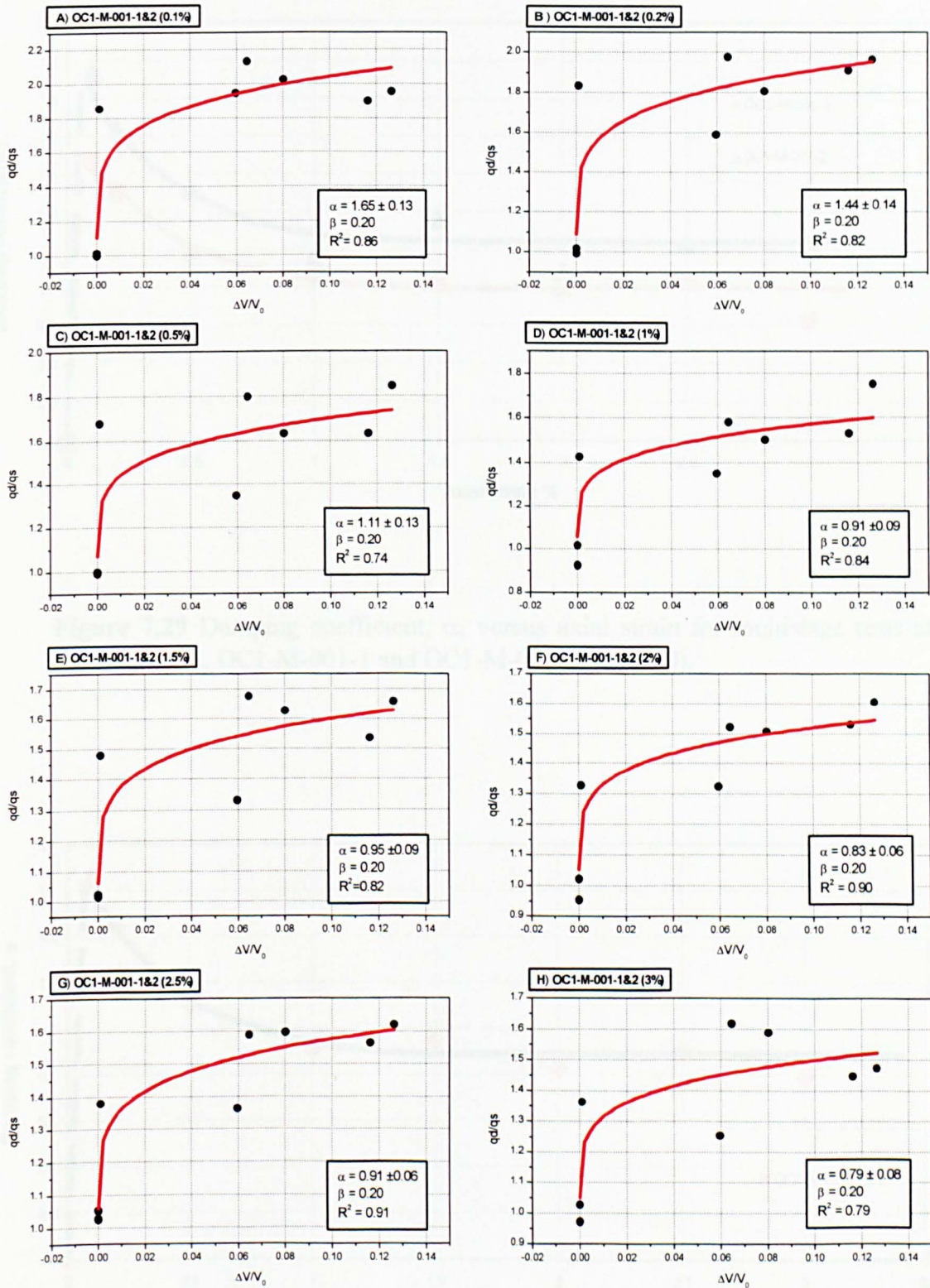


Figure 7.28 Deviator stress versus normalized axial displacement rate ($\Delta V/V_0$) at different strain states for multistage tests at different rates, OC1-M-001-1 and OC1-M-001-2.

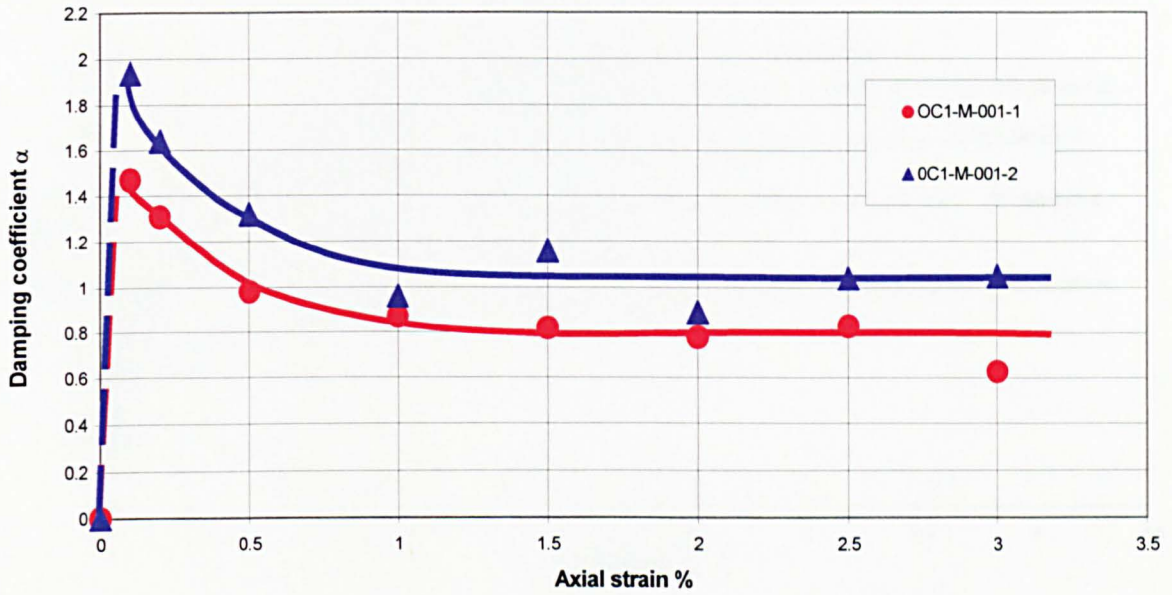


Figure 7.29 Damping coefficient, α , versus axial strain for multistage tests at different rates, OC1-M-001-1 and OC1-M-001-2. ($\beta=0.20$).

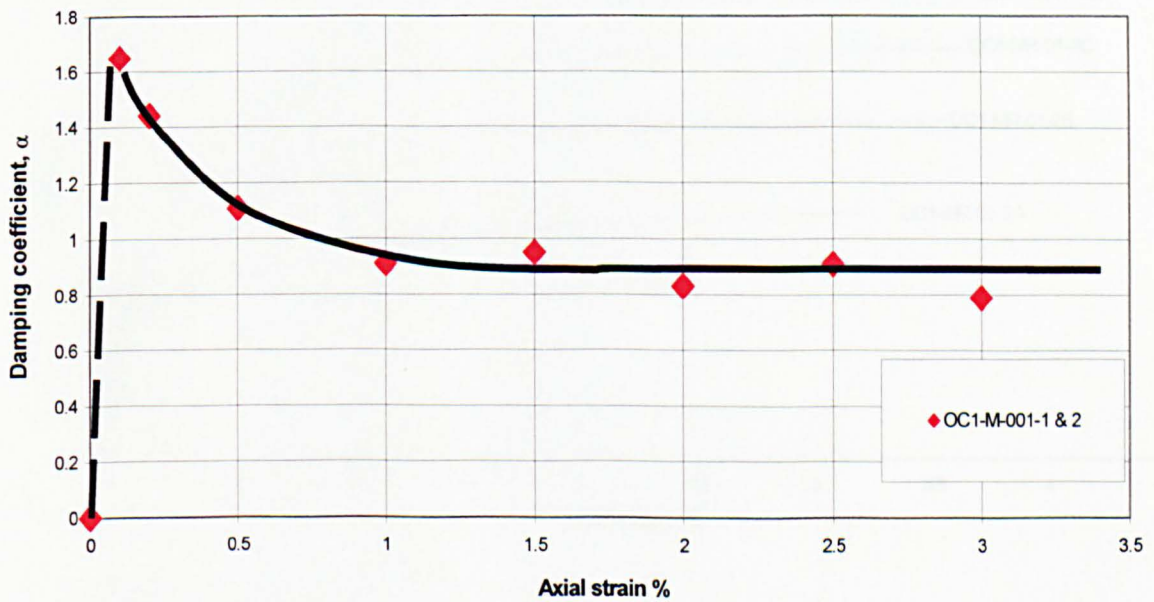


Figure 7.30 Damping coefficient, α , versus axial strain for combined analysis of data from multistage tests at different rates OC1-M-001-1 and OC1-M-001-2. ($\beta=0.20$).

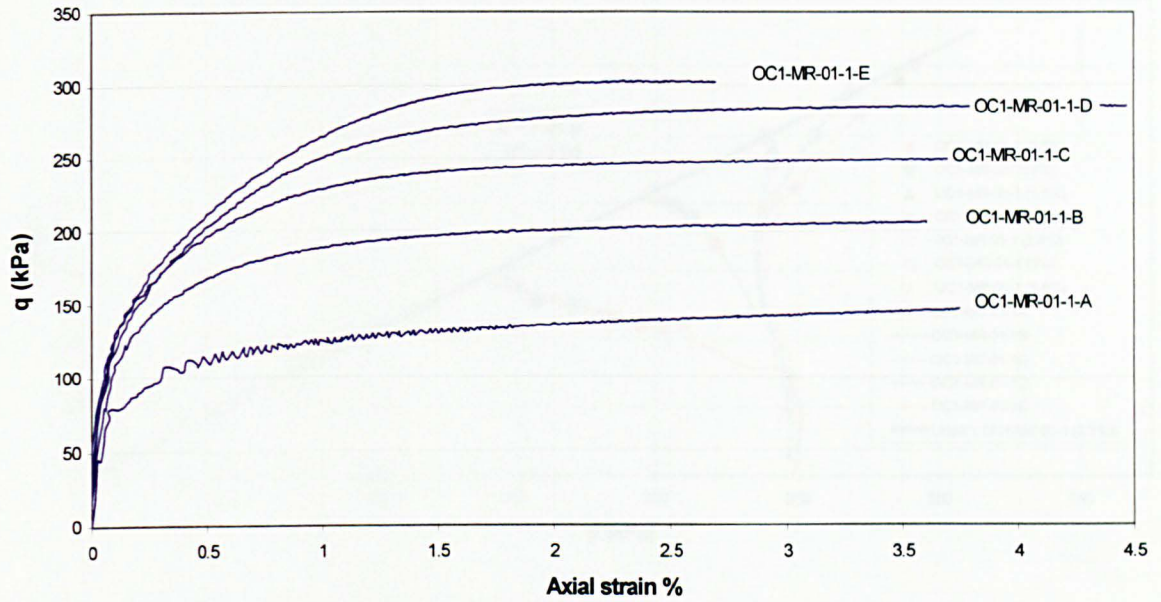


Figure 7.31 Deviator stress versus axial strain for multistage test OC1-MR-01-1 at constant rate (0.01 mm/s).

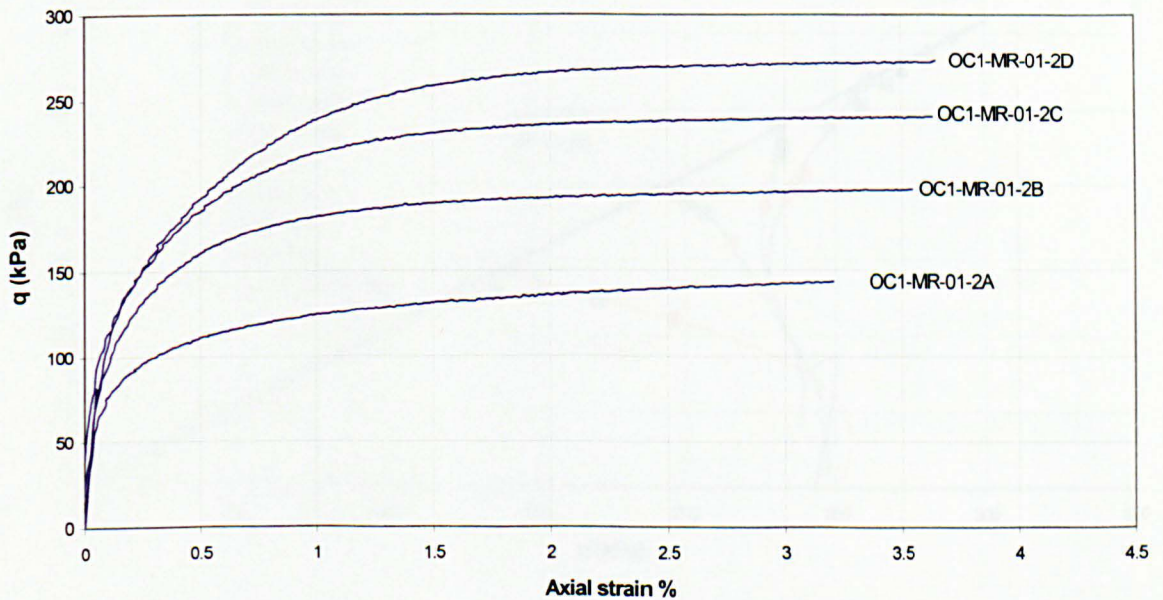


Figure 7.32 Deviator stress versus axial strain for multistage test OC1-MR-01-2 at constant rate (0.01 mm/s).

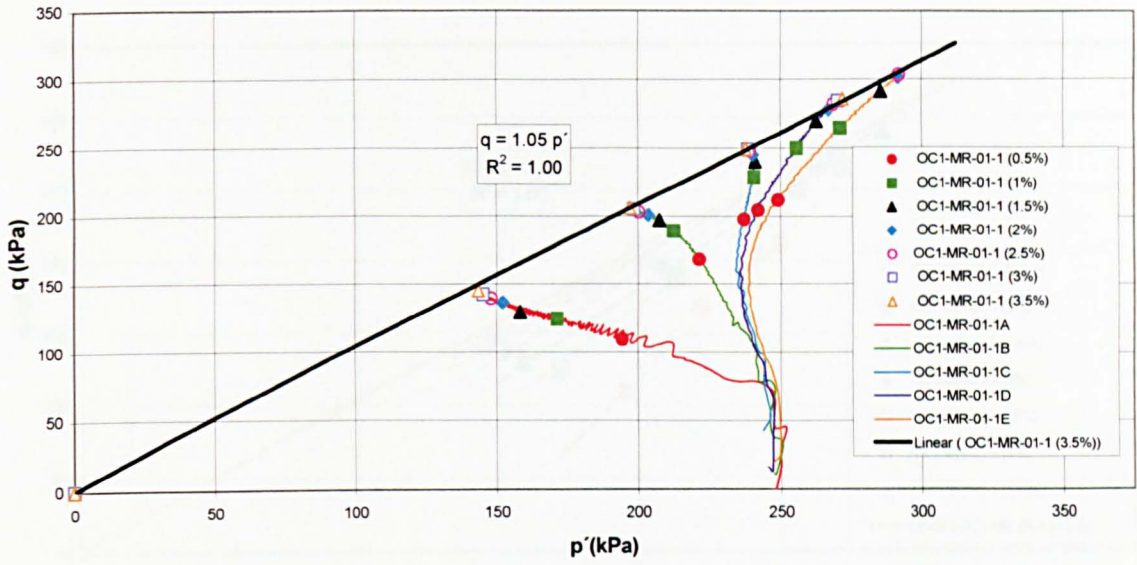


Figure 7.33 Effective stress paths for multistage test OC1-MR-01-1 at constant rate (0.01 mm/s).

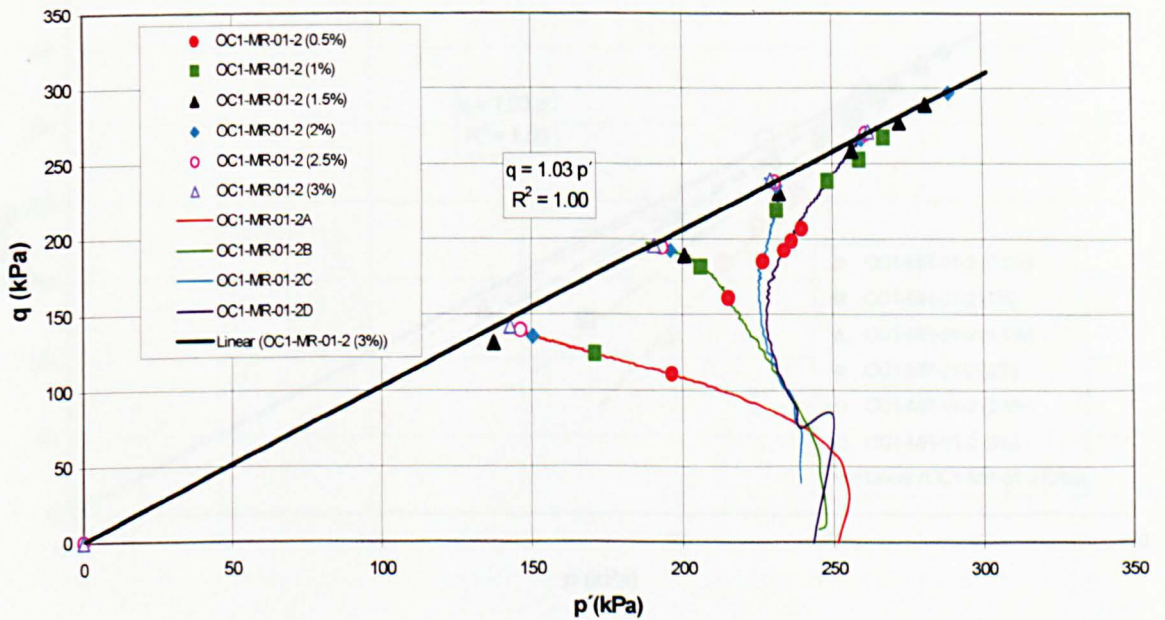


Figure 7.34 Effective stress paths for multistage test OC1-MR-01-2 at constant rate (0.01 mm/s).

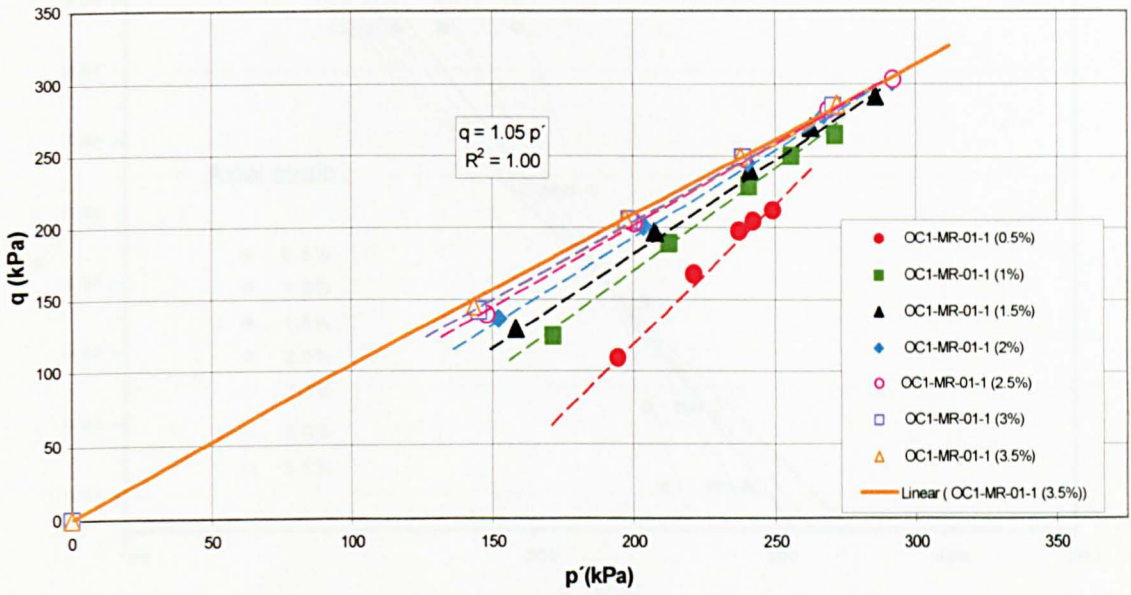


Figure 7.35 Equal strain contours for multistage test OC1-MR-01-1 at constant rate (0.01 mm/s). Deviator stress versus mean effective stress.

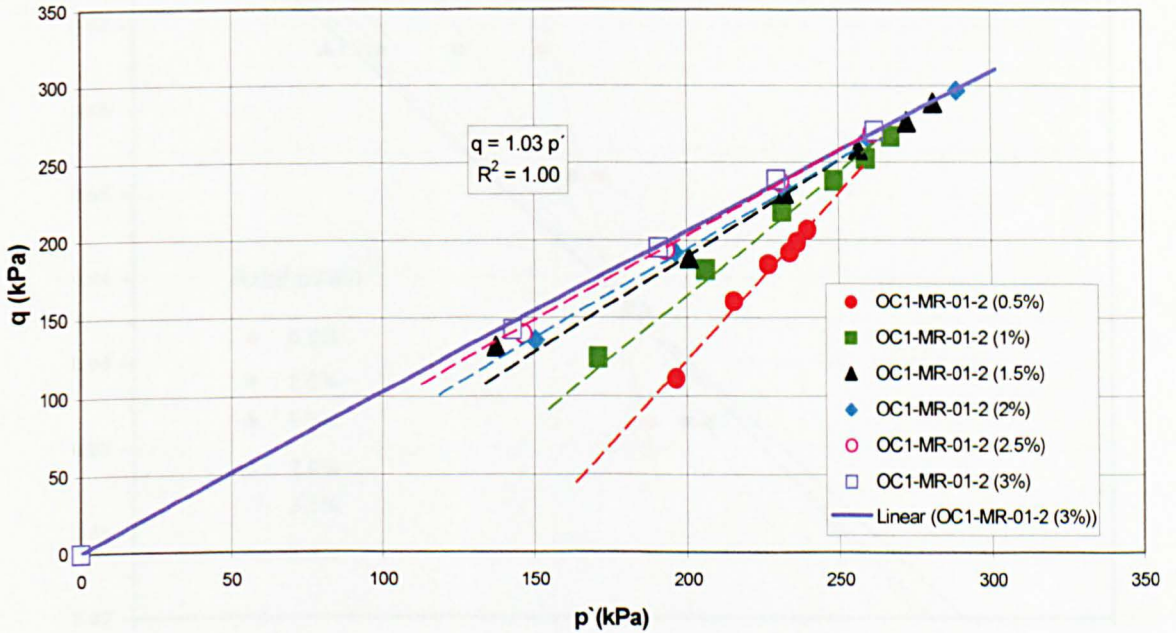


Figure 7.36 Equal strain contours for multistage test OC1-MR-01-2 at constant rate (0.01 mm/s). Deviator stress versus mean effective stress.

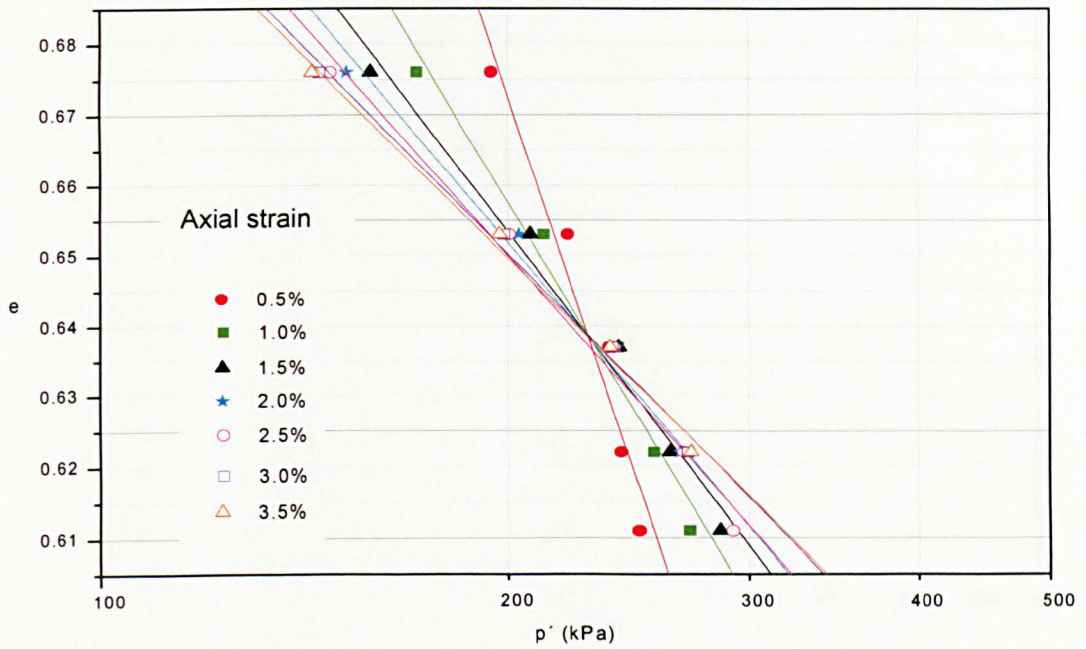


Figure 7.37 Equal strain contours for multistage test OC1-MR-01-1 at constant rate (0.01 mm/s). Voids ratio versus mean effective stress.

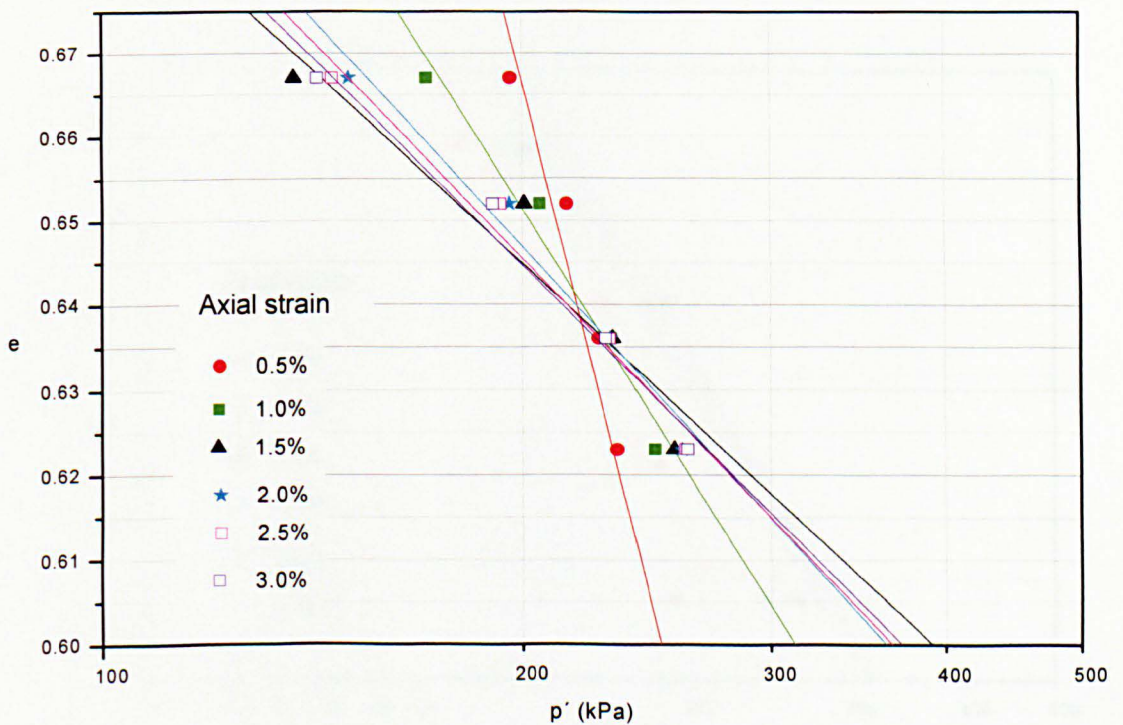


Figure 7.38 Equal strain contours for multistage test OC1-MR-01-2 at constant rate (0.01 mm/s). Voids ratio versus mean effective stress.

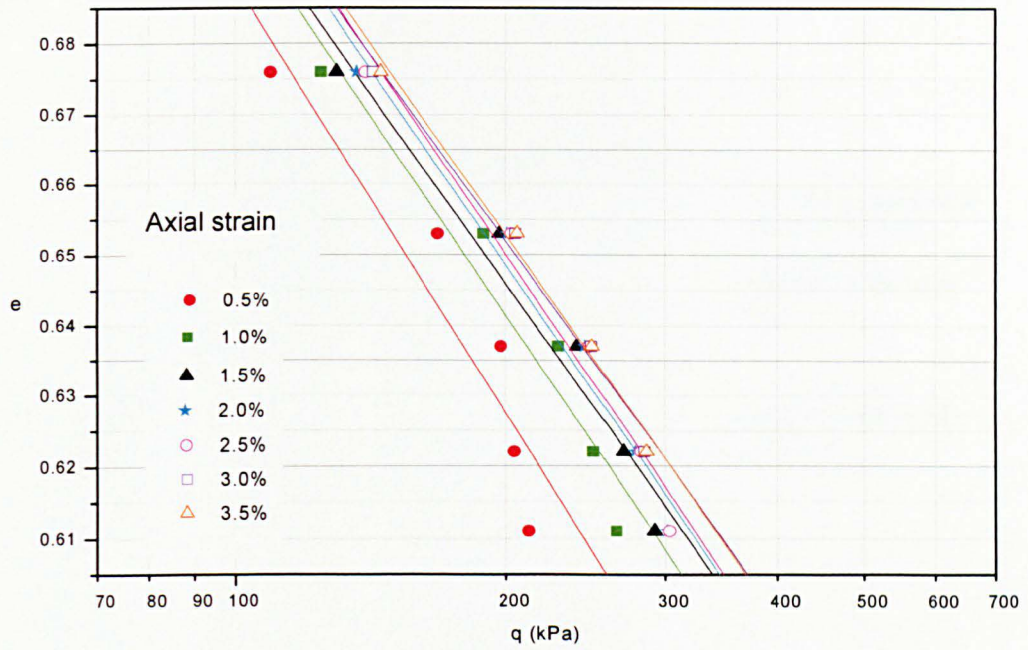


Figure 7.39 Equal strain contours for multistage test OC1-MR-01-1 at constant rate (0.01 mm/s). Voids ratio versus deviator stress.

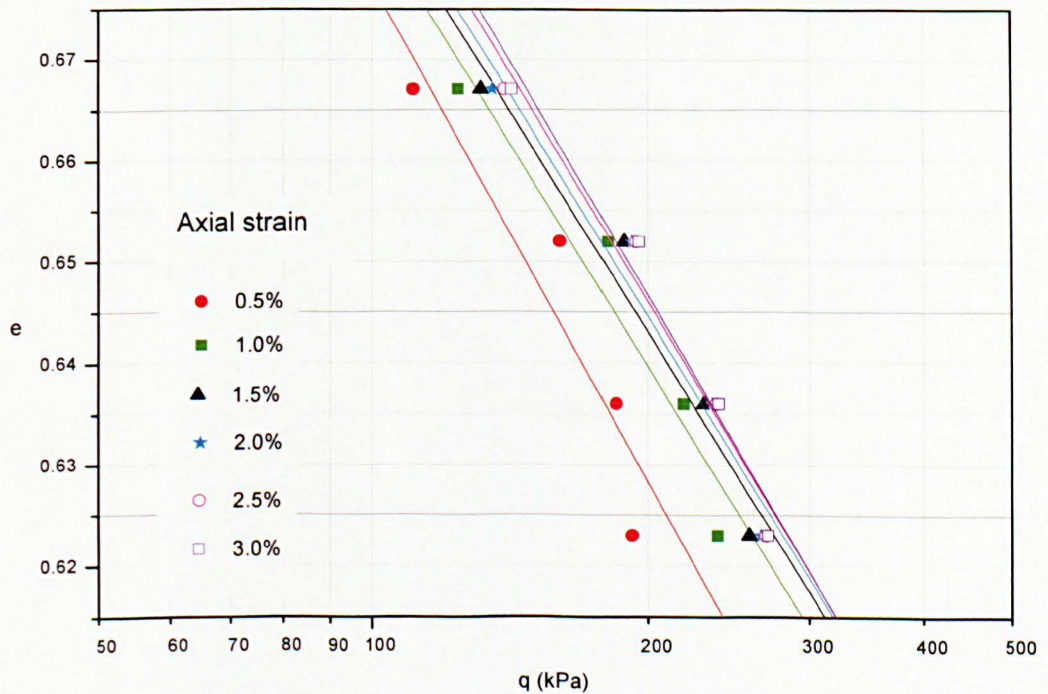


Figure 7.40 Equal strain contours for multistage test OC1-MR-01-2 at constant rate (0.01 mm/s). Voids ratio versus deviator stress.

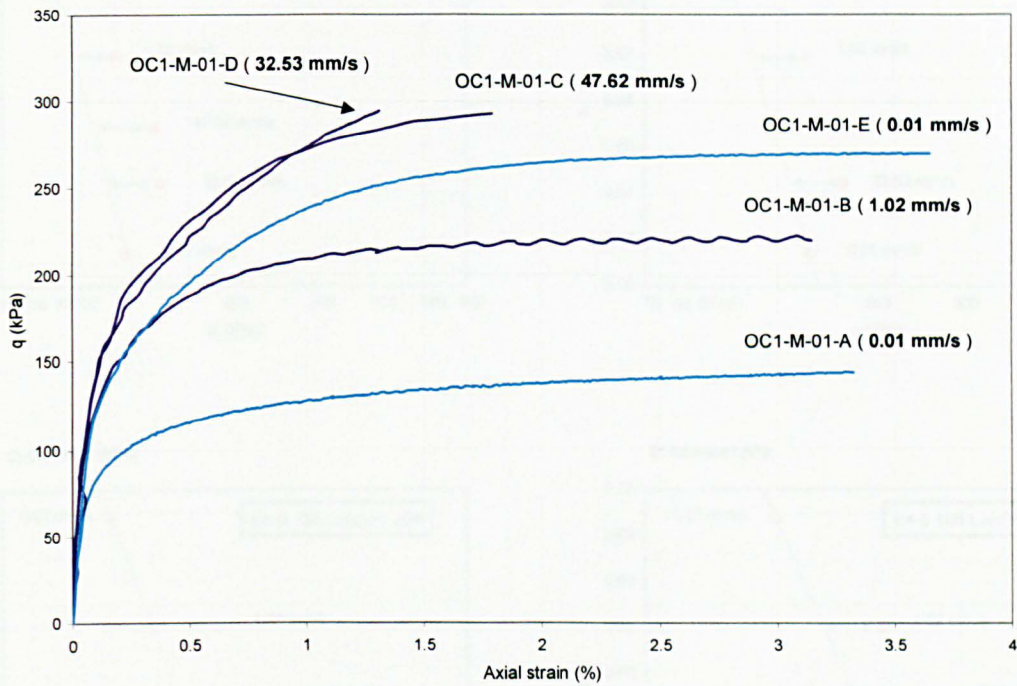


Figure 7.41 Deviator stress versus axial strain curves at different rates for multistage test OC1-M-01. (OCR = 1)

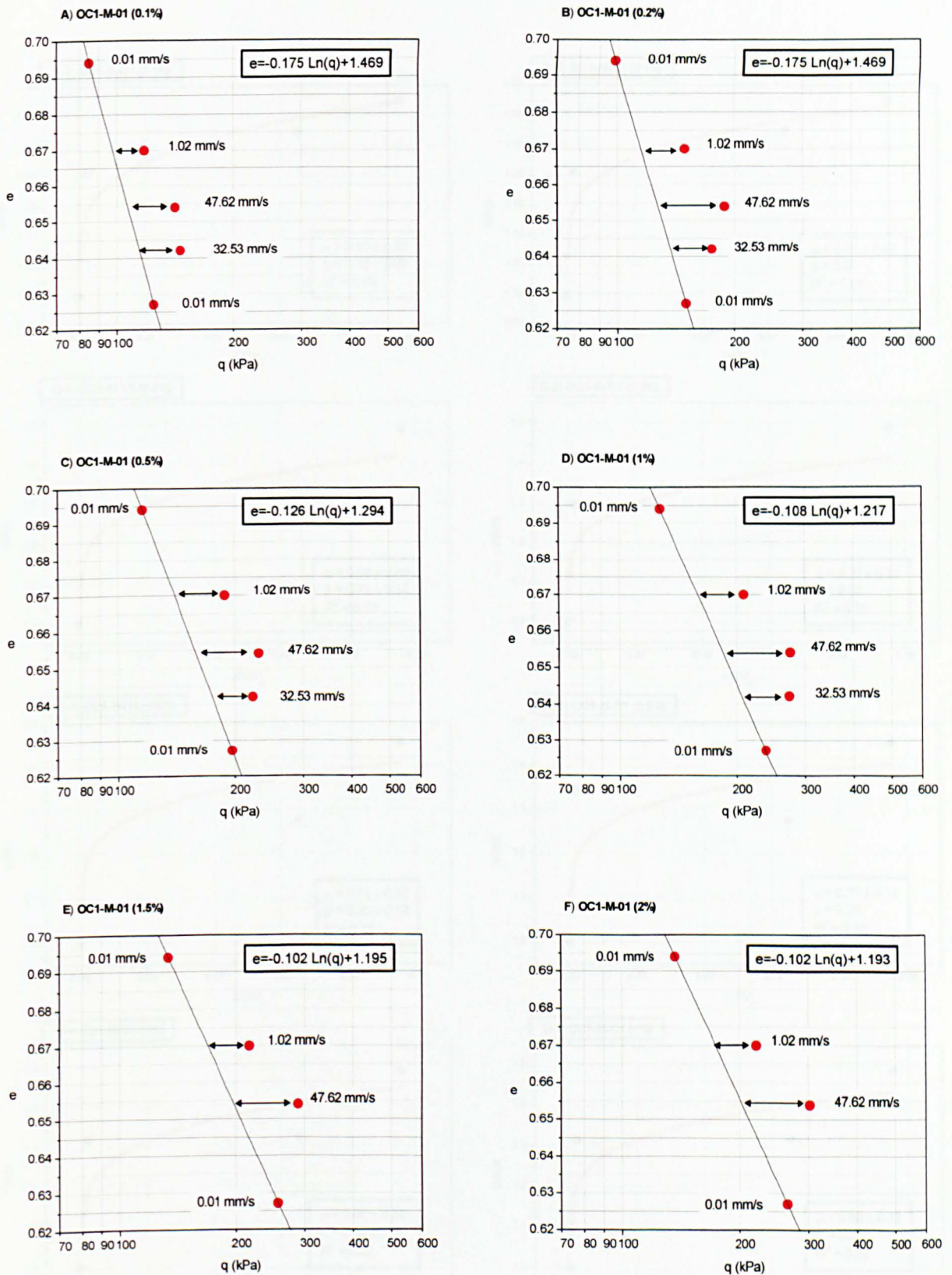


Figure 7.42 Deduced equal strain contours at 0.01 mm/s for multistage test OC1-M-01. Voids ratio versus deviator stress.

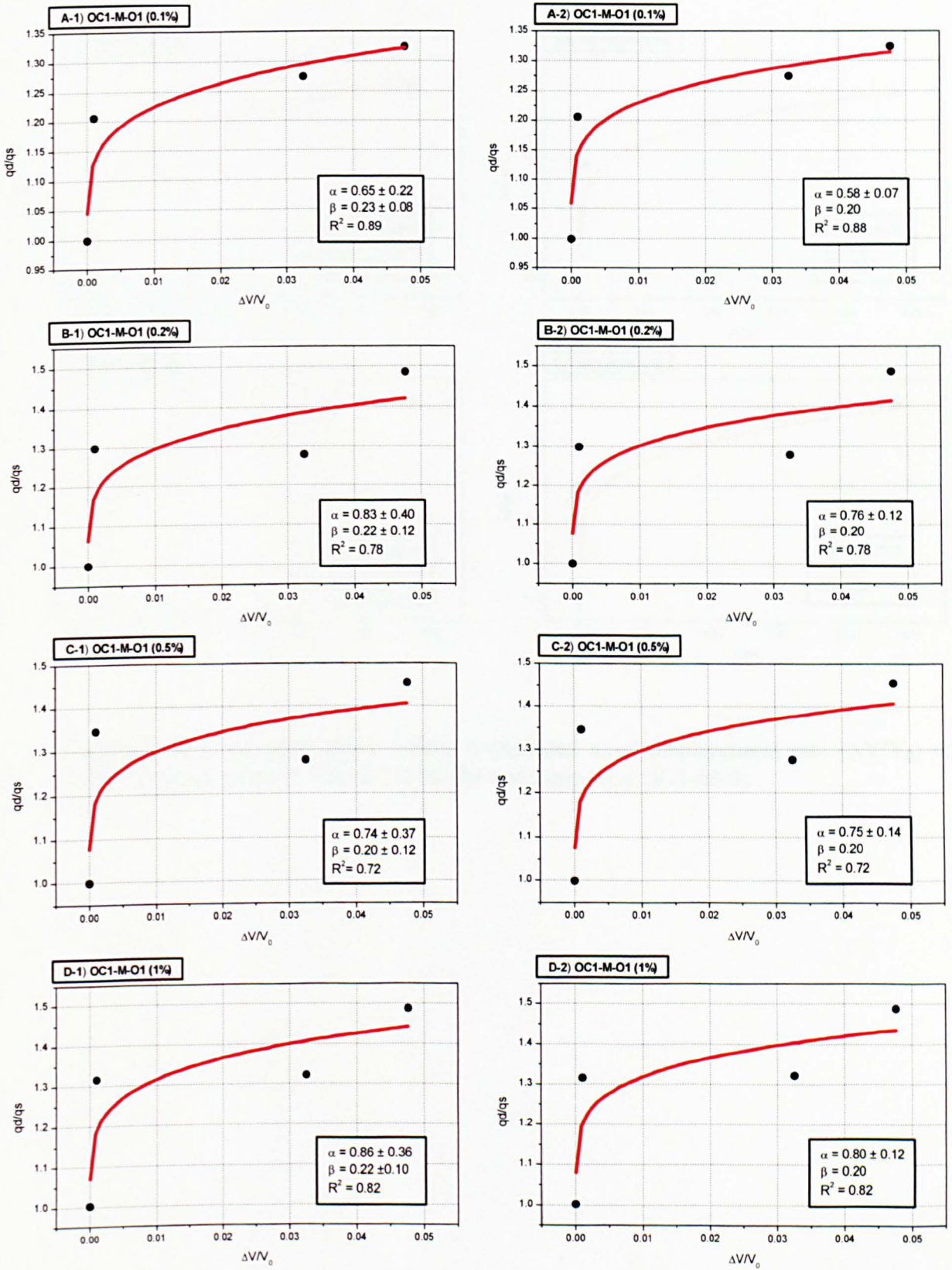


Figure 7.43 a Deviator stress versus normalized axial displacement rate ($\Delta V/V_0$) at different strain states (0.1% to 1.0%) for multistage test OC1-M-01.

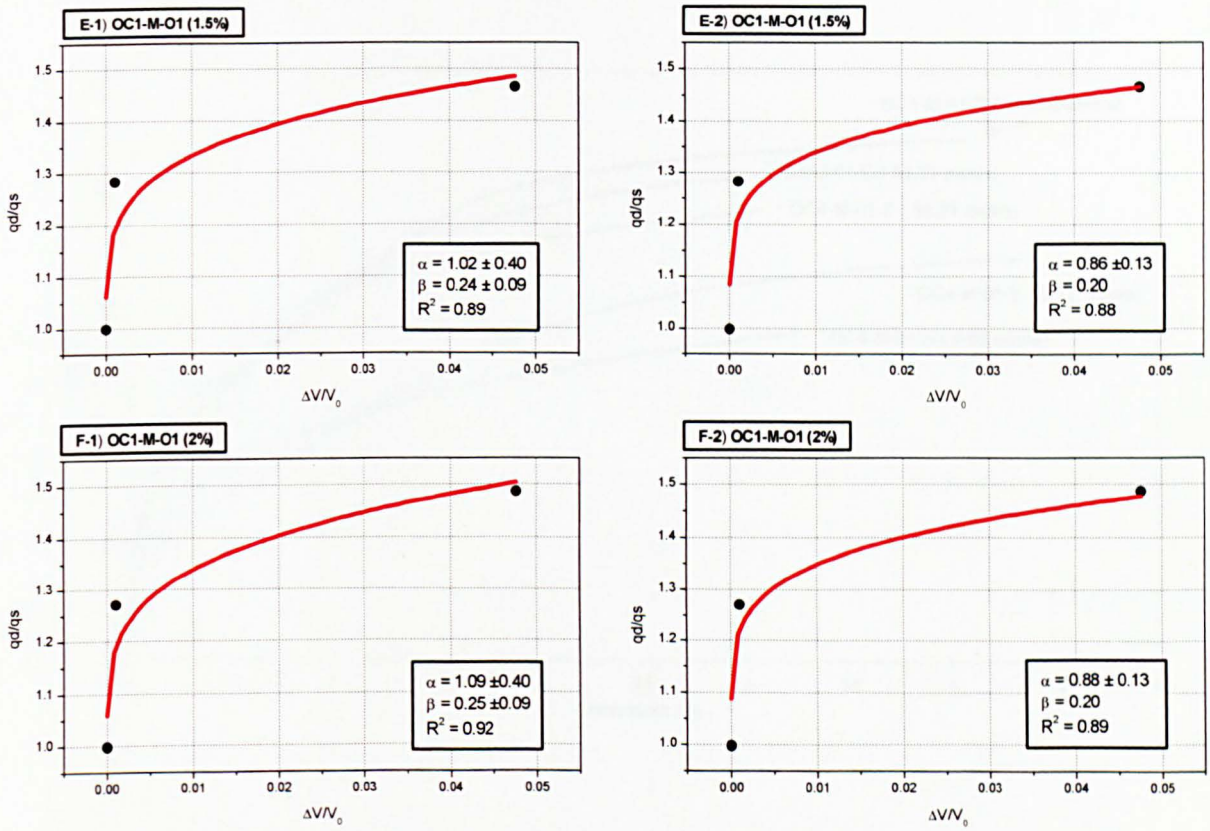


Figure 7.43 b Deviator stress versus normalized axial displacement rate ($\Delta V/V_0$) at different strain states (1.5 % to 2.0 %) for multistage test OC1-M-01.

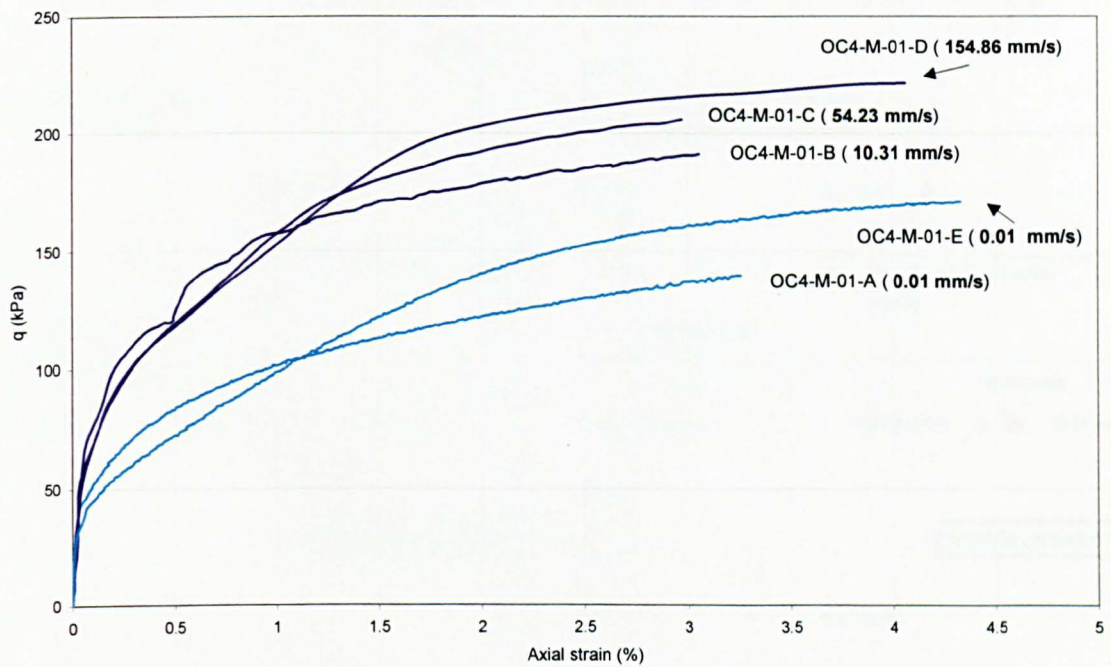


Figure 7.44 Deviator stress versus axial strain curves at different rates for multistage test OC4-M-01. (OCR = 4).

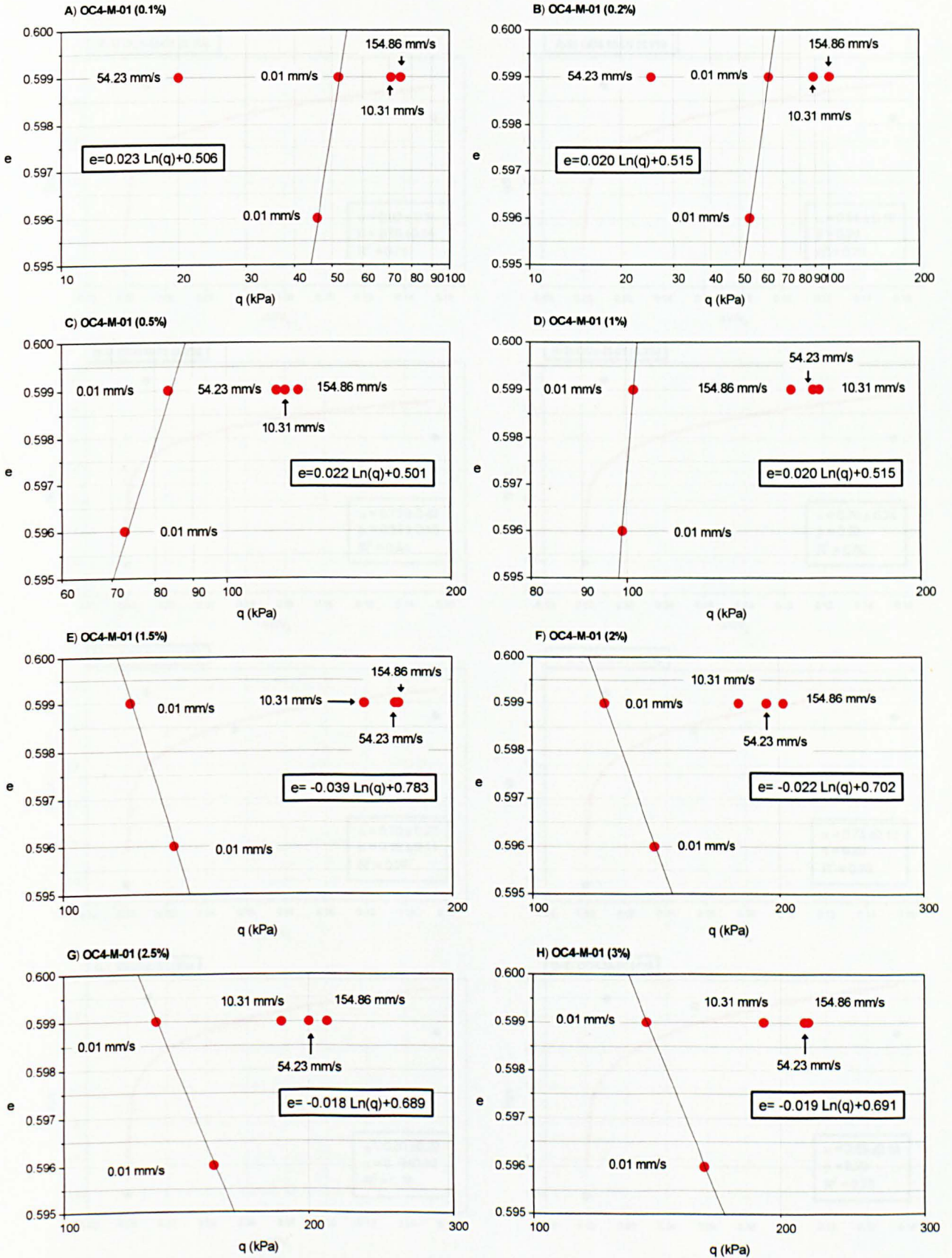


Figure 7.45 Deduced equal strain contours at 0.01 mm/s for multistage test OC4-M-01. Voids ratio versus deviator stress.

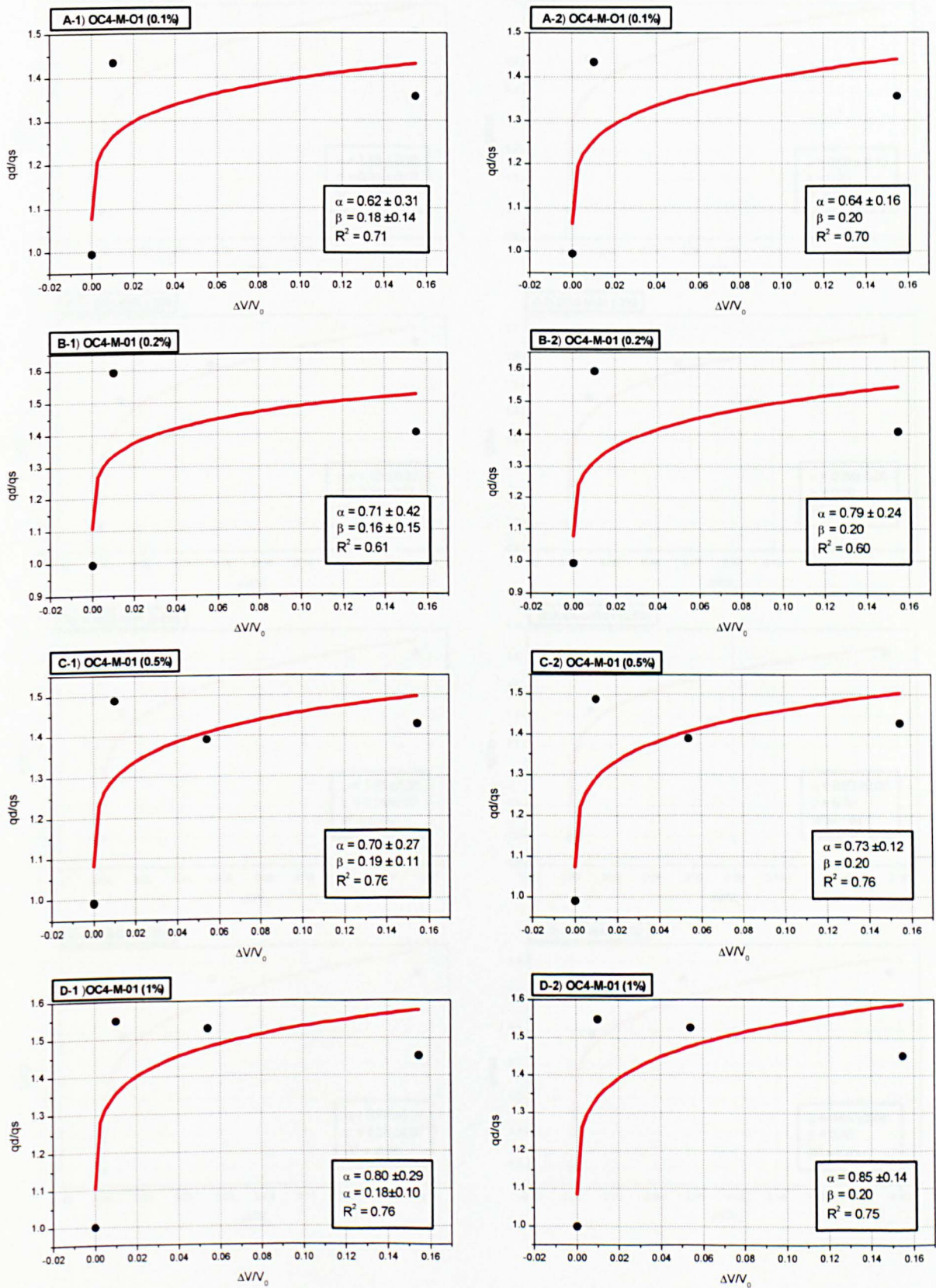


Figure 7.46 a Deviator stress versus normalized axial displacement rate ($\Delta V/V_0$) at different strain states (0.1% to 1.0%) for multistage test OC4-M-01.

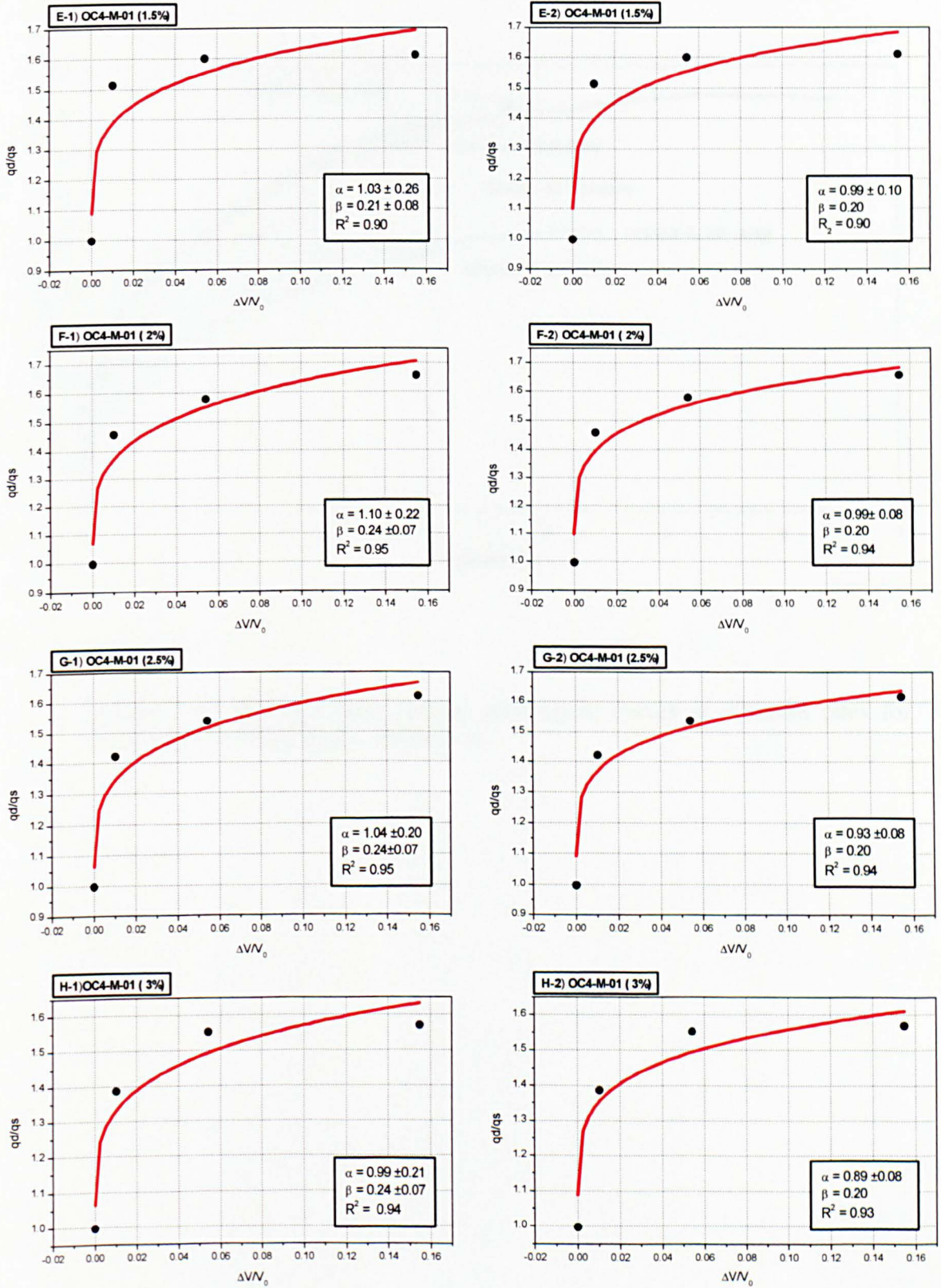


Figure 7.46 b Deviator stress versus normalized axial displacement rate ($\Delta V/V_0$) at different strain states (1.5 % to 3.0%) for multistage test OC4-M-01.

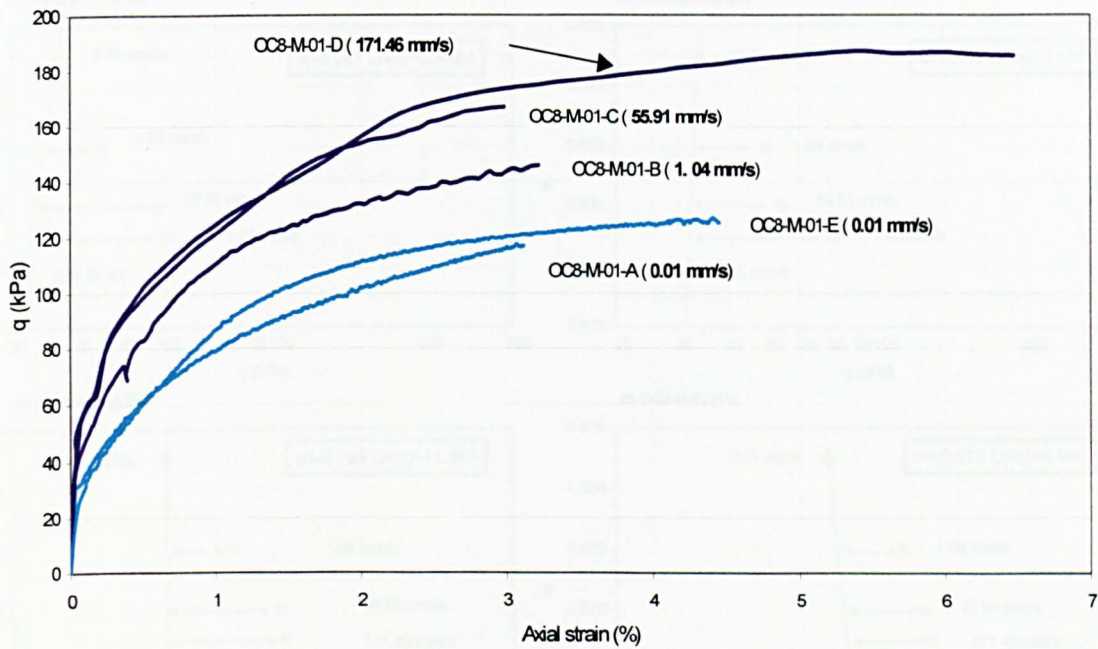


Figure 7.47 Deviator stress versus axial strain curves at different rates for multistage test OC8-M-01. (OCR = 8).

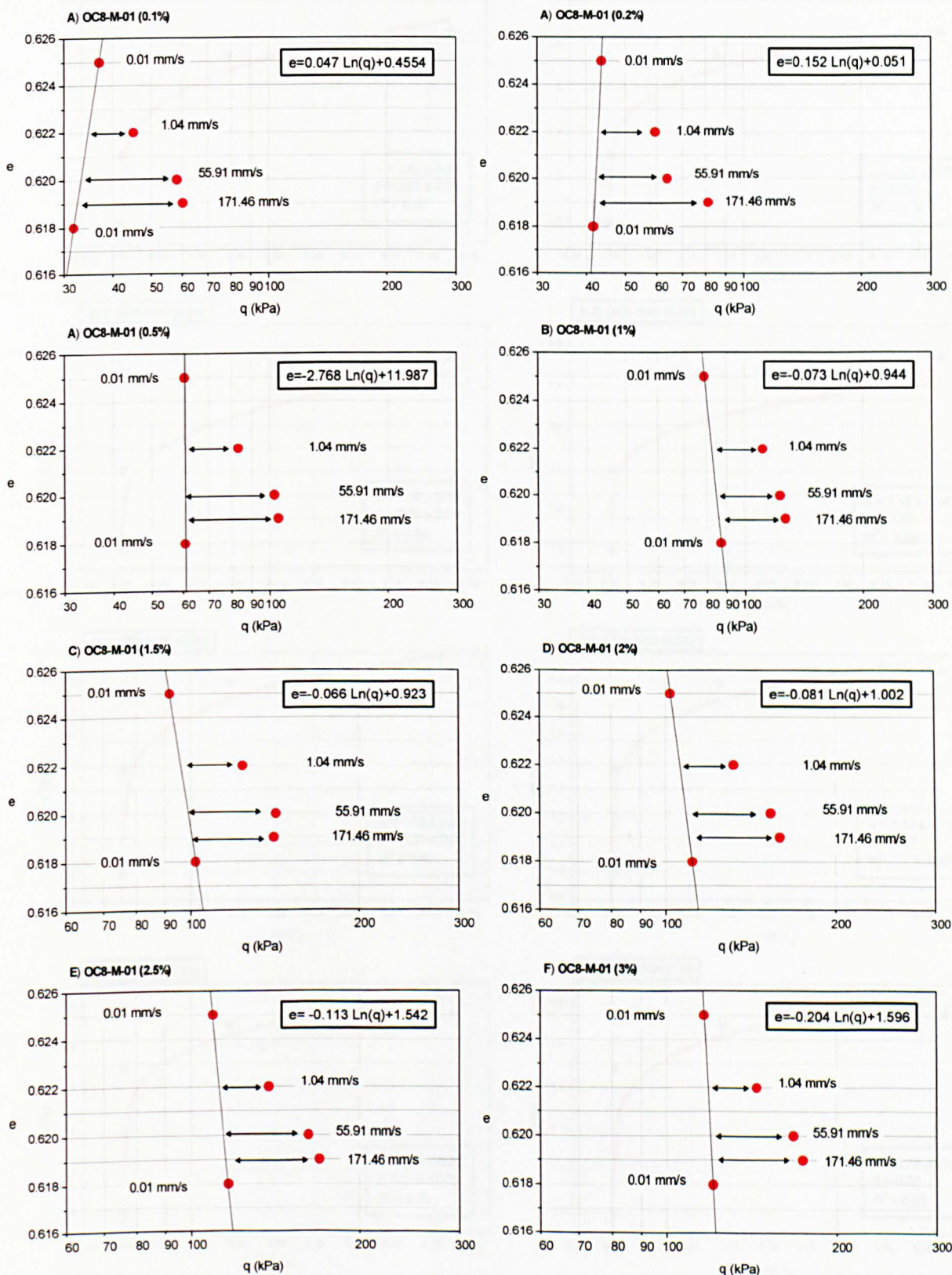


Figure 7.48 Deduced equal strain contours at 0.01 mm/s for multistage test OC8-M-01. Voids ratio versus deviator stress.

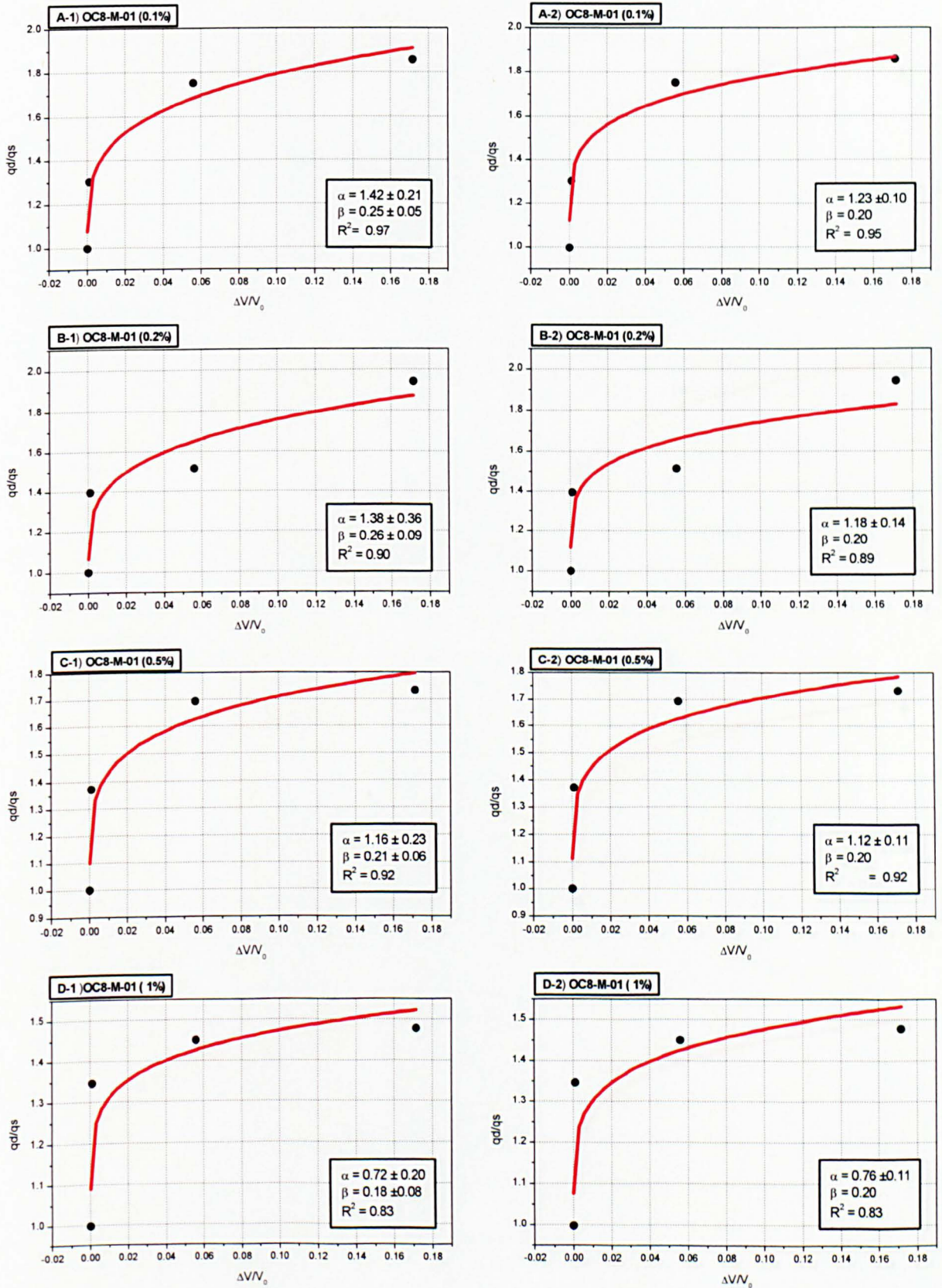


Figure 7.49 a Deviator stress versus normalized axial displacement rate ($\Delta V/V_0$) at different strain states (0.1% to 1.0%) for multistage test OC8-M-01.

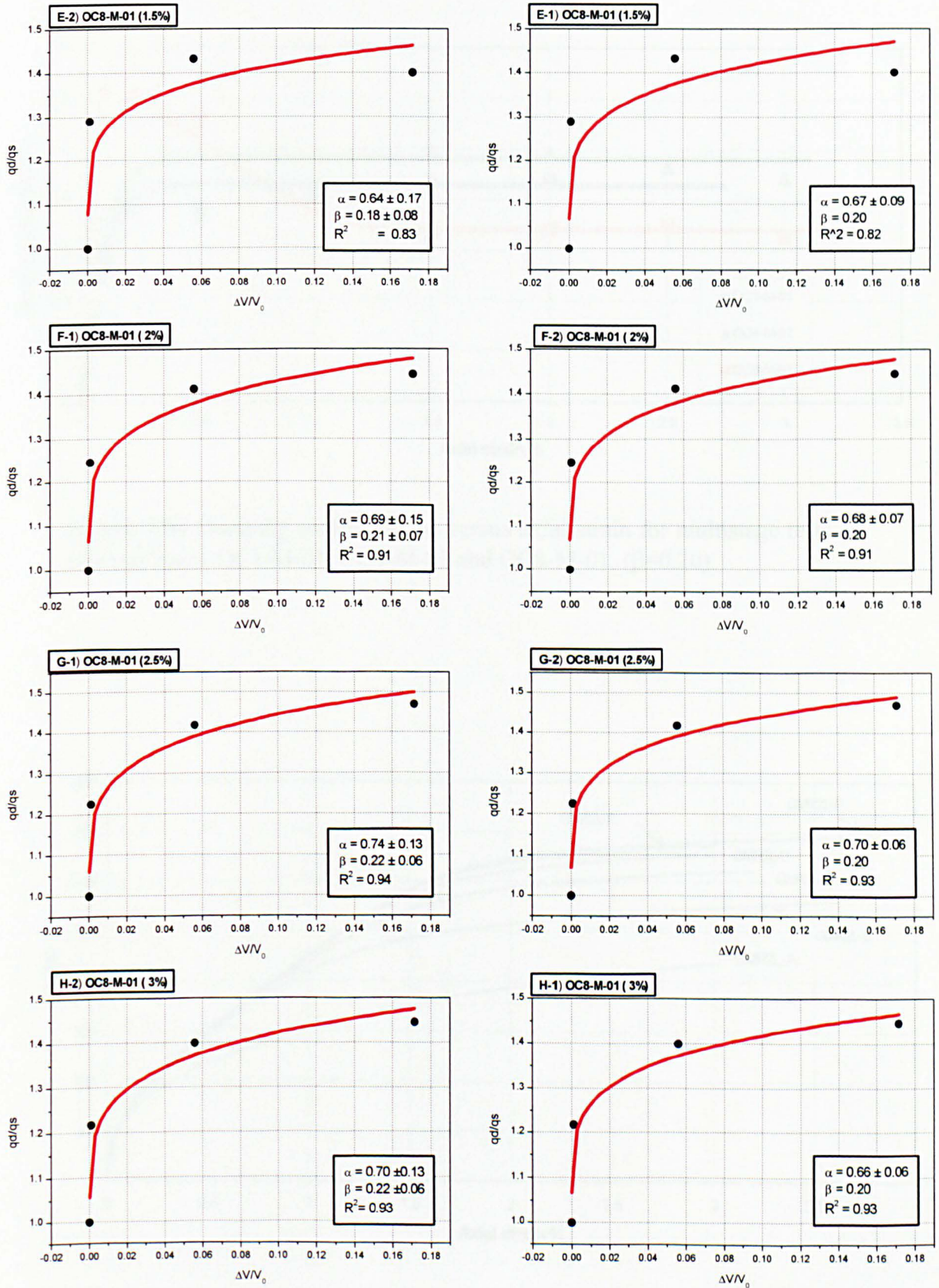


Figure 7.49 b Deviator stress versus normalized axial displacement rate ($\Delta V/V_0$) at different strain states (1.5 % to 3.0 %) for multistage test OC8-M-01.

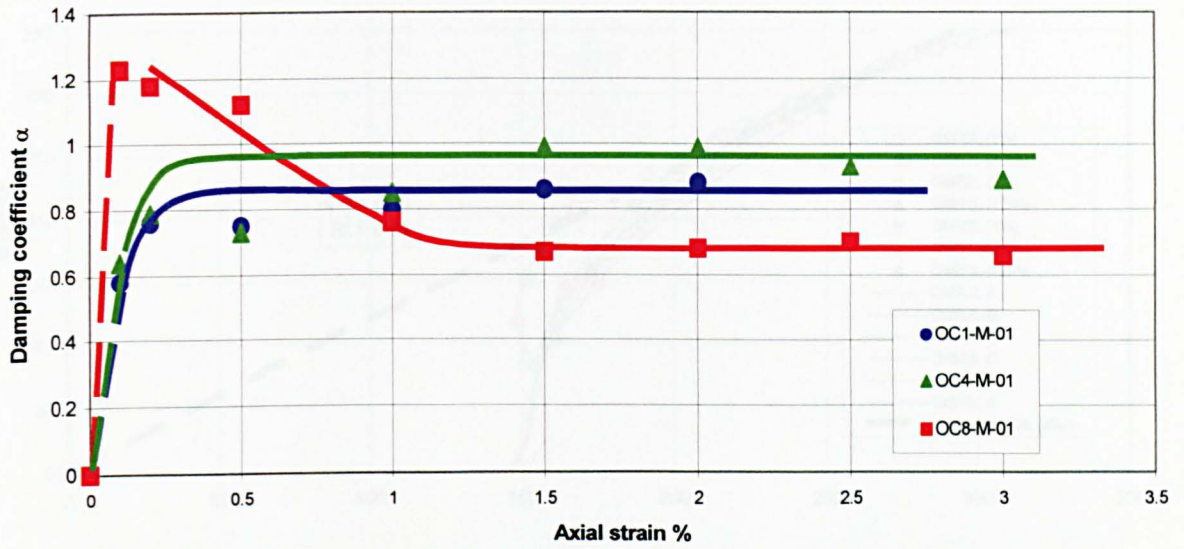


Figure 7.50 Damping coefficient, α , versus axial strain for multistage tests at different rates, OC1-M-01, OC4-M-01 and OC8-M-01. ($\beta=0.20$).

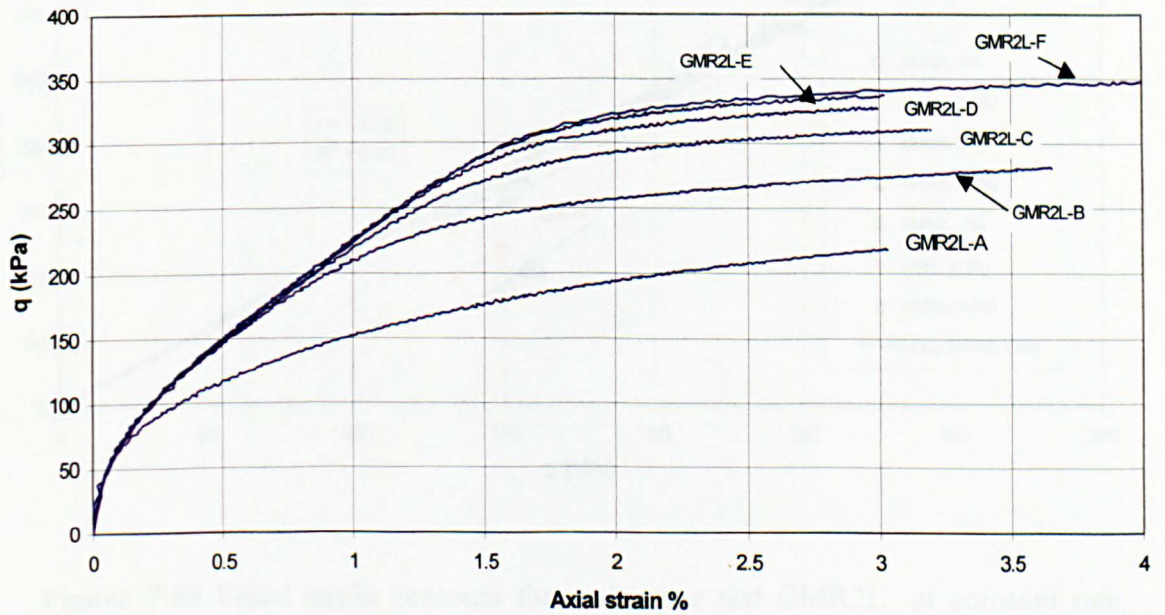


Figure 7.51 Deviator stress versus axial strain curves for multistage test GMR2L at constant rate (0.001 mm/s).

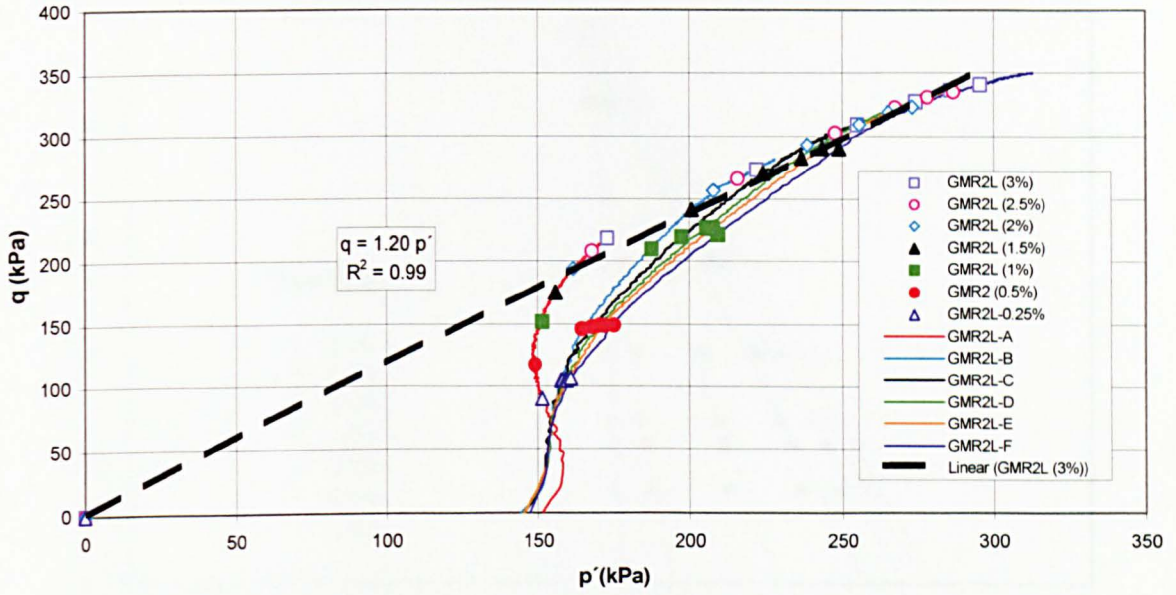


Figure 7.52 Effective stress paths for multistage test GMR2L at constant rate (0.001 mm/s).

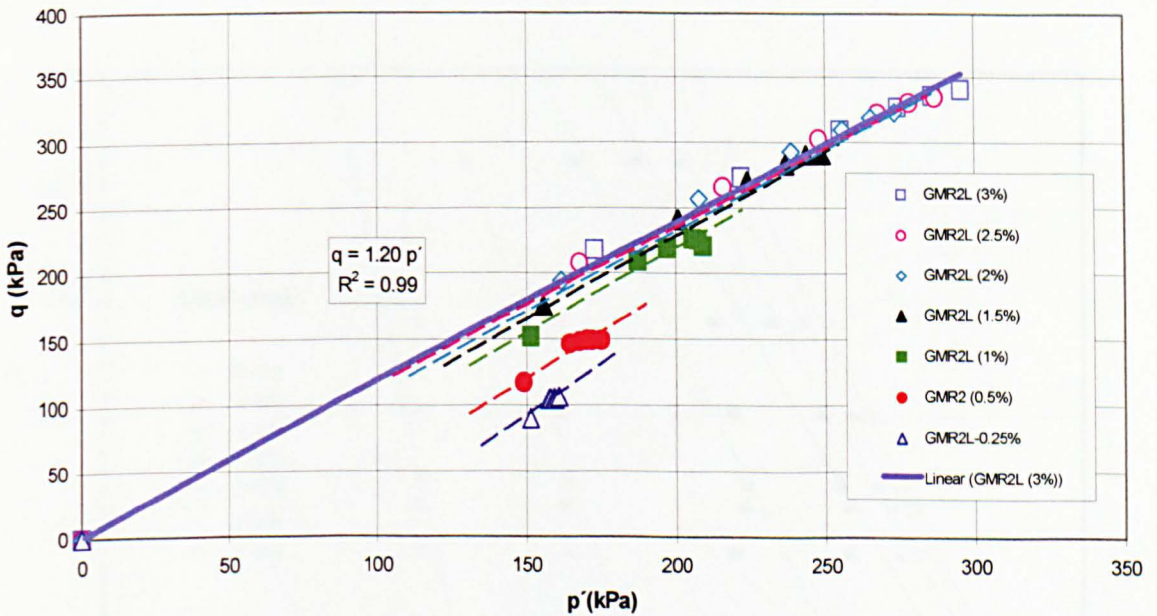


Figure 7.53 Equal strain contours for multistage test GMR2L at constant rate (0.001 mm/s). Deviator stress versus mean effective stress.

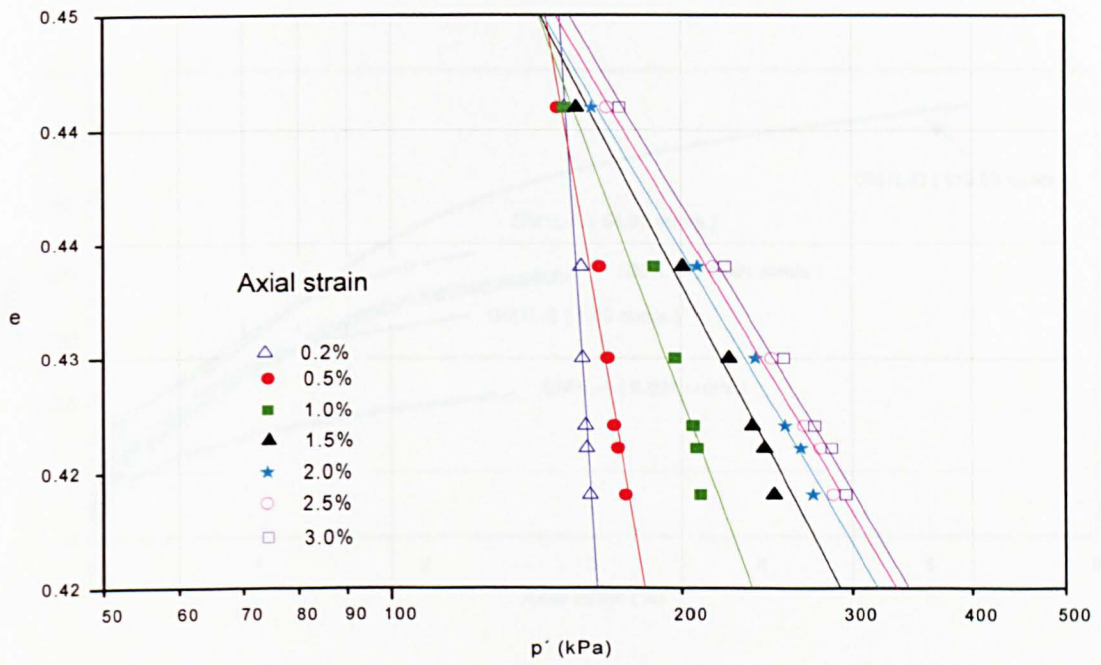


Figure 7.54 Equal strain contours for multistage test GMR2L at constant rate (0.001 mm/s). Voids ratio versus mean effective stress

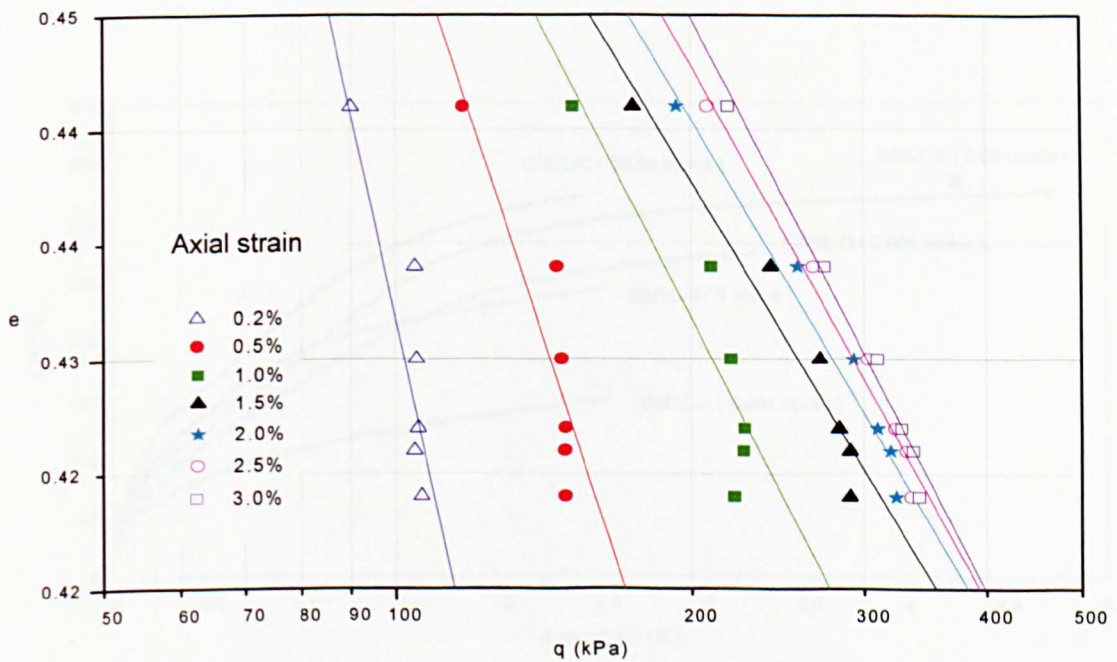


Figure 7.55 Equal strain contours for multistage test GMR2L at constant rate (0.001 mm/s). Voids ratio versus deviator stress.

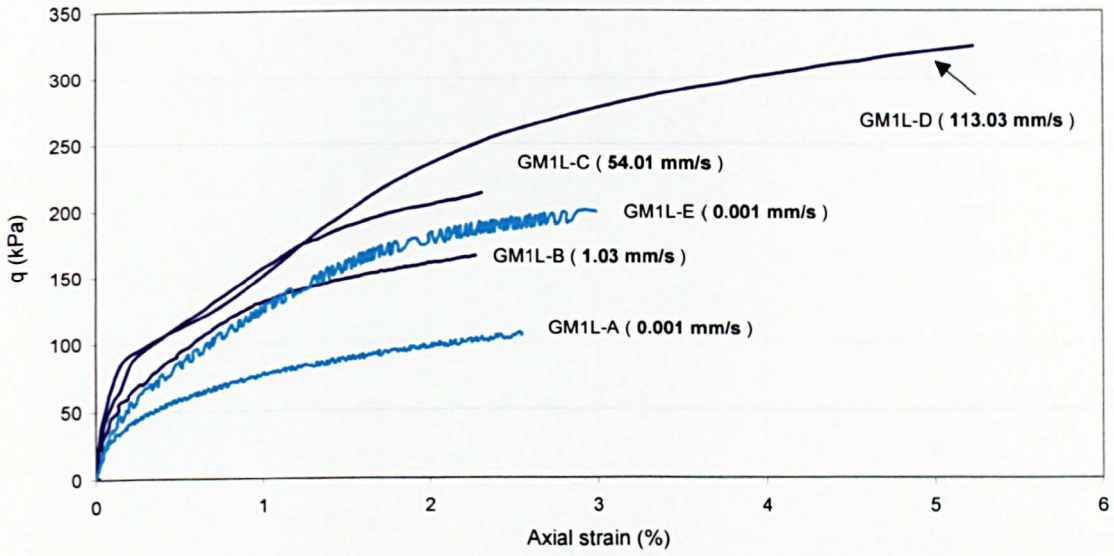


Figure 7.56 Deviator stress versus axial strain curves at different rates for multistage test GM1L.

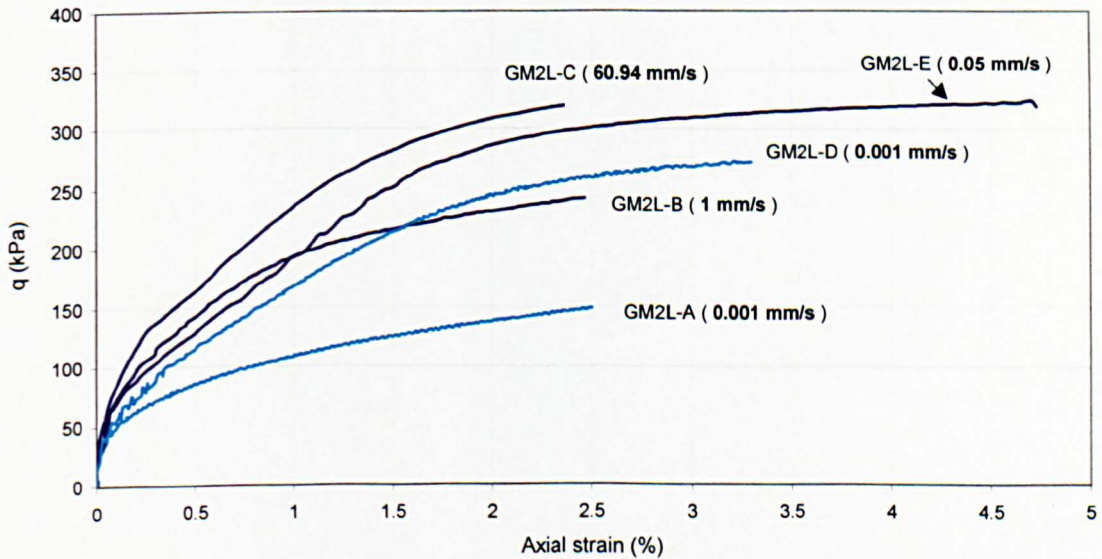


Figure 7.57 Deviator stress versus axial strain curves at different rates for multistage test GM2L.

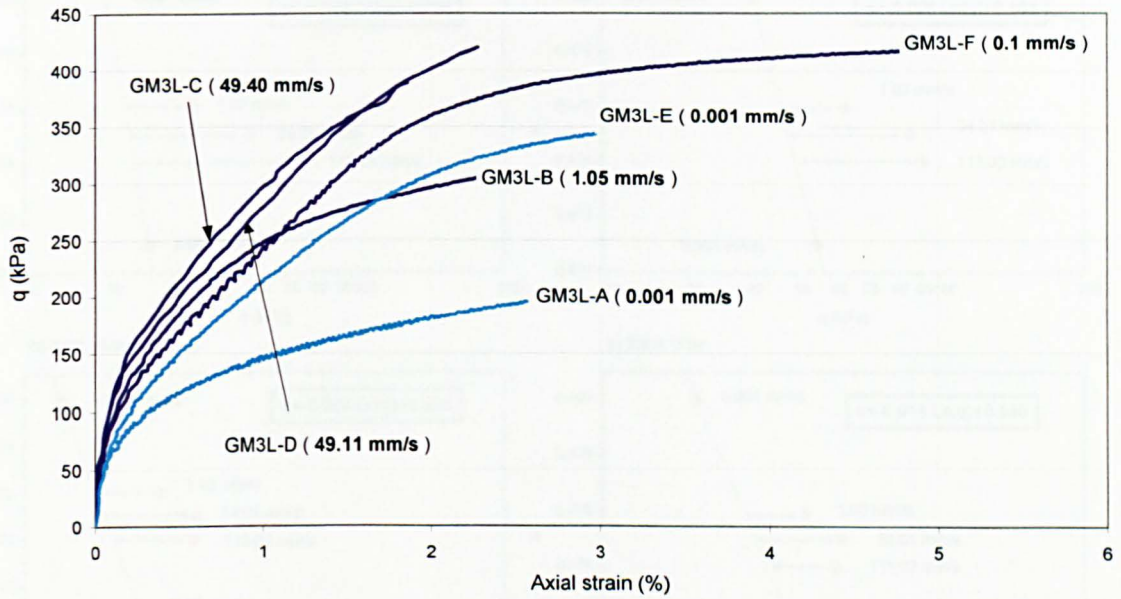


Figure 7.58 Deviator stress versus axial strain curves at different rates for multistage test GM3L.

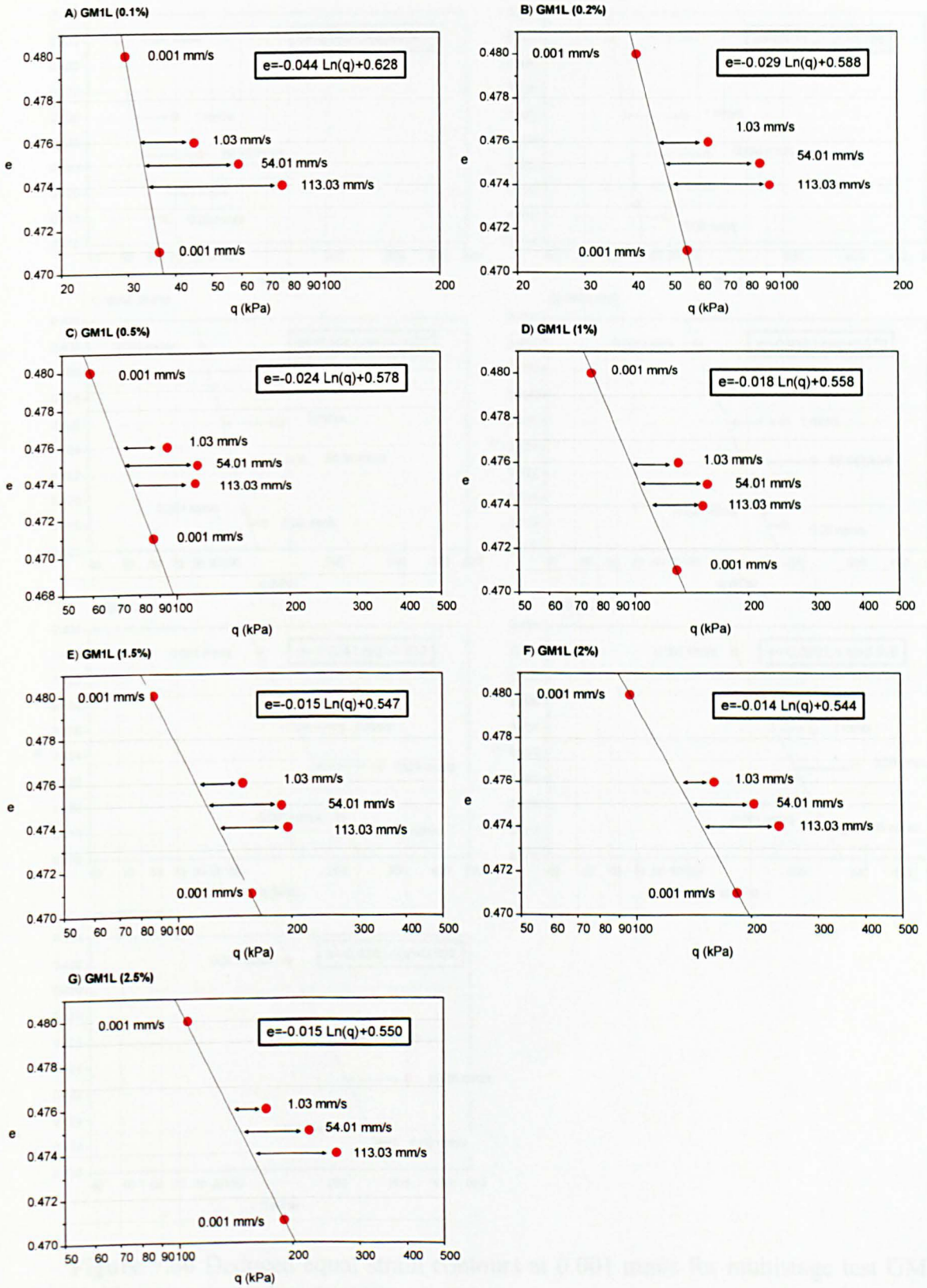


Figure 7.59 Deduced equal strain contours at 0.001 mm/s for multistage test GM1L. Voids ratio versus deviator stress.

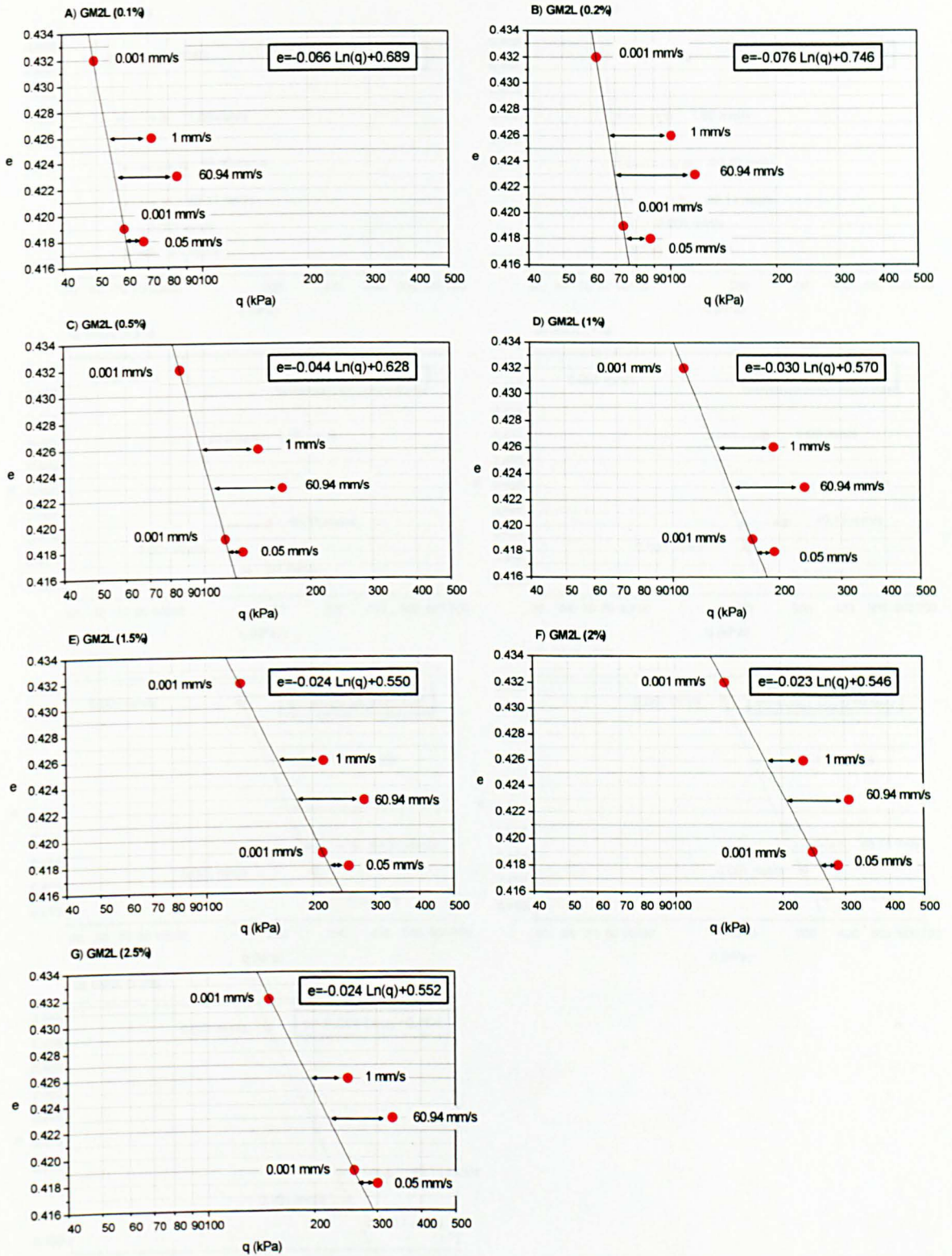


Figure 7.60 Deduced equal strain contours at 0.001 mm/s for multistage test GM2L. Voids ratio versus deviator stress.

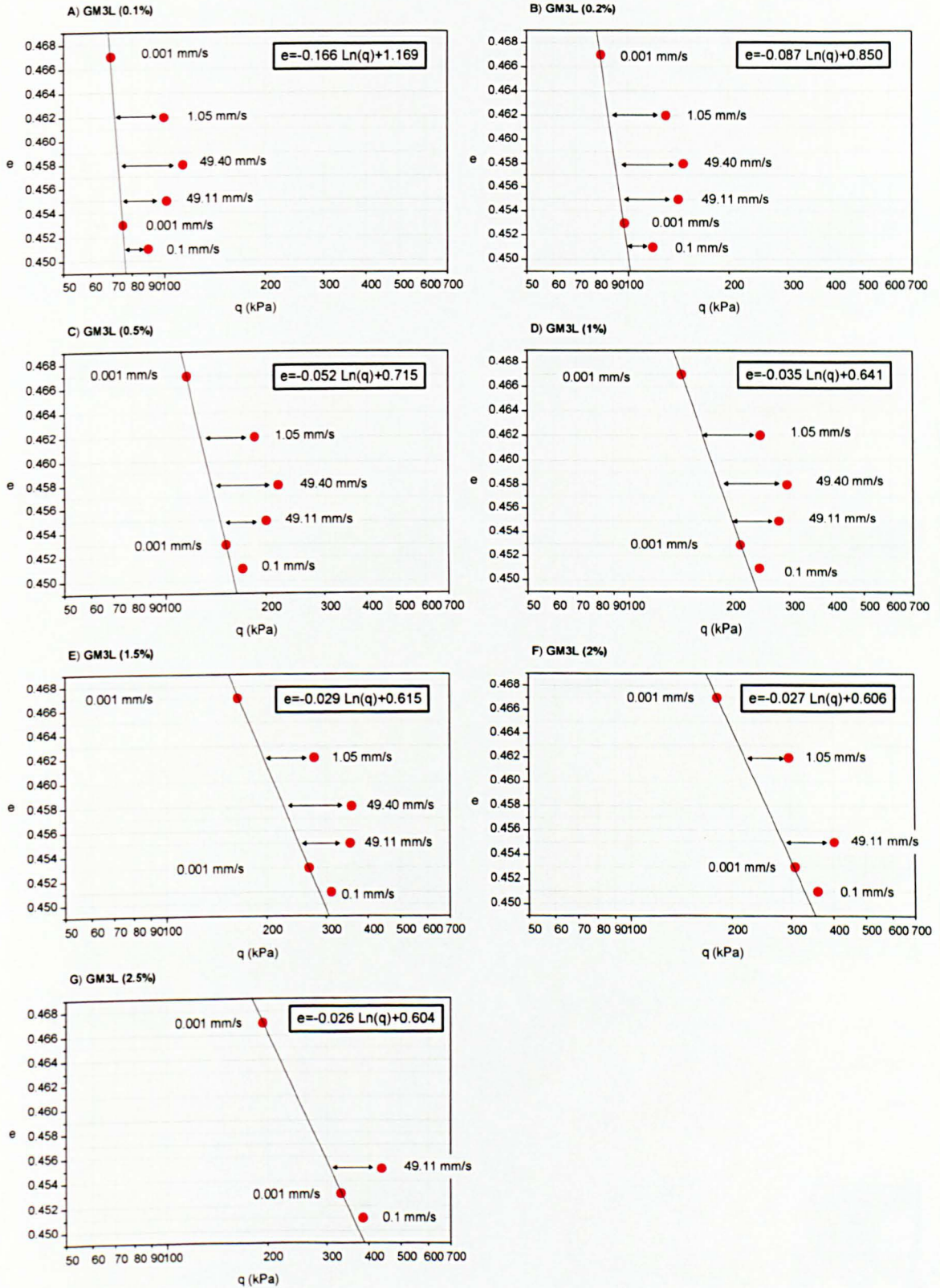


Figure 7.61 Deduced equal strain contours at 0.001 mm/s for multistage test GM3L. Voids ratio versus deviator stress.

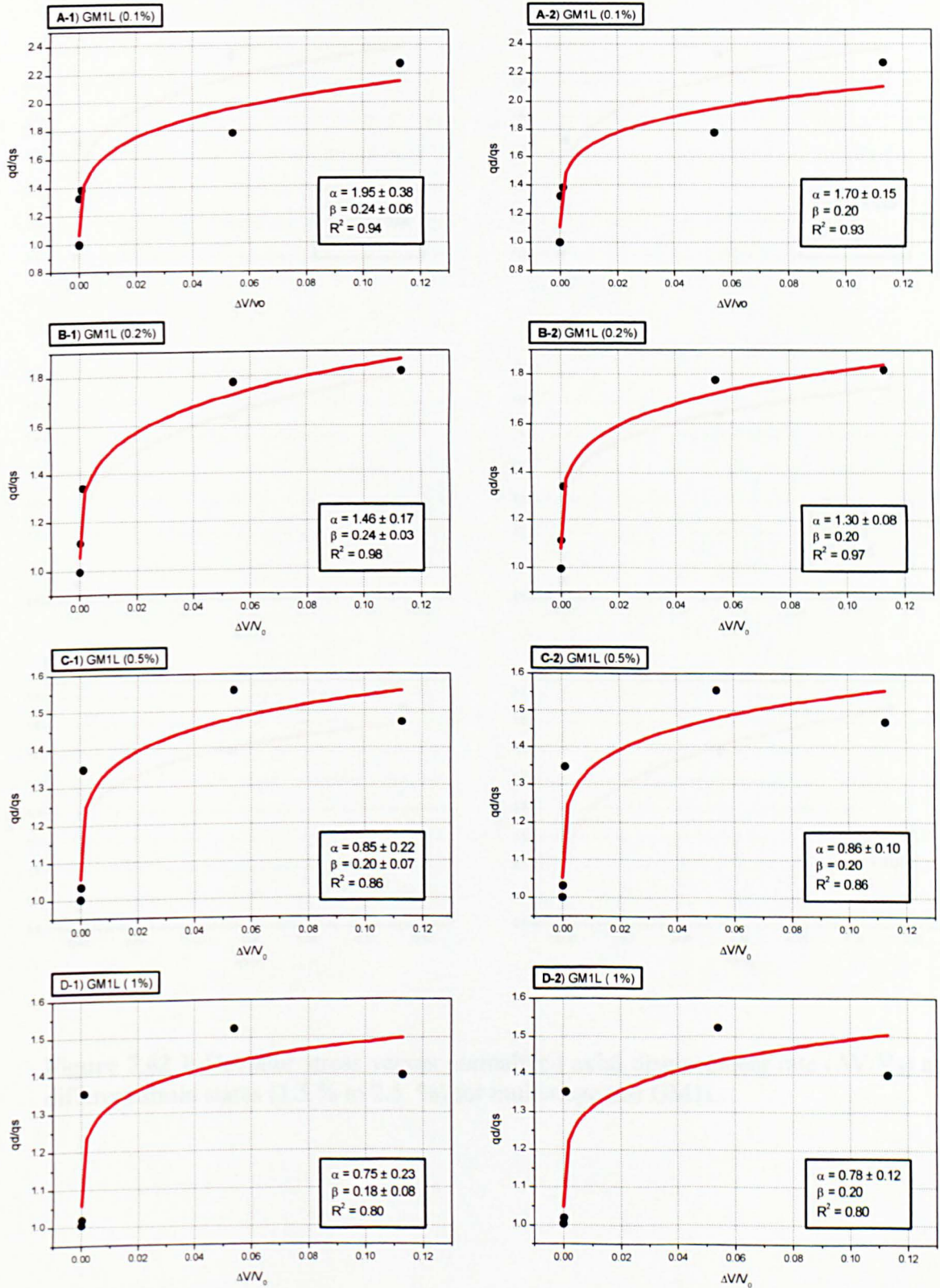


Figure 7.62 a Deviator stress versus normalized axial displacement rate ($\Delta V/V_0$) at different strain states (0.1 % to 1.0 %) for multistage test GM1L.

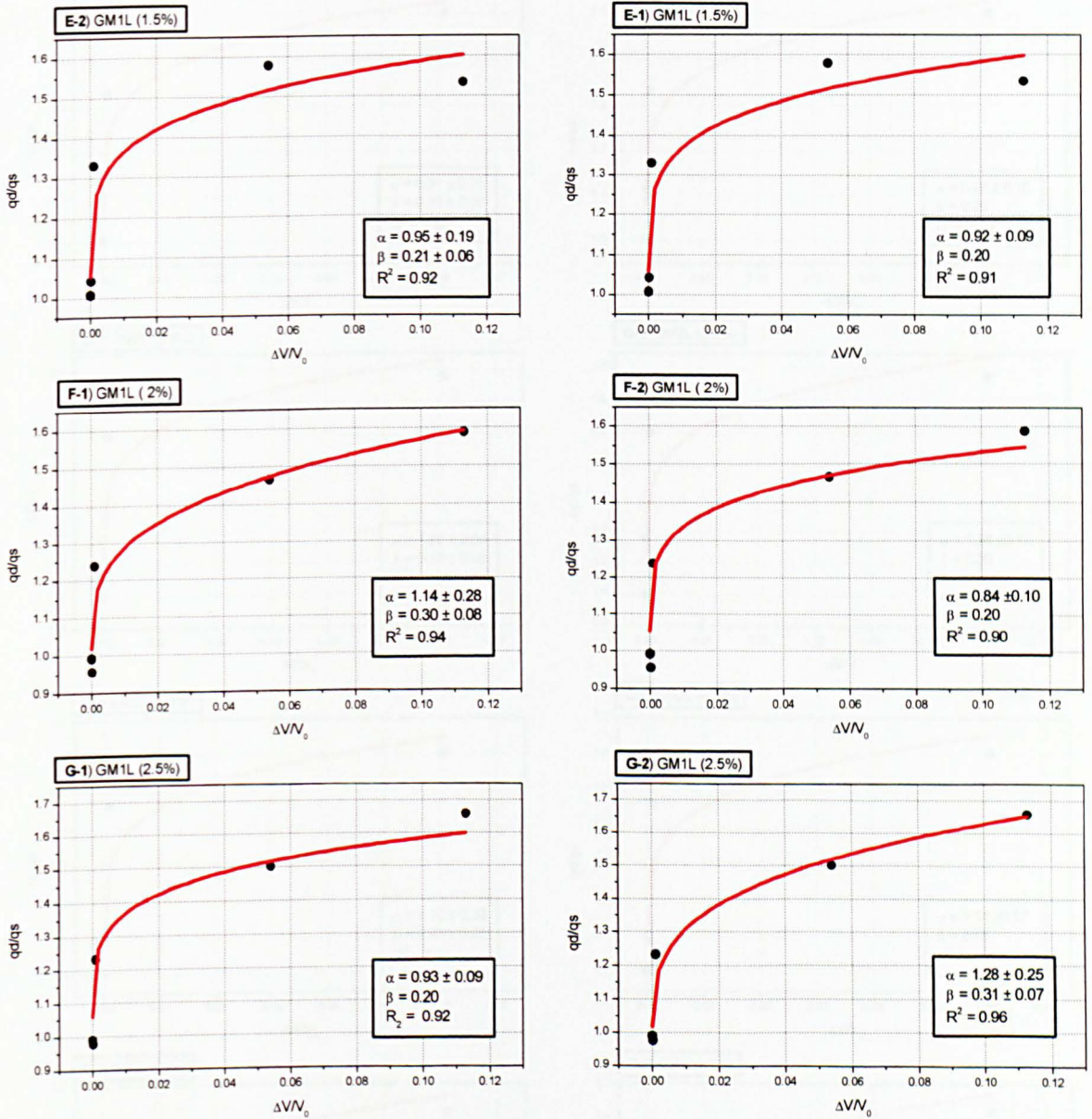


Figure 7.62 b Deviator stress versus normalized axial displacement rate ($\Delta V/V_0$) at different strain states (1.5 % to 2.5 %) for multistage test GM1L.

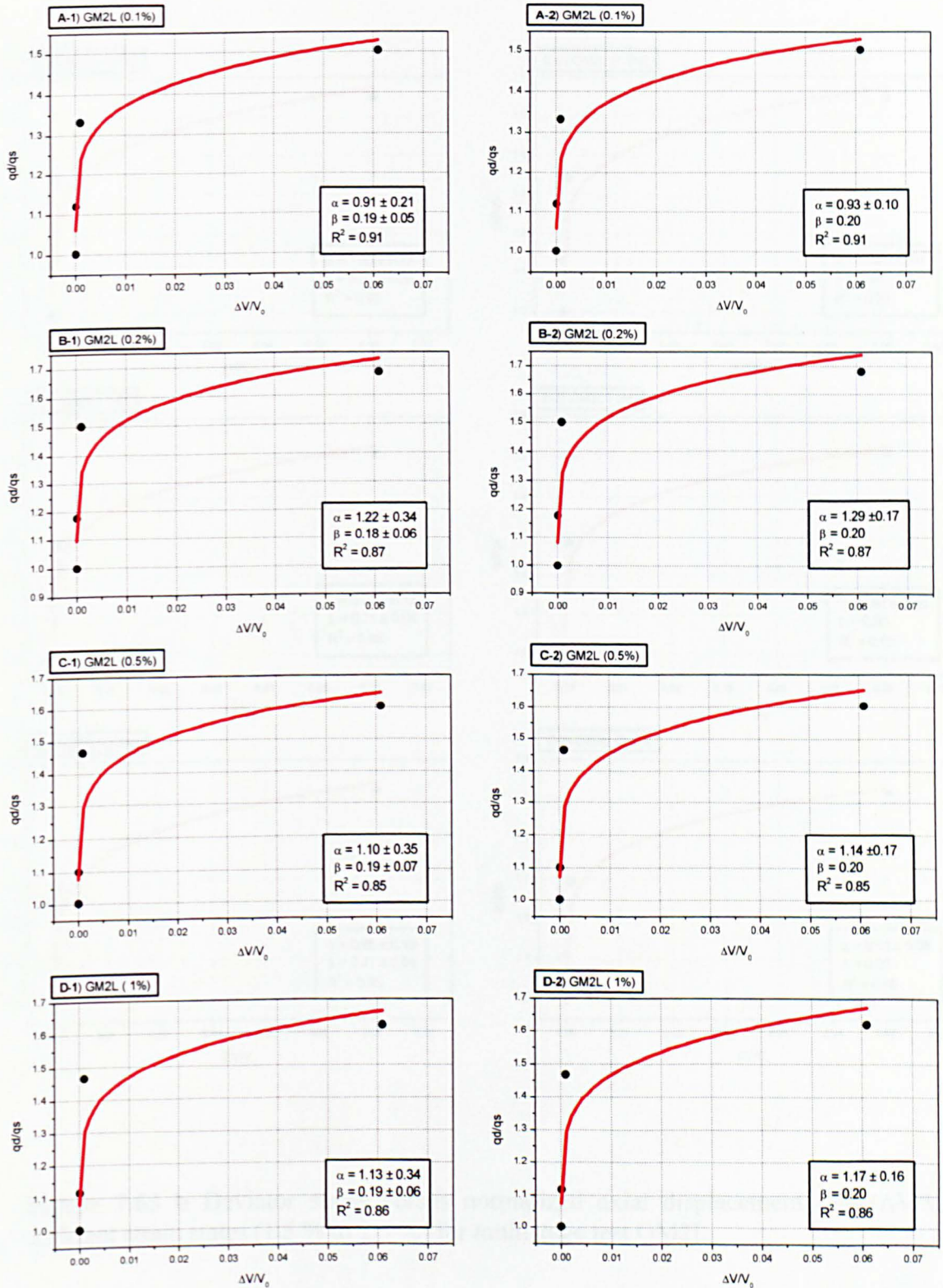


Figure 7.63 a Deviator stress versus normalized axial displacement rate ($\Delta V/V_0$) at different strain states (0.1 % to 1.0 %) for multistage test GM2L.

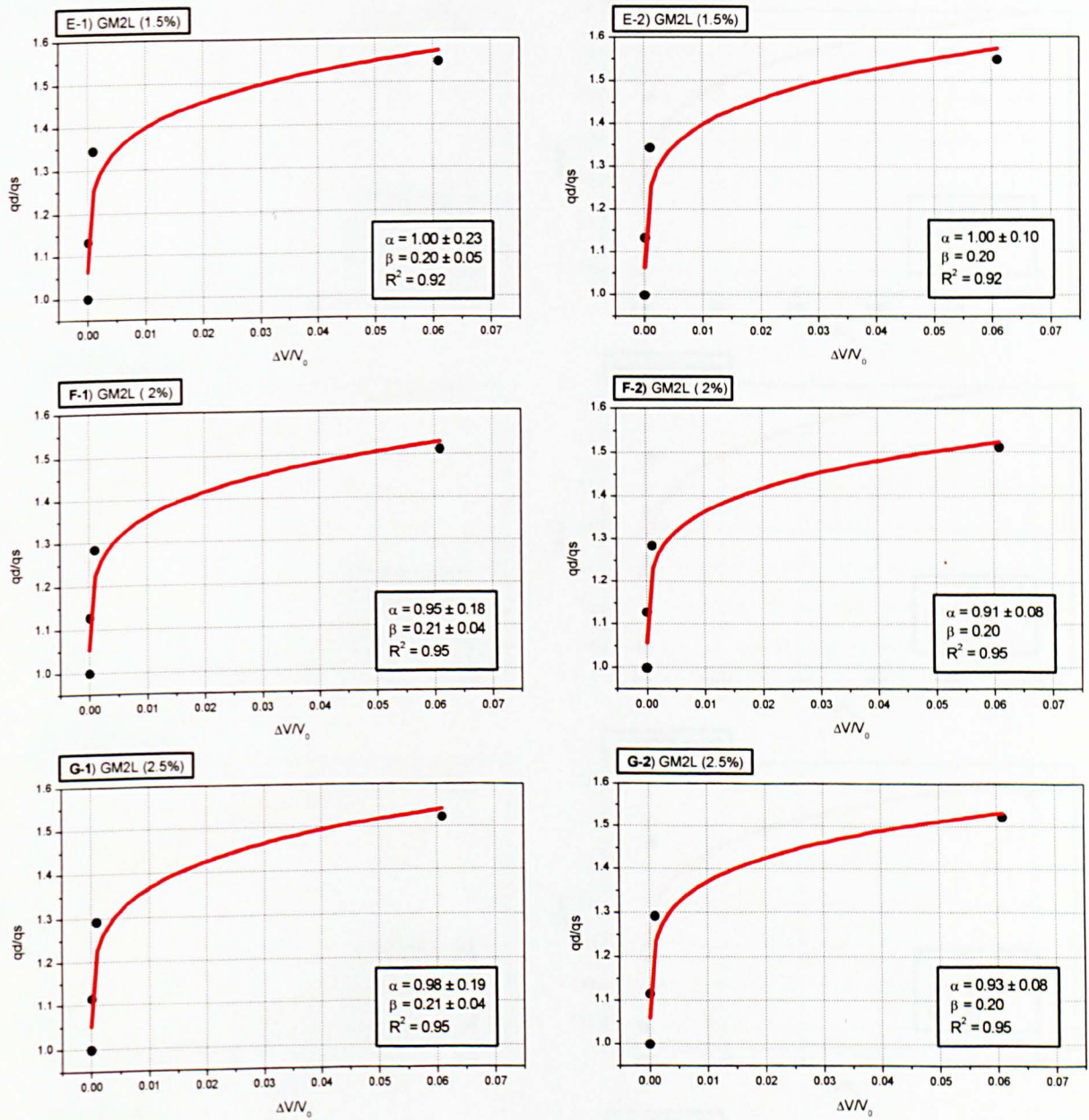


Figure 7.63 b Deviator stress versus normalized axial displacement rate ($\Delta V/V_0$) at different strain states (1.5 % to 2.5 %) for multistage test GM2L.

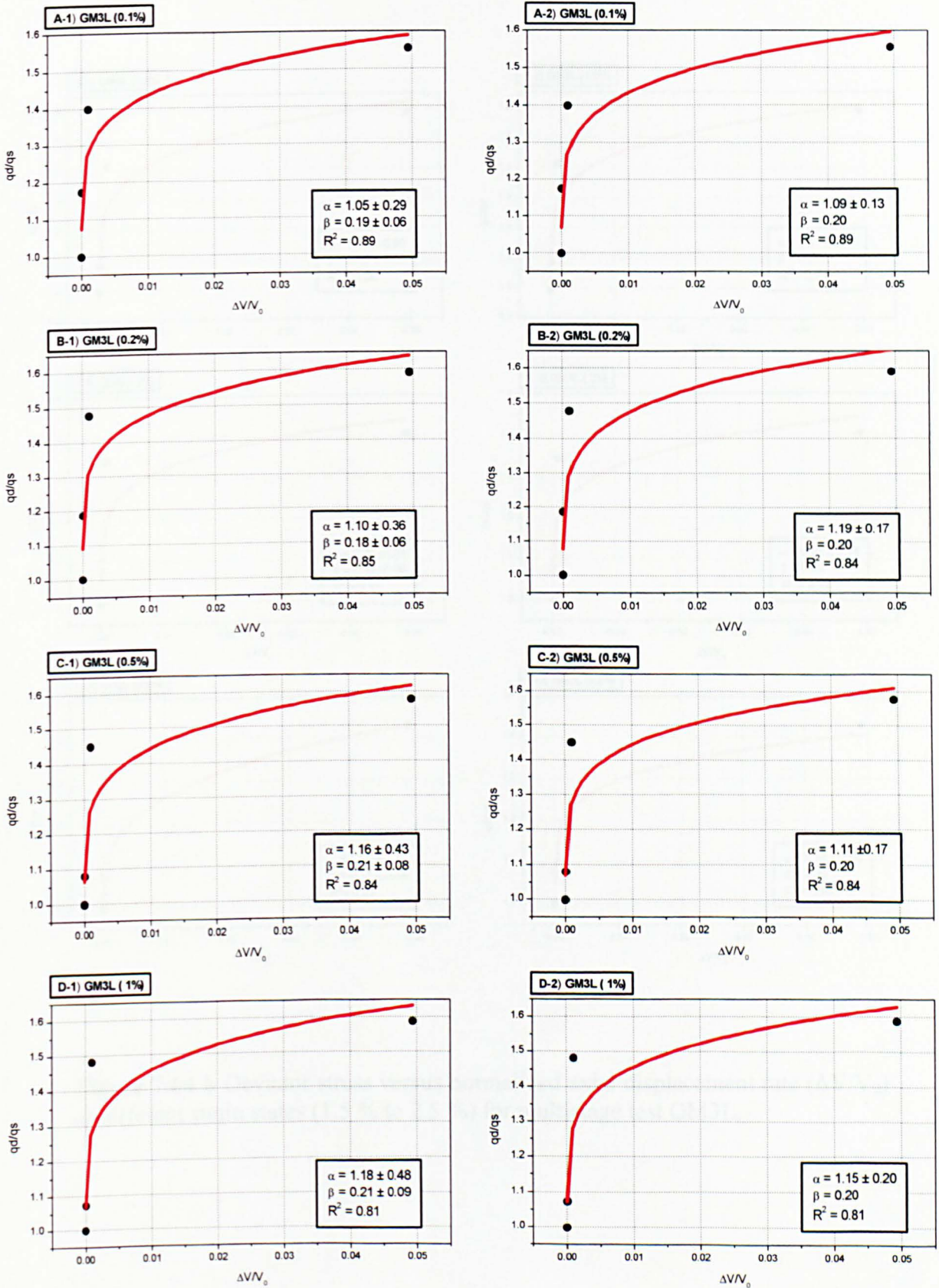


Figure 7.64 a Deviator stress versus normalized axial displacement rate ($\Delta V/V_0$) at different strain states (0.1 % to 1.0 %) for multistage test GM3L.

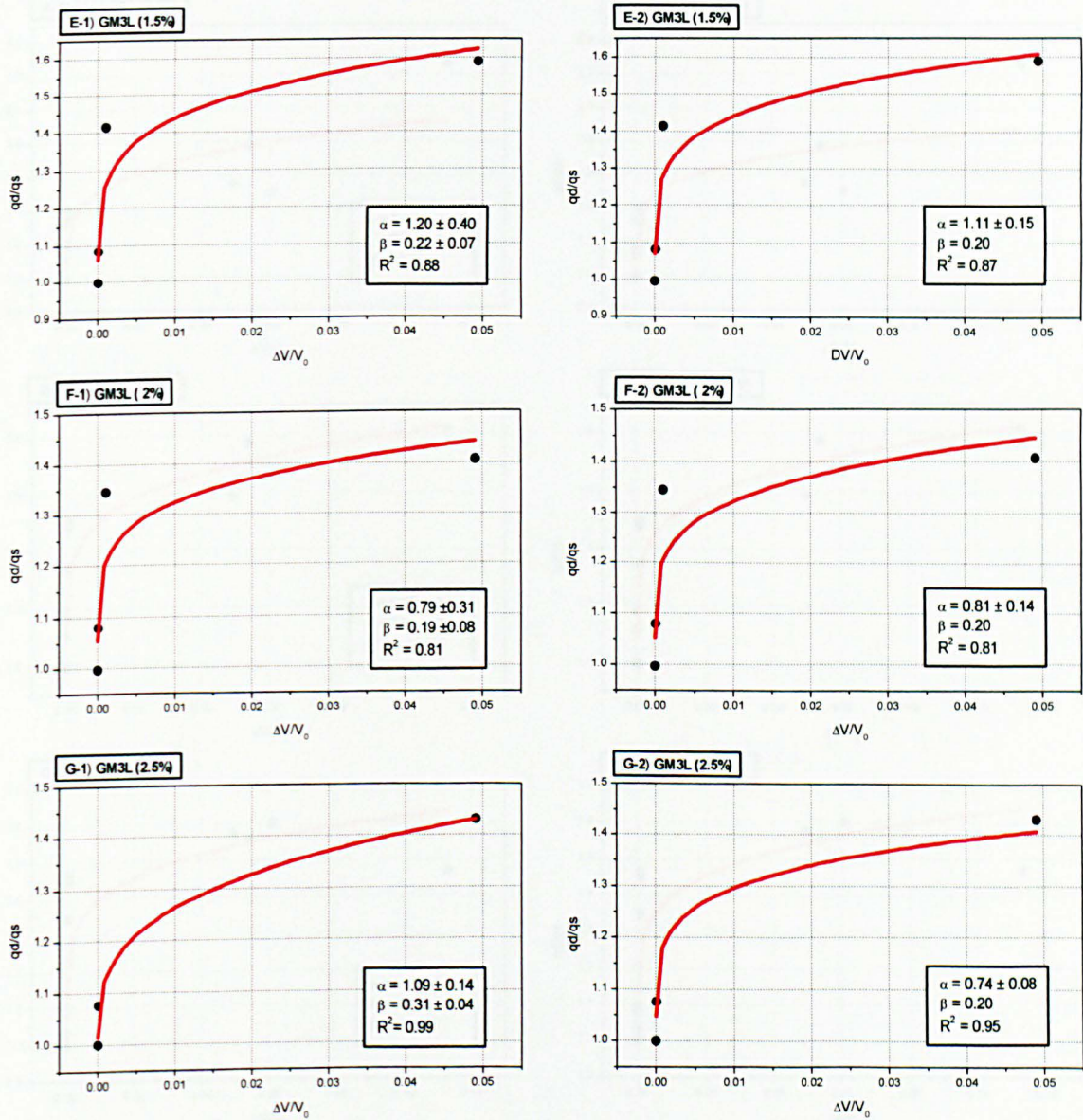


Figure 7.64 b Deviator stress versus normalized axial displacement rate ($\Delta V/V_0$) at different strain states (1.5 % to 2.5 %) for multistage test GM3L.

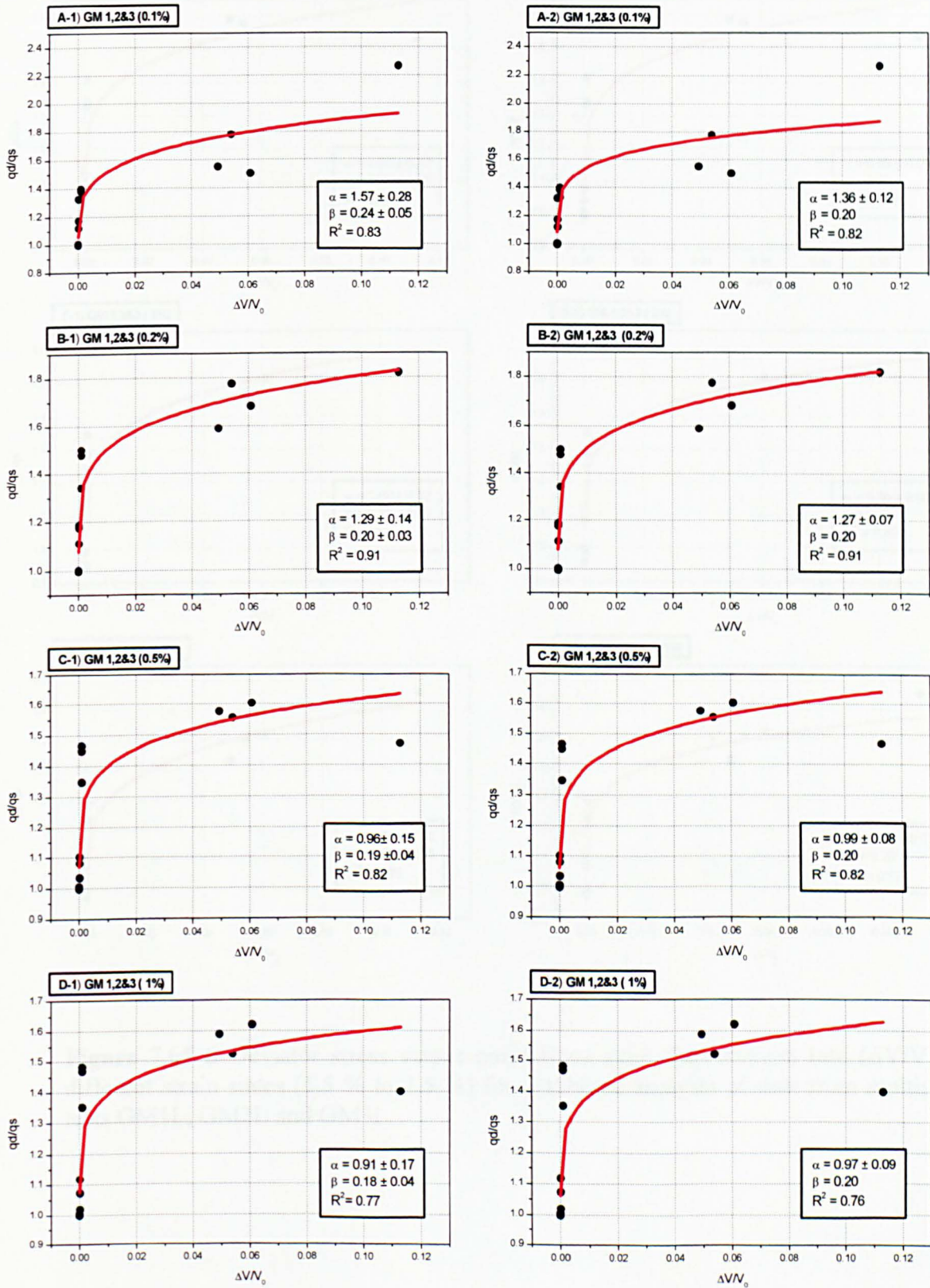


Figure 7.65 a Deviator stress versus normalized axial displacement rate ($\Delta V/V_0$) at different strain states (0.1 % to 1.0 %) for combined analysis of data from multistage tests GM1L, GM2L and GM3L.

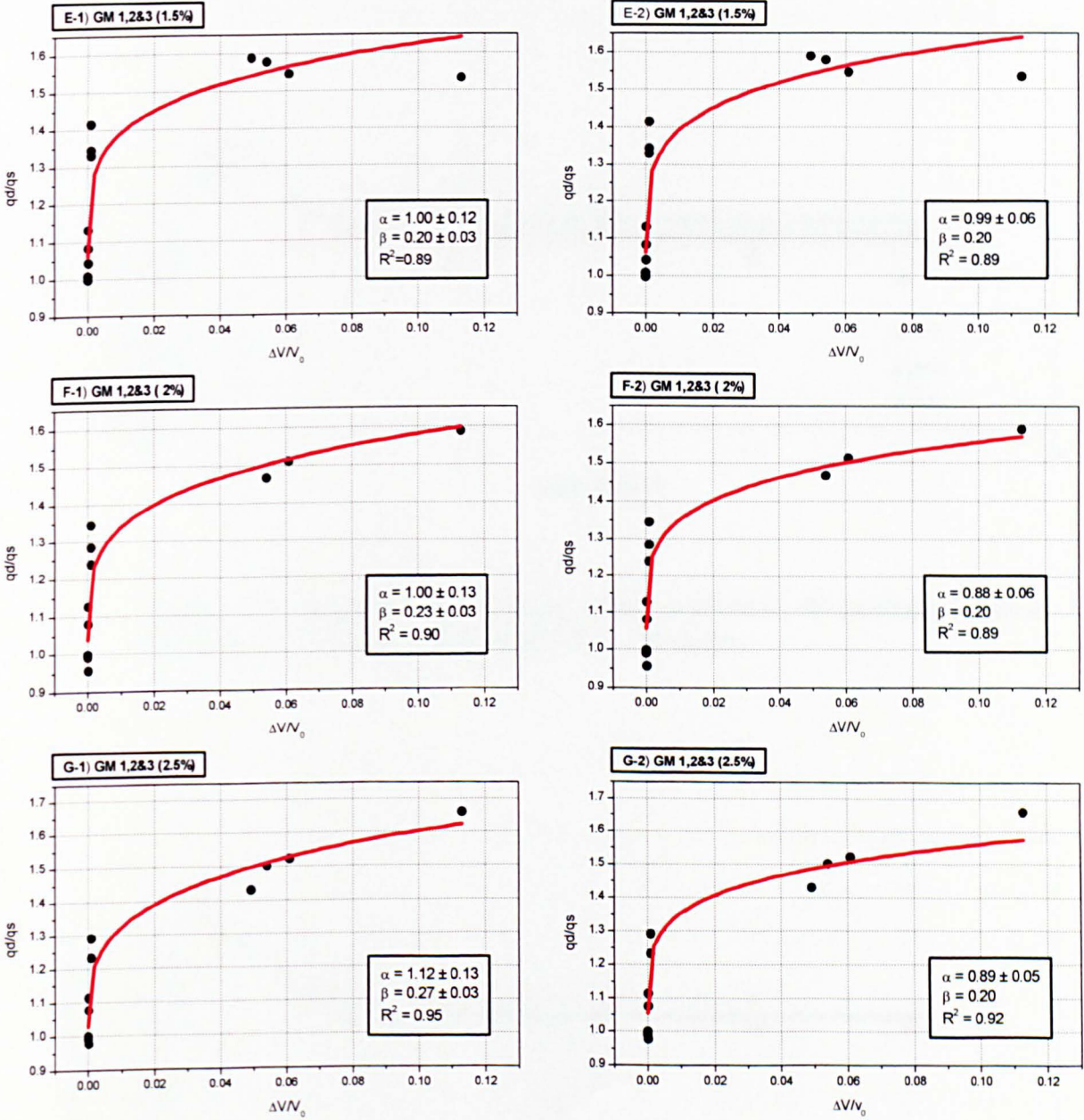


Figure 7.65 b Deviator stress versus normalized axial displacement rate ($\Delta V/V_0$) at different strain states (1.5 % to 2.5 %) for combined analysis of data from multistage tests GM1L, GM2L and GM3L.

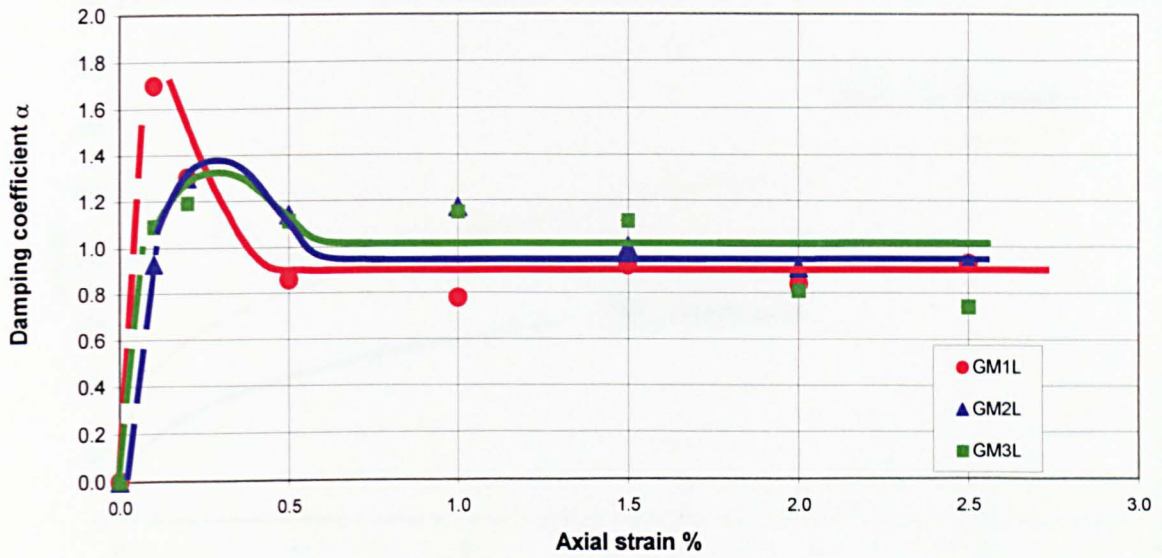


Figure 7.66 Damping coefficient, α , versus axial strain for multistage tests at different rates GM1L, GM2L and GM3L. ($\beta=0.20$).

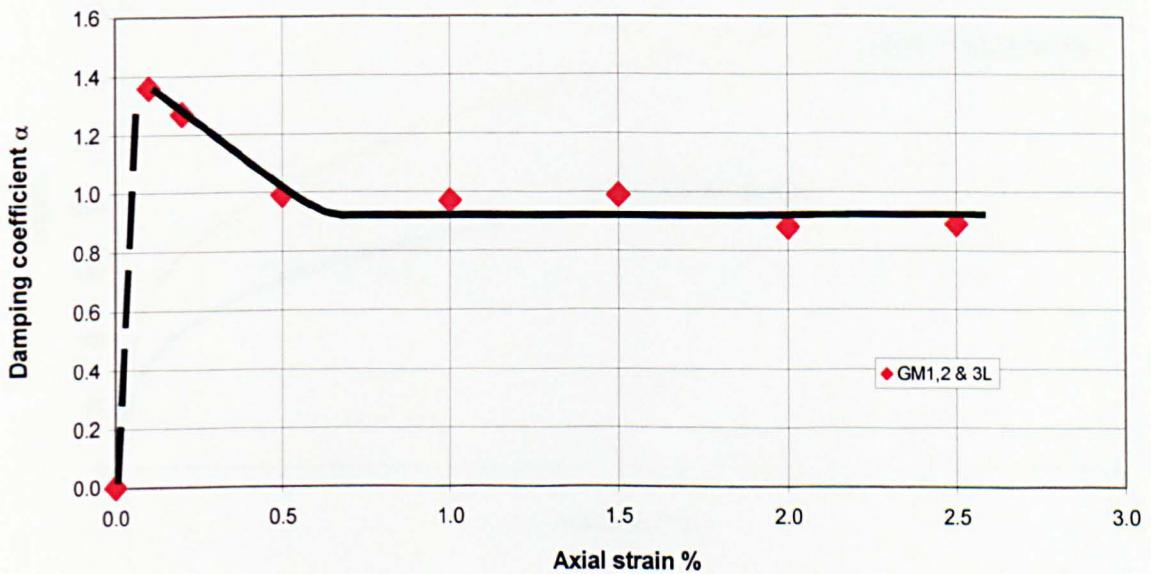


Figure 7.67 Damping coefficient, α , versus axial strain for combined analysis of data from multistage tests at different rates GM1L, GM2L and GM3L. ($\beta=0.20$).

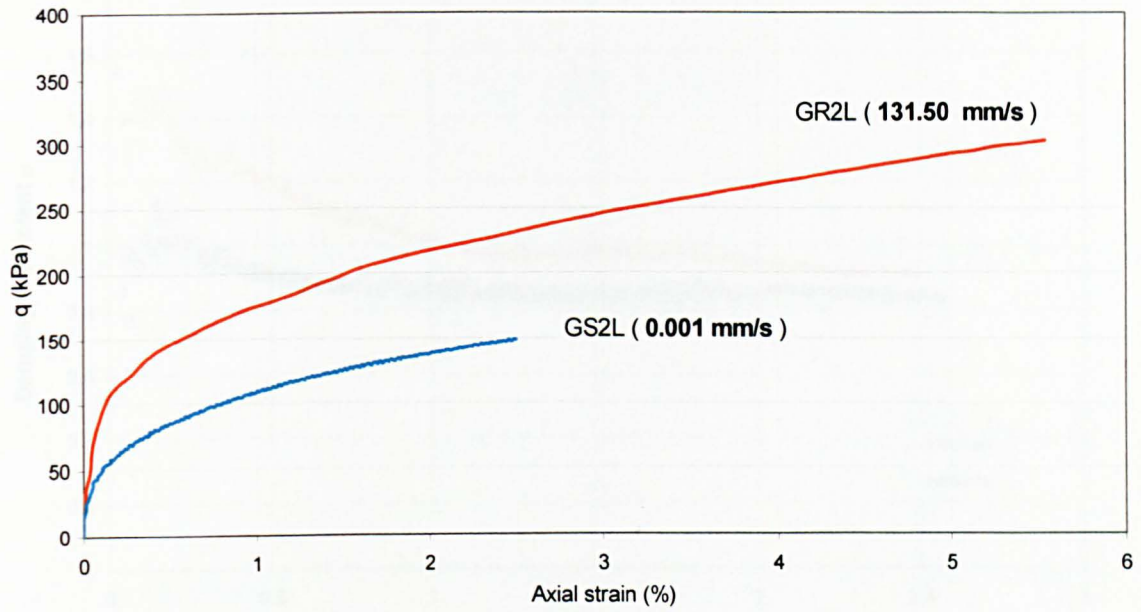


Figure 7.68 Deviator stress versus axial strain curves at for monotonic consolidated undrained triaxial tests GS2L and GR2L.

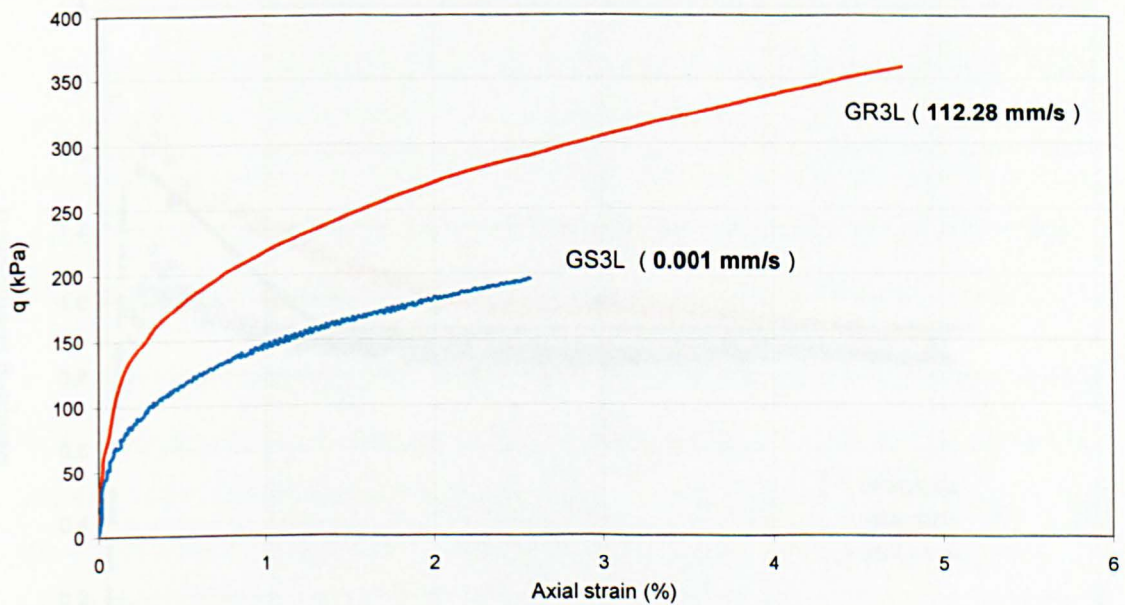


Figure 7.69 Deviator stress versus axial strain curves at for monotonic consolidated undrained triaxial tests GS3L and GR3L.

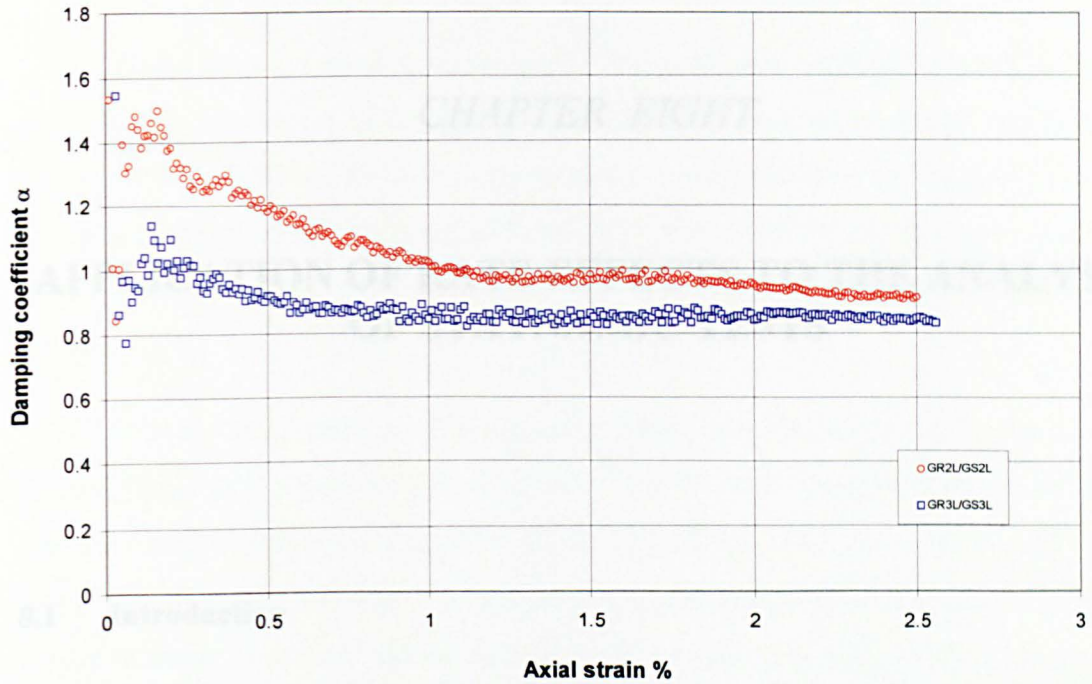


Figure 7.70 Damping coefficient, α , versus axial strain for GR2L versus GS2L and GR3L versus GS3L. ($\beta=0.20$).

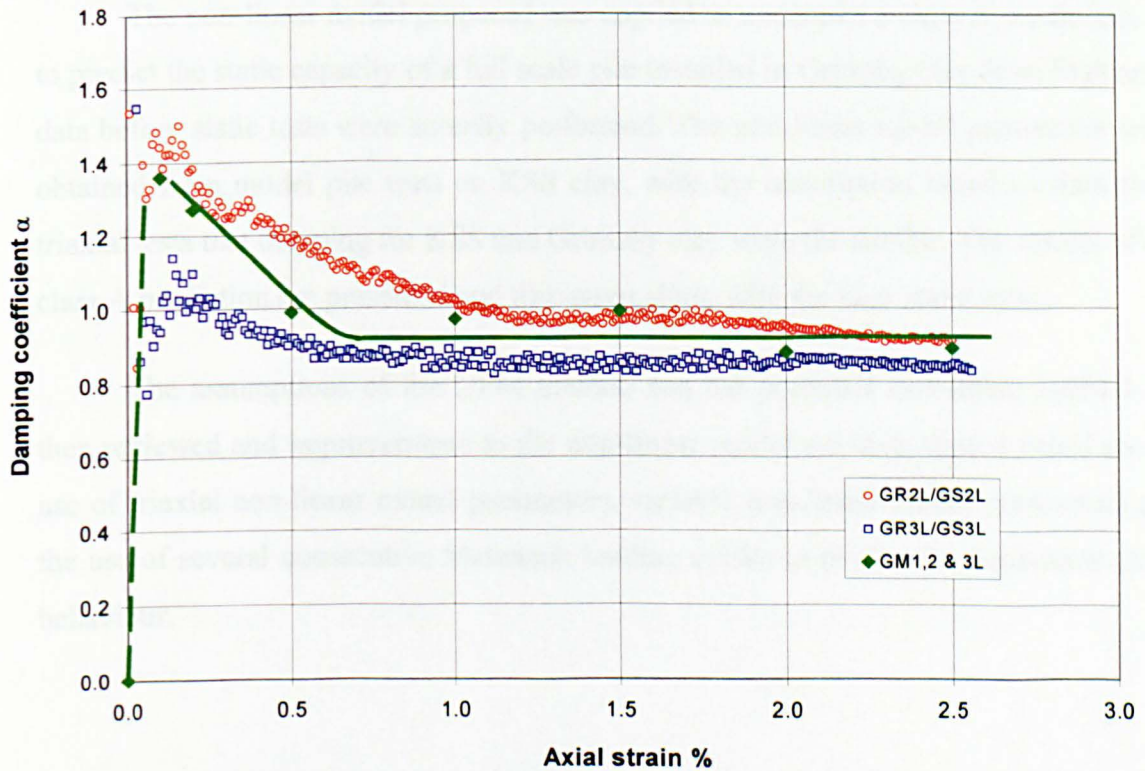


Figure 7.71 Damping coefficient, α , versus axial strain for for GR2L versus GS2L, GR3L versus GS3L and for combined analysis of data from multistage tests at different rates GM1L, GM2L and GM3L. ($\beta=0.20$).

CHAPTER EIGHT

APPLICATION OF RATE EFFECTS TO THE ANALYSIS OF STATNAMIC TESTS

8.1 Introduction

This Chapter explores the application of rate effects to the interpretation of Statnamic tests by introducing a non-linear model based on triaxial tests on Grimsby and KSS clay and model pile tests on KSS clay.

The non-linear model proposed was applied to undertake a class A prediction, i.e. to predict the static capacity of a full scale pile installed in Grimsby clay from Statnamic data before static tests were actually performed. The non-linear model parameters were obtained from model pile tests on KSS clay, with the assumption based on data from triaxial tests that damping for KSS and Grimsby clay were the similar. The results of the class A prediction are presented and discussed along with the later static tests.

The assumptions of the UPM method and the proposed non-linear method are then reviewed and improvements to the non-linear model are investigated based on the use of triaxial non-linear model parameters, variable non-linear model parameters and the use of several consecutive Statnamic loading cycles to predict the equivalent static behaviour.

8.2 A non-linear Statnamic analysis method.

While the most often used method of Statnamic test analysis, UPM (Middendorp *et al*, 1992), assumes a linear variation of damping with velocity, the results of the triaxial tests on KSS and Grimsby clay at various rates presented in Chapter 7 suggest a non linear variation of damping with velocity and therefore an empirical non-linear model relating kinematic and static shear resistance (Equation 7.4) as was discussed in Section 7.2.1.

Brown (2004) carried out model pile testing in a large clay calibration chamber to investigate rate effects on pile resistance in KSS clay. The model pile was 75 mm diameter with an initial embedded length of 720 mm and was installed in a 1.0 m high and 0.78m diameter clay bed. The pile response was monitored by means of a load cell, a pore pressure transducer and an accelerometer on the tip of the pile and a skin friction sleeve with load cell and a pore pressure transducer to measure shaft resistance and pore pressure on the face of the pile. In addition pore pressure transducers and accelerometers were installed in the clay bed to monitor the response of the soil to pile loading events. Loading was applied to the pile using a closed loop computer controlled high-speed servo-hydraulic actuator mounted rigidly above the calibration chamber to produce Statnamic type pulses and constant rapid penetration rates. The actuator was fixed with a co-axially mounted LVDT and load cell mounted directly between the actuator and the pile. Further detail of the instrumentation and tests results are given in Brown (2004). Based on constant rate of penetration (CRP) testing at varying rates from 0.01mm/s to 500 mm/s. Brown (2004) proposed an empirical non-linear model relating dynamic and static total pile resistance (Equation 8.1) analogous to the model proposed in Section 7.2.1 (Equation 7.2) relating kinematic and static shear resistance in triaxial tests. By comparing the high rate pile resistances, at pile penetration equal to 10% of the pile diameter, with the low rate resistances obtained for CRP tests at 0.01 mm/s it was possible to define R_d and R_s , as the dynamic and static total resistance of the pile respectively.

$$\frac{R_d}{R_s} = 1 + \alpha_{mp} \left(\frac{\Delta V}{V_0} \right)^{\beta_{mp}} - \alpha_{mp} \left(\frac{0.01}{V_0} \right)^{\beta_{mp}} \quad \text{Equation 8.1}$$

where α_{mp} and β_{mp} are the coefficients of damping, ΔV is axial rate of displacement in mm/s, V_0 is a rate of 1000 mm/s used to normalise the rate.

The prediction of static pile resistance from Statnamic test data taking into account both the inertia of the pile and the non linear variation of damping with velocity, can thus be obtained by rewriting Eqn. 8.1 as:

$$\frac{F_{STN} - Ma}{F_s} = 1 + \alpha_{STN} \left(\frac{v}{v_0} \right)^{\beta_{STN}} - \alpha_{STN} \left(\frac{0.01}{v_0} \right)^{\beta_{STN}} \quad \text{Equation 8.2}$$

where $(F_{STN} - Ma)$ represents the dynamic resistance. F_{STN} is the measured Statnamic load on the head of the pile. $M*a$ is the inertial force on the pile, where M^* is the mass of the pile and a is the acceleration of the pile. F_s is the static load in a CRP pile test carried out at 0.01 mm/s. And hence the static resistance of the pile

$$F_s = \frac{F_{STN} - M^* a}{1 + \alpha_{STN} \left(\left(\frac{\Delta V}{V_0} \right)^{\beta_{STN}} - \left(\frac{0.01}{V_0} \right)^{\beta_{STN}} \right)} \quad \text{Equation 8.3}$$

The coefficients of damping quoted by Brown (2004) for the KSS material reflecting testing on four different clay beds were $\alpha_{mp} = 1.22$ and $\beta_{mp} = 0.32$. However, it was found that coefficients of damping from multistage triaxial tests on KSS clay were $\beta = 0.20$ and α was a function of the strain ($\alpha=f(\epsilon)$) that tended to 0.90 when $\epsilon \geq 0.5\%$. (Figures 7.28, 7.29 and 8.1)

8.3 The class A prediction

The present research project included the study of the rate effects in undisturbed Grimsby clay from the site where the full-scale pile testing (Brown 2004) was carried out. A class A prediction (Lambe, 1973), consisting of the prediction of the static capacity of the full scale pile installed in clay before the static tests were carried out, was undertaken based on the information from the model pile testing in the calibration chamber (KSS), varying rate triaxial tests carried out in both reconstituted clay (KSS)

and undisturbed clay (Grimsby) and the Statnamic test data. On completion of the Statnamic testing of the insitu prototype pile the results of the predictions (Hyde *et al*, 2003,a) were forwarded to Prof. Malcolm Bolton of Cambridge University for safe keeping prior to static pile testing. The static testing, consisting of constant rate of penetration (CRP) and maintained load tests (MLT), was carried out three weeks after the Statnamic tests were undertaken. Finally a comparison of the static pile test results and predicted values (Hyde *et al*, 2003,b) was completed and submitted to Prof. Malcolm Bolton for verification of the prediction.

8.3.1 Prediction method

The Class A prediction was realized using the non-linear algorithm (Equation 8.3) proposed in Section 8.2. The results of the multistage triaxial tests at different rates were used to compare the rate effects and the damping coefficients for the KSS material on the calibration chamber and the glacial clay from the full-scale test site. It was found that both materials had similar triaxial damping coefficients (Figures 7.28, 7.29, 7.49, 7.69 and 8.1). This justified the use of the damping coefficients α_{STN} and β_{STN} derived directly from the model pile tests in KSS, α_{mp} equal to 1.22 and β_{mp} equal to 0.32 (Brown 2004), to the full-scale pile in the glacial clay (Grimsby). Although Statnamic testing was undertaken for several consecutive loading cycles, only the last maximum target load, of 3000 kN, was chosen for the prediction. The analysis of the Statnamic data was also carried out using the Unloading Point Method (UPM) to allow the evaluation of the class A prediction versus both the results from the static pile testing and the most commonly used Statnamic method of prediction.

8.3.2 Pile type and installation

An instrumented auger bored cast in-situ pile, designed by Brown (2004) was installed. This consisted of a C35 concrete mix with 10 mm aggregate with 36 N/mm² strength after 28 days and an average density of 2.345 Mg/m³. The pile had a nominal diameter of 600 mm and was installed to 12.06m BGL. A steel casing of 610 mm outer diameter and 8mm wall thickness was placed to a depth of 1.8m BGL with 480mm left above the ground level. The main reinforcement consisted of six 12m long T16 bars

with a single horizontal helical reinforcement consisting of T12 bar spaced at 300 mm centres. The instrumentation of the pile consisted of three main elements. A pile tip load cell, concrete strain gauging and embedded accelerometers. In addition to the instrumentation in the pile, accelerometers were placed in the adjacent ground at different depths at various horizontal distances from the pile. Further details of pile design, installation and instrumentation are given by Brown(2004)

8.3.3 Pile testing

Statnamic testing was carried out using a 3MN Statnamic device with a hydraulic catch mechanism provided by PMC limited (PMC, 2003). The Statnamic testing programme consisted of a series of six loading steps of 1000, 1500, 2000, 1500, 2500, 3000 kN on the auger bored pile. The loads quoted were the maximum target loads. The tests were carried out over two days. The first loading step of 1000 kN on the auger bored pile was undertaken on the first day and the remaining loading steps were carried out on the second day. The time between loading steps did not exceed one hour, that was the time needed to reset the reaction mass and the combustion charge for the next test, except between 1000 kN and 1500 kN, when the pile was left overnight. During the Statnamic events, the load on the head of the pile and the displacement were measured and recorded at a logging rate of 1kHz. The velocity and acceleration, used for predictions, were calculated by differentiation of the measured displacement versus time logs and velocity versus time respectively. Before the calculation of the acceleration five point adjacent averaging was used to smooth the deduced velocity.

A constant rate of penetration (CRP) test was carried on the auger bored pile three weeks after the Statnamic testing, allowing any excess pore pressure, generated during the Statnamic loading events, to dissipate. Four days later the pile was subjected to a maintained load test (MLT), carried out over two days. The tests were aimed at providing reference static values to compare the predicted results based on Statnamic data with standard UK practice pile testing results. Both the CRP test and the MLT were carried out by PMC Ltd in accordance with the ICE Specification for Piling and Embedded Retaining Walls (ICE, 1997), with the same equipment and arrangements. The load was applied to the pile by means of a hydraulic jack connected to compressor via an air-hydraulic interface. Reaction for the jack consisted of reaction beams

anchored to three 600mm diameter and 11.5 m length auger bored piles. Further detail of the reaction system is given by Bell (2001). A load cell and four LVDT's, placed on the pile head, measured the applied load and displacement during the tests. The CRP test was carried out at 0.01mm/s, the same rate as used by Brown (2004) in the laboratory scale model pile testing. The readings of load and displacement were logged every 12 seconds and the test was undertaken up to 26.78 mm displacement. The MLT test was carried out for a proof load test, followed by an extended proof load test. The proof load test was carried out up to a maximum load of 1350 kN and the extended proof load test up to a maximum load of 1800 kN.

8.3.4 Prediction results

The load displacement curves for the Statnamic tests are shown in Figure 8.2, with the pile tests set at zero for the beginning of each new cycle. Figure 8.3 , shows the load displacement curves for the 3000 kN Statnamic load cycle together with the Class A static prediction and the UPM static prediction. Figure 8.4, shows the load displacement curves for the Class A prediction together with the unloading point method (UPM) prediction and the CRP and MLT tests.

The prediction was divided in two parts: Pile static stiffness prediction and ultimate static prediction. Table 8.1 (Measured CRP/ Class A prediction/ UPM) shows the measured and predicted secant stiffness values at a pile load of 1500 kN. It was uncertain if the full shaft and end bearing capacities of the bored pile were reached at the Statnamic device's maximum capacity of 3000 kN. Assuming that the ultimate load might have been reached at the maximum value of Statnamic load, the corresponding load was then corrected for damping and presented as the predicted ultimate pile capacity. Table 8.2 (Measured CRP/ Class A prediction/ UPM) shows the measured and predicted ultimate pile capacity at a pile head displacement of 8.85 mm.

8.3.5 Discussion of the class A prediction

The pile stiffness during CRP loading was higher than both the class A and the UPM prediction. The CRP test results Figure 8.4, show that the pile capacity after an initial yield at about 1800kN continued to increase up to 16 mm of pile head

displacement. The prediction of ultimate pile capacity coincided with the yield point of CRP after 1800 kN. The predicted ultimate capacity of 1746 kN at 8.85 mm was 10% less than the measured CRP load of 1946 kN at 8.85 mm.

The UPM method over predicted the ultimate pile capacity by 17% at 8.85 mm of head displacement and up to 23% if the analysis is extended past the peak Statnamic load to the unloading point. Although the class A prediction was made for the CRP tests, it is interesting to compare with MLT data. The measured MLT load of 1574 kN at 8.85 mm is 19 % lower than CRP load of 1946 kN at 8.85 mm. The ultimate capacity of the class A prediction lay between the MLT and CRP test results. The initial pile stiffness coincides for both CRP and MLT up to 3.27 mm of head displacement and hence the Class A prediction also under-predicts the stiffness when the MLT is chosen as the static reference value.

8.4 Improvements to the non-linear Statnamic method.

The Unloading Point Method (UPM), described in Chapter 2, is based on the following assumptions:

- a) A linear variation of damping with velocity.
- b) Damping coefficient constant.
- c) Static value of force constant between the point of maximum load and maximum displacement.
- d) Dynamic force and static forces equal at $v = 0$ mm/s.
- e) Only one loading cycle is analysed.

A linear variation of damping force with velocity has been proved to be unrealistic for the clay soils investigated in this research. Based on the findings from triaxial tests at different rates reported in Chapter 7 and the findings reported by Brown (2004) in the associated research on large scale laboratory pile testing an empirical nonlinear model relating Statnamic and static pile resistance (Equation 8.3) is proposed.

The hypothesis of a nonlinear model for clays agrees with the findings of previous researchers such as Gibson & Coyle (1968), Randolph & Deeks (1992) or Hyde *et al.* (2000) as was discussed in Section 2.6

Hypotheses c) and d) are an essential part of the UPM when obtaining the coefficient of damping, C_{UPM} , directly from the measured Statnamic data regardless of any further information about the type of soil or maximum load applied. However none of these two hypotheses has ever been validated. The assumption of the static resistance being constant between the points of maximum load and maximum displacement might only be applicable if the displacement of the pile was enough to guarantee that the pile had failed and achieved its ultimate capacity for the equivalent static conditions at the point of maximum load. The equivalent static force could then be assumed to be constant after this point.

The determination of the ultimate capacity by means of the UPM is purely based on the assumption that the Statnamic force corrected to take into account the inertia of the pile coincides with the equivalent static force at one point, the unloading point, when the velocity of the pile becomes zero. The experimental work reported by Brown (2004) for both the large scale model pile testing in KSS clay and full scale pile testing in Grimsby clay shows that at the unloading point the Statnamic and static load do not coincide. The Statnamic force at that point might be higher than the static by up to 30% and this is the origin of the widely reported over-prediction when the UPM is used to analyse Statnamic events in clay soils. (Brown, 1994 & 1995) (Goble *et al.*, 1995) (Seidel, 1996).

The method used for the Class A prediction stays away from the use of the UPM assumptions a), c) and d) by introducing a non-linear model (Equation 8.3) where the non-linear parameters (damping coefficients), α_{STN} and β_{STN} , were obtained directly from the model pile tests in KSS. The Class A prediction still coincides with the UPM on the assumptions of constant coefficients of damping during the full Statnamic event and the use of a single Stanamic loading cycle to deduce the equivalent static curve.

In the following sections the possibility of using damping coefficients obtained from triaxial testing is explored and the assumption of “constant“ coefficients of

damping and the use of a single Statnamic pulse are re-examined in order to propose improvements to the non-linear model presented in Section 8.2.

8.4.1 Triaxial damping coefficients

The application of the damping coefficients α_{STN} and β_{STN} , derived directly from the model pile tests in KSS to the full scale tests in Grimsby clay was justified because it was found that both materials had similar triaxial damping coefficients, and hence similar rate effects can be assumed. This does not however allow the use of the same principle for different soils or even different types of clay.

The new non-linear method cannot be considered a feasible alternative to the analysis of a Statnamic test in different soil conditions if a laboratory model pile testing programme is previously required to obtain the damping coefficients to be implemented in Equation 8.3. The option of applying the damping coefficients obtained from triaxial testing instead of those obtained from the model pile tests was explored for both Statnamic tests carried out in the laboratory and in the field. This offers the possibility of being able to evaluate the values of the damping parameters for different type of soils and stress conditions using a relatively simple laboratory test.

Figure 8.5 shows the results of the prediction conducted for KSS in calibration chamber bed 5 by means of Equation 8.3 with damping parameters obtained from multistage triaxial testing, i.e. β equal to 0.20 and α equal to 0.90. The prediction provides a good correlation with static measured data (errors less than 5 %). Figure 8.6 shows the result of a prediction conducted for the full scale pile test in Grimsby clay for the 3000 kN Statnamic loading cycle. The prediction coincides with the static measured values (CRP) for displacements higher than 8 mm (approximately 1.2 % of the pile diameter), close to the point of maximum load, providing an excellent correlation for ultimate capacity but as for the class A and UPM predictions it still under-predicts the stiffness by as much as 24% (Figure 8.4 and Figure 8.6).

8.4.2 Variable non-linear model parameters. Bilinear α_{STN} model

The variability of the UPM “constant” coefficient of damping, C_{UPM} , through the full Statnamic loading pulse was investigated, confirmed and stated as a shortcoming of the method by Seidel (1996) and acknowledged by Mullins *et al*, (2002).

The results from the monotonic and multistage triaxial tests carried out at different rates for both KSS and Grimsby clay show that the coefficient of damping α , in Equation 7.4, varies with strain while the coefficient of damping β can be considered constant and equal to 0.20. (Figure .8.1)

The analysis of Statnamic test results together with the corresponding CRP test results, for the same pile, on the associated laboratory model pile testing programme conducted in KSS clay and full scale model pile testing in Grimsby clay (Brown, 2004), can be used to explore the variability of the coefficient α_{STN} with pile displacement in Equation 8.3. Assuming β_{STN} equal to 0.20, Equation 8.3 can be rewritten as Equation 8.4, where the values of α_{STN} that match predicted and actual static (CRP) capacity at each pile displacement state are deduced using the measured Statnamic and static CRP data.

$$\alpha_{STN} = \frac{\frac{F_{STN} - M * a}{F_s} - 1}{\left[\left(\frac{\Delta V}{V_0} \right)^{0.20} - \left(\frac{0.01}{V_0} \right)^{0.20} \right]} \quad \text{Equation 8.4}$$

Figure 8.7 shows the deduced α_{STN} values for Statnamic data from the model pile testing (Brown 2004) calibration chamber beds 4 and 5 in KSS clay. The results from both beds for loading cycles of 20, 25 and 30 kN confirm the variability of α_{STN} , in Equation 8.3, such that it could be defined as a bilinear function of displacement. In the first zone from zero to approximately 0.7 mm pile head displacement (equivalent to 1% of the model pile diameter) α_{STN} increases linearly with displacement. In the second zone α_{STN} can be assumed to be constant. The backfigured α_{STN} values for Statnamic data from prototype pile tests in Grimsby clay, for Statnamic loading cycles of 2000,

2500 and 3000 kN, are shown in Figure 8.8. In this case α_{STN} also varies with displacement and the same two zones can be identified with the displacement limit between zones being between 1% to 1.2% of the pile diameter.

Based on these observations the possibility of proposing a simplified model for α_{STN} , taking into account its variability, was investigated. Figure 8.9 shows a Bilinear α_{STN} model, suggested for Grimsby clay, where the coefficient of damping, α_{STN} , (Equation 8.3) is assumed to be a function of the normalized displacement, d , defined as the ratio between pile head displacement and pile diameter. The value of α_{STN} increases linearly, with d , from zero until $d = 1\%$ where it is assumed to become constant and equal to 0.90 (the ultimate triaxial damping parameter, α , for both KSS and Grimsby clay (Figure 8.1)). The value of $d = 1\%$ is not arbitrary but coincides with the definition of “quake” (Smith, 1960), known as the local pile displacement to cause slip between the pile and soil (Randolph & Deeks, 1992). It is the limit between the elastic and plastic zones of soil behaviour (Svinkin, 1996) and the point where the full static capacity is assumed to be mobilized, generally taken in the range 2-3 mm for a 300 mm diameter pile (Randolph & Simons, 1986).

The result of applying the bilinear α_{STN} model (Figure 8.9) (with quake equal to 1% and maximum α equal to 0.90) in Equation 8.3, to modify the 3000 kN Statnamic loading cycle in Grimsby clay are shown in Figure 8.10. The prediction, plotted along with the non-linear model based predictions with damping parameters obtained from the model pile testing in KSS clay (Class A prediction) and from triaxial testing, provides a good correlation in the plastic zone (for pile head displacement higher than 6 mm, equivalent to 1% of the pile diameter). It actually coincides with the measured static capacity (CRP) and the prediction based on “constant” triaxial damping parameters in the plastic zone and improves the correlation between predicted and measured static capacity in the elastic zone (for normalized pile head displacement lower than the quake = 1%) with less than 14 % under-prediction. In contrast, class A and triaxial damping parameter based under-predictions were as much as 33 % and 24 % respectively in the same area (pile head displacement = 4 mm). If the bilinear α_{STN} model (Figure 8.9) is applied with quake equal to 1.2 % (purely based on observations of the back analysis of the empirical results for the 3000 kN Statnamic loading cycle and maximum α_{STN} equal

to 0.90, the prediction in the plastic zone (now assumed to be at 1.2 % of pile diameter) remains the same and the maximum under-prediction in the elastic zone decreases to 9% (Figure 8.11).

Figure 8.12 and Figure 8.13 show the results after the application of the same bilinear α_{STN} model, with quake equal to 1% and α_{STN} equal to 0.90, to the analysis of Statnamic model pile testing data, based on Equation 8.3, for calibration chamber beds 4 and 5 in KSS clay (Brown 2004). The application of the model in bed 4 over-predicts the static (CRP) capacity by as much as 13.5 % for 7 mm displacement (equivalent to 10 % of pile diameter) while the application of the same model to bed 5 provides a good correlation between predicted and measured static data (CRP) with an under-prediction of less than 3.0 % at 10% of the pile diameter. The prediction for bed 5 closely matches the measured static values for displacements lower than 1%, and this constitutes an improvement with respect to the prediction based on “constant” triaxial damping parameters (Figure 8.5).

8.4.3 Several consecutive Statnamic loading cycles. Multistage Bilinear α_{STN} model

The UPM and the non-linear model, in any of the forms proposed in previous sections, use a single loading Statnamic cycle to derive the equivalent static capacity of the pile.

The pile testing carried out on the full scale prototype in Grimsby consisted of a series six consecutive loading steps of 1000, 1500, 2000, 1500, 2500, 3000 KN. For the class A prediction and the different applications of the non-linear model, in previous sections, the loading history of the pile before each loading step was ignored and the results plotted with the pile tests set at zero pile head displacement for the beginning of each new cycle (Figure 8.8).

The back analysis of Statnamic data for each loading cycle versus the measured static CRP test, all set at zero pile head displacement for the beginning of each new loading step, showed that the deduced non-linear model parameter α_{STN} , for β_{STN} assumed equal to 0.20 (Equation 8.4) was different for different loading stages, the value of α_{STN} appears to increase when the load increases (Figure 8.8). This seems to

agree with the results of Statnamic data reported by Janes (1995) that show that the Statnamic UPM damping “constant” C_{UPM} , in the same area of the Statnamic cycle, varied on the same pile by a factor of 3 when the applied Statnamic force was doubled. But in that case, as in the non-linear analysis in previous sections, the preloading history of the piles was ignored.

If the results of the successive loading steps are plotted taking into account the actual pile head displacement or un-recovered deformation before each loading stage (Figure 8.14), the combination of all the loading steps could be considered as a single loading test consisted of a succession of loading and unloading cycles. The bilinear α_{STN} model (Figure 8.15), with the maximum α_{STN} equal to 0.90 and the quake equal to 1% where d is now the normalized initial pile head displacement (Pile head displacement/ diameter %) before each loading stage, could be used as an empirical approach to obtain the corresponding maximum α_{STN} value for each loading stage, (and hence the ratio between α values for different loading stages equal to the ratio between their initial normalized pile head displacements).

Figure 8.16 shows the maximum α_{STN} values for the Statnamic tests on Grimsby clay obtained applying this method. i.e. α_{STN} equal to 0.00, 0.11, 0.32, 0.65, and 0.90 for normalized pile head displacements of 0.00%, 0.12%, 0.35%, 0.72%, 1.11% corresponding to nominal target Statnamic loading cycles of 1000, 15000, 2000, 2500 and 3000 kN respectively. The deduced α_{STN} values can be applied to the non-linear model (Equation 8.3) with β_{STN} equal to 0.20, to modify the Statnamic data for each loading cycle (Figure 8.17) and the predicted static capacity can be defined as the envelope of the modified Statnamic data. Figure 8.18 shows the multistage bilinear α_{STN} model prediction for Statnamic tests on Grimsby clay and measured static CRP set at zero pile head displacement. The multistage prediction defined as the envelope of the successive modified Statnamic loading cycles slightly under-predicts the static CRP capacity of the pile set at zero pile head displacement (maximum error at 15.88mm head displacement, with predicted value equal to 1950 kN and the measured value equal to 2065 kN, is equal to 5.6%). But if, being consistent with the idea of considering the preloading history of the pile, the static (CRP) test results are set at the un-recovered

initial displacement before the test (Figure 8.19), then the predicted static capacity provides an excellent correlation with the measured static (CRP) capacity .

The multistage bilinear α_{STN} model prediction so defined takes into account the preloading history of the pile, justifies the variability of α for different loading stages and allows the extension of the prediction to a wider range of pile head displacements compared with the single loading cycle analysis.

The α values determined from single stage triaxial tests on KSS were lower than those obtained from corresponding multistage triaxial tests. This testing anomaly was not observed in the case of the data from tests on Grimsby clay where as can be observed in Figure 7.70 similar α values were obtained for both single and multistage tests. The author felt justified therefore using a maximum value of 0.90 for α_{STN} in the bilinear model when applied to the full scale pile prediction in Grimsby clay.

Further research is required in order to check the validity of the empirical approach using the non-linear model (Equation 8.3) for different types of clay soil, conditions (effective stress, stress history and combination of different soils at different levels) and pile lengths.

The non-linear model proposed (Equation 8.3) for Statnamic analysis is in fact the same model proposed by Randolph & Deeks (1992) (Equation 2.6) for the dynamic shaft response of pile, including the term suggested by Hyde *et al* (1998) such that the dynamic friction reverts to the static value when the slip velocity is equal to that at which τ_s is defined. It is similar to non-linear viscous laws proposed by Gibson *and* Coyle (1968), Heerema (1979) and Litkouhi *and* Poskit (1980). The values of β equal to 0.20 and α equal to 0.90 obtained from the triaxial testing agree with the values of α_{RD} varying from 0.10 for sand to 1.00 for clay soils and β_{RD} close to 0.20 suggested by Randolph & Deeks (1992), Gibson *and* Coyle (1968), Heerema (1979) and Litkouhi *and* Poskit (1980).

The value of α obtained from the triaxial testing based on the best fit of the experimental data to the power law that represents the proposed non-linear model (Equation 7.2) relating static and dynamic shear resistance has an associated standard

error of ± 0.1 . It might be then convenient to consider α_{STN} defined within an interval 0.90 ± 0.10 rather than a single value.

The analysis of the parametric sensitivity of the prediction of static load pile response from Statnamic data based on the non-linear model (Equation 8.3), assuming β_{STN} equal to 0.20 and varying the value of α_{STN} from 0.60 to 1.20, shows that an increase of α by 0.1 represents about 3% reduction of the predicted static response (percentage referred to measured dynamic load (F_{STN-Ma})).

Model	Pile Load kN	Pile Head Displacement mm	Secant Stiffness kN/mm
Measured CRP	1500	3.90	385
Class A prediction	1500	6.32	236
UPM	1500	5.30	283
For comparison only			
F_{STN}	1500	2.89	519
F_{STN} - Ma	1500	3.24	463

Table 8.1 Measured and predicted secant stiffness at a pile load of 1500 kN

Model	Pile Load kN	Pile Head Displacement mm
Measured CRP	1946	8.85
Class A prediction	1746	8.85
UPM	2343	8.85
For comparison only		
F_{STN}	3037	8.85
F_{STN} - Ma	3210	8.85

Table 8.2 Measured and predicted ultimate pile capacity at pile head displacement of 8.85 mm (point of maximum Statnamic load)

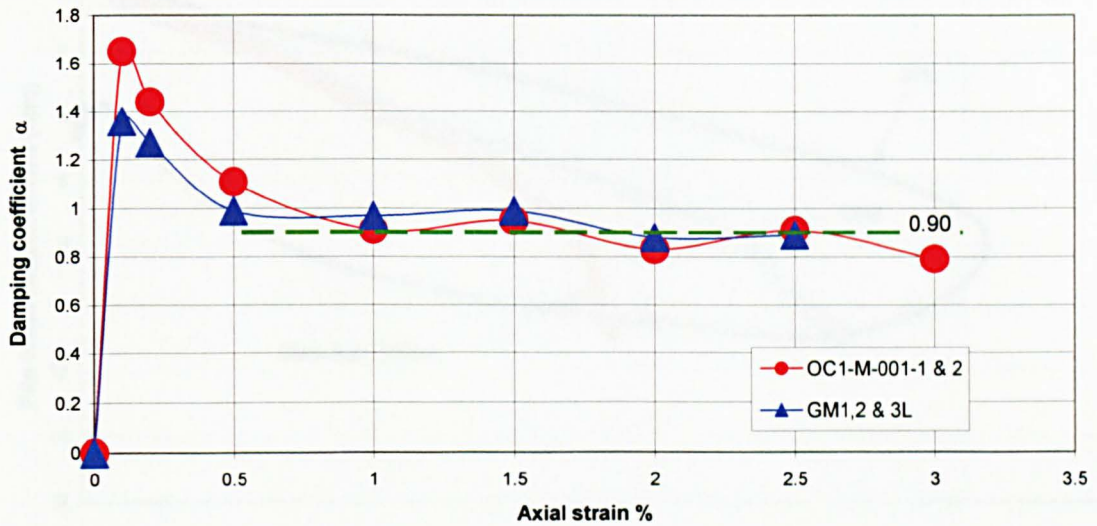


Figure 8.1 Damping coefficients, α , from multistage triaxial tests on KSS clay and Grimsby clay. ($\beta = 0.20$)

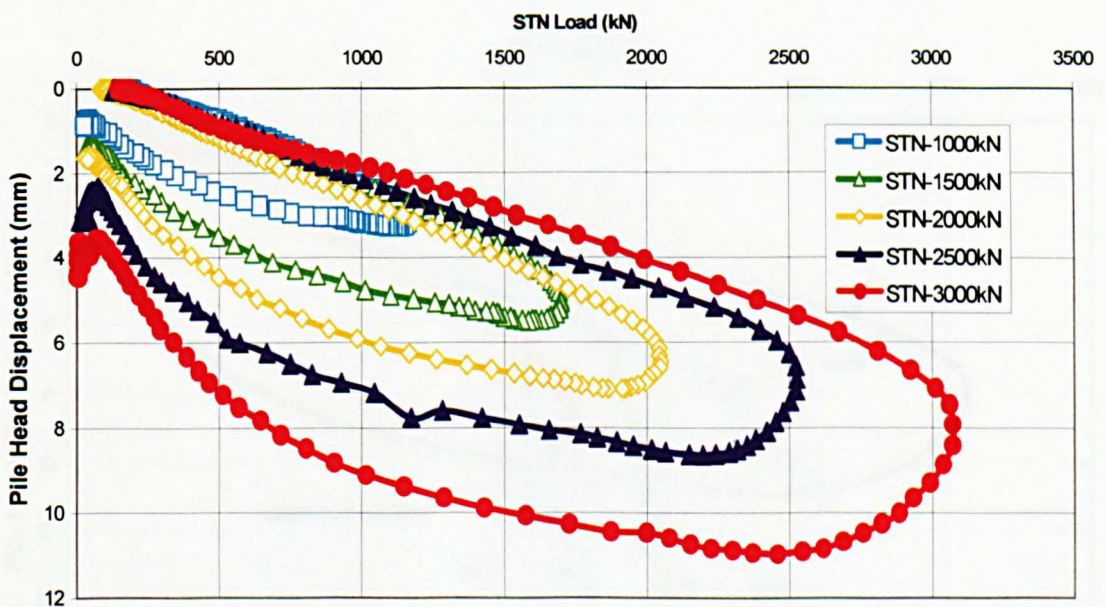


Figure 8.2 Load displacement curves for Statnamic tests with pile tests set at zero at the beginning of each new cycle. (Grimsby clay)

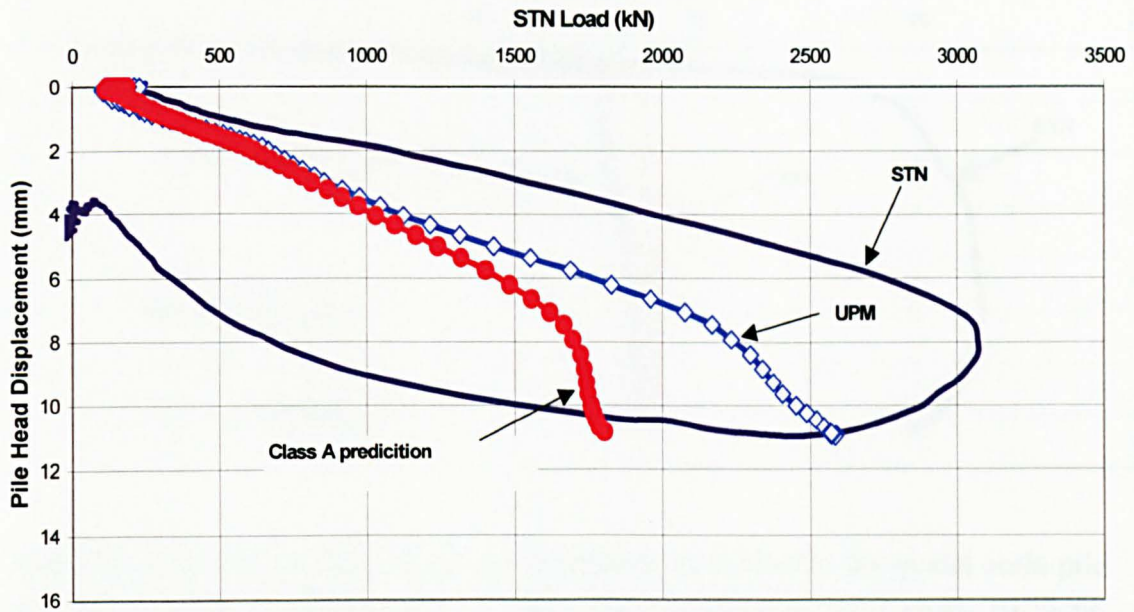


Figure 8.3 Load displacement curves for 3000 kN Statnamic load cycle, class A prediction and UPM static prediction.

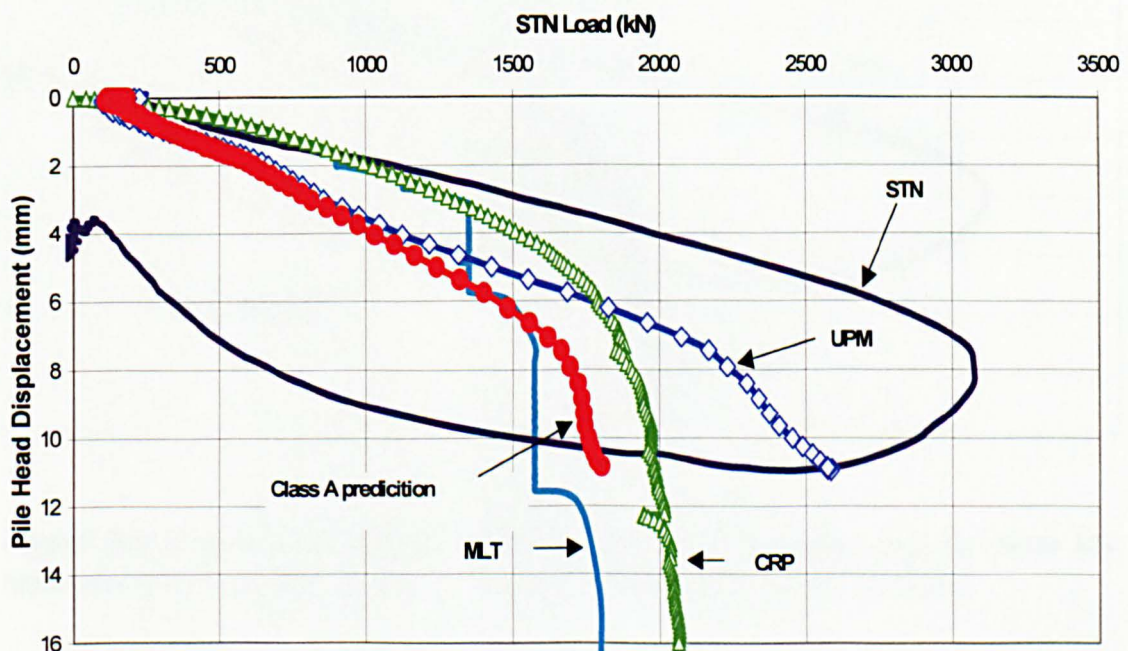


Figure 8.4 Load displacement curves for 3000 kN Statnamic load cycle, class A prediction, UPM static prediction, CRP and MLT test results.

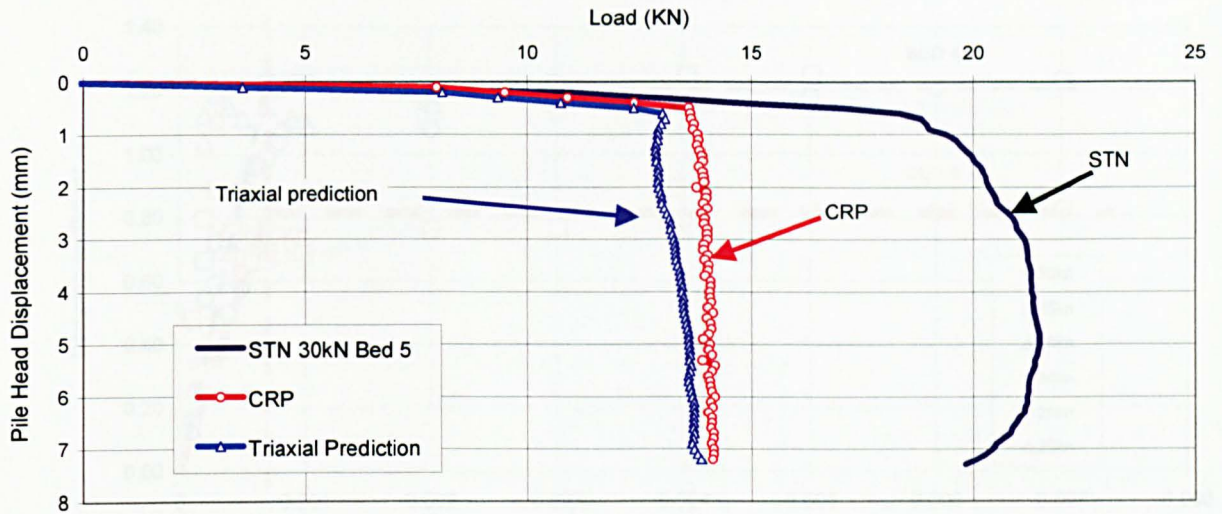


Figure 8.5 Non-linear damping model prediction on KSS clay for model scale pile test on calibration chamber bed 5 using triaxial damping coefficients ($\alpha=0.90$; $\beta=0.20$).

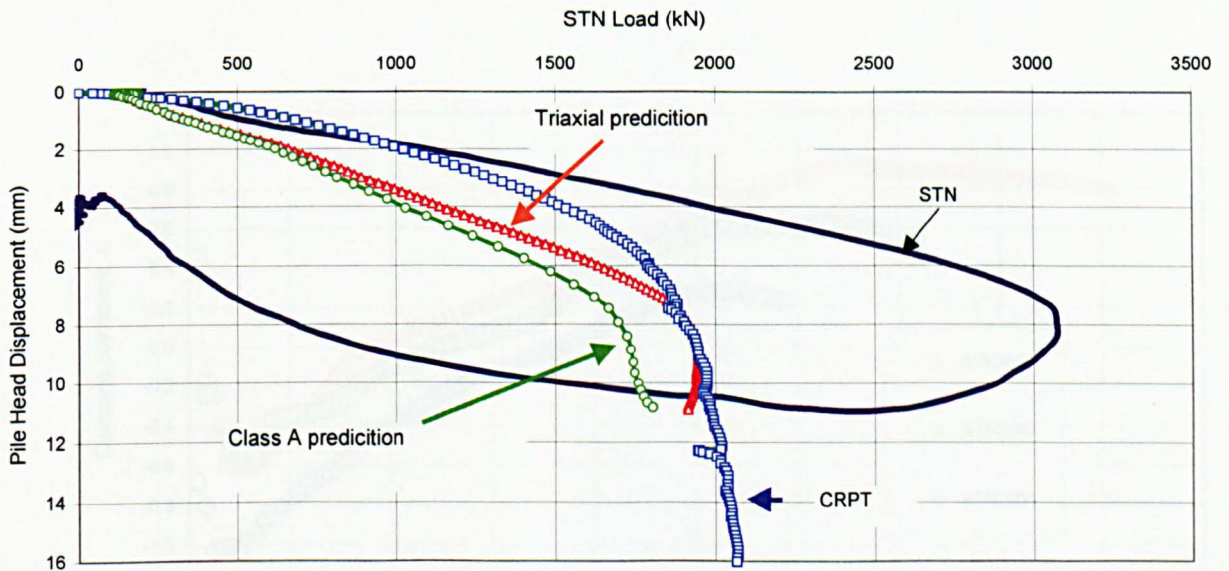


Figure 8.6 Non-linear damping model prediction on Grimsby clay for 3000 kN Statnamic load cycle using triaxial damping coefficients ($\alpha=0.90$; $\beta=0.20$).

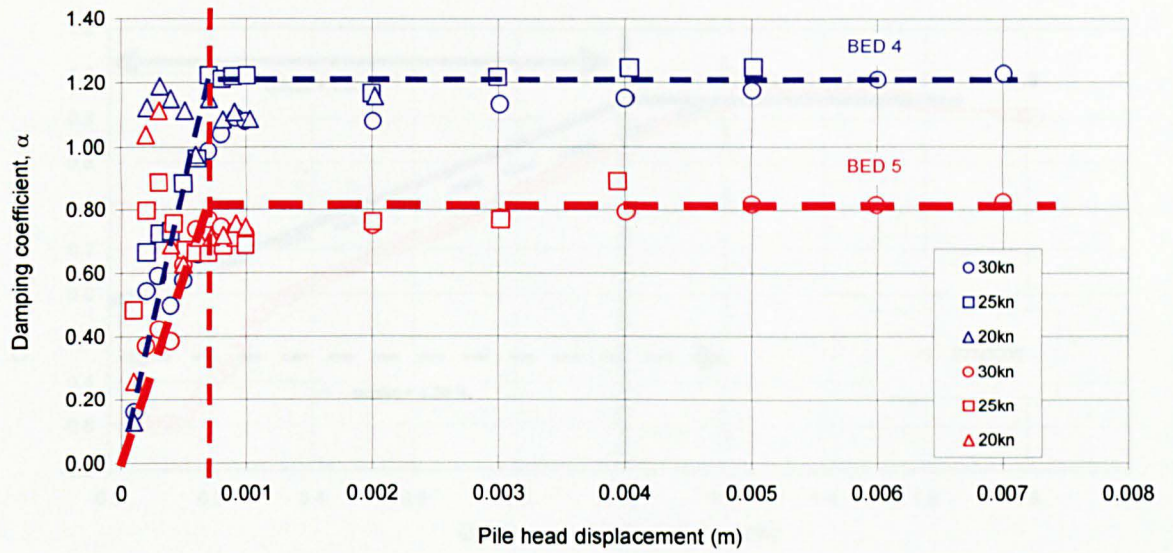


Figure 8.7 Deduced α_{STN} values from the measured Statnamic and static data on KSS clay for model pile tests on the calibration chamber beds 4 and 5.

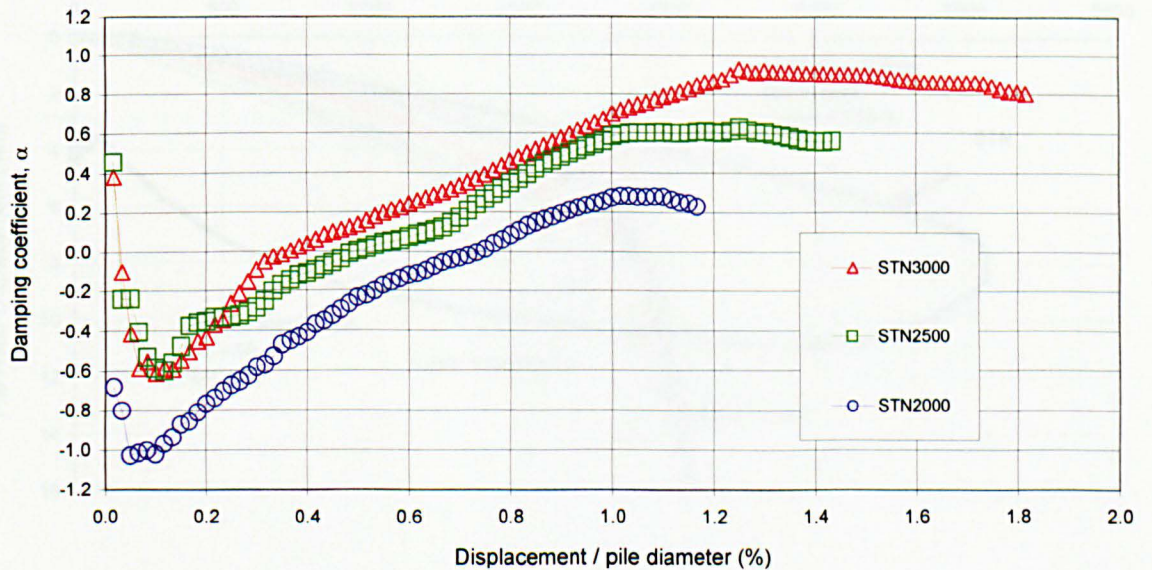


Figure 8.8 Deduced α_{STN} values from the measured Statnamic and static data on Grimsby clay for full scale pile tests.

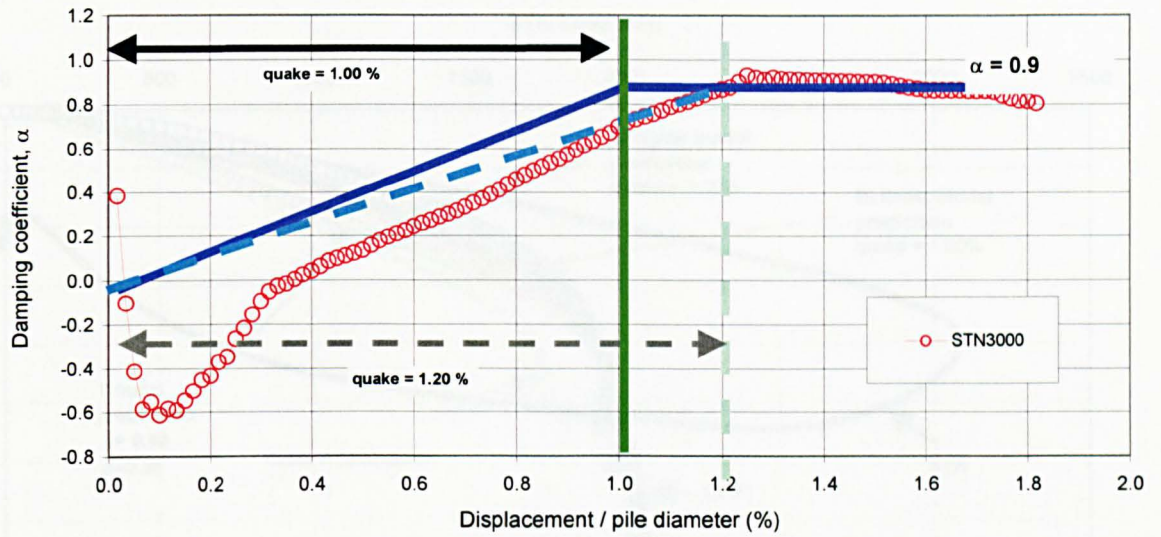


Figure 8.9 Bilinear α_{STN} model for Grimsby clay. ($\alpha_{STN} = f(d)$; $\beta_{STN} = 0.20$)

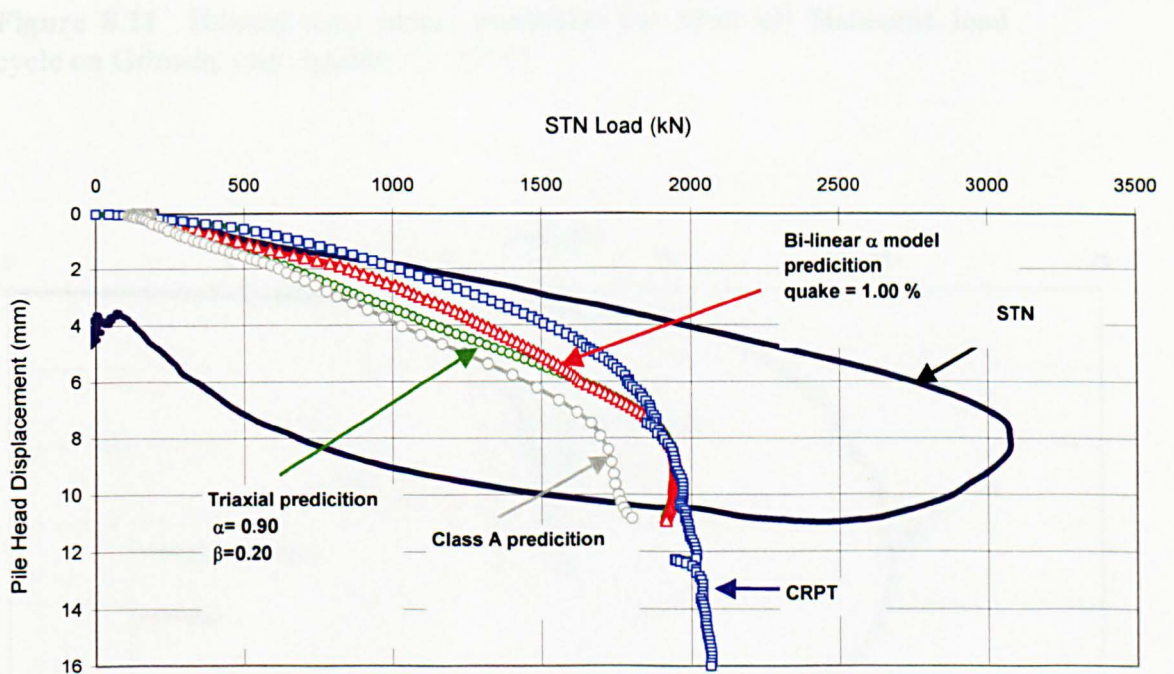


Figure 8.10 Bilinear α_{STN} model prediction for 3000 kN Statnamic load cycle on Grimsby clay. (quake = 1%)

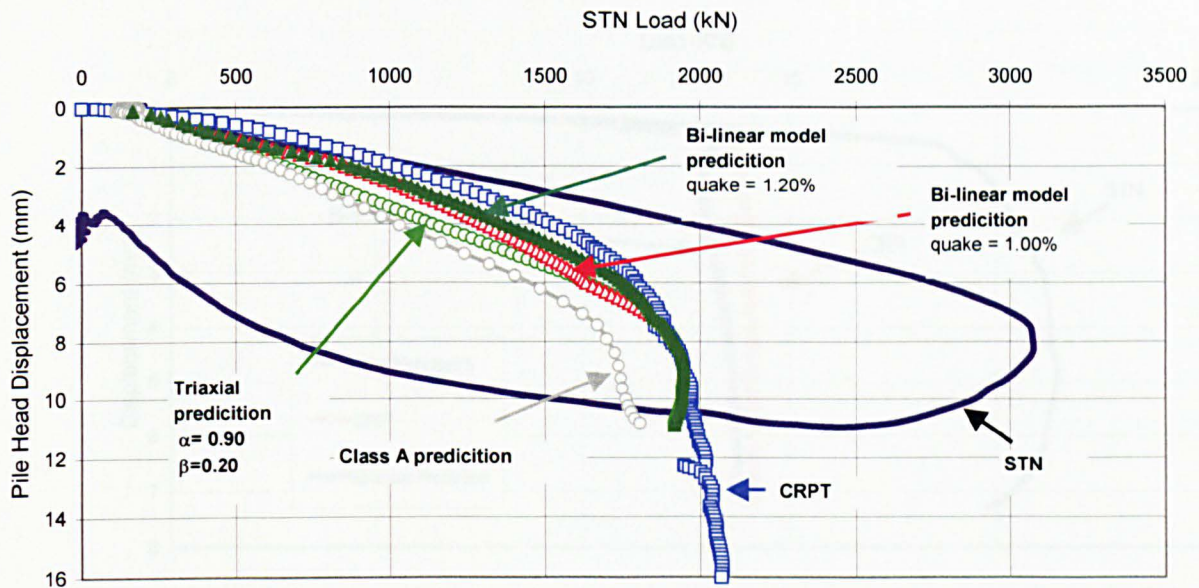


Figure 8.11 Bilinear α_{STN} model prediction for 3000 kN Statnamic load cycle on Grimsby clay. (quake = 1.20 %)

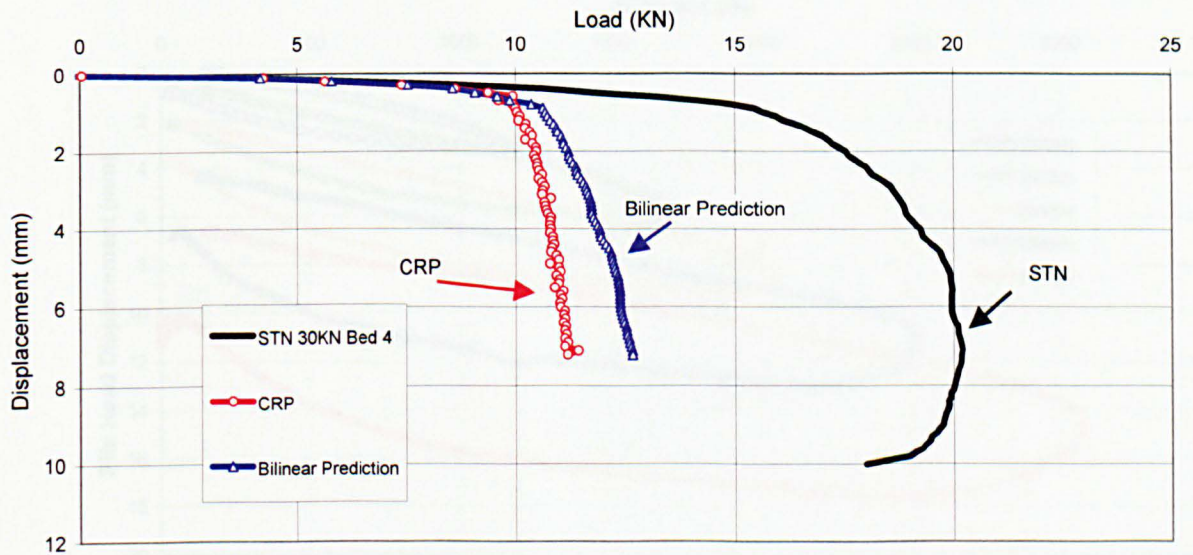


Figure 8.12 Bilinear α_{STN} model prediction for the maximum Statnamic load cycle on KSS clay for calibration chamber bed 4. (quake = 1 %; $\alpha_{STNmax} = 0.90$)

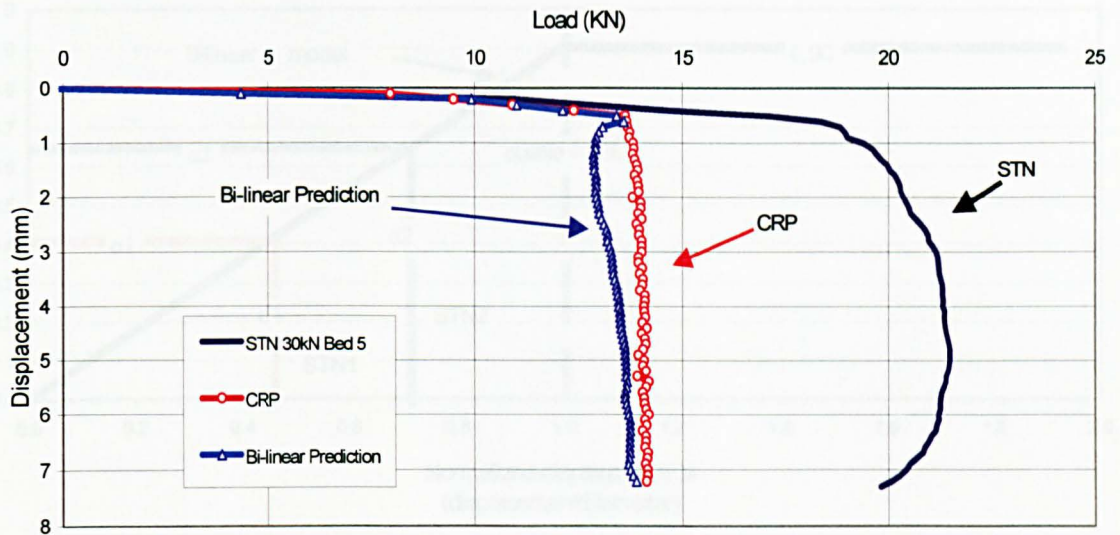


Figure 8.13 Multistage bilinear clay model

Figure 8.13 Bilinear α_{STN} model prediction for the maximum Statnamic load cycle on KSS clay for calibration chamber bed 5. (quake = 1 %; $\alpha_{STNmax} = 0.90$)

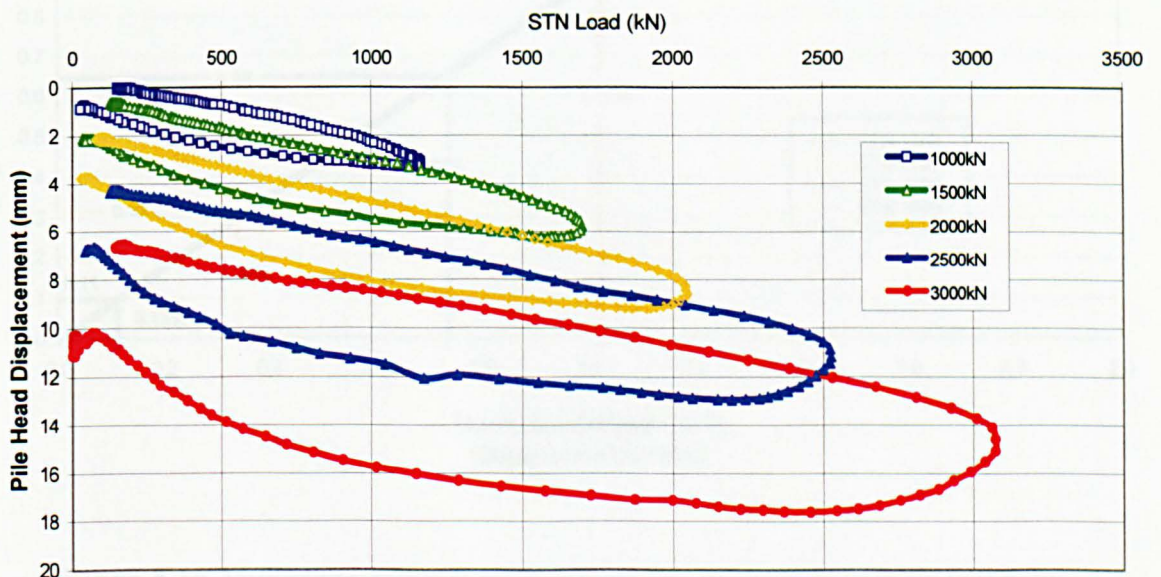


Figure 8.14 Load displacement curves for Statnamic tests with the pile test set at the initial un-recovered displacement at the beginning of each new cycle. (Grimsby clay).

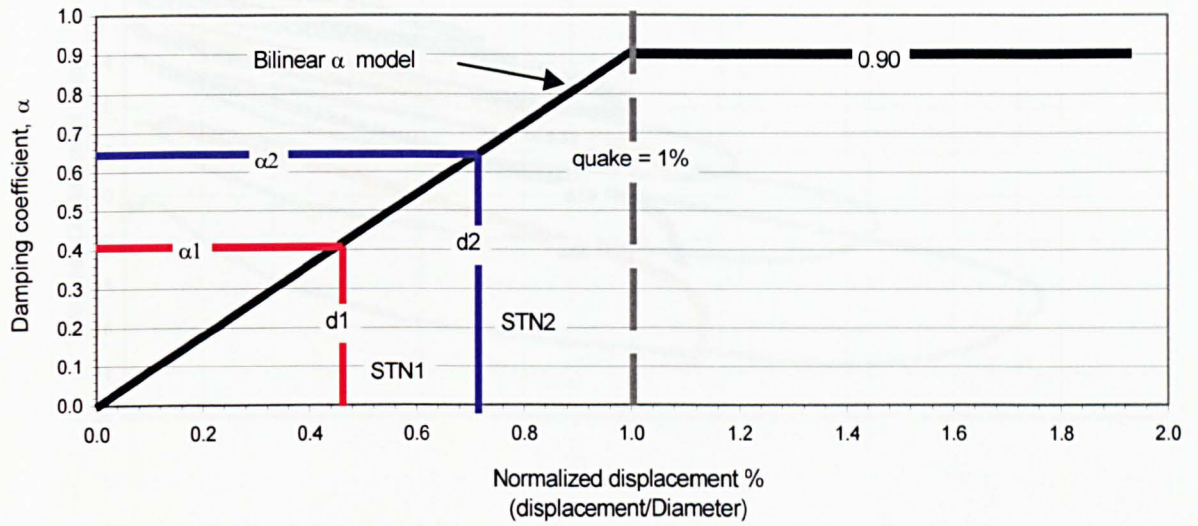


Figure 8.15 Multistage bilinear α_{STN} model.

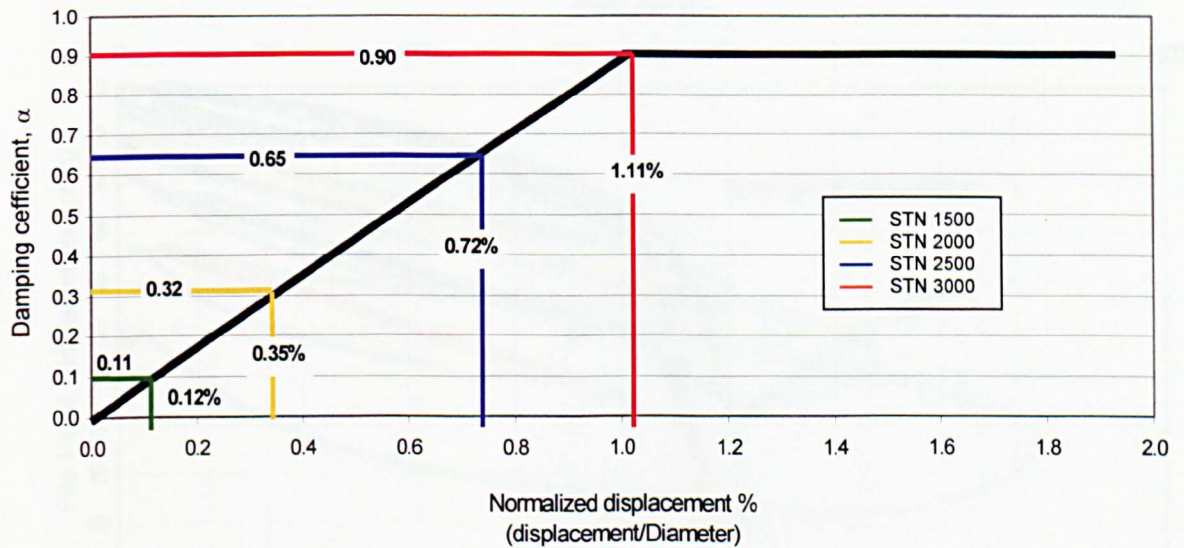


Figure 8.16 Multistage bilinear α_{STN} model for Statnamic tests on Grimsby clay.

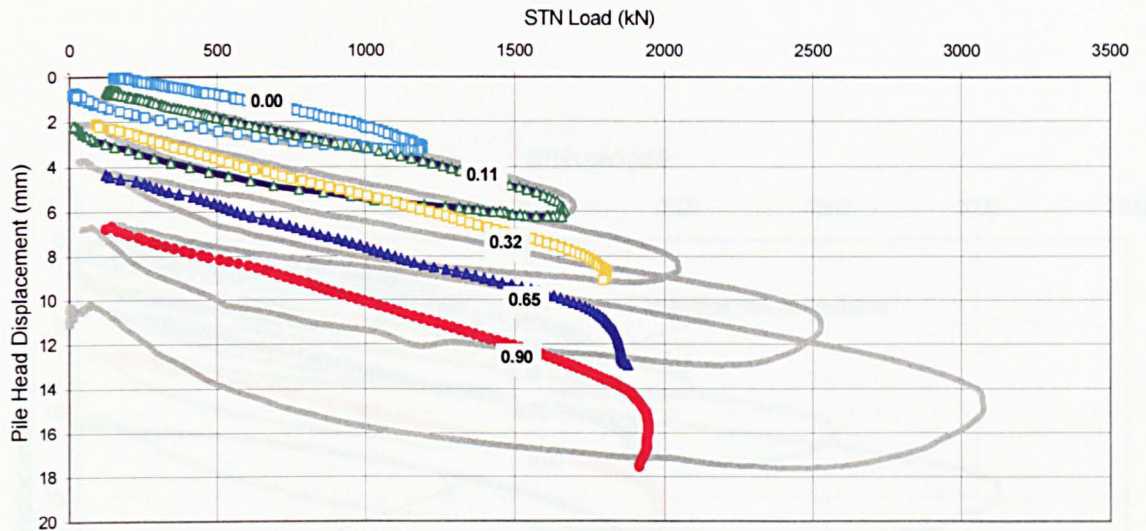


Figure 8.17 Multistage bilinear α_{STN} model prediction for Statnamic tests on Grimsby clay.

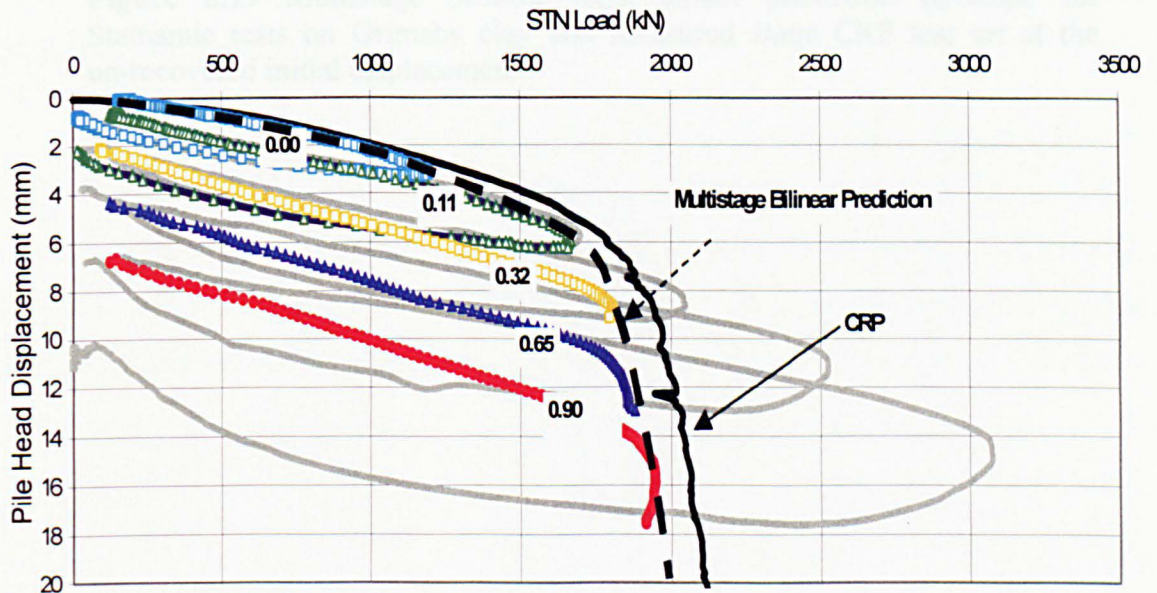


Figure 8.18 Multistage bilinear α_{STN} model prediction envelope for Statnamic tests on Grimsby clay and measured static CRP test set at zero.

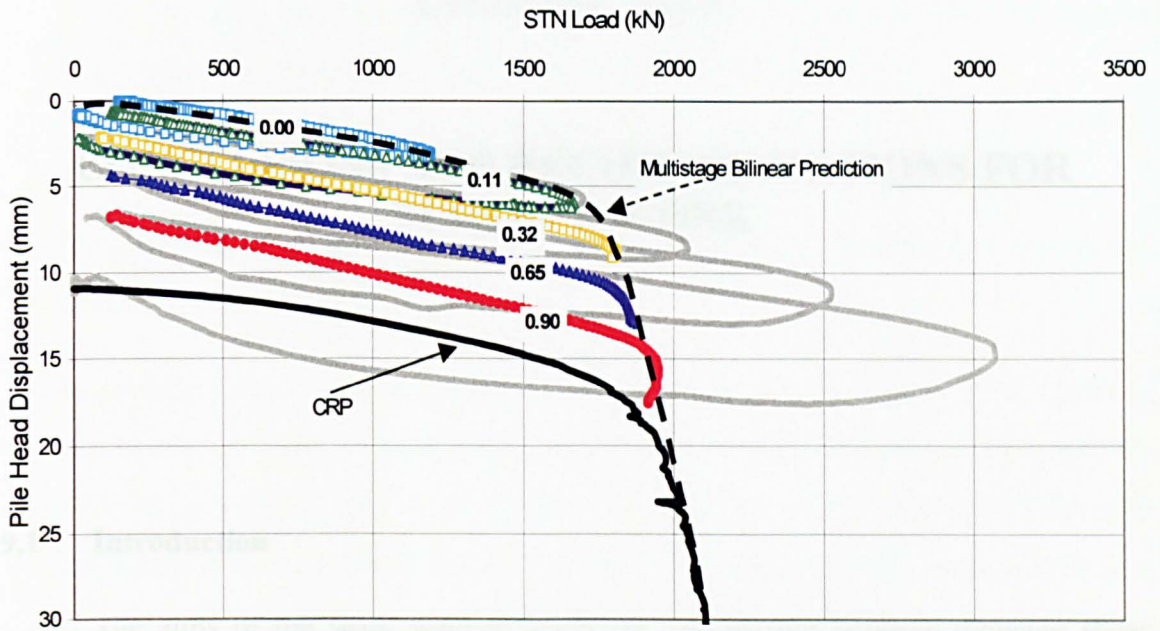


Figure 8.19 Multistage bilinear α_{STN} model prediction envelope for Statnamic tests on Grimsby clay and measured static CRP test set at the un-recovered initial displacement.

9.2 Rapid loading tests

The objectives of the work on reconstituted clay (KSS) and undisturbed clay (Grimsby) were

- to determine rate effects by means of monotonic static tests carried out at different rates on a series of samples.

CHAPTER NINE

CONCLUSIONS AND RECOMMENDATIONS FOR FURTHER WORK

9.1 Introduction

The aims of the work were to study the relationship between dynamic shear resistance and rate of shearing in clay soils and to apply the results to refine and develop models of soil behaviour in order to improve the current method (UPM) of analysis for Statnamic pile tests.

The objectives of the investigation were to carry out a triaxial testing programme on reconstituted clay (KSS) and undisturbed clay (Grimsby), to interpret the results in relation to current soil models, to calibrate the results against large scale model pile tests on KSS clay and in situ pile tests on Grimsby clay (Brown, 2004) and to establish models of soil behaviour taking into account rate effects for the analysis of Statnamic tests.

9.2 Rapid loading tests

The objectives of the work on reconstituted clay (KSS) and undisturbed clay (Grimsby) were

- to determine rate effects by means of monotonic triaxial tests carried out at different rates on a series of samples;

- to develop a multistage technique to study the rate effects on a single sample and
- to apply the multistage technique to a comparison of rate effect parameters for KSS with those obtained for undisturbed Grimsby clay.

The main conclusions from the rapid loading tests are:

- 1) The shear strength increased and the excess pore pressure decreased as the rate of shearing increased.
- 2) A power law was proposed relating dynamic and static shear strength. The model is similar to the models proposed by Gibson & Coyle (1968), Randolph & Deeks (1992), Hyde et al (2000), with β equal to 0.20 as suggested by Heerema (1979) and Litkouhi and Poskitt (1980), but with α equal to a function of axial strain ($\alpha(\epsilon)$) that becomes approximately constant for axial strains higher than 1%.
- 3) The coefficients of damping α and β for reconstituted clay (KSS) and undisturbed clay (Grimsby) were obtained by multistage testing at various rates, with static reference rate equal to 0.001 mm/s.. The values were similar for both KSS and Grimsby clay and hence the same rate effects can be assumed for both materials. Based on the observations it was possible to define β equal to 0.20 and α as function of axial strain ($\alpha(\epsilon)$) that tended to 0.90 when the axial strain was higher than 1%.
- 4) Good agreement was observed between α values obtained from single stage tests and those from multistage tests thus validating the use of multistage rapid loading tests to obtain reliable damping parameters (α and β) for undisturbed Grimsby clay.

9.3 Application of rate effects to the analysis of Statnamic test results

The main conclusions from application of rate effects to the analysis of Statnamic test results are:

- 1) A method has been proposed, and validated, that allows full interpretation of Statnamic results on the basis of relatively simple laboratory tests.

- 2) Based on the triaxial tests on Grimsby and KSS clay reported in this thesis and model pile tests on KSS clay (Brown, 2004) a non-linear model (Equation 8.3) has been proposed relating the static resistance of a pile to the measured Statnamic load taking into account the rate effects and the inertia of the pile.
- 3) The use of damping parameters, α equal to 0.90 and β equal to 0.20, obtained from the triaxial tests for the non-linear analysis of Statnamic tests in both KSS and Grimsby clay provided good correlation for the ultimate static capacity (under-prediction of less than 5% for KSS and less than 0.5 % for Grimsby) but still under-predicted the secant stiffness.
- 4) A simplified bi-linear model was proposed for α_{STN} which differentiates elastic and plastic zones of behaviour in the load-displacement response of a pile using the concept of quake, previously introduced by Smith (1960) for the analysis of the dynamic response of piles. In the elastic zone, defined from zero to quake (assumed to be a displacement equal to 1% of the pile diameter), α_{STN} was assumed to increase linearly from zero to 0.90. In the plastic zone, defined from quake upwards, α_{STN} was assumed to be constant and equal to 0.90. The application of the bi-linear model of α_{STN} gave a good correlation in the plastic zone and represents a significant improvement of the prediction of static behaviour of the pile from Statnamic data in the elastic zone, providing a better prediction of the secant stiffness in this area.
- 5) A multistage bi-linear α_{STN} model prediction was proposed when a pile is loaded in a series of consecutive Statnamic cycles with increasing maximum targeted load. The multistage bi-linear α_{STN} model takes into account the preloading history of the pile, justifies the variability of α_{STN} for different loading stages and allows the extension of the prediction to a wider range of pile head displacements than by means of a single loading cycle analysis. The application of this empirical approach to the Statnamic data series for the prototype pile in Grimsby clay provided an excellent correlation with measured static (CRP) tests.

9.4 Application of multistage tests to determine critical state parameters

- 1) The results from multistage triaxial tests at constant rate (0.001 mm/s) carried out on reconstituted clay (KSS) and undisturbed clay (Grimsby) showed that the slope of equal strain contours defined in q - p' space and the parameters a_1 and a_2 that fit the same equal strain contours in the e - p' space could be used to determine the critical state parameters, M , λ and Γ . The slope of the equal strain contours in q - p' tended to M and a_1 and a_2 tended to λ and $(\Gamma+1)$ respectively.

9.5 Recommendations for further Work

- 1) The rate effect investigation has been carried out on reconstituted clay (KSS) and undisturbed Grimsby clay. A similar research programme should be conducted on a wider range of soils in order to investigate the rate effects and correlation between damping coefficients and fundamental soil properties.
- 2) The application of rapid loading triaxial tests to obtain the damping coefficients, used for the analysis of Statnamic data, is limited by the need to use a non-conventional rapid loading triaxial system. It is therefore desirable to investigate the possibility of determining the coefficients of damping from monotonic or multistage tests carried out up to 1 mm/s (usually achievable with conventional triaxial system), adopting the non-linear model (Equation 7.4) to fit the experimental data.
- 3) The triaxial investigation has been carried out using constant strain rate tests. A testing programme consisting of stress controlled transient loading tests, simulating Statnamic pulses, and constant rate static loading tests would allow an investigation of the validity of application of the non-linear models to transient loading tests and further investigation into the concept of "quake" used in the proposed empirical approach for analysing Statnamic data on piles.
- 4) A significant cell pressure increment was observed during rapid loading tests caused by the ram as it penetrated the cell. If a similar testing programme is carried out in the future with the same system a pressure transducer should be incorporated in the

- cell to measure the actual confining pressure and an air gap cushion should be left to reduce the effect.
- 5) Further research is required to check the validity of the constant rate multistage test method for determining critical state parameters. It is recommended that a testing programme needs to be conducted including multistage and monotonic triaxial and consolidation tests for different soils.
 - 6) The application of rate effects to the analysis of Statnamic data requires further investigation in order to check the validity of the empirical approach, using the non-linear model (Equation 8.3), for different types of clay soil, conditions (effective stress, stress history and combination of different soils at different levels) and pile lengths.
 - 7) It is desirable to conduct a laboratory large scale pile testing programme, consisting of consecutive Statnamic loading stages (without consolidation between them), to check the validity of the multistage bilinear α model on reconstituted clay (KSS) and extend the investigation to different soils and conditions, including those incorporating different layers of soil.
 - 8) In order to check the validity of the bi-linear α model on different soils and types of pile, the existing data base of Statnamic-and static tests should be analysed.
 - 9) Further research is required into the determination of damping coefficients by means of different methods. CPT (Cone Penetration Tests) should be carried out at different rates, from 0.001 mm/s upwards, in order to investigate the possibility of obtaining in-situ damping coefficients, and evaluate the rate effects associated with this testing method.

REFERENCES

- ADACHI, T. & OKANO, M (1974). A constitutive equation for normally consolidated clay. *Soils and Foundations* Vol.14, No.4, pp. 53-73.
- ADACHI, T. & OKA, F. (1982). Constitutive equations for normally consolidated clay based on elasto-viscoplasticity. *Soils and Foundations*. Vol.22, No.4, pp. 57-70.
- ADACHI, T., OKA, F. HIRATA, T., HASHIMOTO, T., PRADHAN, T.B.S NAGAYA J. & MIMURA M. (1991). Triaxial and torsional hollow cylinder tests of sensitive natural clay an elasto-viscoplastic constitutive model. 10th Int. European Conference on SMFE deformation of soils and displacement of structures., Florence, Italy, Balkema..Vol.1, pp.3-6
- AKAI, K. ADACHI, T. & ANDO, N., (1975). Existence of a unique stress-strain-time relation of clays. *Soil and Foundations*. Vol. 15 No.1 March, pp.1-16
- AKAI, K. YAMAMOTO, J. & OZAWA, Y. (1962). On behaviour of pore pressure during shear of saturated clay. *Trans. JSCE*, No. 85, pp. 1-6 (in Japanese).
- AKAI, K., ADACHI, T. & OKANO, M. (1972). Deformation characteristics of saturated clay under vibrational loading in terms of effective stress. *Proc 7th Annual Meeting of JSSMM*, pp. 273-276 (in Japanese)
- AL-MHAIDIB, A.I. (2001). Effect of rate of loading on uplift capacity of a model pile in clay. *Proc. 11th International Offshore and Polar Engineering Conference*. Stavanger, Norway, June 17-22. ISOPE, Vol 2, pp 656-661
- AMERICAN STANDARD TESTING METHODS. Standard test method for piles under static axial compressive load. ASTM D1143-81:1994.
- ANDERSON, W.F., BROWN, M.J., HYDE, A.F.L. & BALDERAS MECA, J. (2003) A laboratory study of Statnamic testing of piles in clays. *Proc. Int. Conf. on Advances in Soft Soil Engineering and Technology*, 2nd, Putrajaya, Malaysia, 2-4 July 2003. pp. 117-127.
- ANDERSON, W.F., PYRAH, I.C. & FRYER, S.J. (1991) A clay calibration chamber for testing field devices. *ASTM Geotechnical Testing Journal*, Vol. 14, No. 4, December 1991. pp. 440-450.
- ATKINSON, J. H., BRANSBY .P.L. (1978). *The mechanics of soils. An introduction to critical state soil mechanics*, McGraw-Hill.
- BELL, A (2001) Investigation into the increase in capacity with time of precast piles driven into stiff overconsolidated clay. MSc Thesis, University of Sheffield, UK.

- BEMBEN, S.M. & MYERS D.A. (1974). The influence of rate of penetration on static cone resistance values in Connecticut River Valley Varved Clay. Proc. European Symposium on penetration testing. Stockholm. ESOPT, Vol 2, No. 2 , pp 33-34.
- BERMINHAM, P., & JANES, M. (1989). An innovative approach to load of high capacity of piles. International Conference on Piling and Deep Foundations, London. pp.409-413
- BISHOP, A.W. AND HENKEL, D.J. (1964): The Measurement of Soil Properties ithe Triaxial Test, Edward Arnord Publishers Ltd., UK.
- BJERRUM, L., SIMONS N. & TORBLAA , I. (1958). The effect of time on the shear strength of a soft marine clay. Brussels Conf. On Earth Pressure Probs.Vol.1.pp.148-158
- BOND, A. J. (1989). Behaviour of displacement piles in an overconsolidated clay. PhD Thesis. Imperial College, University of London.UK. 1989
- BOND, A.J. & JARDINE, R.J. (1991) Effects of installing displacement piles in a high OCR clay. Geotechnique, Vol. 41, No. 3, 1991. pp. 341-363.
- BRIAUD, J.L., GARLAND, E. & FELIO, G.Y. (1984) Rate of loading parameters for vertically loaded piles in clay. Proc. of the Annual Offshore Technology Conference, 16th, Houston, Texas, 7-9 May 1984. pp. 407-412.
- BRITISH STANDARDS INSTITUTION. Code of practice for foundations. BS8004:1986.
- BRITISH STANDARDS INSTITUTION.Code of practice for site investigations,. BS 5930:1981
- BRITISH STANDARDS INSTITUTION. Methods of test for soils for civil engineering purposes. BS1377:1990.
- BRITISH STANDARDS INSTITUTION. Part 121: Testing concrete-Method for determination of static modulus of elasticity in compression. BS1881:1983
- BROWN (2004). The Rapid Load Testing of Piles in Fine Grain Soils.PhD Thesis. University of Sheffield. UK. 2004 (In preparation)
- BROWN, D.A. (1994) Evaluation of static capacity of deep foundations from Statnamic testing. ASTM Geotechnical Testing Journal, Vol.17, No. 4, December 1994. pp. 403-414.
- BROWN, D. A. (1995). Discussion closure on "Evaluation of static capacity of deep foundations from Statnamic testing" by Dan Brown. ASTM Geotechnical Testing Journal, GTJODJ ,Vol.18, No.4, pp 495-498.

- BROWN, M.J. (2003) Research Developments-Progress Report. *Ground Engineering Journal*. Vol. 36, No.4, April 2003. pp. 31-32.
- BROWN, M.J., HYDE, A.F.L. & ANDERSON, W.F. (2002) The influence of loading rate on pile behaviour in clay. In R. Philips, P.J. Guo & R. Popescu (eds), *Int. Conf. On Physical Modelling in Geotechnics ICPMG'02*, Newfoundland, Canada, 10-12 July, 2002. Rotterdam, A.A. Balkema. pp. 667-672.
- CASAGRANDE, A & SHANNON, W.L. (1948) Stress deformation and strength characteristics of soils under dynamic loads. *Int. Conf. on Soil Mechanics and Foundation Engineering*, 2nd, Vol. 5, 1948. pp. 29-34.
- CASAGRANDE, A & WILSON, S.D. (1951) Effect of rate of loading on the strength of clays and shales at constant water content. *Geotechnique*, Vol. 2, No. 3, June 1951. pp. 251-263.
- CHIN, M. C. (1998). Application of signal matching techniques to statnamic testing. 2nd International Statnamic Seminar, Tokio. Japan, 28-30 October 1998 pp 311-312.
- CRAWFORD C.B. (1959) .The influence of rate of strain on effective stresses in a sensitive clay. *Amer. Soc. Test. Mat. Special Tech Pub. No. 254*, pp 36-61
- DAYAL, U. & ALLEN, J.H. (1975) The effect of penetration rate on the strength of remoulded clay and sand samples. *Canadian Geotechnical Journal*, Vol. 12, 1975. pp. 336-348.
- EIBER, R.J. (1958). A preliminary Laboratory Investigation of the Prediction of Static Pile Resistances in Sand. Master's thesis, Department of Civil Engineering, Case Institute of Technology, Clevelant, OH.
- EL NAGGAR, M.H. & BALDUNELLI, M. (1998). Signal mathching technique of statnamic load tests for pile capacity prediction. 8th International Colloquium on Structural and Geotechnical Engineering, Cairo, Egypt.3:366-375
- FELLENIIUS, B. (1995) Welcome form the Chairman, First International Statnamic Seminar, Vancouver, British Columbia Canada. 1995
- FOEKEN, R.J., MIDDENDORP, P. & COURAGE, W.M, (1998). Application of stress wave method for automatic matching and statnamic prediction. 2nd International Statnamic Seminar, Tokyo. Japan, 28-30 October 1998 pp 345-354.
- GARBIN, E.J. (1999) Data interpretation for axial Statnamic testing and the development of the Statnamic Analysis Workbook. MSc Thesis, University of South Florida, USA, 1999.
- GIBSON, G.C. & COYLE, H.M. (1968) Soil damping constants related to common soil properties in sands and clays (Bearing Capacity for Axially Loaded Piles). Texas A&M University, Texas, USA, Texas Transportation Institute. September 1968. Research Report 125-1, Study 2-5-67-125.

- GOBLE, G. G, SCANLAN, R.H, & TOMKO, J.J. (1967). Dynamic studies of the bearing capacity of piles. Highway Research Record No. 167, Bridges and Structures, April
- GOBLE, G. G. & RAUSCHE, F. (1970). Pile load tests by impact driving. Highway Research Record No. 333
- GOBLE, G.G., RAUSCHE, F & LIKINS, G. (1995). Discussion on "Evaluation of Static Capacity of Deep Foundation from Statnamic Testing" by Dan Brown. Geotechnical Testing Journal,GTJODJ. Vol.18, No.4, pp 493-498.
- HEEREMA (1979) Relationship between wall friction, displacement velocity and horizontal stress in clay and in sand, for pile driveability analysis. Ground Engineering Journal, January 1979. pp. 55-65.
- HIGHT, D.W.(1982). A simple piezometer probe for the routine measurement of pore pressure in triaxial tests on saturated soils. Geotechnique Vol.32. No. 4. pp 396-401.
- HIGUCHI, T. (2001). Liquefaction of Silts. PhD Thesis. University of Sheffield. UK. 2001.
- HORVATH, R.G. (1995) Influence of loading rate on the capacity of a model pile in clay. Canadian Geotechnical Journal, Vol. 32, 1995. pp. 364-368.
- HYDE, A. ANDERSON, W.F. BROWN, M. & BALDERAS-MECA, J. (2003a) The prediction of static pile behaviour from Statnamic testing of an auger bored pile in glacial clay. University of Sheffield internal report. Submitted to Prof. Malcolm Bolton (University of Cambridge)
- HYDE, A. ANDERSON, W.F. BROWN, M. & BALDERAS-MECA, J. (2003b) The prediction of static pile behaviour from Statnamic testing of an auger bored pile in glacial clay. Comparison of Static pile testing results and predicted values. Internal report University of Sheffield. Submitted to Prof. Malcolm Bolton (University of Cambridge)
- HYDE, A.F.L., ROBINSON, S.A. & ANDERSON W.F. (2000) Rate effects in clay soils and their relevance to Statnamic pile testing. In O. Kusakabe, F. Kuwabara & T. Matsumoto (eds), Int. Statnamic Seminar, 2nd, Tokyo, Japan, 28-30 October 1998. Rotterdam, A.A. Balkema. pp. 303-309.
- JAMES, R.C. (1967) The effect of electro osmosis on the bearing capacity of bored piles in clay soils. PhD Thesis, University of Sheffield, UK, 1967.
- JANES, M. (1995). Statnamic load testing of bridge pier foundations in North America. Proc. 36th Symposium on Engineering Geology and Geotechnical Engineering, Utah State University, Logan, Utah.

- JANES, M.C. JUSTANSON, M.D. BROWN, D.A. (2000). Long period dynamic load testing ASTM standard draft. Proc. 2nd International Statnamic Seminar, Tokyo, Japan, October, 1998, pp 199-218
- JUSTASSON, M. D. (1997). Report of Load Testing at the Taipei municipal incinerator expansion works. Tapei.
- KANTONA, M. G. (1984). Evaluation of viscoplastic cap model. Getechnical Engineering Journal. ASCE Vol 110, No. 8, pp 1106-1125.
- KUSAKABE, KUWABARA, & MATSUMOTO (eds), (2000). "Statnamic Load Tests", Draft of method for rapid load test of singles piles (JGS 1815-2000). Proc 2nd International Statnamic Seminar, Tokyo, Japan, October, 1998, pp 237-242
- LAMBE, T.W. (1973) Predictions in soil engineering. Geotechnique, Vol. 23, No. 2, 1973. pp. 149-202.
- LEFEBVRE, G. & LEOEUF, D. (1987) Rate effects and cyclic loading of sensitive clays. ASCE, Journal of Geotechnical Engineering, Vol. 113, No. 5, May 1987, pp. 476-489.
- LEMOS, L.J.L. (1986). Rate effects on residual strength. PhD Thesis. Imperial College of Science and Technology, University of London. U.K. 1986
- LEMOS, L.J.L. (1991) Shear strength of shear surfaces under fast loading. Eur. Conf. Soil Mech. Florence. Vol.1, pp. 137-141
- LITKOUHI, S. & POSKITT, T.J. (1980) Damping constants for pile driveability calculations. Geotechnique, Vol. 30, No. 1, 1980. pp. 77-86.
- LITTLE, J. A., WOOD, D.M, PAUL, M.A. & BOUAZZA, A. (1992). Some laboratory measurement of Bothkennar clay in relation to soil fabric. Geotechnique Vol. 42. No.2. pp 355-361.
- LO, K.Y. (1969). The pore pressure-strain relationship of normally consolidated undrained clays. Canadian Geotechnical Journal. Vol 6. pp 383-412.
- LUNNE, T., ROBERTSON, P.K. & POWELL, J.J.M (1997) Cone penetration testing in geotechnical practice. 1st ed. London, UK, Blackie Academic and Professional, 1997.
- LUPINI, J.F., SKINNER, A.E. & VAUGHAN, P.R. (1981) The drained residual strength of cohesive soils. Geotechnique, Vol. 31, No. 2, 1981. pp. 181-213.
- MATSUI, T. & ABE, N. (1985). Elasto/viscoplastic constitutive equation of normally consolidated clays based on flow surface theory. 5th ICONMG. Vol 1, pp 407-413.

- MATSUMOTO, T. (1998) A FEM Analysis of a Statnamic loading test on open-ended steel pile. Proc. of 2nd International Statnamic Seminar, Tokyo, Japan, October, 1998, pp 287-294.
- MIDDENDORP, P., BERMINGHAM, P. & KUIPER, B. (1992) Statnamic load testing of foundation piles. In F.B.J. Barends (ed), Int. Conf. on the Application of Stress Wave Theory to Piles, 4th, The Hague, The Netherlands, 21-24 September 1992. Rotterdam, A.A. Balkema, 1992. pp. 581-588
- MIDDENDORP, P. (1993) First experiences with Statnamic load testing of foundation piles in Europe. In W.F. van Impe (ed), Proc Int. Geotechnical Seminar on Deep Foundations on Bored and Auger Piles, 2nd, Ghent, Belgium, 01-04 January, 1993. Rotterdam, A.A. Balkema. pp. 265-272.
- MIDDENDORP, P. & BIELEFELD, M.W (1995) Statnamic load testing and the influence of stress wave phenomena. Proc. of Int Statnamic Seminar, 1st, Vancouver, Canada, 27-30 September 1995. pp. 207-220.
- MIDDENDORP, P. (2000) Keynote lecture: Statnamic the engineering of art. In S. Niyama & J. Beim (eds), Int. Conf. on the Application of Stress Wave Theory to Piles, 6th, Sao Paulo, Brazil, 11-13 September 2000, Rotterdam, A.A. Balkema. pp. 551-562.
- MIDDENDORP, P., GINNEKEN, G.J.J. van & FOEKEN R.J. van. (2000) The advantages and disadvantages of dynamic load testing and Statnamic load testing. In S. Niyama & J. Beim (eds), Int. Conf. on the Application of Stress Wave Theory to Piles, 6th, Sao Paulo, Brazil, 11-13 September 2000. Rotterdam, A.A. Balkema. pp. 625-632.
- MULLINS, G., LEWIS, C.L. & JUSTASON, M.D (2002). Advancements in Statnamic data regression techniques. In M.W. O'Neill (ed), Proc. ASTM Conf. Int. Deep Foundations Congress, 2002, Florida, ASTM Geotechnical Special Publication No.116, Vol. 2. pp 915-930.
- MURAYAMA, S. SEKIGUCHI, H. & UEDA, T. (1972). Stress relaxation of clays. Proc. Kansai Regional Meeting of JSCE, pp. III-1 (in Japanese)
- NISHIMURA, S. & MATSUMOTO, T. (1995) Wave propagation analysis during Statnamic loading of a steel pipe. Proc. of 1st Int Statnamic Seminar, Vancouver, Canada, 27-30 September 1995. pp. 23-33.
- OKA, F. (1981). Prediction of time dependent behaviour of clay. 10th ICSMFE. Vol.1. pp 215-218
- OKA, F. (1982). Elasto-viscoplastic constitutive equation for overconsolidated clay. International Symposium on Numerical Models in Geomechanic, Zurich.1982. pp147-156
- OLSON, R.E. & PAROLA, J.F. (1967) Dynamic shearing properties of compacted clay. Proc. of Int. Symp. on Wave Propagation and Dynamic Properties of Earth Materials,

- University of New Mexico, 23-25 August 1967. University of New Mexico Press, Albuquerque, New Mexico, 1967, pp. 173-182.
- O'NEILL, H. M. (1962). Direct-shear test for effective-strength parameters. Proc. Amer. Soc. Civ. Engrs(88:SM4:), pp 109-137.
- PAIKOWSKY, S.G. & CHERNAUSKAS, L.R. Soil inertia and the use of pseudo viscous damping parameters. 5th International conference on the application of stress wave theory to piles. Orlando, Florida, September 11th-13th. Townsed, F.C., Hussein, M., Mcway, M.C. pp 203-216
- PERYZNA, P. (1963). The constitutive equations for workhardening and rate sensitive plastic materials. Proc. of Vibrational Problems, Warsaw, Vol.4, No.3, pp 281-290
- PIERPOINT, N. D. (1996). The Prediction and Back Analysis of Excavation behaviour in Oxford Clay. PhD Thesis. University of Sheffield.U.K. 1996.
- PMC (2003) Company website. www.piletest.co.uk.
- POOROOSHAB, H.B. & ROSCOE, K. H. (1961). The correlation of the results of shear tests with varying degrees of dilatation. Proc. 5th Int. Conf. Soil. Mech., Vol 1. pp 297-304.
- POWELL, J.J.M. & QUARTERMAN, R.S.T. (1998). The interpretation of cone penetration tests in clays, with particular reference to rate effects. Proc. International Symposium on penetration testing. Orlando. Balkema, Rotterdam. Vol 2, pp 903-909.
- RANDOLPH, M.F. & DEEKS, A.J. (1992) Dynamic and static soil models for axial response. In F.B.J. Barends (ed), Int. Conf. on the Application of Stress Wave Theory to Piles, 4th, The Hague, The Netherlands, 21-24 September 1992. Rotterdam, A.A. Balkema. pp. 3-14.
- RANDOLPH, M.F. & SIMONS, H.A. (1986) An improved soil model for one-dimensional pile driving analysis. Int. Conf. On Numerical Methods in Offshore Piling, 3rd, Nantes, France, 21-22 May 1986. Paris, Editions Technip. pp. 3-17.
- RANDOLPH, M.F (2003) Science and empiricism in pile foundation of pile capacity. Geotechnique.Vol. 53, No. 10, pp- 847-875
- RICHARDSON, A.M. & WHITMAN, R.V. (1963) Effect of strain rate upon undrained shear resistance of a saturated remoulded fat clay. Geotechnique, Vol. 13, No. 4, 1963. pp. 310-324.
- ROSCOE, K. H., SCHOFIELD, A.N. & THURAIRJAH, A. (1963). Yielding of clays in states wetter than critical. Geotechnique Vol. 13, No.3, pp 211-240.
- ROSCOE, K.H. & PROOROOSHAB, H.B. (1963). A theoretical and experimental study of strains in triaxial tests on normally consolidated clays. Geotechnique, Vol 13, No.1, pp12-28.

ROSCOE, K.H. SCHOEFFIELD, A.N. & WROTH, C.P. (1958). On the yielding of soils. *Geotechnique*, Vol.8, No.1, pp22-53.

ROSSATO, G., NINIS, L. & JARDINE, R.J. (1992) Properties of some kaolin based model clay soils. *ASTM Geotechnical Testing Journal*, Vol. 15, No. 2, June 1992. pp. 166-179.

SCHOFIELD, A.N. & WROTH, C.P. (1968). *Critical State Soil Mechanics*. McGraw-Hill. London.

SEIDEL, J.P. (1996) The use of the signal matching approach to the analysis of Statnamic tests. In Townsend, M. Hussein & M.C. McVay (eds), *Int. Conf. on the Application of Stress Wave Theory to Piles*, 5th, Orlando, Florida, 11-13 September, 1996. Rotterdam, A.A. Balkema. pp. 1051-1061.

SEKIGUCHI, H. (1977) Rheological characteristics of clays. *Proc. 9th ICSMFE*, Vol.1, pp 289-292.

SHEAHAN, T. C., LADD, C. C. & GERMAINE J. T. (1996). Rate-dependent undrained shear behavior of saturated clays. *Journal of Geotechnical Engineering*. February 1996. pp 99-108.

SHOGAKI, T. & SHIRAKAWA, S. (1999). Undrained strength from various shear tests for undisturbed Kumamoto clay. *Characterization of Soft Marine Clays*. Tsuchida & Nakase (eds). Rotterdam, Balkema.

SINGH, A. & MITCHELL, J.K. (1968). General stress-strain-time function of soils. *Proc. ASCE, SM 1*, pp 21-46.

SKEMPTON, A.W. (1948) Vane tests in the alluvial plain of the River Forth near Grangemouth. *Geotechnique*, Vol. 1, No. 2, December 1948. pp. 111-118.

SKEMPTON, A.W. (1954). The pore pressure coefficients A and B, *Geotechnique*, Vol. 4, pp. 143-147.

SMITH, E. A. L. (1960). Pile driving analysis by the wave equation. *ASCE, Journal of the Soil Mechanics and Foundation Engineering Div.* 86: 35-61.

SRISAKTIHIVEL, S. (2003) Laboratory measurements of the permeability of clay soils assisted by a self-boring device. PhD Thesis. University of Sheffield. UK. 2003.

SVINKIN, M.R (1996) Soil damping in wave equation analysis of pile capacity. 5th International Conference on the Application of Stress Wave Theory to Piles. Orlando, Florida, September 1996. Townsend, F.C., Hussein, M, Mcvay, M.B (eds), pp 11-13.

TAYLOR, D.W. (1942) Research on consolidation of clays. Massachusetts Institute of Technology, Dept. of Civil & Sanitary Engineering, Serial 82.

- TAYLOR, P.T. (1966) Age effects on shaft resistance and effect of loading rate on load distribution of bored piles. PhD Thesis, University of Sheffield, UK, 1966.
- THE INSTITUTION OF CIVIL ENGINEERS. (1997) Specification for piling and embedded retaining walls. 1st ed. London, UK, Thomas Telford Publishing, 1997.
- TIKA, T. M. (1989). The effect of fast shearing on the residual strength of soils. PhD Thesis. Imperial College of Science and Technology, University of London. U.K. 1989
- TIKA, T.E., VAUGHAN, P.R. & LEMOS, L.J.L. (1996) Fast shearing of pre-existing shear zones in soil. *Geotechnique*, Vol. 46, No. 2. 1996. pp. 197-233.
- TIKA-VASSILIKOS, T. (1991). "Clay-on-Steel Ring Shear Tests and Their Implications for Displacement Piles." *Geotechnical Testing Journal*, GTJODJ Vol 14, No. 4. pp 457-463.
- TURNER, M. J. (1995). The Role of Integrity and other Non-destructive Testing in the Evaluation of Pile Foundation., CIRIA Founders.
- WHITMAN, R.V. (1957) The behaviour of soils under transient loadings. Proc. Int. Conf. on Soil Mechanics and Foundation Engineering, 4th, 1957. pp. 207-210.
- WOOD, D. M. (1990). Soil behaviour and critical state soil mechanics, Cambridge University Press.
- WOOD, T (2003) An investigation into the validation of pile performance using Statnamic tests. MSc Thesis, Imperial College, London, UK, 2003.
- WROTH, C. P., & LOUDON P.A, (1967). The correlation of strain within a family of triaxial tests on overconsolidated samples of kaolin. Proc. Geotechnical Conference, Oslo. pp163-189.
- YONG, R.N. & JAPP, R.D. (1969). Stress-strain behaviour of clays in dynamic compression. *Vibration Effects of Earth-quakes on Soils and Foundation*, ASTM STP 450, American Society for Testing Materials, pp 233-262
- ZHU, J.G. & YIN, J.H. (2000) Strain rate dependent stress strain behaviour of overconsolidated Hong Kong marine clay. *Canadian Geotechnical Journal*, Vol. 37, pp. 1272-1282

APPENDIX 1

CELL PRESSURE CORRECTIONS

The following notes offer an explanation of the cell pressure corrections carried out on data for rapid loading tests performed with the pneumatic computer controlled rapid loading triaxial system (Section 4.3).

It was found that during rapid loading tests, for rates higher than 10mm/s, the cell pressure increased due to the rapid change in volume caused by the ram as it penetrated the cell. The duration of these tests was 100 ms and the cell pressure system regulated by a servo valve (described in Section 4.3.1) was unable to compensate for the induced cell pressure increment. Although the cell pressure system included a pore pressure transducer, the software (Universal Testing Machine) did not allow monitoring and logging of cell pressure values under the cyclic test mode that was used for the rapid loading tests and hence the actual cell pressure value during these tests was unknown.

It was decided to carry out a testing programme to find out the actual value of cell pressure during rapid load tests. A miniature pore pressure transducer (Section 4.3) was immersed in the cell to log the cell pressure values during the test. The testing programme consisted of six series of monotonic rapid loading tests. Each series consisted of six tests carried out at different rates from 1 mm/s up to 200 mm/s. One series of tests was undertaken for each of the cell pressures used in the *main testing* programme i.e. 470 kPa (Series OC1 and multistage tests at OCR1 on KSS clay), 320 kPa (Series OC4 and multistage test at OCR4 on KSS clay), 270 kPa (multistage test at

OCR8 on KSS clay), 360 kPa (GM1L Grimsby clay), 435 kPa (GM2L Grimsby clay) and 545 kPa (GM3L Grimsby clay).

Figure A1-1 shows the results of measured cell pressure increase versus displacement obtained for rapid loading triaxial tests at different rates for an initial cell pressure equal to 470 KPa. Similar results were obtained for each series of tests and hence for each initial cell pressure. It was observed that the increase of cell pressure was significant for rates higher than 50 mm/s although it could be assumed negligible for rates lower than 10 mm/s.

The change in cell pressure seemed to depend on the initial cell pressure, the rate of testing and the axial displacement. It was found that for each series, and hence for each initial cell pressure value, it was possible to define the cell pressure increase as a function of both rate of testing and axial displacement and therefore predict the cell pressure value for tests carried at different rates within the range of 50 to 200 mm/s as shown in Figure A1-2. The cell pressure increase (ΔCP) was approximated by the function

$$\Delta CP = A v^2 d^2 + B v^2 d + C v^2 + D d \quad \text{Equation A1-1}$$

where d is the axial displacement (mm) and v is the testing rate (mm/s).

The Equation A1-1 was determined using a least squares fit to the experimental results for tests carried out at 270, 320, 360, 435, 470 and 545 kPa initial cell pressure. The values of the parameters A , B , C and D obtained for each series are shown in Table A1-1. A good agreement was observed between measured and predicted cell pressure increments for all the tests. Figure A1-3 shows this for the series carried out at an initial cell pressure equal to 470 kPa. The actual cell pressure value during rapid loading tests is assumed to be equal to the sum of the initial cell pressure value and the calculated cell pressure increment. These corrections only affected the interpretation of the pore pressure response and stress path analysis on series OC1 and OC4 (Sections 7.2.1 and 7.2.2 respectively).

Further investigation was carried out in an attempt to suggest recommendations for the reduction of the increase in cell pressure during future testing. Figure A1-4

shows the results of a series of test carried out at initial cell pressure equal to 470 and rate of testing equal to 200 mm/s where different air gaps were left in the cell when it was filled with water, before the initial cell pressure was applied. The heights of the air gaps at the top of the cell (mm) were 10, 20 70 and 200 mm. The results of these tests (Figure A1-4) show that the air gaps acted as a cushion and reduced the cell pressure increase as the ram penetrated the cell. The larger the air gap the greater the reduction of the increase. It is recommended for future testing to leave an air gap to reduce the increase of cell pressure during testing and to measure the actual cell pressure by means of a transducer.

	Initial Cell Pressure (kPa)					
	270	320	360	435	470	545
A	-0.0001	-0.0001	-0.0001	-0.0001	-0.0001	-0.0002
B	0.0261	0.0322	0.0344	0.0383	0.0406	0.0417
C	-2.2017	-2.7524	-2.9518	-3.2792	-3.4545	-3.5676
D	9.6048	11.9064	12.6013	13.5525	14.0842	14.3858

Table A1-1 Parameters A, B, C, D in Equation A1-1 for different initial cell pressures.

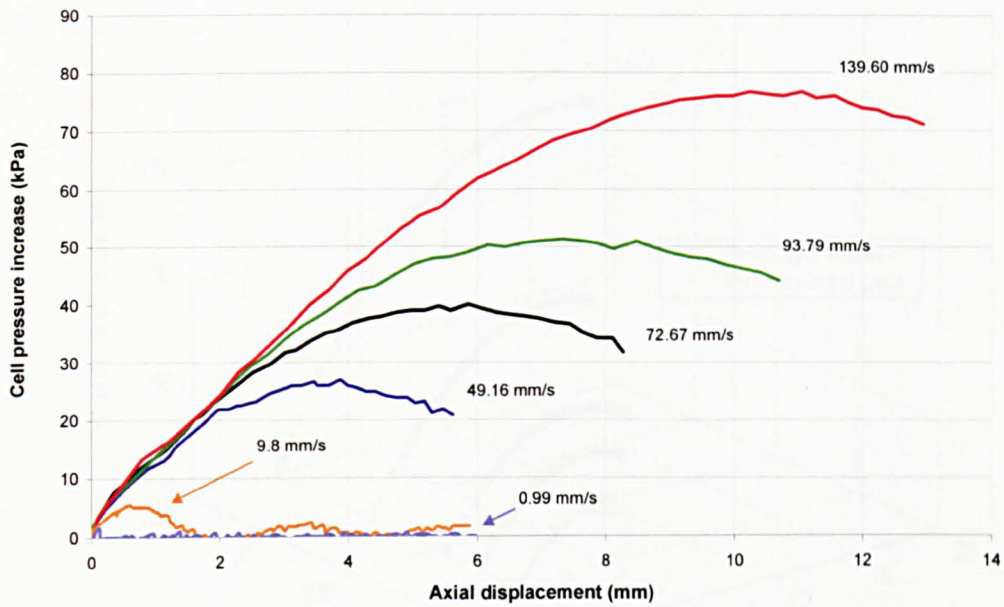


Figure A1-1 Measured cell pressure increase versus axial displacement for rapid loading triaxial tests at different rates. (Initial cell pressure = 470 kPa)

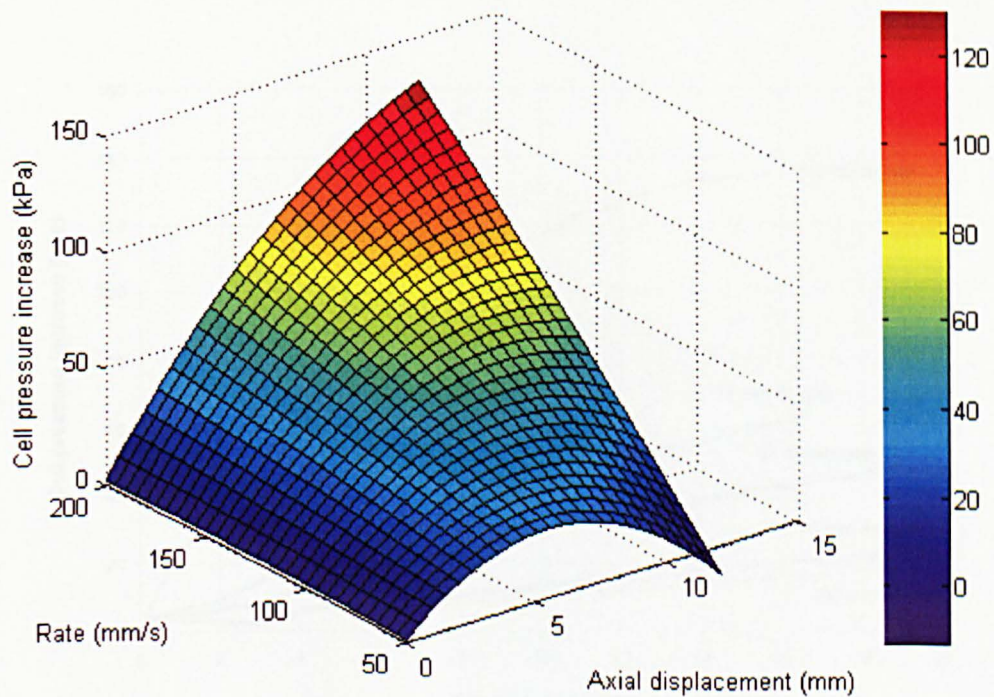


Figure A1-2 Predicted cell pressure increase with axial displacement during rapid loading triaxial tests at different rates. (Initial cell pressure = 470 kPa)

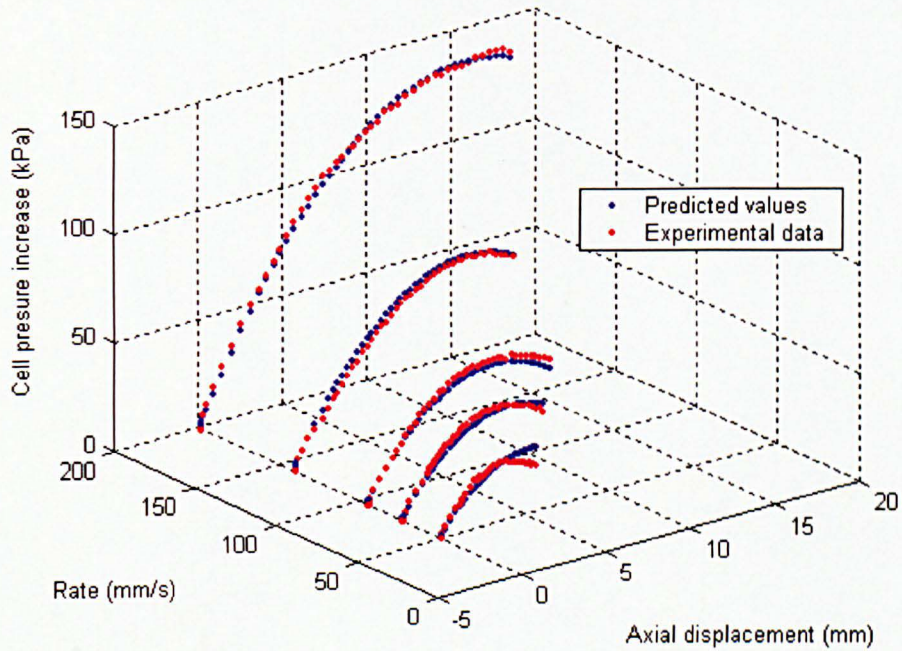


Figure A1-3 Measured and predicted cell pressure increase with axial displacement during rapid load triaxial tests at different rates. (Initial cell pressure = 470 kPa)

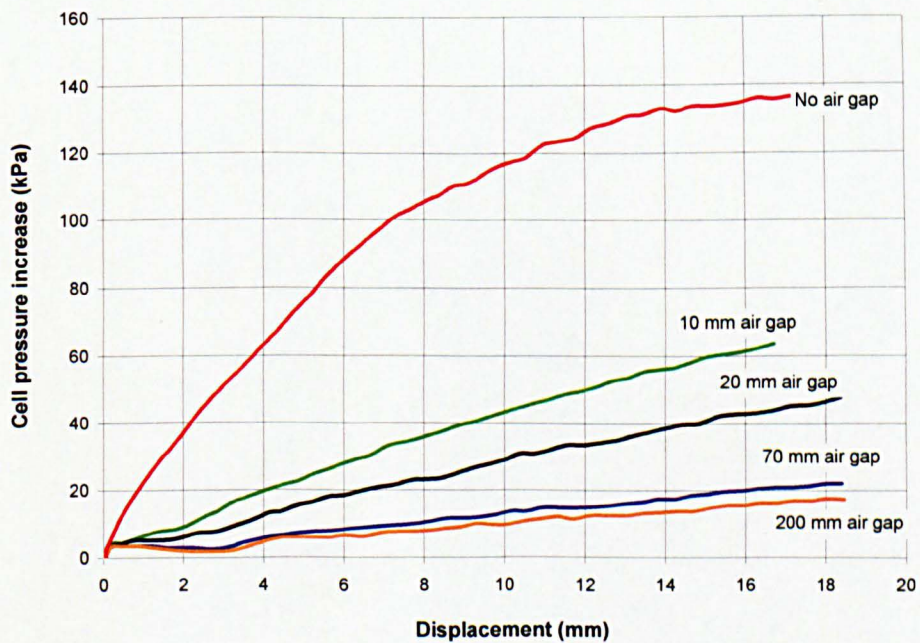


Figure A1-4 Cell pressure increase versus axial displacement for rapid load triaxial tests at 200 mm/s for different cushion air gaps in the cell. (Initial cell pressure = 470 kPa)